SEISMIC RESPONSE OF TUNNEL AND TUNNEL SUPPORTS IN JOINTED ROCKS

A THESIS

submitted by

MALAVIKA VARMA

for the award of the degree

of

DOCTOR OF PHILOSOPHY

GEOTECHNICAL ENGINEERING DIVISION

DEPARTMENT OF CIVIL ENGINEERING

INDIAN INSTITUTE OF TECHNOLOGY MADRAS

AUGUST 2019

Dedicated to

YOU

THESIS CERTIFICATE

This is to certify that the thesis titled **SEISMIC RESPONSE OF TUNNEL AND TUNNEL SUPPORTS IN JOINTED ROCKS**, submitted by **MALAVIKA VARMA** (CE14D047), to the Indian Institute of Technology Madras, Chennai for the award of the degree of **Doctor of Philosophy**, is a bona fide record of the research work done by her under our supervision. The contents of this thesis, in full or in parts, have not been submitted to any other Institute or University for the award of any degree or diploma.

Dr. V.B. Maji
Associate Professor
Department of Civil Engineering
Indian Institute of Technology Madras
Chennai-600 036.

Prof. A. Boominathan
Professor
Department of Civil Engineering
Indian Institute of Technology Madras
Chennai-600 036.

Place: Chennai

Date: 14th August 2019

ACKNOWLEDGEMENTS

I wish to express my sincere gratitude to my research advisors Dr. Vidya Bhushan Maji and Prof. A. Boominathan, for their constant encouragement, immense support, active involvement in all phases of this research work. They helped me expand my knowledge and horizon and allowed me to explore diversely. They helped me understand patience, which ultimately remoulded my research mentality and motivated me to achieve perfection.

I sincerely thank Prof. K. Ramamurthy, Head of the Department, for his support, suggestions and all the facilities provided for pursuing this research work. I am greatly obliged to Prof. S. R. Gandhi, Prof. K. Rajagopal, Prof. G. R. Dodagoudar Prof. R. G. Robinson, Dr. T. Thyagaraj, Dr. Dali Naidu Arnepalli, Dr. Tarun Naskar and Dr. Ramesh Kannan K. for their frequent advice and precious suggestions for refining the quality of research. I would like to extend my gratitude to the members of my doctoral committee, Dr. Rupen Goswami, Dr. Subhadeep Banerjee and Dr. C.S. Shankar Ram for their continuous review of my research progress and valuable suggestions. A special thanks to Prof. Manu Santhanam and Ms. Malarrvizhi A. for providing me all the necessary support for the experimental works in the Building Technology and Construction Management Division. I thank Mr. Soundarapandian M., Mr. Om Prakash K., Mr. Suresh P., Mr. Gasper Arumairaj J. for helping with various technical and non technical requirements in the campus. I thank Mr. Muthusamy R, Mr. Jalaludhin and Mr. Kumar for responding immediately and helping me rectify the issues I had with my computational system. A special thanks to the staff of Departmental Workshop: Mr. Prince Anandraj, Mr. G. Balasubramanaian and Mr. P. Nagarajan, for fabricating the models and experimental set-up. I also thank the staffs from Dept. of Civil Engg. and Administrative section, who were welcoming and supportive at each point.

I thank Dr. Jay Aglawae for responding to my queries regarding UDEC modelling at different stages of my work.

I am honoured to know and be encouraged by Dr. Wesley Patrick, Executive Director, Center for Nuclear Waste Regulatory Analyses, Southwest Research Institute, San Antonio, United States of America. I thank him for his valuable insights, references and motivation.

I thank Prof. K.S. Rao, IIT Delhi a mentor, who encouraged me to follow my PhD dreams.

I thank project staff, Mr. Dharani Raj and Mani from the Dept of Civil Engg. who found extra time in helping me during various phases of my work and being such good friends.

Heartfelt thanks to my friends at IIT Madras: Ms. Swagatika Senapati, Ms. Surabhi Jain, Mr. Ramon Vargheese, Ms. Vijaya Ramananthan, Dr. Jitesh Chavda, Ms. Jyotsna Venkatesh, Mr. Dinesh Natrajan, Ms. Dhanya J.S., Dr. Suganya Kuppusamy, Dr. Sivakumar, Ms. Manasa Hanumanthappa, Ms. Priya Beena Sudaven, Ms. Vineetha K, Mr. Nikhil John, Ms. Aparna G Pillai, Ms. Aarti Shivan, Dr. Balu George, Dr. Deepthi Yarala, Mr. Aravind Raj, Mr. Biju M.S., Ms. Jayalakshmi Arunkumar, Mr. Sandeep Bandipally, Ms. Dhanalakshmi, Ms. Arsha laksmi, Ms. Amal Azad Sahib, Ms. Anu Jose, Ms. Reshma Bhoodesan, Mr. Akshay Sakhare, Mr. Deviprasad B.S., Ms. Sona Gokuldas, Ramanandan, Ms. Ambili, Arun C, Dr. Dhanya Jaya, Mr. Ananthapadmanabhan, Ms. Resmi G., Dr. Salini Unnikrishnan, Dr. Lini Dev, Dr. Julina Johnson, Mr. Soumya Ranjan Misra, Dr. Sunil Ranjan Mohapatra, Dr. Nithin Sudarsanan, Dr. Chinchu Cheriyan, Ms. Prathyusha Naik, Dr. Raheena Moozhikkal, Mr. Vivek Roy, Ms. Rini Prakash, Ms. Anna George, Ms. Ayesha, Mr. Manan Patel and Ms. Kruti Patel whose association leaves a very sweet memory in my mind. Special wishes and thanks to all my fellow research scholars of the Geotechnical Engineering Division, Department of Civil Engineering, IIT Madras, Chennai.

I am obliged to Mr. Sampath and Mrs. Dhanalakshmi Sampath, my previous houseowners who took care of me during the flood of 2015 and cyclone of 2016 like family. They also looked out for me and my safety when I used to come home late at night from the lab.

My heartfelt gratitude to my friends Aryasree, Nileena, Sivapraveen, Rajesh, Revathy, Pooja, Praneetha, Kamal Nanda, Akshay Mitra Pawar, Cini Philip, Sanju John, Nima Soman who always loved me and stayed next to me.

I thank Dr. Shyam Kerala Varma, Ms. Vidya Varma, Dr. Yadu Vasudev, Ms. Pallavi Varma, Col. Haridas, Ms. Indira Haridas, Mr. Brijesh Varma, Ms. Surabhi Raja, Mr. Suresh Varma, Mr. Sreekumar Kaloor, Ms. Pratyusha Sridharan and Mr. Pranoy Varma for providing the comfort of family and home during various occasions. Thanks to darlings Trayi, Avanika and Advait for making me laugh and forget my tensions.

I express my gratitude to my family Mrs. Easwari Varma, Er. Sreeram Rajan, Dr. Chandni Varma, Mr. Raveendra Varma, Mrs. Sajini Varma, Mr. Dileep Varma, Mrs. Girija Varma, Mr. Pradhu Varma, Mr. Prem Varma, Mrs. Devi Varma, Mr. Jishnu Varma, Mrs. Meera Varma, Mrs. Praseeda Varma, Mr. Ajith Varma, Mrs. Sheila Varma, Mr. Suraj Varma, Dr. Archana Varma, Mr. Sharat Varma, Ms. Lakshmi Varma and Dr. Anoop Varma who understood, whenever I couldn't be there for you. My siblings, Aswin, Parvathy, Ritwik, Manyu, Sreelekshmi Vasudev, Parthiv, Satchit, Advait, Ambarish and Anagha for teasing me, encouraging me, motivating me and grounding me, all at the same time. You kept the grit in me alive. My darlings Dhruv, Vihaan and Anushka, the very thought of you made me smile.

I would like to express my gratitude and love to my parents Mr. Varma K Raghu and Mrs. Beena Varma for their immense love, moral support, encouragement, inspiration, affection and blessings throughout my life. And I thank my love, my world, Arjun for all the patience you have shown towards me. You three have been my punching bag and my stress relief. Knowing that you had my back helped me gather myself and stand tall, everytime I broke down. I don't know what I would have done without you.

I am grateful to everyone who always wished the best for me and those who have done their duty and responsibilities on time so that my life continues with convenience.

I thank every entity and energy in the universe that shaped me and helped me stay focused.

Malavika Varma

ABSTRACT

The underground structures are considered to be comparatively safe under the action of dynamic loads and hence the effect of seismic loads are hardly considered. The presence of discontinuity increases the complexity in the behaviour of the rock under dynamic loading, especially joints, which are very common in the field. Present study attempts to understand the effect of stress waves propagating through jointed rocks. The first part of the study focuses on the wave propagation through single and multiple joints. The second part of the study focuses on the performance of unsupported tunnels under the action of seismic loads. These underground structures are mostly supported by one or more support systems. And the behaviour of these support systems under the action of seismic load comprises the third and last part of the study.

Most of the previous studies focussed on the transmission and reflection coefficient of the propagating wave. The current study is aimed to understand the variation in wave velocity according to different joint conditions. Experimental studies aided with numerical methods are adopted. The experimental program consists of low strain ultrasonic pulse velocity tests on laboratory prepared gypsum samples. Rock samples with various joint configurations namely joint angle, joint spacing and joint roughness are studied. The joint angle is found to influence the wave velocity and for a certain range of incidence angle, it increases. The increase in the joint roughness tends to reduce the wave velocity. This study is limited to high frequency ranges and a numerical model based on distinct element method (DEM) is developed to extend for other frequencies. The DEM model is systematically validated with laboratory studies. The increase in wave velocity after certain joint angle was prominent in case of relatively high and low frequencies. Also, the size of the block used for the study, the position of the joint in the block, the number of joints and joint spacings are found to have considerable influence on the wave velocity. Empirical relationships are proposed based on the results to predict longitudinal wave velocity in jointed rock mass with respect to intact wave velocity.

To understand the behaviour of unsupported jointed rock tunnel under seismic loading, a case study of Lucky Friday mine is analysed on a laboratory scale model. The scaled 1985 Mexican earthquake is provided as the seismic input. The tunnel deformations are studied and compared with that of static conditions. The study considers failures occurring due to joint slip and a parametric study is done to understand the effect of insitu stress, joint orientation, joint

stiffness and joint friction angle on the deformation and stability. The joint stiffness and joint friction angle are found to produce a pronounced effect on the tunnel deformation under seismic conditions. Moreover, certain joint angle combinations and wedge angles are found to create complete failure of the tunnel. Investigation with different lateral stress coefficients confirms that the shallow tunnels are more vulnerable under seismic loading.

The response of tunnel support systems under earthquake conditions are important as they decide on the overall stability. For this, a study is conducted on the headrace tunnel of Tehri dam situated at seismic zone V and passing through jointed rockmass. Uttarkashi earthquake (1991, M_w=6.8) and Nepal earthquake (2015, M_w=8.1) are provided as seismic input, based on its location and magnitude respectively. The stresses and deformations acting on rockbolts and shotcrete as support systems individually and as a combined system are analysed. A detailed study on the force and deformation behaviour of each rockbolts placed around the tunnel is discussed. Rockbolts are found to undergo higher forces and deformation under the action of seismic loads with a visible effect on the bolts passing through joints. The study on shotcrete showed the presence of spalling and stress concentrations at areas of intersection between the support and rock joints. For a combined support system, a transfer of forces between the rockbolt and shotcrete can be observed. There is an increase in the stress concentration on the tunnel sidewalls along with the reduction of stresses on rockbolts passing through joints at shoulders. A parametric study is performed on the support systems to understand the effect of various joint parameters and incoming wave characteristics. The stress waves acting on the joints are found to produce a loosening effect in the rock mass leading to tunnel instability. The stability of underground openings under dynamic conditions is essential for its safe design, especially for the prediction of performance under seismic loading. The present study attempts to bring clarity and provide better insight into this important domain.

TABLE OF CONTENTS

LIST OF FIGURES

LIST OF TABLES

NOTATIONS

$\theta_{\text{P-incident}}$	Incident angle of the primary wave
$\theta_{\text{P-reflected}}$	Reflected angle of the primary wave
$\theta_{\text{P-transmitted}}$	Transmitted angle of the primary wave
$\theta_{\text{S-incident}}$	Incident angle of the secondary wave
$\theta_{\text{S-reflected}}$	Reflected angle of the secondary wave
$\theta_{\text{S-transmitted}}$	Transmitted angle of the secondary wave
u	Displacement
α_p	P wave velocity
x	Distance
t	Time
v	Particle velocity, $\frac{\partial u}{\partial t}$
ε	Stain, $\frac{\partial u}{\partial x}$
U	Group velocity in intact rock
θ	Angle of incidence
N	The number of fractures
ω	Angular frequency
K	Specific stiffness
Z	Seismic impedance
ξ	Ratio of fracture spacing to wavelength
$\lvert T_N \rvert$	Transmission coefficient of normally propagating waves along multiple parallel fractures

$\lvert T_1 \rvert$	Transmission coefficient of normally propagating waves along single fracture
φ	Friction angle
Ω	Dimensionless frequency
Y_c	Critical depth for tunnels
D_t	Diameter or span of the tunnel
D_b	Block length
W_t	Tunnel wall length
$L_{b,roof}$	Length of rock bolt for roof
$L_{b,wall}$	Length of rock bolt for sidewall
σ	Normal force
τ	Shear force
Δx	Small length
E	Modulus of elasticity
F	Function of
JRC	Joint Roughness Coefficient
λ	Wavelength
V_j	Wave velocity through jointed rock
V_i	Wave velocity through intact rock
A_1, A_2, B_1,B_2	Constants
L_B	Block length
L	Distance to joint position
s	Joint spacing
ς	Defined function of L, L_B and λ

L_{bolt}	Length of rockbolt
B	Width of the tunnel
H	Height of the tunnel
I	Moment of inertia
cs_{sstiff}	Shear stiffness on coupling springs
cs_{nstiff}	Normal stiffness on coupling springs

ABBREVIATIONS

ISRM	International Society for Rock Mechanics
UDEC	Universal Distinct Element Code
DDM	Displacement Discontinuity Method
EMM	Equivalent Medium Method
VWS	Virtual Wave Source
TLPM	Thin Layer Plate Method
TLIM	Thin Layer Ineterface Method
EVMM	Equivalent Viscoelastic Medium Method
UPV	Ultrasonic Pulse Velocity
SHPB	Split Hopkinson Pressure Bar
DIANE	Discontinous Inhomogeneous Anisotropic and Non Elastic
BEM	Boundary Element Method
FEM	Finite Element Method
FDM	Finite Difference Method
DEM	Discrete Element Method
DDA	Discontinous Deformation Analysis
DFN	Discrete Fracture Network
3DEC	3 dimensional Distinct Element Code
PFC	Particle Flow Code
MRTS	Metro Rail Transport System
NATM	New Austrian Tunnelling Method
CNWRA	Centre for Nuclear Waste Regulatory Analysis
SCL	Sprayed Concrete Lining
SEM	Sequential Excavation Method
s	Second
kN	Kilo Newton
kNm	Kilo Newton metre
m	metre
USGS	United States Geological Survey

CHAPTER 1

INTRODUCTION

1.1 GENERAL OVERVIEW

The behaviour and response of rocks under the action of dynamic loads are broadly classified as the study area called rock dynamics. The dynamic loads acting on the rocks are considered as stress waves propagating through the rocks. The source of these stress waves might be blasting, earthquake, rockburst, airblast, pressure bumps or impact loadings. The study of rock dynamics deals with both the effect of stress waves and the process of wave transmission through the rocks which, may vary from micro-scale fracturing in the rock to large fault displacements. With the increasing dependence on rock structures in the urban environment for infrastructural development, mining or petroleum sectors, a need for standards of rock dynamic testing, design and practice was felt. This led to the establishment of a Commission on Rock Dynamics in 2008 by the International Society for Rock Mechanics (ISRM). The current study is inspired by the rigorous ongoing studies around the world in that direction.

Rocks are never truly intact, and the presence of discontinuities are ubiquitous. The discontinuities may be in the form of fissures, microcracks, joints, bedding planes or faults. These discontinuities separate intact rock blocks in the field. The presence of any discontinuity produces significant ambiguity in the behaviour of rocks in both static and dynamic conditions. The stress waves according to its amplitude and strain rate also causes changes in the rock or displacements along the joints. The strain rate of most waves in rocks is comparatively low unless the rock is near to the source of the dynamic load. Thus these waves propagate as elastic waves through the rocks. Stress waves propagating in rocks undergo attenuation on the intersection with a discontinuity. These stress waves thus travelling as elastic waves along the rock on the joints undergo transmission, reflection and absorption. The percentage of wave transmitted, reflected and absorbed depended on whether the joints are welded, non-welded or open. Welded joints in most cases are so strong that their presence is usually nullified. Hence the stress waves striking welded joints are fully transmitted. Open joints undergo full reflection, and no transmission takes place. The stress waves passing through non-welded joints are partially reflected and partially transmitted. The wave propagation pattern would be affected by the properties of the joint. These changes in wave propagation also affect the time required for the wave to travel through the joints and causing a change in its wave velocity.

The construction of a tunnel in discontinuous rocks leads to the possibility of joint slip conditions. These tunnels which have chances of a potential slip in static conditions due to the presence of free blocks are likely to find an aggravated response under the action of dynamic loads. The understanding is essential with an increasing number of important and critical projects in major seismic zones. The stress waves acting on the joints or discontinuities are likely to produce a loosening effect or opening of the joints, especially near the excavations and underground structures. This leads to some associated problems regarding the response of tunnels and its support systems under the action of earthquake loads. The stability of openings under dynamic conditions is essential, even under the action of multiple earthquakes or other dynamic behaviour. The research area still being new with relatively fewer insights on rock dynamics behaviour, this study would attempt to bring more clarity and put light into this important subject.

1.2 OBJECTIVES AND SCOPE

This research mostly focuses on the seismic response of tunnels in jointed rocks. The aim is to understand the effect of joints on the wave propagation and effect of dynamic loading on tunnels in jointed rock and corresponding support systems. The main objectives are:

1. To study the effect of rock joints and rock masses on wave propagation.
2. To study the response of jointed rock tunnels and tunnel supports under earthquake load.

The scopes of the study are,

- Study the effect of rock joints, namely joint spacing, roughness and inclination on wave propagation using laboratory experiments.

- Develop a numerical model using distinct element method to capture the effect of wave propagation through joints and simulate the wave propagation in jointed rocks for different joint configurations.
- Extend the applicability of the model for tunnels and study the effect of rock joint characteristics under the action of earthquake loads.
- Numerical analysis of tunnel considering the interaction of rock supports with the surrounding rock mass under the action of earthquake loads.

1.3 ORGANIZATION OF THE THESIS

This thesis is organised into nine chapters,

Chapter 1 presents the background to the area of study and the significance of the study along with the importance of understanding wave propagation through joints and various phenomena leading to the dynamic loading on joints. The chapter provides an insight into the thesis and its significance. A general overview of the thesis along with the scopes and objectives are provided.

Chapter 2 focuses on the details of the literature available and the state of art description of the work. A review of work done analytically, experimentally and numerically to understand wave propagation has been provided. A study on the response of tunnels when acted upon by dynamic loading is also discussed. The effect of tunnels with and without supports and the performance of various support systems have also been discussed.

Chapter 3 aims at understanding the behaviour of the wave, change in wave propagation and wave velocity for a laboratory study by ultrasonic pulse velocity test on samples of gypsum. Various joint configurations are studied to understand the behaviour of longitudinal waves with varying joint properties.

Chapter 4 extends the laboratory experiments discussed in chapter 3 to numerical modelling using Universal Distinct Element Code (UDEC). The chapter attempts to understand the change in wave velocity with various joint and wave parameters like joint angle, joint roughness, block length, joint position and frequency. Empirical relationships are proposed for the prediction of wave velocity through the rock mass and presented.

Chapter 5 tries to understand rock joint behaviour under seismic wave history obtained from an actual earthquake. In this chapter, a scaled model study of Lucky Friday Mine is conducted to understand the performance of unsupported jointed rock tunnel with two sets of joints. The study is conducted numerically simulated to understand the effect of the same on joint slippage and tunnel failures with varying joint parameters and stress conditions.

Chapter 6 tries to understand the behaviour of rockbolts as support system under the action of earthquake loads. The study uses the headrace tunnel from Tehri dam project. Uttarkashi (1991, Mw=6.8) and Nepal (2015, Mw= 8.1) earthquakes are being used for the study. This chapter focuses on the effect of these earthquakes on rockbolt as the tunnel support. A detailed study on the forces acting on each rockbolt is done to understand the effect of dynamic loading on it relative to its position in the tunnel. The effect of parameters like joint friction, bolt length, bolt diameter, frequency of the incoming wave, duration of loading and amplitude of loading on the performance of the rockbolts are also discussed.

Chapter 7 extends chapter 6 by using shotcrete as the only support for the headrace tunnel in Tehri dam. The shotcrete deformations under the action of Uttarkashi and Nepal earthquakes is compared to its performance under static conditions. The forces acting on different parts of the shotcrete is used to understand the stress concentrations on the action of an earthquake load. The study is extended to understand the performance of the shotcrete with the change in various parameters, namely joint stiffness, shotcrete thickness, wave frequency, duration of loading and amplitude of loading.

Chapter 8 attempts to understand the behaviour of a combined support system, namely rockbolts and shotcrete. With chapter 6 and chapter 7 focusing on the performance of rockbolt and shotcrete as individual support systems, in chapter 8, the combination is investigated under earthquake loads for the same case study of Tehri dam. A comparison is made for the change in forces, deformation and moments when the support systems are used individually and in combination.

Chapter 9 gives a summary of the work done as a part of this thesis and the results obtained from the study. The major conclusions are provided with the scopes for future work.

1.4 MAJOR CONTRIBUTIONS FROM THE WORK

The major contributions from this work can be divided into three main headings:

- Effect of joints on wave propagation
    - Experimental study on the variation in the wave velocity with rock joints using ultrasonic pulse velocity test.
    - Confirming the adaptability of numerical models in the study of wave propagation through jointed rock mass.
    - Understanding the variation in wave velocity with various joint characteristics.
    - Comparison of wave velocity change for all frequency ranges.
    - Providing empirical relations to predict wave velocity through rock mass for different joint characteristics.
- Performance of unsupported jointed rock tunnels under seismic loading.
- Performance of support systems in jointed rock tunnels for earthquake loading.
    - Tunnel analysis with rockbolt - when the same is used as the only support system.
    - Tunnel analysis with shotcrete - when the same is used as the only support system.
    - Performance of rockbolt and shotcrete in jointed rock tunnels when used in combination.

CHAPTER 2

LITERATURE REVIEW

2.1 INTRODUCTION

Rock dynamics is the study of responses of rocks and rock structures under the action of any dynamic load and is one of the most important areas of study in the field of rock mechanics (Aydan et al., 2011; Aydan, 2016; Zhou and Zhao, 2011). The action of dynamic load on rocks may be in the form of deformation, load/stress or fractures and failures which varies with time. Hence, the area of rock dynamics covers a wide range, varying from wave propagation through rocks to the effects of fault displacements. Among these, the effect of the dynamic load on rock discontinuity is very important, and the effect these joints under dynamic loads need to be understood.. The chapter gives an insight into the previous analytical, experimental and numerical studies conducted to understand wave propagation through rocks and rock joints. The detailed review tries to understand the response of tunnels under the action of various dynamic loads. The performance of tunnel supports under the action of dynamic loads are also studied and reviewed

2.2 INTRODUCTION TO THE PROPAGATION OF STRESS WAVES

The dynamic loads acting on a medium are represented as waves. The stress waves travel as body waves (Figure 2.1) and surface waves (Figure 2.2). Body waves mainly consist of primary wave or secondary wave. These waves pass through the medium under consideration. Whereas the surface wave consists of Rayleigh waves or Love waves, and they propagate near the surface of the medium under consideration.

Primary waves are commonly known as P waves. They are also called compression waves because of the compressional force it imparts. The particles in the medium propagate along or opposite to the direction of wave propagation. Secondary waves are generally referred to as S waves.. The particles in the medium move perpendicular to the direction of the wave, which induces a shearing force on the medium and causing distortion to the body.

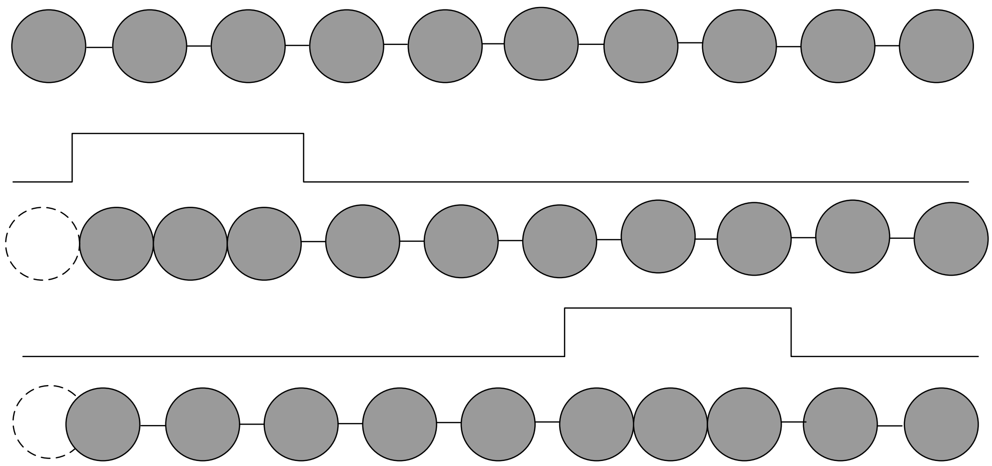

Figure 2.1: Propagation of P wave (Adapted and redrawn from Zhang, 2016)

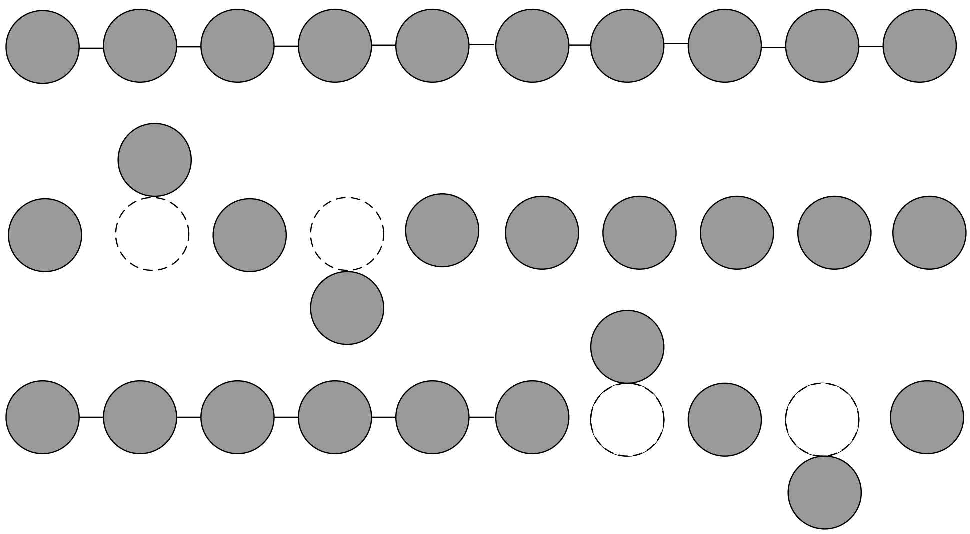

Figure 2.2: Propagation of S wave (Adapted and redrawn from Zhang, 2016)

The action of the stress waves may be an effect of drilling, blasting, impact, earthquake, rockburst, airblast or bumps propagate through the rocks. And the stress waves produced by the dynamic loads are classified as an elastic wave, plastic wave or shock wave according to the stress-strain relation it builds on the materials. If the strain acting on the medium is directly proportional to the stress acting on the medium, the waves are known as elastic waves. But when the stress produced is more than the yield stress in the body and elastic-plastic deformation occurs, the waves are known as plastic waves. Explosion or blasting creates shock waves causing the particles to experience a very high strain in an infinitesimal duration.

When these stress waves intersect a surface or discontinuity, the stresses undergo reflection, transmission, and absorption (Figure 2.3). This affects the wave propagation pattern, amplitude and the velocity of the wave. The problem faced by a rock mass on being intersected by a stress wave depends on the scale of analysis. This has been well explained by Zhao et al. (1999).

In the micro-scale, the dynamic stress may induce particle displacements, micro cracking. While in a large scale, the dynamic stresses may be the cause of displacements along discontinuities. Sometimes, the micro-scale fracturing extending over long time induces large deformations and failure. Compared to the micro-scale, on a large scale, discontinuities contribute a significant role in wave propagation and attenuation. The stress waves incident on a joint gets reflected, transmitted and absorbed according to the joint under consideration. The various studies on the effect of wave propagation while passing through joints have been discussed in this chapter. The study has been extended to understand the effects of stress waves on underground structures and the tunnel support systems.

2.3 WAVE PROPAGATION IN JOINTED ROCKS

Dynamic loads create stress waves which move and exert forces at adjacent points. Speed of the stress wave is a constant for a medium while it is unperturbed by any disturbances. But waves, as they get intersected by a discontinuity or undergo a change in medium, gets scattered. The incident wave will be partly transmitted and partly reflected. Waves travelling through rock, governed by laws of linear elasticity are known as seismic waves, and the speed with which the wave propagates is known as seismic velocity. The speed with which these particles move is known as particle velocity, which is relatively very small compared to seismic velocity. Although the elastic waves are often assumed to travel in a unidirectional manner, the coupling between different normal stress and strain due to Poisson's effect, causes the motion never to be truly one dimensional in the mathematical sense. Most studies on stress wave propagation across joints are limited to the assumption that the joint may deform but does not get damaged. Several studies have been made using analytical, numerical and experimental methods on wave propagation across rocks.

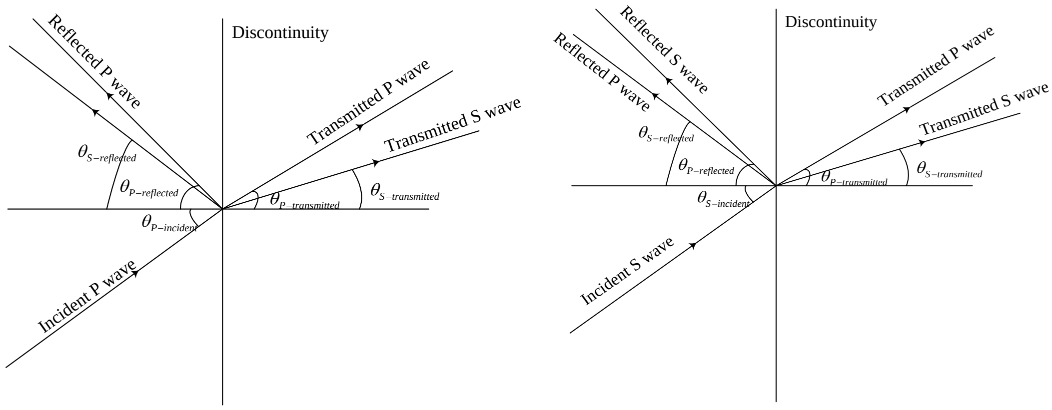

Figure 2.3: Transmission and reflection of P wave and S wave at a discontinuity

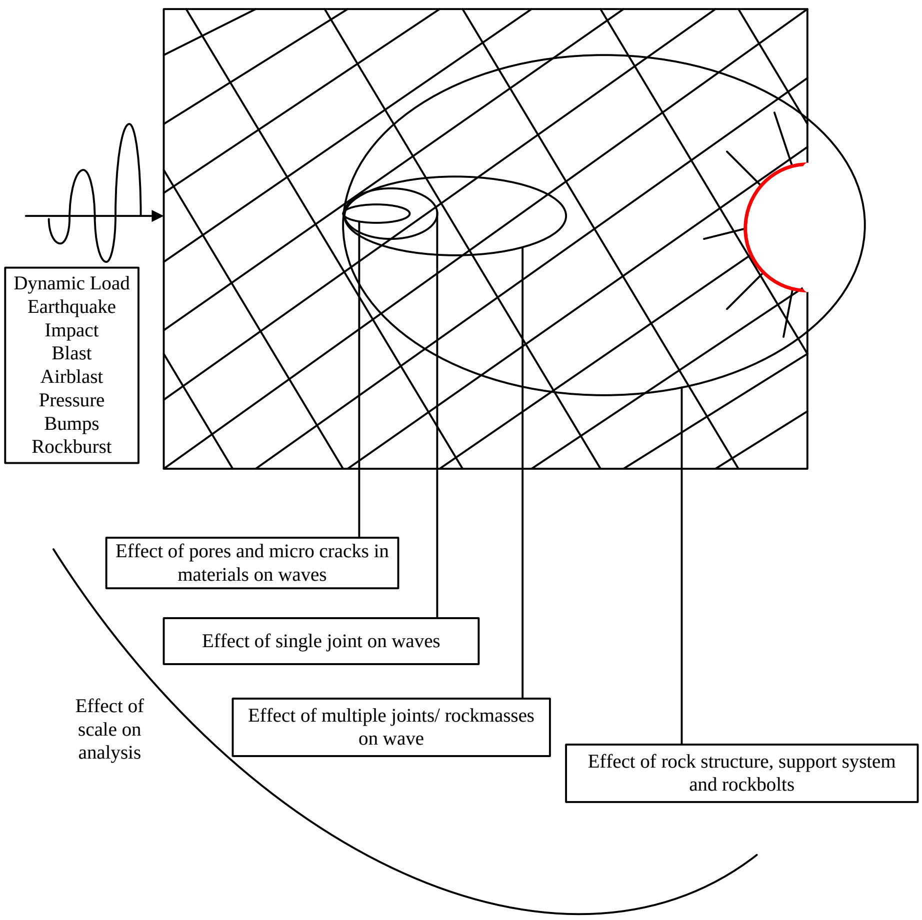

Figure 2.4: Typical rock dynamic problem in tunnels and caverns (Adapted and redrawn Zhao et al., 1999)

2.3.1 Analytical Studies

In a continuous elastic medium, the equation of a one dimensional P wave propagation is given as Eq. 2.1 according to Jean D' Alembert (1747)

$$\frac{\partial^2 u}{\partial t^2} = \alpha_p^2 \frac{\partial^2 u}{\partial x^2} \qquad \text{(Eq. 2.1)}$$

Where,

u is the displacement,

α_p is the P wave velocity,

x is the distance and ;

t is the time.

The wave equation is also expressed in terms of particle velocity and strain as

$$\frac{\partial v}{\partial t} = \alpha_p^2 \frac{\partial \varepsilon}{\partial x} \qquad \text{(Eq. 2.2)}$$

where, $v = \frac{\partial u}{\partial t}$ and $\varepsilon = \frac{\partial u}{\partial t}$.

The change in wave velocity and transmission pattern are analysed by different analytical methods. The analytical techniques mostly used in wave propagation studies can be generally characterized as

- Approximate Methods (Walsh, 1966; Miller, 1977; 1978)
- Displacement Discontinuity Method (DDM) (Schoenberg, 1980; Pyrak-Nolte et al., 1990; Cai and Zhao, 2000; Perino et al., 2010)
- Equivalent Medium Method (EMM)(Li et al., 2010; Fan et al., 2012; Zou et al., 2016)

Most research in the area of wave propagation through joints are analysed using DDM method. In DDM method, the stress along the joints is assumed to be continuous while the displacements are discontinuous. But, most of the early research in the field used approximate methods. Walsh (1966) reported that specific attenuation of waves in rocks is because of two factors; (a) by assuming the cracks to be approximate elliptical slits in plane strain and; (b) relation for specific energy loss.

Rock fractures have displacements as slip along the joints due to normal, and shear stresses acting on them, and the fracture surfaces are dominated by friction acting on them. By approximating this theory, Miller (1977) found that a large part of the energy is dissipated as frictional energy and that the frictional boundary stresses are nonlinear. Miller (1977) had analysed the steady state solution of nonlinear systems by the method of equivalent linearization. The wave propagation is found to depend on the ratio of the amplitude of incident stress to frictional stress associated with the nonlinear model. In the absence of kinematic interlocking, the transmission is nearly complete for very low values of the stress ratio, whereas reflection is nearly complete for high stress ratio values. Instead of Coulomb slip model, Miller (1978) analysed wave propagation using other non-linear joint models like Fortsch model (linear spring parallel to frictional damper) and Leob model (linear spring parallel to Coulomb damper where slip stress is not constant but proportional to slip displacement). An approximate solution method was used in these models. The results were found to be in accordance with Miller (1977) for all the models.

Schoenberg (1980) studied obliquely incident waves on joints by DMM assuming linear slip. Welded and non-welded joints were considered in the analysis. Equations for displacement, reflection coefficient, and transmission coefficient were derived analytically. Pyrak-Nolte et al. (1990) observed that specific stiffness is the most relevant parameter that determines the seismic properties of the fracture since it gives the quantitative description of mechanical coupling between two fractures affecting wave transmission. The variation of group velocity was studied using DDM for different frequencies under different specific stiffness. Group velocity was described as the wave velocity through a single fracture. The variation of velocity with the angle of incidence was also plotted. The variation of velocity was found to be influenced by frequency and ratio of specific stiffness of joint to impedance. The variation P wave velocity with angle of incidence was also analysed, and the velocity was found to increase as the incident angle nears 90°. This effect was the influence of the phase shift in the incident waves. An equation for group travel time for a medium having N fractures were proposed by Pyrak-Nolte et al. (1990) as,

$$t_{eff} = \frac{L}{U\cos\theta} + Nt_{gT} \qquad \text{(Eq. 2.3)}$$

where,

L is the total path length along a line normal to the planes,

U is the group velocity in intact rock,

θ is the angle of incidence and

N the number of fractures.

The group time delay for each fracture t_{gT} according to Pyrak-Nolte et al. (1990) is a function of angular frequency (ω), specific stiffness (k) and seismic impedance (Z).

$$t_{gT} = 2\frac{\left(\frac{k}{Z}\right)}{\left[4\left(\frac{k}{Z}\right)^2 + \omega^2\right]} \qquad \text{(Eq. 2.4)}$$

Cai and Zhao (2000) derived theoretical formulation using DDM approach and method of characteristics for calculating the transmission coefficient of normally propagating waves along multiple parallel fractures ($|T_N|$). It is a function of the ratio (ξ) of fracture spacing to wavelength. The study leads to the understanding of a critical and threshold fracture spacing to wavelength ratio, which determines the action of multiple fractures. The $|T_N|$ is independent of fracture spacing if $\xi \geq \xi_{thr}$ and $|T_N| = |T_1|^N$. When $\xi_{thr} < \xi < \xi_{cri}$, $|T_N|$ increases as fractures spacing reduces and when $\xi \leq \xi_{cri}$ $|T_N|$ decreases with fracture spacing. But, as the stiffness of the fractures were found to increase $|T_N|$ is not affected by the number of fractures, even if their ξ is very small. Zhao and Cai (2001) analysed the transmission of P waves across fractures. The study was limited to single fractures which are dry following a nonlinear deformation pattern. The results obtained for transmission and reflection coefficients from nonlinear deformations were found to be special conditions of solutions by linear deformations.

Li and Cai (2010) proposed a virtual wave source (VWS) method for understanding the effect of multiple joints on the transmission coefficient. The results obtained from the equivalent elastic model and virtual wave source method depended on the frequency and spacing under consideration. Perino et al. (2010) studied wave propagation across the joints for single and multiple joints to understand the effect of the transmission coefficient as a factor of normalised stiffness. Normalised stiffness is the ratio of specific stiffness to the product of radial frequency and impedance along with the effect of wavelength and joint spacing. The DDM and thin layer plate method (TLPM) provided a successful solution only when the joint thickness was much smaller than the wavelength. Zhu et al. (2011) verified the usage of distinct lattice spring model for wave propagation studies by comparing it against VWS.

Fan et al. (2012) analysed viscoelastic behaviour of rock mass by DDM and EMM considering individual discontinuities to be micro-joints and the rock mass to be macro joints in sedimentary rock. The equivalent medium method treats the rock mass as a whole and predicts the effect of joints on the behaviour of the rock mass. The influence of amplitude and frequency on wave propagation and transmission coefficient was analysed to find a decrease in transmission coefficient as the frequency increases. Wu et al. (2014) used the method of characteristics to determine the effect of an infilling material and the stiffness induced by it on the P wave propagation and transmission coefficient. Li et al. (2014, 2015) analysed rock mass with different rock mass seismic quality factor using thin layer interface model (TLIM) and equivalent viscoelastic medium method (EVMM) respectively. A new, improved equivalent viscoelastic medium method was proposed by Li et al. (2015). A rock mass of higher quality was observed to be having less transmission losses and higher phase velocity. As frequency neared infinity, velocity was found to near intact wave velocity in jointed rock blocks. Zou et al. (2016) studied the obliquely incident waves through single oblique joints for P and S wave using wave superposition states in different areas adjacent to the fracture. In their studies, the time delay between reflected and refracted P and S waves are calculated analytically. Also, the effect of reflection of waves in limited area conditions as in laboratory experiments has also been taken into consideration.

2.3.2 Experimental Studies

Zhang and Zhao (2014) compiled different testing methods on dynamic loads under intermediate and high strain testing. Different test methods are used to understand the performance of rocks for different strain rates. The studies regarding wave propagation pattern mostly focus on the transmission and reflection characteristics of the waves. Different test methods were used to understand the wave propagation pattern depending on the strain levels. At low strain levels, the wave propagation through rocks mostly affected the wave patterns, transmission, and reflection rather than the rock in itself. The laboratory studies under low strain were mostly using ultrasonic pulse velocity test, bender element test and resonant column method. But for tests on high strain conditions, split Hopkinson pressure bar (SHPB) is usually adopted.

Studies using ultrasonic pulse velocity is one of the simplest methods of low strain dynamic testing. This method has been used by various researchers over the time to understand the wave propagation using piezoelectric transducers placed across the samples. Myer et al. (1990) conducted an experimental study on rock samples to understand the seismic behaviour of different joints under axial loading varied from 10 to 85 MPa. The effect of confining pressure on the wave propagation pattern using ultrasonic pulse study showed that, with an increase in confining pressure, the transmission coefficient increases due to the increase in joint stiffness properties. This was correlated with the analytical solutions for reflection and transmission coefficients by Miller (1978). This study was later extended on various other materials and different joint characteristics (Cook, 1992; Pyrak-Nolte, 1992, 1996; Chen et al., 1993).

Fratta and Santamarina (2002) used a resonant column device to study wave propagation along joints. Shear wave velocity was obtained for samples with and without infilling material. The presence of an infilling material was found to bring a decrease in the wave velocity and transmission coefficient. This research was extended by Cha et al. (2009) for P waves and to find the effect of other joint properties. The results with P wave velocity followed a similar trend as in the study by Fratta and Santamarina (2002). For saturated samples, the variation of P and S wave velocities were studied by Rodriguez- Sastre and Calleja (2006) using ultrasonic pulse velocity test. The study gave results on the effect of multiple foliations and foliation angles on the wave velocity. Ju et al. (2007) studied the effect of rough joints on the stress wave propagation under large strain loading using the Split Hopkinson Pressure Bar (SHPB) test. It was found that rougher the surfaces more the permanent deformations and hence higher the wave attenuations. Li and Pyrak-Nolte (2010) analysed the effect of wave transmission on layered carbonate rocks using seismic arrays to produce full-waveform measurements on the samples. The results of the study were used to find the effect of number of layers on the transmission of obliquely incident wave.

Kurtuluz et al. (2011) studied the wave propagation through marbles to understand the wave velocity under different joint patterns. The study was on multiple joints of different inclinations, and the variation of wave velocity and an increase in number of joints were found to decrease the wave velocity. Also, maximum wave velocity was found to be obtained when the angle of incident waves was zero. Perino (2011) used a resonant column for studying wave propagation across intact and jointed specimens with different fracture patterns. Smooth and rough fractures were incorporated as the joints to estimate the wave velocity, shear modulus and damping ratio of the material with different joint conditions.

Resonant column tests were done by Mohd.-Nordin (2014) and Sebastian (2015) for understanding wave propagation through single and multiple fractures. Both the studies were conducted on gypsum to replicate the rock and joint behaviour. The study by Mohd.-Nordin et al. (2014) concentrated on the joint roughness coefficient and its effect under different normal stresses. Sebastian (2015) carried out low strain tests on resonant column apparatus and bender element apparatus. The P wave velocity and shear wave velocity was found to decrease as the number of joints increased for the bender element test. Wu et al. (2015) studied the effect of P wave attenuation across parallel surface using SHPB tests for welded and non-welded joints and found that the wave attenuation increases when the surfaces are joined together with the help of some infilling material. Gui et al. (2016) carried out SHPB test on single filled and unfilled non welded fracture with a striking input pressure of 8 MPa, and it was found that filled non-welded joints have most attenuation. So as the infilling material thickness is increased, the wave attenuation occurring across the joint increases.

2.3.3 Numerical Studies

Many experimental procedures are costly and strenuous to be studied. This is especially true when the size of the rock mass considered for the study is enormous. The studies using numerical methods are according to the problem statements under consideration. Starfield and Cundall (1988) gave general guidelines in the development or use of any modelling technique. According to Harrison and Hudson (2000), the modelling in rock should follow DIANE concept (Discontinuous, Inhomogeneous, Anisotropic and Non-Elastic). The critical aspect of any numerical model is the objective and problem statement, according to Hoek et al. (1990). Division of the study can be done as the continuum method or discontinuum depending on the properties under consideration (Jing, 2003). The different available methods of numerical modelling are:

- Continuum method: Boundary Element Method (BEM), Finite Element Method (FEM) and Finite Difference Method (FDM)
- Discontinuum method: Discrete Element Method (DEM), Discontinuous Deformation Analysis (DDA) and Discrete Fracture Network (DFN)
- Hybrid method: Hybrid BEM/DEM, Hybrid FEM/BEM, Hybrid FEM/DEM and others.

If the presence of discontinuity is vital in the numerical studies, the discontinuum approach is used. Jing (2003) explains the concept of continuity and discontinuity to be problem specific. And hence the generalisation of the same to all areas of study is not possible. The main difference of a discontinuum method over a continuum is the displacement compatibility, where the displacements are not enforced between the internal elements and replaced by boundary contact condition. Kazerani and Zhao (2011) provided various advantages of discontinuum over continuum, such as the capability of discontinuum to examine the initiation and propagation of cracks. Elmo et al. (2012) also specified the disadvantage of discontinuum approach to be lack of information available on contact stiffness.

The wave propagation analysis through joints is done under the assumption of discontinuum concept using the discrete element method. Four programming methods are available under discrete element modelling according to Cundall and Hart (1992) – Distinct Element Method, Modal Methods, Discontinous Deformation Analysis (DDA) and Moment Exchange Methods. The Universal Distinct Element Code (UDEC) and 3 Dimensional Distinct Element Code developed by Itasca is widely used in the rock engineering applications as they are custom made for the same.

Cai and Zhao (2000) did a parametric study on wave transmission and reflection coefficients for single and multiple joints using a discrete element based code UDEC. The theoretical solution was based on displacement discontinuity model considering the presence of multiple parallel fractures. The study was according to the effect of spacing and number of fractures on the transmission coefficients. The transmission coefficients were found to be highly dependent on the number of fractures. The model used for this study was of 300 m length and 1 m in width. The input wave was of frequency 50 Hz is applied as a velocity input sinusoidal wave of unit amplitude. The variation of result with mesh size with respect to wavelength was studied, and the increase in mesh size was found to increase the error when compared to theoretical results. Zhao et al. (2008) extended the work of Cai and Zhao (2000) and considered the effect of nonlinear deformable joints on P wave propagation across fractures using UDEC. The block size used in this study was of 600 m length and 1 m width with a frequency of 50 Hz.

Toomey et al. (2002) used a numerical scheme called Discrete Particle Scheme to study the effect of tensile strength on the joint properties. They analysed the components of wave in tensile condition and compressive conditions for reflection and transmission of the wave along the boundary. Most of the studies were carried out on smooth surface joints. Perino (2011) used UDEC and 3DEC for evaluating the stress wave propagation across joints and reproducing the experimental results. Resende (2010) studied the effect of joint stiffness and insitu stress on the wave transmission using Particle Flow Code, a discrete element method software. Eitzenberger (2012) described the effect of discontinuity on wave propagation considering infill material, the thickness of infill, normal and shear stiffness. Huang (2014) conducted studies using PFC to determine the effect of filled joints. A filled layer with bonded materials which cannot take any tensile stress was modelled. Sebastian (2015) used 3DEC modelling to validate and extend the studies on the bender element test for stress wave propagation across jointed samples. Raffaldi and Loken (2016) used UDEC to help create an understanding of wave propagation and tensile failure using rock fracture ejection. Gui et al. (2016) studied the wave propagation across welded and non-welded joints with and without infilling material. The study was conducted on UDEC to understand the attenuation pattern under different joint conditions. Cui et al. (2016) used 3DEC to know S wave propagation pattern through joints under different joint spacing. The difference in joint patterns was compared for Mohr-Coulomb joint and continuously yielding joints by extending a Time Domain Recursive Method for S wave propagation. Babanouri and Fattahi (2018) analysed wave propagation through 3 orthogonal joints. The modelling was done by replacing the joints with orthotropic continua. Zhan and Qi (2017) extended the research by Cai and Zhao (2000) to understand the acceleration amplification factors acting at different points of a fractured slope. The study provided an understanding on the effect of the acceleration amplification in terms of normalised joint stiffness (K) and normalised joint spacing (ξ).

2.4 THE EFFECT OF SEISMIC LOADING ON TUNNELS

Development of various infrastructure projects is closely linked with the underground structures, such as utility tunnel, metro rail transport service (MRTS), hydropower cavern or a nuclear repository. This creates a need for study on the stability and performance of tunnels. Tunnels built in rock, are always assumed to be strong and stable. The seismic performance of tunnels is hardly considered. However, a number of tunnel failures under during earthquakes are reported in the literature (Dowding and Rozen, 1978; Owen and Scholl, 1981; Sharma and Judd, 1991; Power et al., 1998; Kaneshiro et al., 2000; Asakura et al., 2000; Adyan et al., 2010; Roy and Sarkar, 2017). Hence, it is important to study the performance of tunnels under seismic loading.

One of the earliest research is by Mao and Pow (1971) regarding the hoop stresses acting on a circular tunnel. A circular tunnel on the incidence of simple harmonic P wave was considered for the study (Figure 2.5). Main assumption used in the study is that of an isotropic elastic medium around tunnel which follows Kirch's solutions (1898) of stress concentration. The stress concentrations occurring around the tunnel under static and dynamic conditions were compared using dimensionless frequency Ω. The dimensionless frequency Ω (Mao and Pow, 1971) is a function of circular frequency ω, the radius of the tunnel *a* and the P wave velocity V_p and is expressed as

$$\Omega = \frac{\omega a}{V_p} \quad \text{(Eq. 2.5)}$$

The peak stress concentration under dynamic conditions was found to be 10 to 15% higher than static conditions especially when Ω is 0.25 or when the wavelength of the incoming wave is close to 25 times the tunnel diameter. Design charts were proposed to determine the peak dynamic stress acting for a given Poison's ratio and dimensionless frequency.

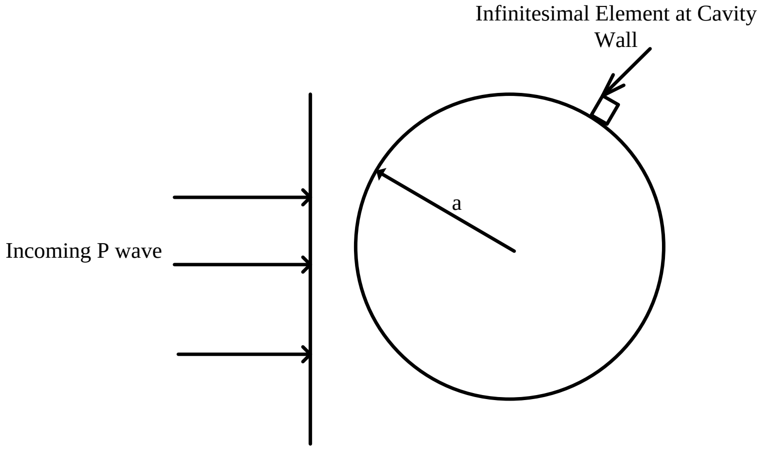

Figure 2.5: Circular cylindrical cavity and incident wave (Adapted and redrawn from Mao and Pow, 1971)

Dowding and Rozen (1978) carried out a seismic response study of different tunnels and it is found that the underground structures underwent damage only when the seismic load acting on it is higher than 0.12g, and no tunnel collapse occurred below 0.5g. Owen and Scholl (1981) studied the response of circular tunnels in an isotropic, homogenous medium. The focus of the researchers was on the effect of P, SV and SH waves on a circular tunnel. The tunnel followed different deformation patterns with forces acting on the tunnel, as shown in Figures 2.6, 2.7 and 2.8. It is found that the shallow tunnels are more susceptible to earthquakes and an equation (Eq.2.6) based on theoretical solutions connecting the distance between a train of waves and the angle of incidence of the waves was proposed to understand the critical depth Y_c,. Beyond the critical depth chances of wave interference due to surface reflections and the incident train of waves is negligible (Figure 2.9).

$$Y_c = \frac{L_o}{2\cos\theta} \quad \text{(Eq. 2.6)}$$

The consideration of seismic load on underground structure design was done by Barton (1984) using the Q system of the rock mass classification, assuming $Q_{seismic}$ to be half of Q_{static}. An application of the factor of safety in the design of tunnels was proposed by increasing the support pressure, as shown in Figure 2.10. Ingerslev and Kiyomiya (1997) in the analysis of underground structures for the Hanshin Earthquake, 1995 and Loma Prieta earthquake, 1989 found that tunnels seated in rocks would undergo the same deformation as the rock itself.

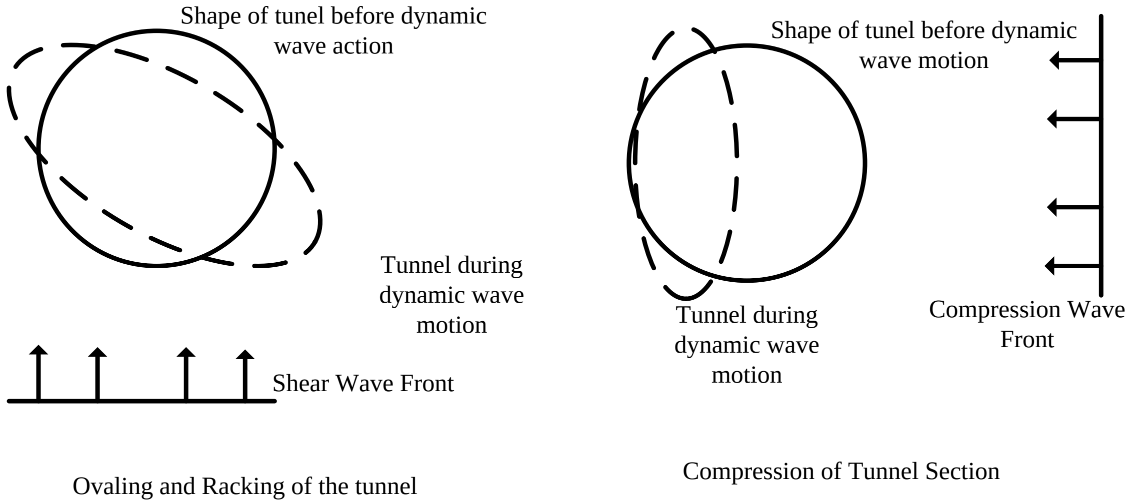

Figure 2.6: Deformation in tunnels due to dynamic load (Adapted and redrawn from Owen and Scholl, 1981)

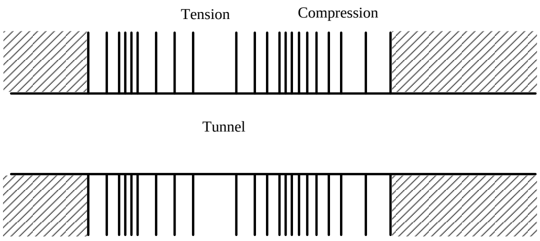

Figure 2.7: Axial deformation along tunnel (Adapted and redrawn from Owen and Scholl, 1981)

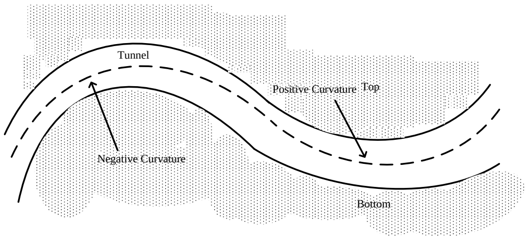

Figure 2.8: Curvature deformation along tunnel (Adapted and redrawn from Owen and Scholl, 1981)

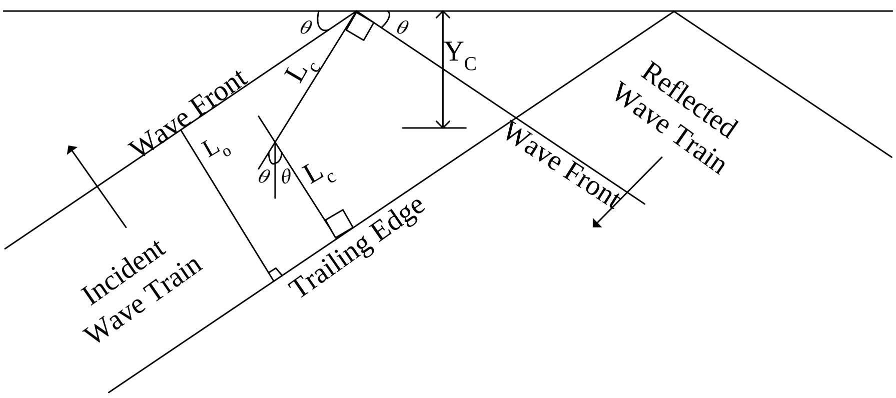

Figure 2.9: Critical depth for interference of incident and reflected train of waves (Adapted and redrawn from Owen and Scholl, 1981)

The planning and design of nuclear waste repository projects in the United States lead the way to a large number of studies. The researchers mainly attempted to understand the behaviour of joints under seismic conditions (Kana et al., 1990; Ahola et al., 1996; Kana et al., 1997). The studies were mostly based on deep mining area of the Lucky Friday mine. Ahola et al. (1996) carried out shake table experiments to find the response of a circular tunnel in jointed medium and identify the tunnel failure by rock slip acting along the joints. The joint displacements were found to be cumulative for recursive loading.

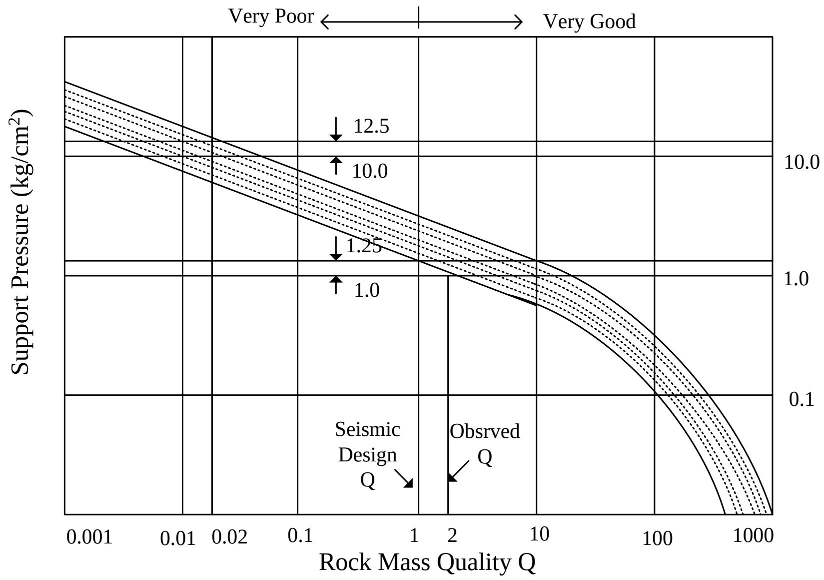

Figure 2.10: Consideration of seismicity on the support pressure using Rock Mass Quality (Adapted from Barton, 1984)

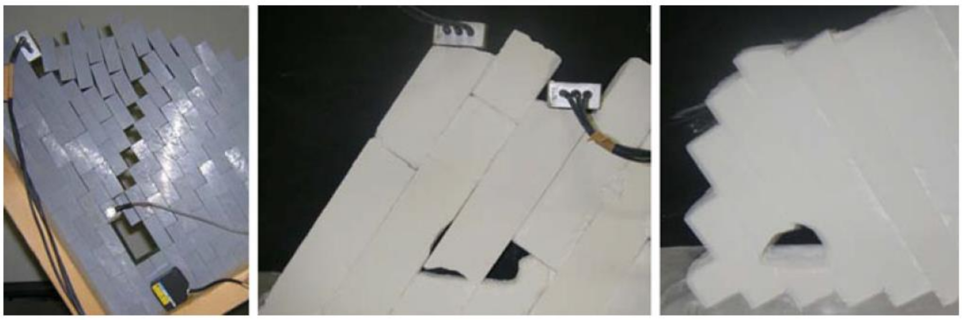

Figure 2.11: Views on some model test in discontinuous rock mass (Adyan et al., 2010)

Adyan and co-workers also conducted model tests on breakable and unbreakable blocks using one-dimensional shake table (Adyan et al., 1994; Adyan and Kawamoto, 2004; Genis and Adyan, 2002, 2008; Adyan et al., 2010). These experiments are mostly focused on shallow unsupported tunnels (Figure 2.11 and 2.12). Dhawan (2004), Abokhalil (2007), Adyan et al. (2010), Yoo et al. (2017) have also worked towards identifying the effect of underground structures in the rock to identify its performance under seismic conditions. While Dhawan et al. (2004) used actual earthquake data of Koynanagar earthquake (1967) in understanding the deformations of multiple underground openings under dynamic conditions, Abokhalil (2007) used pseudo-static methods with a similar interest under focus. Both the studies were done using finite element analysis with plastic behaviour consideration for the rock. It was concluded that plastic damage occurs near the underground opening, which was not transmitted to the surface or other parts.

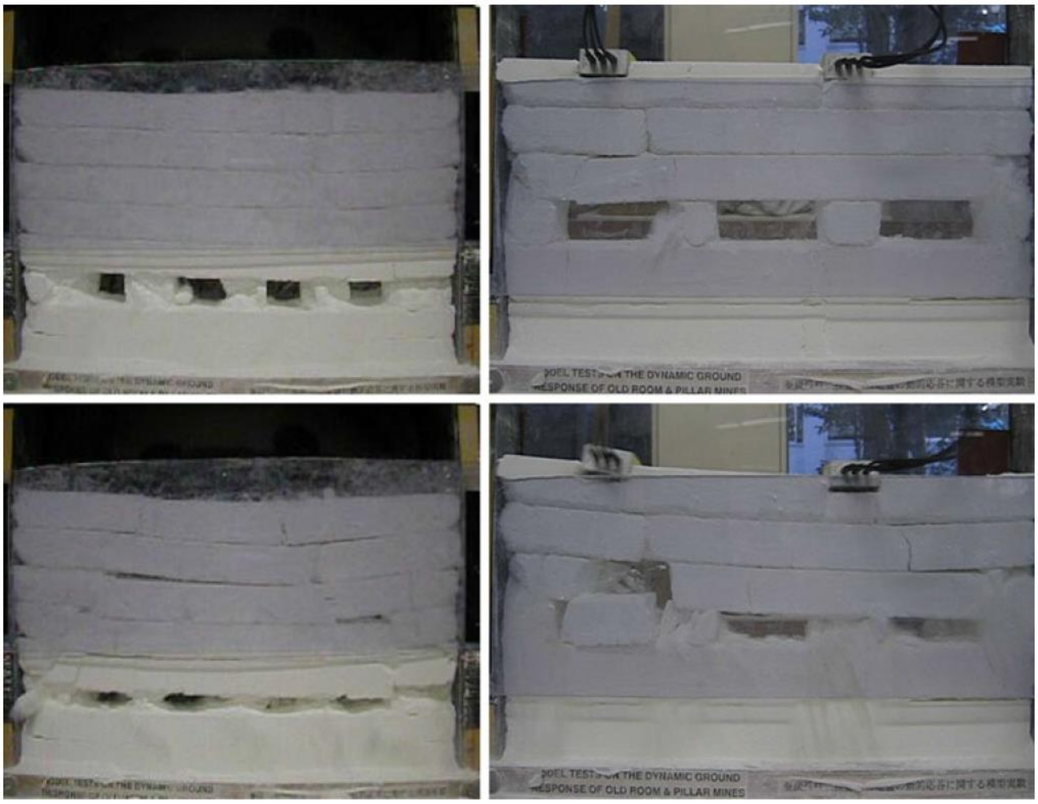

(a) (b)

Figure 2.12: Models of shake table study on abandoned ligmite mine (a) compressive failure of pillars (b) Bending failure of roof layers (Adyan et al., 2010)

Chen et al. (2012) and Yu et al. (2013) extended the studies by Owen and Scholl (1981) on the critical depth to understand the influence of depth on tunnels with the help of numerical analysis. It was concluded that at a depth of 0.25 times the incoming wavelength, the stress state amplification is pronounced. The studies carried out by Yu et al. (2013) also pointed out the higher tunnel response under the action of non-uniform seismic motion compared to uniform seismic motion.

Tao et al. (2015) considered a new classification criterion to classify tunnel damage during the seismic condition. They studied the pattern of Wenchuan Earthquake 2008 and tried to model the same using shake table test to study the behaviour of the tunnel, especially Longdongzi tunnel which suffered damage during the earthquake. With their study, they concluded that the invert, arch and side walls are most susceptible to damage. The interface between bedrock and opening overburden is usually near the portals most. The difference in the surrounding rock properties leads to seismic damage. A study on the stability of tunnels in seismic condition by Cui et al. (2016) using linear continuous yielding and Barton-Bandis models. The majority of the cavern's seismic displacement was found to be made up of elastic body movement. Most of the deformation were found along contact surfaces, making plastic deformation relatively limited. The seismic stability of the cavern was assessed via the overload method giving a seismic safety factor 2-3.

The focus of many studies was on the tunnel response under other types of dynamic loading such as blast loading and rockbursts (Rosengren, 1993; Wang et al., 2007; Heuze and Morris, 2007; Deng, 2014). Hueze and Morris (2007) determined features making the underground facility less resistant to shock. The study was conducted on DE analysis using LDEC while modelling blast load near jointed rock tunnel. Table 2.1 shows the summary of their findings.

Lucky Friday Mine in Coeur d' Alene, Idaho, USA (Ghosh et al., 1996; Hsuing and Ghosh, 2006) was monitored using instrumentation by the Center for Nuclear Waste Regulatory Analyses. Ma and Brady (1999) analysed the dynamic response of a jointed rock excavation for Lucky Friday mine and studied the cumulative accumulation of joint slip deformation in the response of an excavation in a rock mass which experiences repeated seismic loading. The progressive damage at a slip surface was studied for its cumulative displacements, and it was suggested that rock mass fatigue should be considered for the design of tunnels as it becomes increasingly vulnerable to seismic impacts if exposed continuously. The study was done with both Mohr-Coulomb and continuously yielding criteria against actual field data from the Lucky Friday mine, and both were found to reproduce these field results comparatively well. Figure 2.13 shows an image of failure and joint displacements due to mine induced seismicity in Lucky Friday Mine by White and Whyatt (1999).

Table 2.1: Factors under consideration in the tunnel under the action of dynamic load (Adapted from Hueze and Morris, 2007)

Features making the ground facility more resistant to ground shock	Features making the ground facility less resistant to ground shock
Geology	
Non continuous joints	Continuous joints
Wide joint spacing	Smaller joint spacing
Dilatant joints	Non dilatant joints
Higher shear and tensile strength of the joints	Lower shear and tensile strength of the joints
More porous rocks overlying the facility	Less porous rocks overlying the facility
Less water saturation of the viods	More water saturation of the voids
Facility Design	
Smaller span of rock openings	Larger span of rock openings
Rock reinforcement	Un-reinforced rock mass
Tunnel liner	No tunnel lining

Figure 2.13: Failure and disruption in Lucky Friday Mine (White and Whyatt, 1999)

2.5 EFFECT OF DYNAMIC LOADING ON TUNNEL LINING AND TUNNEL SUPPORTS

Support is a term widely used to describe materials that enhance the strength, stability, and load carrying capacity of different excavations. Windsor and Thompson (1993) defined and gave a clear distinction between support and reinforcement.

"*Support is the application of reactive force to the surface of an excavation and includes techniques and devices such as timber, fill, shotcrete, mesh, and steel or concrete sets or liners. Reinforcement is a mean of conserving or improving the overall rock mass properties from within the rock mass by techniques such as rock bolts, cable bolts, and ground anchors.*"

The supports are classified as passive and active according to the load carrying nature. When support exerts a force on the face and imposes a predetermined load at the surface, it is called active support. Tensioned rockbolts or cables, hydraulic props, expandable segmented concrete linings or powered supports are examples of active supports. And when the support is not installed with an applied load but develops capacity as the rock deforms, it is known as passive support. Steel arches, timbered sets, untensioned grouted rockbolts, reinforcing bars or cables work on passive support technique. It is pointed out by Brady and Brown (1993) that a good support system must allow sufficient displacement and restrict the support loads to a practical level. The support pressure displacement curves have explained this perfect combination as shown in Figure 2.14, as suggested by Daemen (1977). This support interaction curve consists of two parts, one which shows the support line of the roof or sidewall and other the support reaction. These curves show the ground characteristics depending on the support pressure and tunnel displacements. This curve shows how redistribution of stresses is carried out by the rock.

The use of tunnel supporting methods like shotcrete, rockbolts, concrete liners, steel shields are commonly used for stabilisation purposes. Table 2.2 shows the recommendations given for rock support in the New Austrian Tunneling Method (NATM) guidelines as suggested by Bieniawski (1989) and Austrian standard for underground works (ONORM B 2203,1993). These stabilisation measures improve the performance of tunnels under static conditions where the load and applications are well defined. But, the performance under dynamic conditions is never taken seriously due to the common assumption that underground structures are very safe under seismic conditions/dynamic loading. Rock bolts and linings typically used in tunnels are designed for the static case where they can handle a large amount of load but no displacements. When subjected to dynamic loading, ground support also needs to dissipate the dynamic stress acting upon it.

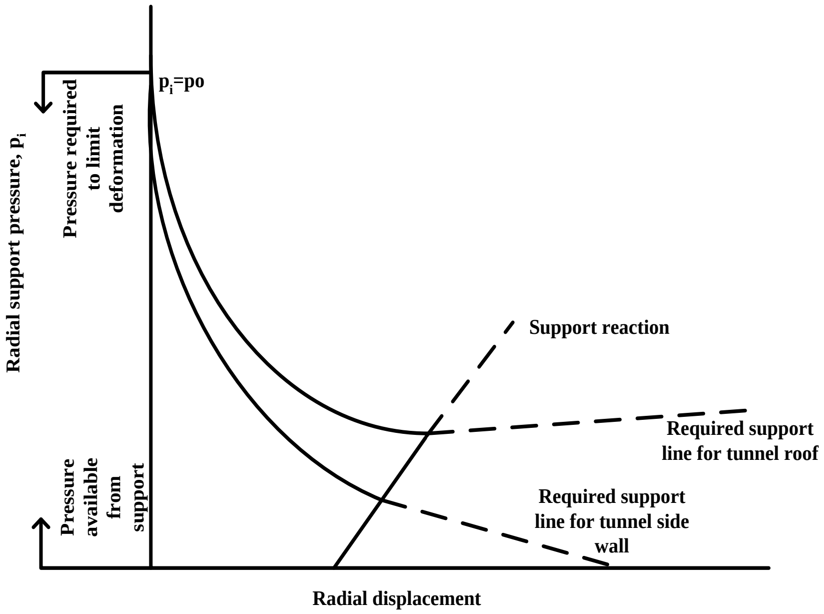

Figure 2.14: Radial support pressure-displacement curves for the rock mass and the support system

Table 2.2: NATM classification and rock support (ONORM B 2203, 1993; Bienwaski, 1989)

Term	**Rock mass condition**	**Requirements to rock support function and excavation measures**	**Principle of roof and wall support**
Stable	Elastic behaviour. Small quick declining deformations. No relief features after scaling The rock masses are long term stable	No need for rock support after scaling. Not necessary to reduce length of round except for technical reasons	Support against dropping rock blocks
Slightly ravelling	Elastic behaviour, with small deformations which quickly decline. Some few small structural relief surfaces from gravity occur in the roof.	Occasional rock support in roof and upper part of the walls necessary to fasten loosened blocks. The length of rounds might only be limited for constructional reasons.	Shotcrete and bolt support in roof
Ravelling	Far-reaching elastic behaviour. Small deformations that quickly decrease. Jointing causes reduced rock mass strength, as well as limited stand up time and active span. This results in relief and loosening along joints and weakness planes, mainly in the roof and upper part of the wall.	Systematic rock support is required, but only in moderate amount. The length of rounds is determined from the stand up time and the time required installing the initial support	Combined shotcrete and bolted round in roof and at springline

Strongly ravelling	Deep non-elastic zone of rock mass. The deformations will be small and reduced when the rock support is quickly installed. Low strength of rock mass results in possible loosening effects to considerable depth followed by gravity loads. Standup time and active span are small with increasing danger for quick and deep loosening from the roof and working face.	Systematic rock support required in roof and walls, and often also of the work face. The cross-section of the heading depends on the size of the tunnel, i.e the face can contribute to stability The length of the rounds must be reduced accordingly, respectively systematic use of support measures such as spiling bolts ahead of the face.	Combined shotcrete and bolted arch in roof and springline, if necessary closed invert
Squeezing or swelling	Plastic zone of considerable size with detrimental structural defects such as joints, seams, shears. Plastic squeezing as well as rock spalling (except for rockburst) phenomena. Moderate but clear time dependent squeezing with only slow reduction of deformations (except for rockburst). The total and rate of displacements of the opening surface is moderate. The rock support can sometimes be overloaded.	Rock support of the whole tunnel surface is required, often also of the working face. The size of the heading should be chosen to effectively utilise the stabilising effect of the face. The effect of the rock support is mainly to limit the breaking up and to maintain the three dimensional stress state. The length of the round must be adjusted according to the support measures ahead of the working face	Support ring of shotcrete with bolted arch and steel set
Strongly squeezing or swelling	Development of a deep squeezing zone with severe inwards movement and slow decrease of the large deformations. Rock support can often be overloaded	Comprehensive rock supporting works required in all the excavated rock surfaces. The size of the unsupported surface after excavation is to be limited according to support measures performed ahead of the face. The large deformations require use of special support designs, for example deformation slotsor or other flexible support layouts. The support should be installed to maintain the three dimensional state of stress in the rock masses	Support ring of shotcrete with steel sets, including invert arch and densely bolted arch

2.5.1 Rockbolt as Support

Rockbolting is a flexible method of support which is used as both initial support and final support. Untensioned grouted rockbolts or dowels are commonly used. A typical rockbolt used in tunnels are of length 2-4 m with a diameter of 20-25 mm. Palmstrom and Nilsen (2000) suggested an expression for finding the length of rockbolts according to the size of the opening and width of the blocks:

$$L_{b,roof} = 1.4 + 0.175 D_t (1 + 0.1 / D_b) \quad \text{(Eq. 2.7)}$$

$$L_{b,wall} = 1.4 + 0.1(D_t + 0.5 W_t)(1 + 0.1 / D_b) \quad \text{(Eq. 2.8)}$$

Where,

D_t =diameter or span of the tunnel (m)

D_b =block length (m)

W_t = tunnel wall length (m)

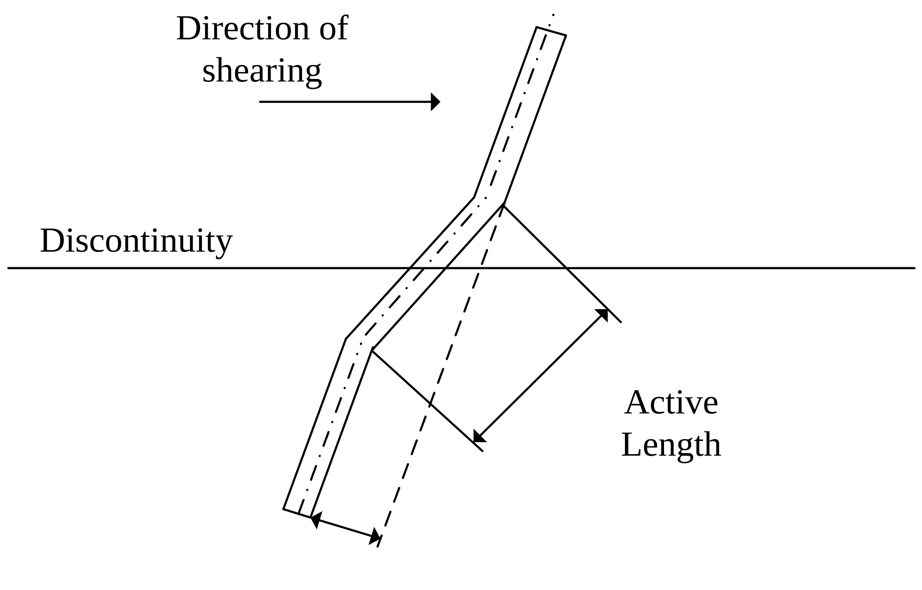

Figure 2.15: Active length of rockbolt (after Brady and Lorig, 1988)

The performance of rockbolt support is according to structural mechanics by yielding. The loads acting on the bolts get mobilised when a relative displacement happens between the rock and the bolt. For a bolt grouted well with resin or concrete, considerable axial stress develops over a short length in the bolt called active length which offers high resistance (Figure 2.15). This resistance may also be in the direction of shear if there is a joint slip. This leads to the observation that reinforcement deformation is concentrated near a discontinuity and triggered by the motion of the joint.

Most studies on the performance of rockbolts under dynamic conditions are concentrated on the performance of rockbolts in deep underground mines in rockburst or blast conditions. Goodman and Dubious (1971) analysed the dynamic forces acting on a rockbolt analytically assuming momentum conservation equations. The velocity and the period of action of the wave pulse were calculated. This value was used to understand the force acting on the rockbolt. Otuonye (1988, 1993) studied the response of axial and bending stresses on grouted rockbolts under the action of blasting. The response of grouted rockbolts near the ground opening was found to have higher vibrations than the bolts deep inside the ground. Tannant et al. (1995) and Ortelapp and Stacy (1996) carried out experimental studies on rockbolt to understand their performance in the case of blast loading and explosives. Tannant et al. (1995) in the study of rockbolt behaviour for blast loading found that the position of the explosive with respect to the rockbolt alignment affects the axial and shear forces produced in the rockbolt. The incoming wave frequency and amplitude were fundamental in determining the duration of vibration in rockbolt, and transfer of load to the tunnel surface and damages in the surrounding rock and shotcrete supports. Ortelapp and Stacy (1996) tried to understand how the yielding of rockbolts helped in the absorption of energy coming from the impulse load. They pointed out that rockbolts which yielded performed better under shear and not under axial conditions. Ortellap and Stacey (1998) considered the impact of impulsive loading on different support members like rockbolt, shotcrete, wired mesh, etc. The study found shotcrete to withstand ejection velocities upto to 3 m/s. Even low-grade shotcretes were found to absorb some energy. And the performance of yielding rockbolts was found to be energy absorbing under dynamic conditions. Ortelapp (2001) summarised the effect of dynamic load on tunnel supports under all ground conditions. The necessity of providing unbreakable bolts with controlled yieldability, together with balanced, compliant cladding, appropriately coupled to or integrated with the bolt was mentioned. Wang et al. (2014), Kaiser and Cai (2012) gave tunnel design criteria for support members in deep mines under rockburst conditions. Out of many factors affecting rockbursts, the support members and its properties were identified to be important.

Mortazavi and Alavi (2013) on the analysis of rockbolt under dynamic loading conditions found the stress concentration occurred in the bolts due to the high rate of loading and multiple reflections of the incoming wave. It was noticed that yielding rockbolts stabilised the rock mass. Pytlik et al. (2016) carried out laboratory experiments to understand the capacity of rockbolts under dynamic loading conditions of a mine. The experiment was based on free fall of a mass on the rockbolt. And the bolts were categorised according to impact resistance and recommended for different mining conditions. Wang et al. (2018) provide an analytical solution for load acting on rockbolts during static and dynamic loading. The force on acting on rockbolt due to a blast load could be found by deriving the forces acting. The force acting on the bolts under the combined action of the static and dynamic load is expressed by Wang et al. (2018) as,

$$\sigma(z) = \left(\rho_r.c_r.k\left(\frac{Q^{1/3}}{d}\right)^{\beta}\right).\exp\left(-\frac{z^2}{2K}\right) + \frac{E_b.a}{b}.\frac{1}{1+e^{-\frac{(L-z)-z_o}{b}}} \qquad \text{(Eq. 2.9)}$$

$$\tau(z) = \left(\rho_r.c_r.k\left(\frac{Q^{1/3}}{d}\right)^{\beta}\right).\frac{z}{K}\exp\left(-\frac{z^2}{2K}\right) + \frac{E_b.D}{4}.\frac{a}{b^2}.\frac{e^{-\frac{(L-z)-z_o}{b}}}{\left(1+e^{-\frac{(L-z)-z_o}{b}}\right)^2} \qquad \text{(Eq. 2.10)}$$

where, ρ_r is the rock density, c_r is the velocity of longitudinal wave in rock, Q is the quantity of explosives, d is the distance between the point of interest and the blasting source, k and β are site specific coefficients dependent on in-situ rock mass conditions and the blast design, E_b is the Young's modulus of the bolt, D is the diameter of the rockbolt, a, and b, are constant dependent on the stiffness and strength of bolt, L of the bolt, z_o and K are parameters that are calculated according to the pullout test and z is the distance to the point of calculation of force. Tahmasebinia et al. (2018) conducted analytical, and numerical studies to understand the performance of a cable bolt in static and dynamic conditions. ABAQUS modelling for the numerical studies explained the failure of cable bolts at the initial high strain loading.

2.5.2 Shotcrete or Liner as Support

Shotcrete support is applied by spraying a concrete mix on to the surface at high pressure. The popularity of shotcrete as a support system is because of its favourable properties, high capacity and flexibility. It is used as an initial support system in jointed rock masses and many times combined with rockbolts to be used as a combined support system.

In the modern mechanised tunnelling, precast or cast in situ tunnel liners are commonly used. This is often used as a preventive measure for large faults or weakness zones with highly unstable rock masses. Though expensive, the main attraction of concrete liners is the aesthetic value and perfection which it provides to the surface. Most research for the effect of dynamic load, mainly seismic is concentrated on liners. A significant reason for this is also the ease in identification of even minor cracks occurring on liner in comparison to shotcrete. The studies consisted of case studies where actual damage was observed on the lining, experimental studies and numerical study. Most of these studies are numerical considering the wide possibilities and controlled scenario.

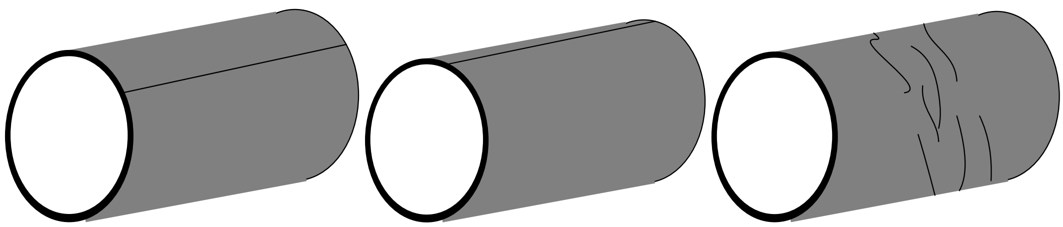

(a) (b) (c)

Figure 2.16: Failure modes of the tunnel (Adapted and redrawn from Zou et al. 2012) (a) Failure at Shoulder (b) Failure at crown (c) Horizontal failure

Failure of tunnel and tunnel lining when it passes through a fault is well noticed (Kimura et al., 1987; Yang et al., 2013; Yu et al., 2016; Manouchehrian and Cai, 2018). These failures range from tunnel caving in or liner/shotcrete break or distortion. The extent of damage near a fault during an earthquake depends on the slippage occurring along the fault plane and the orientation of the fault. Early studies by Dowding (1984) suggested that for lined tunnels the threshold peak particle velocity (PPV) required to cause damage would be roughly double that of unlined tunnels. Studies carried out by Stjern and Myrvang (1998) and Ortlepp and Stacey (1998) have shown that PPV upto 1 m/s will not cause any measurable damage to rock support. Wang (1993) proposed different equations for axial force and bending moment in tunnel linings in soil under seismic condition.

Aakasura et al. (2000, 2007) analysed the different fracture positions in tunnel liners when P and S wave intersect at different angles. The different nature of lining failures for various incoming P and S waves were analysed by Zou et al. (2012). This study made an extension on the research by Aakasura et al. (2000, 2007) for the types of damage occurring in the tunnel liner for incoming S and P waves. Figure 2.16 shows the different types of cracking happening on the tunnel with the nature of incoming waves. Cracking is observed on the shoulders when a vertical S wave or inclined P wave intersects the tunnel. The tunnel roof undergoes cracking when the incoming wave is vertical P wave or inclined S wave. And horizontal cracks are visible when wave passes along the tunnel direction. The study also observed an increase in damage at lower frequencies. The failures along tunnel liners in the studies of Wang et al. (2001), Kongai et al. (2005) and Yu et al. (2016) were found to follow this pattern. Bhasin et al. (2006) investigated the effect of seismicity on rock supports using Phase2 as the numerical tool. The maximum axial force acting on the tunnel lining was found to be highly dependent on the tunnel diameter. The effect was considerably high in the case of elastic-perfectly plastic rock mass compared to elastic assumption.

A field study with extensive instrumentation was conducted by Hsiung and Ghosh (2006) on Lucky Friday Mine to understand the effect of seismicity on tunnels and tunnel supports. It was observed that a threshold seismic amplitude is required for any permanent deformation to occur. Jiang and Zhou (2012) studied the effect of blasting on liners and rocks using LS-DYNA and concluded that there is a notable difference in the PPV and the peak effective tensile stress between the tunnel liner and the surrounding rock at the interface of arch and wall. Romero and Caulfield (2012) studied the Claremont Tunnel and the Bay Tunnel in California. The performance of liners (concrete and steel) under static and dynamic loads both for soil and rock conditions were analysed, and maximum damage was found to occur at transition zones from soil to rock. Kouretzis et al. (2014) analysed the effect of secondary P wave by analytical and numerical solutions. A closed form solution is developed for understanding the hoop stress and bending moment around the tunnel. It was noticed that the hoop stresses developed around the tunnel even under full slip conditions are considerably higher than the stresses produced by S waves of equal or lower magnitudes.

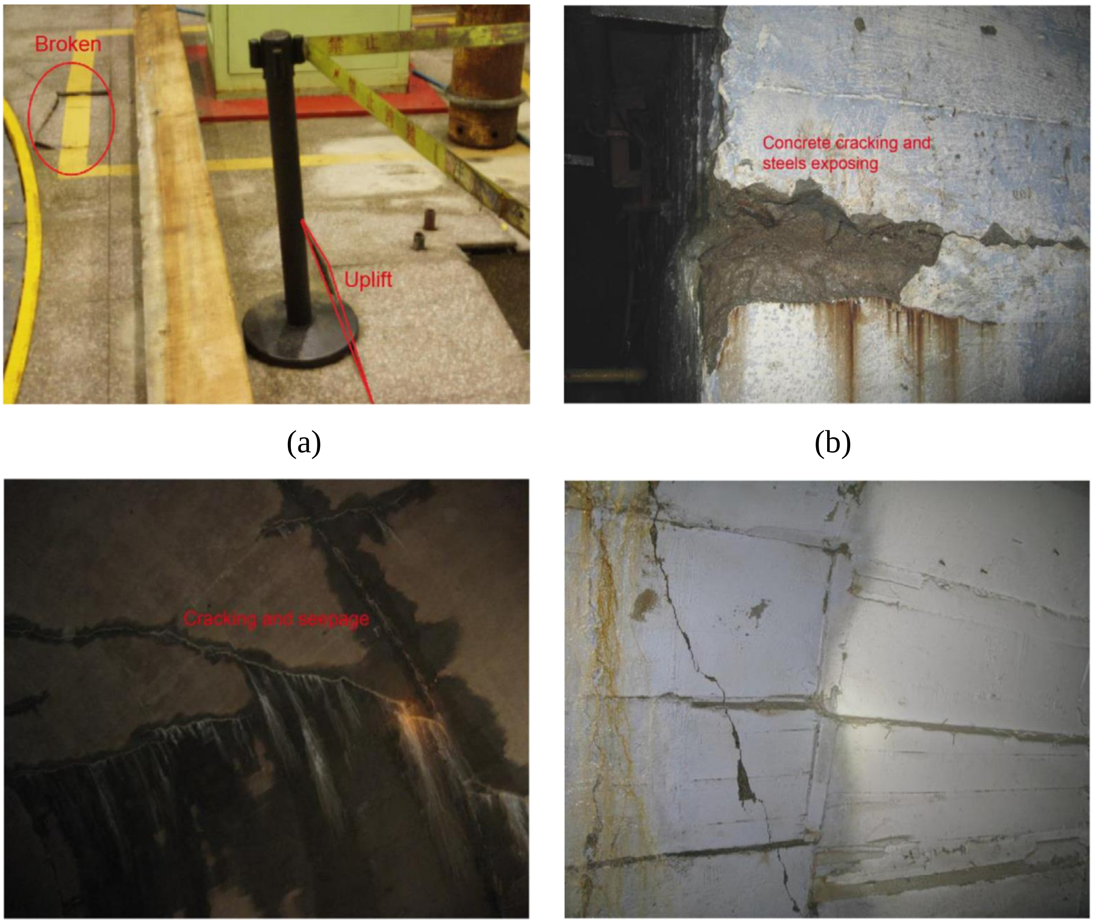

(a) (b)

(c) (d)

Figure 2.17: Yingxiuwan underground powerhouse failure from Wang et al. (2018) (a) Broken and uplift of generator floor (b) Steel corrosion and distortion at the cavern intersection (c) Cracking and seepage of diversion tunnel (d) Cracks on the sidewalls of traffic tunnel

Yi et al. (2014) used wave function expansion method to study the effect of P waves on lined circular tunnels. The dynamic stress concentration factors were discussed for rock mass and the liner under high frequency conditions. Yi et al. (2016) extended the work for low frequency as well. It was observed that when the interface between the rock and liner is weak, resonance may be observed leading to high dynamic stress concentration. Deng et al. (2014) did a set of numerical simulations in UDEC to identify the effect of blast loads on jointed rocks with and without rockbolts under various joint angles, joint spacing and scaled distances. They concluded that the slipping of joints mainly caused the damage of the tunnels. The joint spacing and numbers were identified to have maximum influence on wave propagation in the jointed rock mass. The initial stress condition was found to have very less effect. The tunnels with bolts were found to have comparatively less impact than those without as the bolts were assumed to take some of the vibrations.

Do et al. (2015) tried to find the effect of segmental joints on tunnel liners under seismic condition. An increase in bending moment and normal force was observed to be affected by the joint and joint properties. Wang and Cai (2015) described that the ratio of wavelength to the tunnel diameter is critical in deciding the impact of the earthquake on tunnel support. Only if the ratio is higher than 4.5 a strong impact will be faced and that 4.5 can be considered a critical value. The Wenchuan earthquake (2008) of Richter scale magnitude 8.0 affected many underground structures. The closest large scale structure from the epicentre was Yingxiuwan underground powerhouse, and this was analysed by Wang et al. (2018). The powerhouse was found to undergo severe damage at the portal, and several cracking and spalling of concrete were observed at different parts along with upliftment and breakage of the generator floor (Figure 2.17). A dynamic 3D finite element analysis was done for the powerhouse and the surrounding rock system to understand the nature of the damage. A rock structure interaction of the powerhouse showed the oblique incidence to cause higher damage.

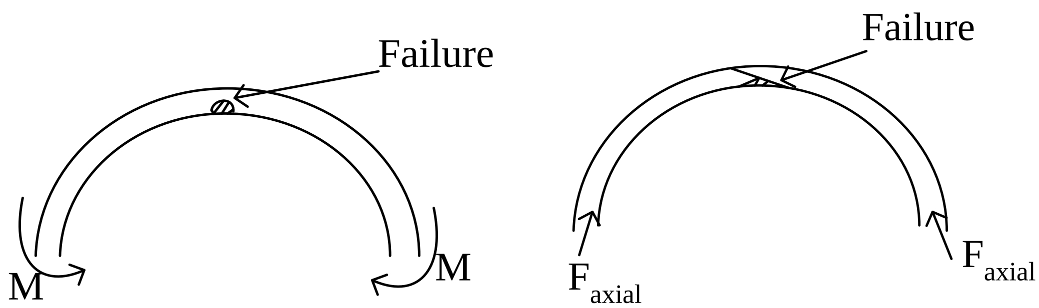

Figure 2.18: Failure due to moment and axial forces (Adapted and redrawn from Zhang et al., 2018)

Zhang et al. (2018) analysed the damages that Tawarayama Tunnel underwent under the 2016 Kumamoto Earthquake. The results of the study were analysed to change in tunnel cross-section with the effect of waves, and the failures were analysed (Figure 2.18) for cracks, spalling and collapse according to hoop stresses and moment acting on it. Roy et al. (2018) analysed the damage occurring on the liners for a tunnel placed in blocky rock mass for various seismic loading scenario. Joints were found to act as filters, and only low frequency waves caused an effect on the tunnel. The types of forces and bending acting on each block was identified as shown in Figure 2.19.

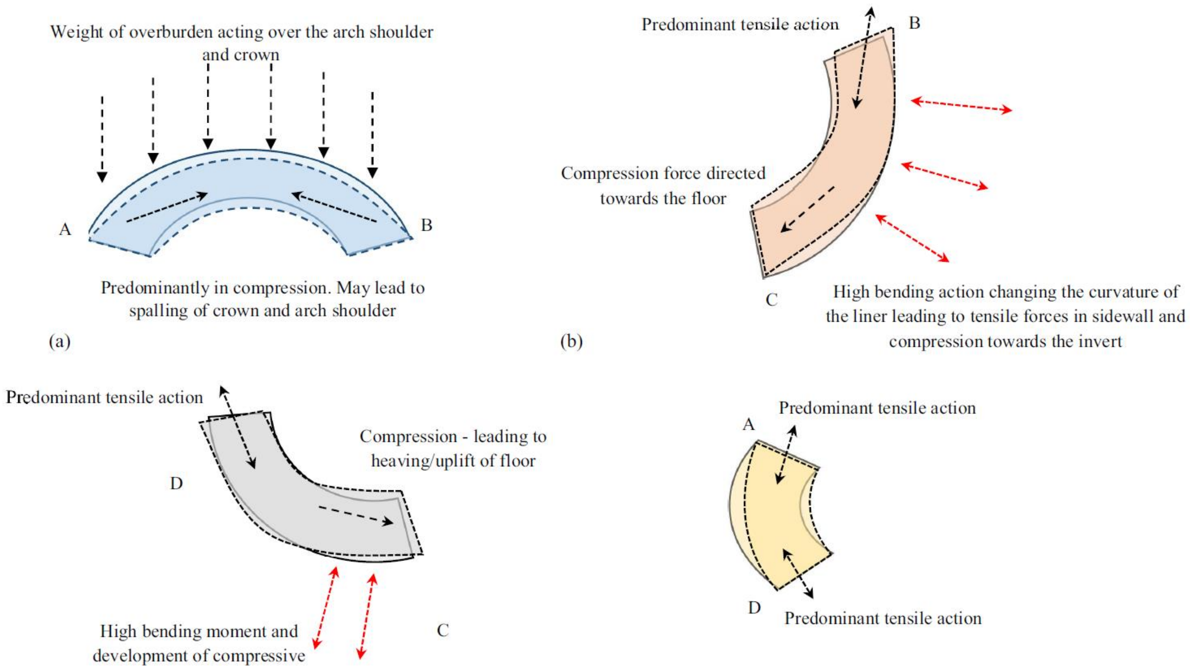

Figure 2.19: Generalised forces acting on different regions of a tunnel liner (Adapted from Roy et al., 2018) (a) Crown (b) and (c) Floor and springline (d) Sidewalls

2.6 SUMMARY

An overview of the existing findings and research in the area of rock dynamics with focus on the performance of rock joints have been presented in this chapter. The dynamic load acting on joints are usually represented in the form of stress waves. The studies on rock joints under the action of the dynamic loads are divided according to three main aspects: (a) the propagation of stress waves through rock joints (b) effect of dynamic load on tunnels (c) the performance of tunnel support system under the action of dynamic load.

The literature on stress wave propagation along joints can be broadly classified as analytical, experimental and numerical studies. Most of the studies concentrate on the transmission and reflection coefficients of the stress waves as they are incident on the rock joint. The analytical studies were verified and extended by different experimental and numerical techniques. The adoption of the experimental technique is according to the strain induced by the stress waves. The numerical studies were according to discontinuum methods to incorporate the joint properties. The studies showed the dependence of wave amplitude and wave velocity on various factors like frequency of the wave, joint angle, joint infilling, joint roughness and number of joints.

The behaviour of tunnels under the action of dynamic loading includes much research on intact rocks compared to jointed rocks. Many of the studies concentrated on blasting and rockburst conditions of deep mines. The failure investigation of tunnels under the action of earthquakes are very limited. Though the tunnels are considered to be safe under the action of earthquakes, studies pointed out failures of tunnels under the action of different earthquakes. Case studies, experimental studies and numerical modelling were done to understand the behaviour of tunnels under the action of dynamic loads. The studies on the presence of joints showed an increased risk of failure in dynamic conditions due to joint slippage. Reinforcements are used to support the tunnels in the field. The studies on rockbolt as a support system is mostly for dynamic loading and rockburst conditions. The effect of rockbolts under earthquake loading is given little importance. Shotcrete and liners are also used as supports. Many studies show the presence of cracks, spalling or breakage under dynamic loading.

Based on the current state of the art covered in this chapter, the study of dynamic loading on rock joints is divided into the effect of joint properties under the action of stress waves, deformations of the unsupported tunnels under earthquake loading and the behaviour of tunnel supports under the action of earthquake loads. The propagation of stress waves through joints is analysed experimentally and numerically for different joint parameters and discussed in the subsequent chapters. The study on jointed rock tunnels and its support system under earthquake loading is conducted numerically and is also presented.

CHAPTER 3

EXPERIMENTAL STUDY ON WAVE PROPAGATION THROUGH ROCK JOINTS

3.1 INTRODUCTION

Knowledge on the wave propagation through rocks is important for any construction in them. The wave propagation pattern and wave velocity changes with the presence of discontinuities. A detailed study is needed for understanding wave propagation under different joint conditions. Waves commonly induce low strains in rock mass while passing through it, except in the neighbourhood of the source (Barton, 2007). Mostly the small strains acting on the rock are elastic. Different test methods are available for understanding the wave propagation pattern and wave velocity according to the intended strain level. Split Hopkinson pressure bar test (Ju et al., 2007; Wu et al. 2014; Wu et al., 2015), resonant column test (Fratta and Santamarina, 2002; Cha et al., 2009; Perino, 2011; Mohd-Nordin et al., 2014, Sebastian and Sitharam, 2014), bender element test (Sebastian, 2015) and ultrasonic pulse velocity test (Pyrak Nolte, 1996; Li and Pyrak- Nolte, 2010; Zhao et al., 2006; Mollhoff et al., 2010; Huang et al., 2014; Yang et al., 2018) are the different types of tests used in understanding the dynamic behaviour of rocks. A rock mass with its high strength and stiffness is regarded to have low strain values due to the waves compared to soil mass (Sebastian, 2015). So, the experiment focuses on wave propagation under low strain conditions. Among these tests, the bender element test and ultrasonic pulse velocity test serves in understanding wave propagation under low strain conditions. Ultrasonic pulse velocity (UPV) test is a widely accepted testing mechanism which is fundamental, simple and reliable. The details of ultrasonic pulse velocity test (UPV) carried out on artificially prepared jointed rock samples are presented in this chapter. The UPV results are used to understand the change in wave velocity with different joints under low strain conditions.

The laboratory tests are done to determine the effect of joint angle, joint roughness, number of joints and joint spacing on the change in wave velocity.

3.2 ONE DIMENSIONAL PROPAGATION OF ELASTIC STRESS WAVES

Wave propagation across an isotropic medium is considered to be one dimensional. But inherently, it is never one dimensional due to the coupling of various stresses and strains. However, the propagation of stress along a long cylindrical object can be considered one dimensional under the assumptions:

- Deformation happens only in the longitudinal direction, and torsional and lateral deformations are neglected.
- Wavelengths are large compared to the diameter of the bar.
- Each plane of cross-section always remains plane.
- Stress over the cross-section is uniform.

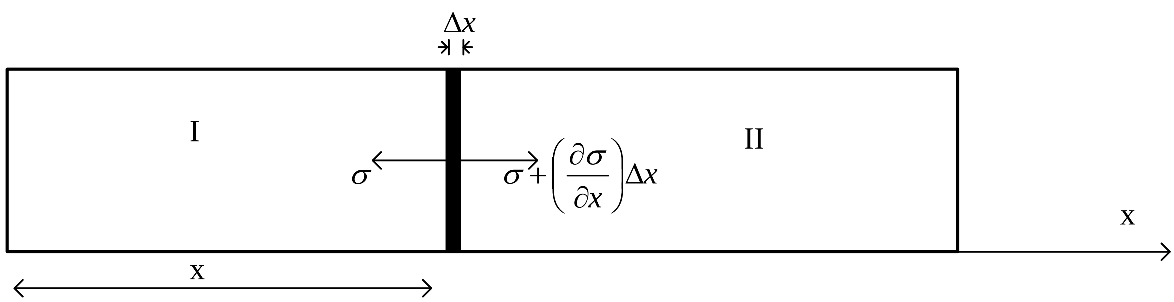

Figure 3.1: Stress acting on an element bar in longitudinal motion

A thin cylindrical rod of uniform cross-section is assumed to have stress along the longitudinal direction does not vary over the length of the rod (Figure 3.1). For a small length Δx over the section, with a wave propagating in the longitudinal direction, stress on the face I is σ. The stress on the other side II will be $\sigma + (\partial\sigma / \partial x)\Delta x$, and u gives the displacement of the element. Then ρ being the density of the bar, according to Newton's law of motion

$$\rho A \Delta x \frac{\partial^2 u}{\partial t^2} = A \frac{\partial \sigma}{\partial x} \Delta x \tag{Eq. 3.1}$$

As the ratio of stress σ and strain $\partial u/\partial x$ is Young's modulus E, the equation changes to

$$\rho\frac{\partial^2 u}{\partial t^2} = E\frac{\partial^2 u}{\partial x^2} \quad \text{(Eq 3.2)}$$

This is the wave equation in the one-dimensional condition. Jean D' Alembert (1747) first gave the wave like nature of Eq. 3.2 in 1747. The velocity of the longitudinal wave along the bar is

$$c_L = \sqrt{\frac{E}{\rho}} \quad \text{(Eq. 3.3)}$$

The solution of equation 3.2 is

$$u = f(c_L t - x) + F(c_L t + x) \quad \text{(Eq. 3.4)}$$

Where 'F' and 'f' are functions depending on initial conditions. The function 'f' corresponds to a wave travelling in the longitudinal direction along increasing x and F corresponds to a wave in the opposite direction. Considering the wave travelling in the direction of increasing x,

$$u = f(c_L t - x) \quad \text{(Eq. 3.5)}$$

Differentiating both sides with respect to x and t gives

$$\frac{\partial u}{\partial x} = -f'(c_L t - x) \quad \text{(Eq 3.6)}$$

$$\frac{\partial u}{\partial t} = c_L f'(c_L t - x) \quad \text{(Eq. 3.7)}$$

Solving with equations produce,

$$\frac{\partial u}{\partial t} = -c_L\frac{\partial u}{\partial x} \quad \text{(Eq. 3.8)}$$

When Hooke's law is applied to the equation,

$$\sigma = -\left(\frac{E}{c_L}\right)\frac{\partial u}{\partial t} = -\rho c_L\frac{\partial u}{\partial t} \quad \text{(Eq. 3.9)}$$

Equation 3.9 shows a linear relation between stress and particle velocity $\frac{\partial u}{\partial t}$. A similar result exists for a wave travelling in the direction of decreasing x where,

$$u = F(c_L t + x) \tag{Eq. 3.10}$$

Similar operation of differentiating by x and t will produce,

$$\sigma = \left(\frac{E}{c_L}\right)\frac{\partial u}{\partial t} = \rho c_L \frac{\partial u}{\partial t} \tag{Eq. 3.11}$$

In these results, a particle velocity greater than zero indicated tensile stress while the particle velocity less than zero the stress is compressive. When a compressive wave moves and intersects with the free surface, it gets reflected. This reflected stress wave is tensile.

3.3 FACTORS AFFECTING WAVE VELOCITY OF A ROCK MASS

Several factors are responsible for the nature of wave propagation through a rock mass. Many researchers explained different parameters affecting wave propagation across a jointed medium. The frequency has been identified to be an important factor which affects the wave velocity while travelling through joints. The frequency of the propagating wave does not affect the wave velocity if there are no joints present in the rock. The current experimental study has been done only for the ultrasonic frequency of 150 kHz. The wave behaviour under other frequencies is studied using numerical modelling and presented in Chapter 4. The major factors that are considered in the experimental study are joint angle, joint roughness and joint frequency.

3.3.1 Joint Angle

A wave when incident on a joint undergoes transmission and reflection. If the incidence is normal to the joint, the transmitted and reflected waves are also normal. However, the transmission pattern is much more complex when the angle of incidence is not normal to the joint. P wave incident on a joint at an angle gets converted to a pair of reflected and transmitted P wave and SV waves (Figure 3.2). These waves get further reflected from the sides of the sample, and the resulting waves undergo superimposition with other reflected and transmitted waves. This causes a change in the measured longitudinal wave velocity. Studies regarding the change in wave velocity with different angles of incidence were studied by Pyrak-Nolte (1990), Sebastian and Sitharam (2014), Zou (2016) for a particular frequency range.

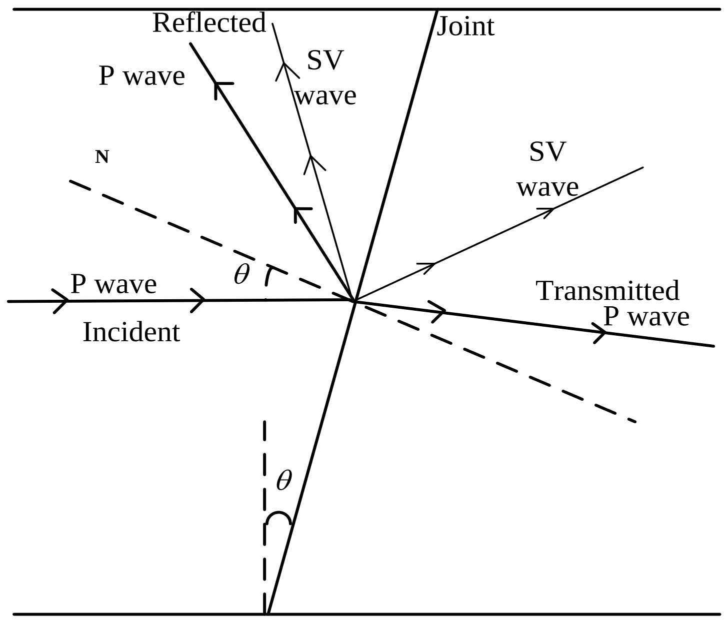

Figure 3.2: Behaviour of a wave when incident on a joint

3.3.2 Joint Roughness

Waves incident on a rough joint behaves similar to a wave incident on an inclined joint. However, rather than a single angle, each part of the joint has different angles, and hence, the overall behaviour of the rough joint on the wave needs to be understood. The joint roughness values can be represented as joint roughness coefficient (JRC) (Barton, 1973; Barton and Choubey 1977). The JRC value of any joint varies from 0-20, with 0 representing a planar joint whereas 20 is the roughest joint. Corresponding JRC values with respect to roughness profiles are shown in Figure 3.3. Various researchers proposed different methodologies for the identification, classification and evaluation the joint roughness (Barton, 1984; Develi and Babadagali, 1998; Belem et al., 2000; Beer et al., 2002; Jiang et al.; 2006; Shigui et al., 2009).

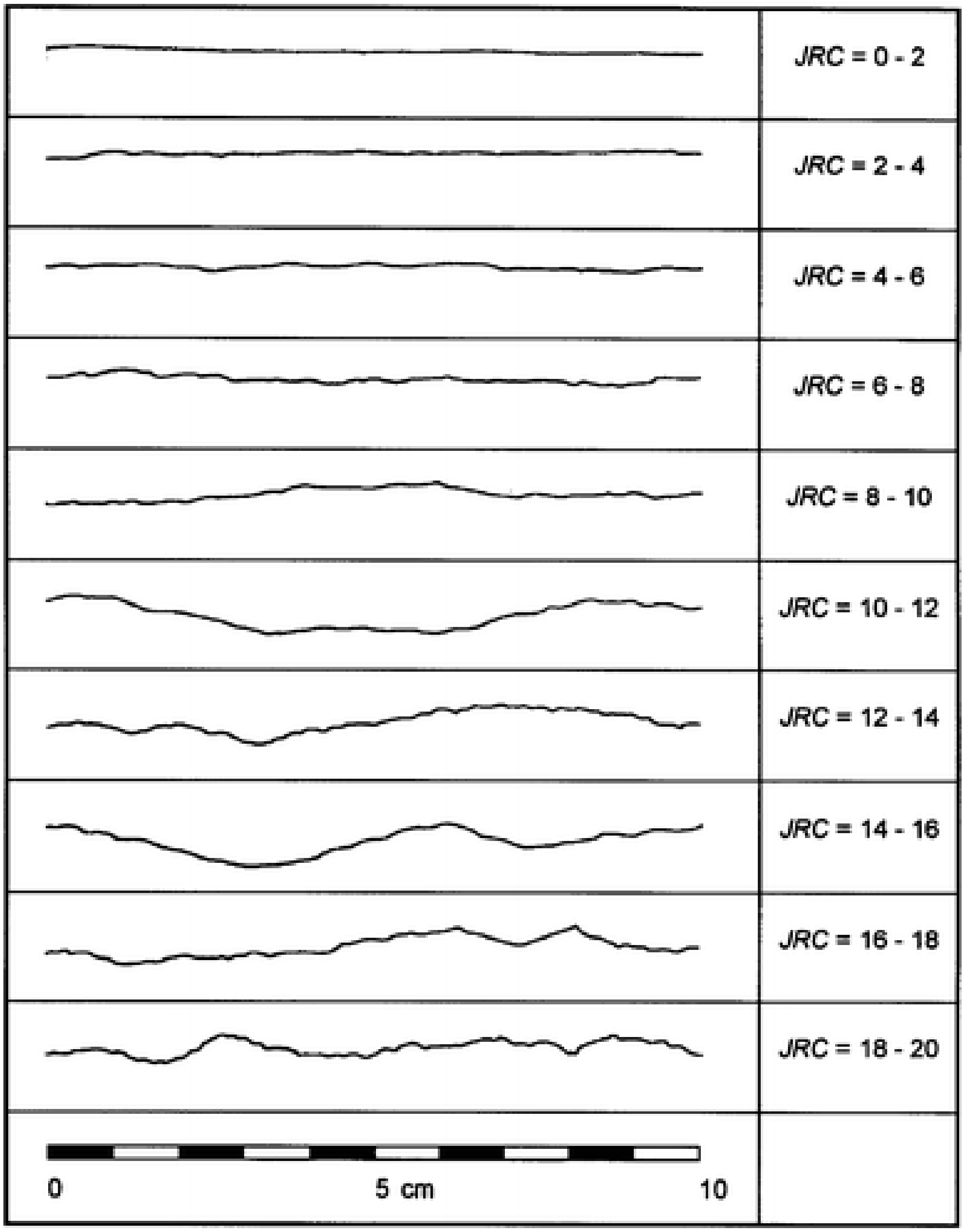

Figure 3.3: Description of JRC by Barton and Choubey (1977)

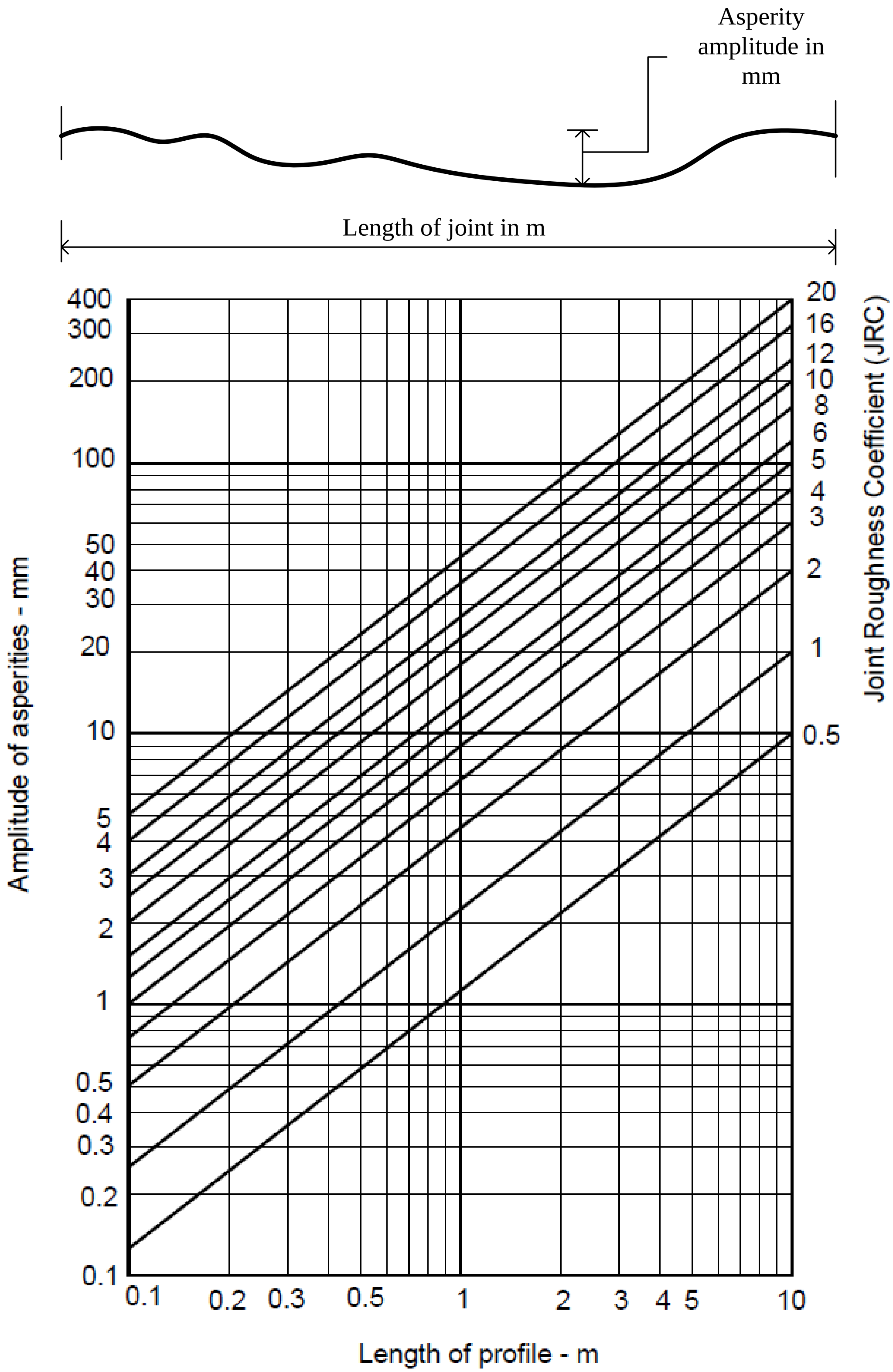

Figure 3.4: Barton (1982) JRC identification chart

Barton (1982) established an alternative method for finding the joint roughness coefficient. The method uses a chart to identify the JRC using the asperity value and length of the joint. The combination of asperity and length of the joint provides the JRC value (Figure 3.4). The estimation of JRC by the graph is for a generalised length of 10 cm. The normalised value of JRC for a given length is provided as

$$JRC_n = JRC_o \left[\frac{L_n}{L_o}\right]^{-0.02 JRC_o} \qquad \text{(Eq. 3.12)}$$

3.3.3 Number of Joints

The increase in the number of joints leads to multiple transmissions and reflections. The increase in the number of reflections and transmissions leads to multiple wave intersections and a decrease in wave amplitude. The change is not only to the wave amplitude but the travel time as well. This is the theory applied in ultrasonic pulse velocity test for the identification of cracks in concrete. Sebastian and Sitharam (2015) have also tried to understand the change in wave velocity for various joint numbers for long wavelengths. However, a lack of understanding is still prominent for the change in wave velocity for different frequencies as the number of joints increases.

3.4 SAMPLE PREPARATION FOR UPV TEST

The joint properties vary over small distances in the field. Thus, the study on the effect of these properties become important. The operations of extracting core samples without any disturbance are tough. Obtaining rock samples of required specification and preparation of corresponding joint configurations are practically difficult. So rock model materials like plaster of Paris, gypsum and cement have been adopted by various researchers (Ramamurthy and Arora, 1994; Indraratna and Haque, 2000; Cha et al., 2009; Sebastian, 2015 and Yang et al., 2018). Gypsum is commonly used as an alternative for rock and is widely popular for experimental studies since it is easily available, flexible and economical. Cha et al. (2009), Sebastian (2015) also conducted experimental studies using gypsum samples to replicate the behaviour.

Samples of required shape and size are made using customized moulds. Moulds of 20 cm length with slots on the covering plate are used as shown in Figure 3.5. The slots help to introduce dividers and simulate the joints as required. The dividers used for making the joints are thin plastic sheets. Acrylic sheets of 10 mm thickness and polypropylene sheets of 4 mm thickness are used in the fabrication of the moulds and dividers respectively. The materials are adopted so that the adhesive property of the gypsum to the mould and dividers would be minimum along with ensuring enough strength to cast samples without any damage. The samples are extracted from the mould with the help of screws, as shown in Figure 3.5. This enables the moulds to be separated from the specimen after the sample hardens.

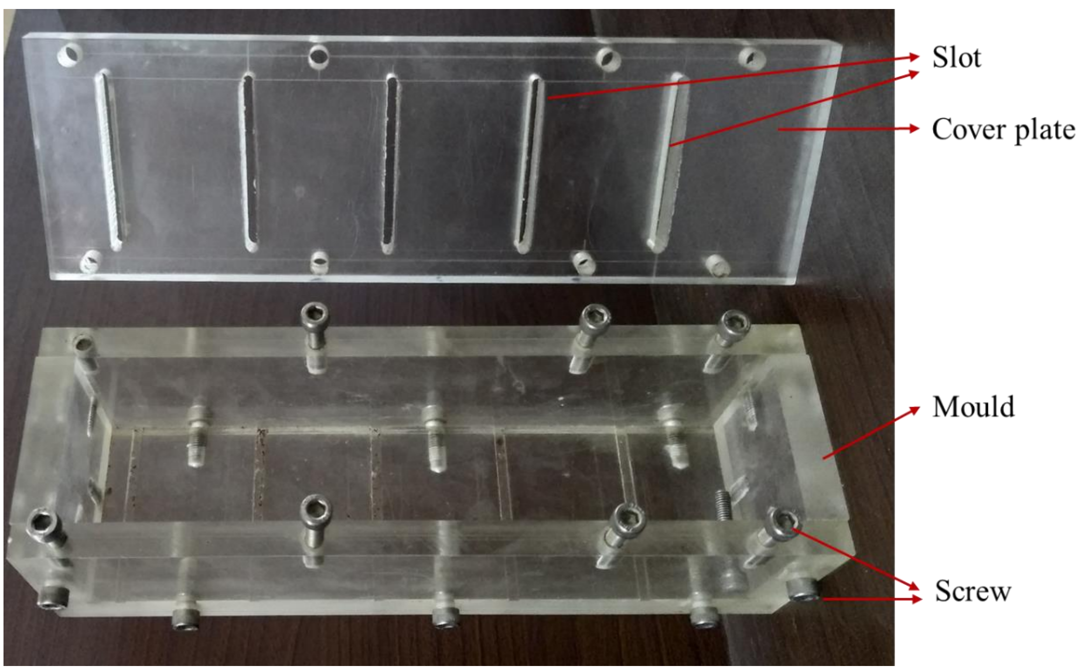

Figure 3.5: 20 cm mould with slits and dividers

The current study used capping Gypsum of grade 35. 24% of water by weight is added and mixed until no lumps of gypsum are present. The slurry should be of flowing consistency. This consistency is essential for the shaping and moulding of gypsum. The slurry is then transferred to the mould, and the dividers are introduced to simulate the required joints. Once the sample attains its initial strength and shape, the moulds are removed. The sample is then set to dry at room temperature for 28 days to obtain its maximum strength. The density and strength properties of the material tested in the laboratory are given in Table 3.1.

Table 3.1: Properties of the gypsum sample

Property	Value
Density	1800 kg/m^3
Elastic Modulus	23.4 GPa
Poisson's ratio	0.17
Unconfined Compressive Strength	35 MPa

3.4.1 Joint Angle

For inclined joints, all the joint angles are placed at the centre, so that the centre of the joint coincides with the centre of the sample. The angle measurement is such that 0˚angle is the normal incidence of the wave. The joint angle is measured such that it is equal to the angle of incidence. The joint angle is varied from 0˚ to 60˚ with an interval of 10˚ with an exception of 55˚. Figure 3.6 shows the mould cover with slits for joint angles 10˚, 20˚, 55˚ and 60˚. Figure 3.7 shows different samples with joint angles 10˚, 20˚, 30˚ and 60˚. It was ensured that the divider passed the slit with ease and reached the bottom of the mould without creating any voids. The same moulds are used in the preparation of samples with multiple joints and different joint roughness.

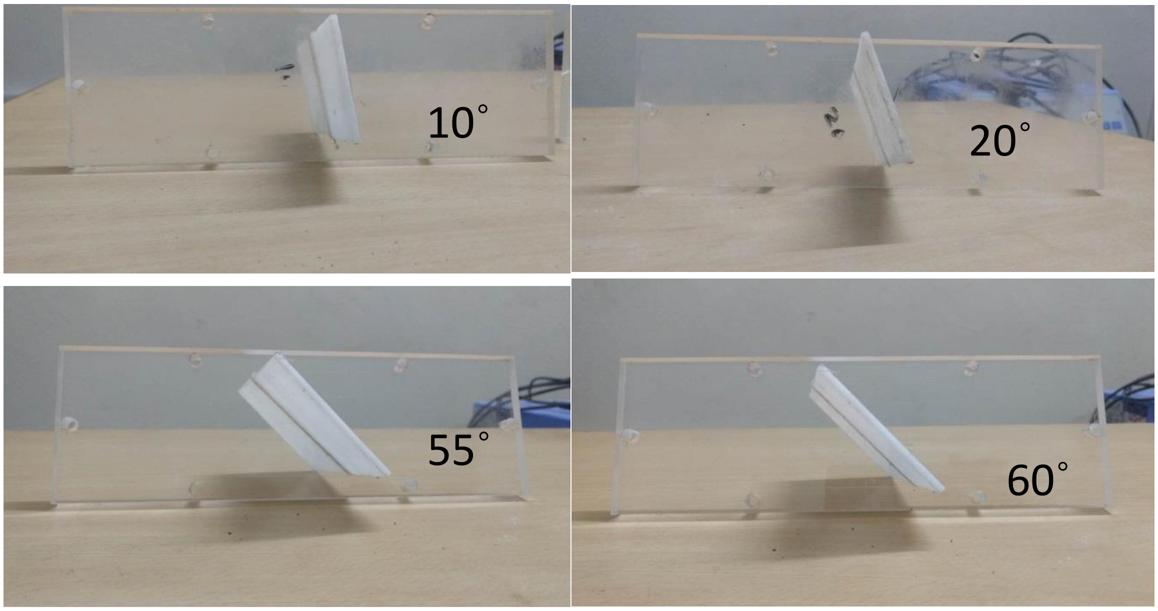

Figure 3.6: Mould caps for different joint angles

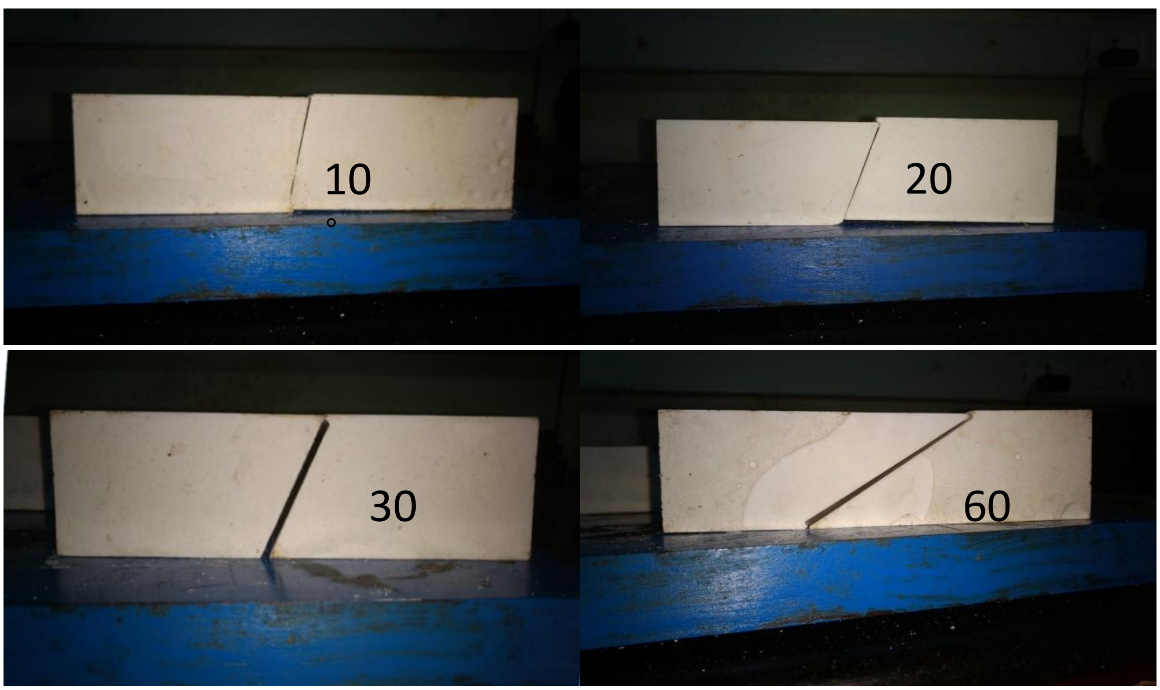

Figure 3.7: Samples of different joint angles

3.4.2 Joint Roughness

Four different joint roughness profiles are adopted for the study. Dividers of varying roughness are introduced to simulate the rough joints at the centre of 20 cm blocks (Figure

3.8). Figure 3.9 shows the rough joints simulated on the rocks. The JRC values are measured by comparison with Barton and Choubey (1977) and from the charts of Barton (1982) for the blocks shown in Figure 3.9. The values found by the charts are then converted to 5 cm length by the Eq. 3.1. Table 3.2 shows the JRC by the figure comparison and by the chart.

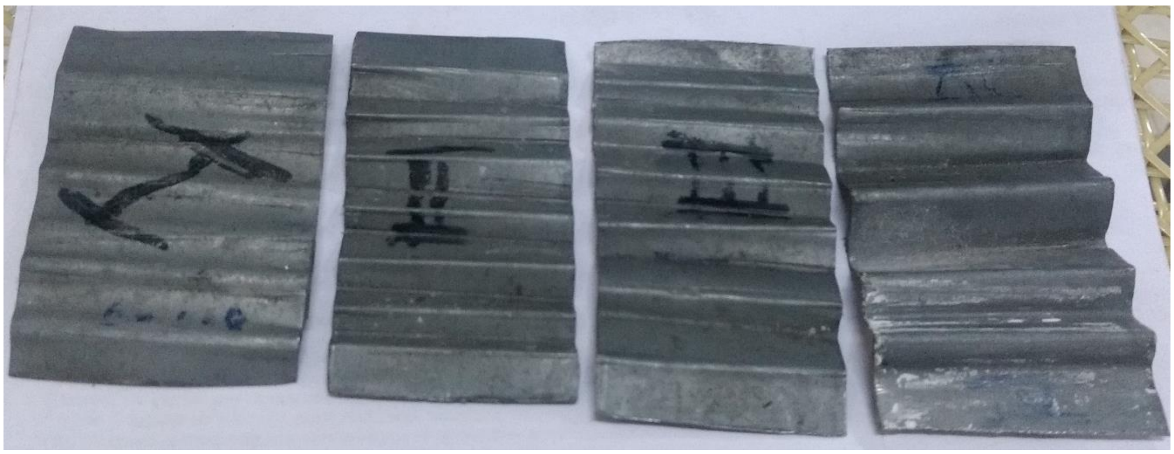

Figure 3.8: Stirrups used in the creation of rough joints

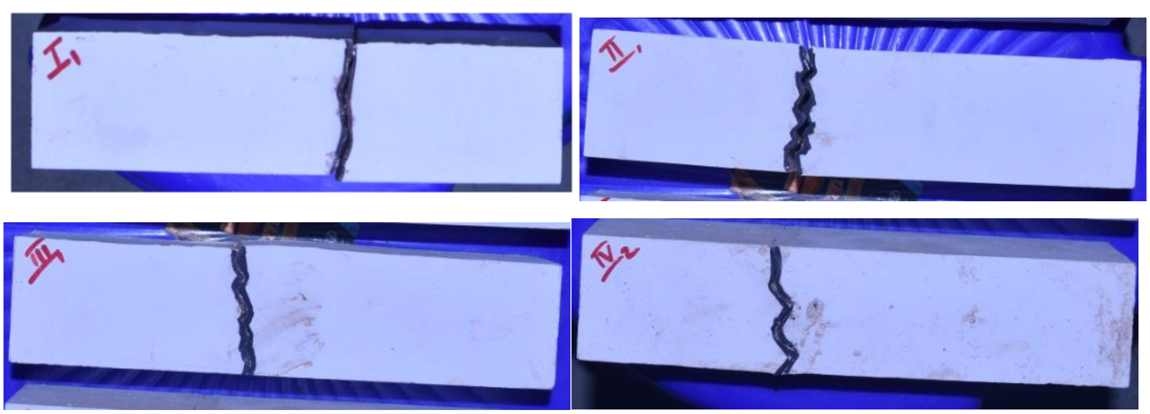

Figure 3.9: Blocks with different JRC values

Table 3.2: JRC value for different samples

Sample type	JRC by comparison Barton and Choubey (1977)	JRC from chart Barton (1982)
I	6-8	6.52
II	14-16	17
III	10-12	11.48
IV	18-20	20.12

3.4.3 Single and Multiple Joints with varying Block Size

Figure 3.10: Samples tested for single joint

For samples having multiple joints, the covering acrylic plate is provided with multiple slots. The dividers are introduced at different positions to create the required joints. The slots are such that single or multiple joints can be made from the same mould. Different blocks of length 1, 3, 4, 5, 9, 11 and 15 cm are adopted to create different combinations. These blocks are combined to form single and double joints of different length. Figures 3.10 and 3.11 shows the different block combinations for single or double jointed blocks.

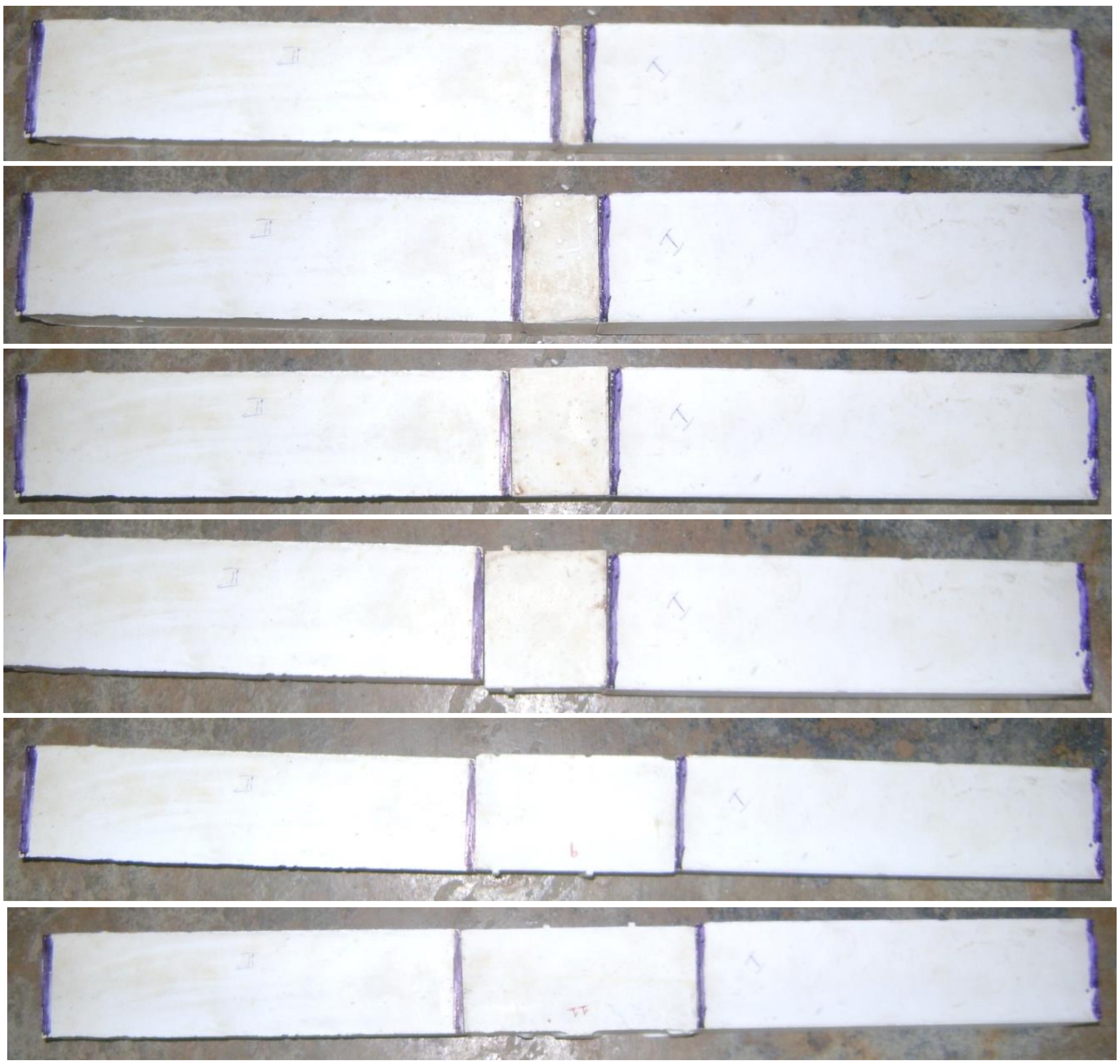

Figure 3.11: Samples tested for two joints

3.5 PRINCIPLES OF UPV TEST

Ultrasonic pulse velocity test is one of the easiest and economical tests to understand the wave velocity. The test is based on the vibration of atoms at the atomic level called acoustics. The vibrations are in four principal directions that will help the wave propagate in four modes: longitudinal, shear, surface and plate waves. Longitudinal waves and shear waves are the most commonly used for testing in laboratories.

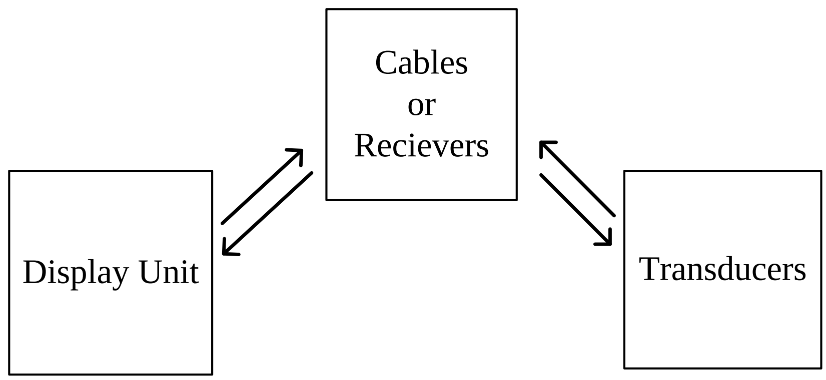

Figure 3.12: Schematic diagram for an ultrasonic wave test

Electric pulses of controlled energy are generated by the pulser, which is converted in the ultrasonic transducer (Figure 3.12). The pulse length and shape can be controlled using the display and control unit. The signals are normally positive half wave, negative half wave or full wave of a given frequency. In longitudinal waves, the vibrations occur in the direction of the wave transmission. And as for shear waves, the vibrations occur perpendicular to the direction of wave transmission. For any given material, the longitudinal and shear wave velocities are a constant and does not depend on the amplitude of the wave as long as the wave amplitude is in its elastic range. The wavelength and frequency of the wave hold a relation with the wave velocity as

$$\lambda f = v \qquad \text{(Eq. 3.2)}$$

where, λ is the wavelength, f is the frequency and v is the wave velocity. The velocity of a wave propagating through a material depends on the strength moduli and density of the material. The velocity of the propagating waves can be obtained by the following expression:

$$v_p = \sqrt{\frac{E}{\rho}} \qquad \text{(Eq. 3.3)}$$

$$v_s = \sqrt{\frac{G}{\rho}} \qquad \text{(Eq. 3.4)}$$

where v_p is longitudinal wave velocity

v_s is shear wave velocity

E is the elastic modulus of the material

G is the bulk modulus of the material

ρ is the material density

As the wave is transmitted through a joint, a part of energy contained by the wave also gets attenuated. In this process of wave attenuation, a time delay occurs in transmission and brings a change in wave velocity. The receiver transducers record the arrival time and amplitude of the pulses, which helps in analysing the wave propagation pattern. The measurement of velocity in an ultrasonic pulse velocity test is by checking the arrival time of waves. The length of the block, when divided by the travel time, calculates the wave velocity. Popular methods in the calculation time travel are the first arrival time method, peak to peak method and cross-relation method (Viggiani and Atkinson 1995, Arulnathan et al. 1998, Chan 2010). In the current study, the first arrival time method is used and is shown in Figure 3.13 It is preferred over the other methods due to its ease of calculation, and the inaccuracy of peak to peak method, where choosing the right peak plays a major role in understanding the wave velocity. First arrival time method calculates the travel time as the point where the signal starts to show and leaves the time axis. Since the frequency under consideration is ultrasonic, the effect of near field errors is less likely to happen (Bringnoli et al., 1996; Viggiani and Atkinson, 1995; Arulnathan et al., 1998; Lee and Santamarina, 2005; Patel et al., 2010).

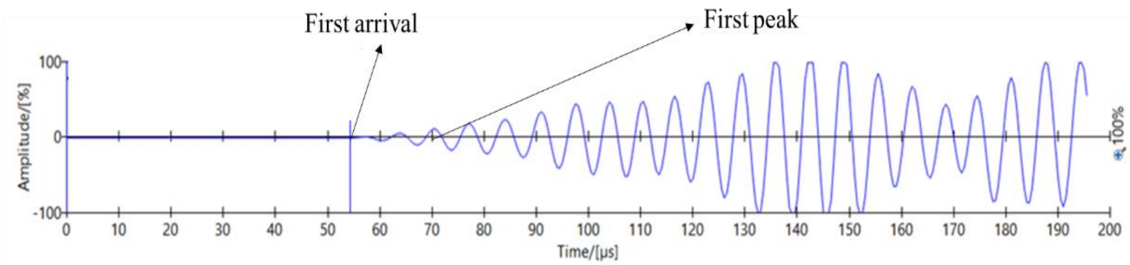

Figure 3.13: Measurement of first arrival and peak to peak arrival

3.6 UPV TEST SETUP AND TEST PROCEDURE

The experimental study was conducted using ultrasonic pulse velocity tester manufactured by Proceq PunditLab^{+}. The machine consists of a pair of transducers (of various sizes with different input voltage), 2 BNC cables, couplant, calibration rod, battery charger with USB-cable and data carrier with software (Figure 3.14). The test works on the principle of identifying the travel time of the waves across the distance, which will give the velocity of the wave in the medium. The frequency of the pulse generated in this test, by the machine will be in the range of 20 kHz to 500 kHz. Also, the amplitude of the input pulse can be adjusted by changing the input voltage. The available codes for the test are ASTM C 597-02, ASTM D 2845 and IS 13311 (1992). In the current study IS 13311(1992) has been followed The complete test setup in diagram is presented in Figure 3.15. Longitudinal waves iare produced using transmission probes at an input voltage of 500V. Before the test is carried out, the equipment needs to be calibrated using the calibration rod provided by the manufactures for the given travel time of 25µs.

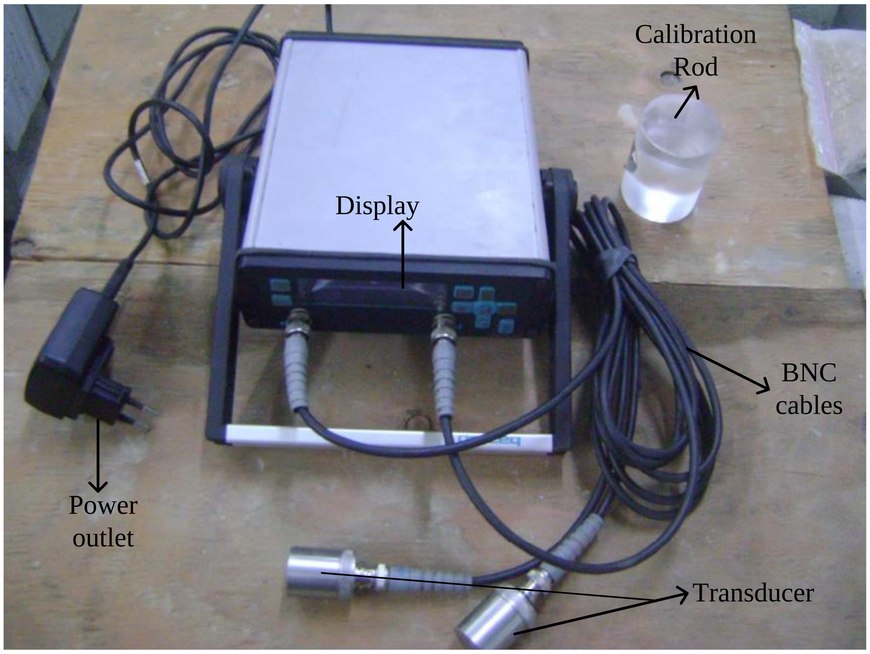

Figure 3.14: Ultrasonic pulse velocity (UPV) test device

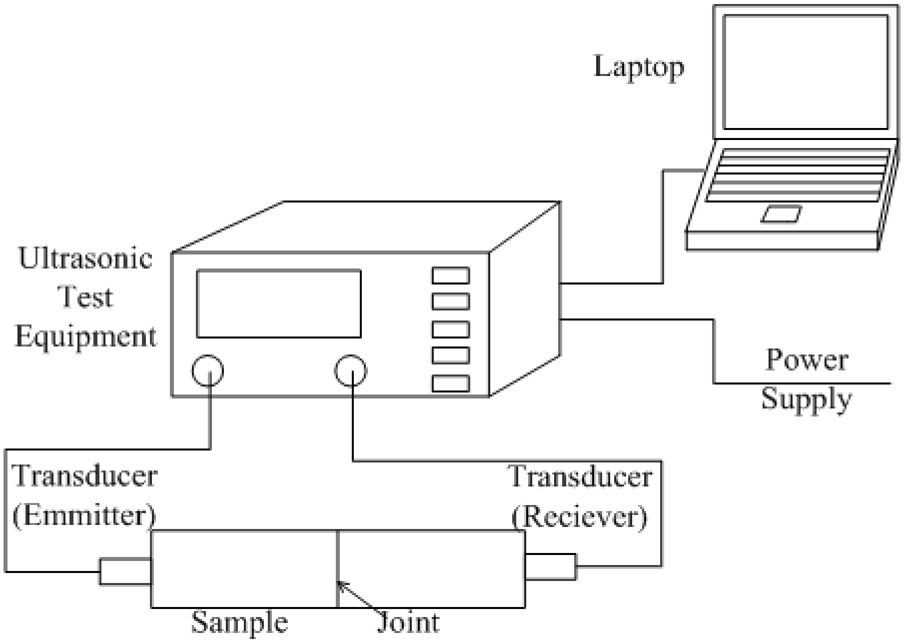

Figure 3.15: Ultrasonic pulse velocity (UPV) test setup

.

3.7 RESULTS FROM EXPERIMENTAL STUDY

The results of the tests are obtained using dedicated software. The output wave signals obtained from the screen, provide information regarding travel time, the amplitude and shape of the arrival wave. First arrival time method is used in the velocity calculation throughout the thesis. Figure 3.16 shows the experimental procedure. The ultrasonic tests are conducted so as to analyse the variation of wave velocity according to the different types of joints. Block samples of length 20 cm are used for the experimental studies to understand joint angle and joint roughness. For both the conditions, the joint is positioned at the centre of the sample. Samples with joint angles 0˚, 10˚, 20˚, 30˚, 55˚ and 60˚ are studied. And the joint roughness of 0, 6.5, 11.5, 17 and 20 are studied. To understand the effect of number of joints, different block sizes and varying joint positions studies of blocks with multiple joints are conducted. The summary of the joints studied is provided in Table 3.3. The intact wave velocity is also measured for all intact samples.

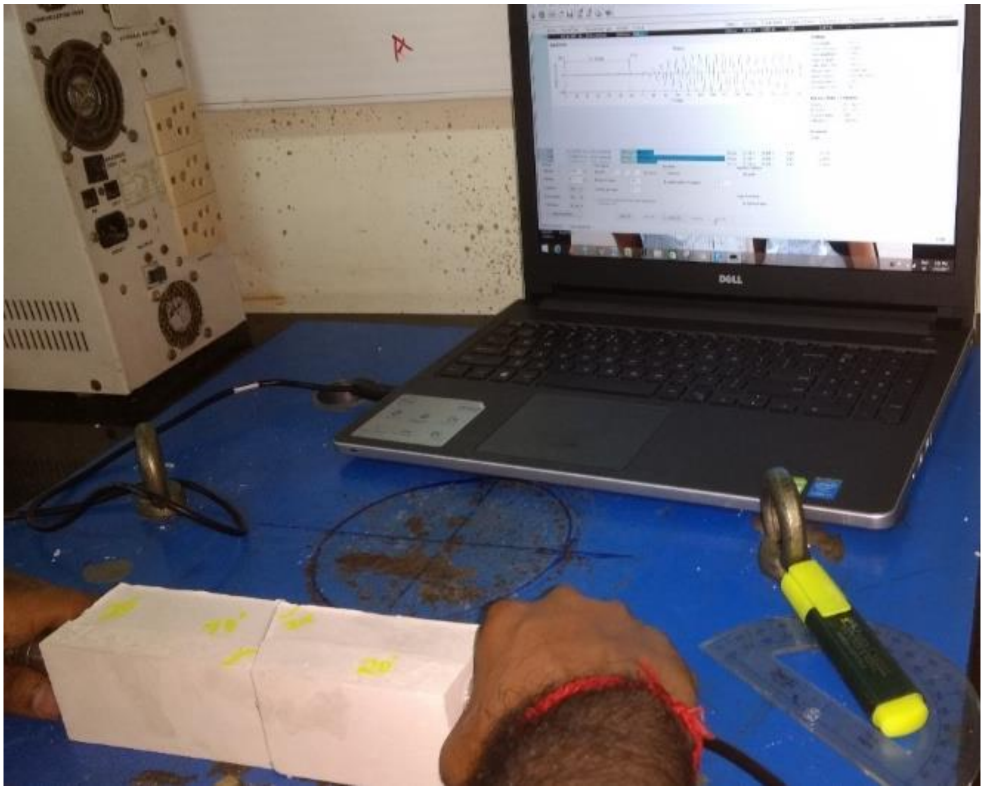

Figure 3.16: Experimentation using ultrasonic pulse tester

Table 3.3: Laboratory test program

Test Sample	Block length	Joint Angle	Joint Roughness	Number of Joints	Position of 1st joint	Position of 2nd joint
1	20 cm	0	0	1	10 cm	-
2	20 cm	10	0	1	10 cm	-
3	20 cm	20	0	1	10 cm	-
4	20 cm	30	0	1	10 cm	-
5	20 cm	55	0	1	10 cm	-
6	20 cm	60	0	1	10 cm	-
7	20 cm	0	0	1	10 cm	-
8	20 cm	0	6.5	1	10 cm	-
9	20 cm	0	11.5	1	10 cm	-
10	20 cm	0	17	1	10 cm	-
11	20 cm	0	20	1	10 cm	-
12	40 cm	0	0	1	20 cm	-
13	35 cm	0	0	1	15 cm	-
14	26 cm	0	0	1	11 cm	-
15	31 cm	0	0	1	11 cm	-
16	29 cm	0	0	1	9 cm	-
17	21 cm	0	0	1	1 cm	-
18	41 cm	0	0	2	20 cm	21 cm
19	43 cm	0	0	2	20 cm	23 cm
20	44 cm	0	0	2	20 cm	24 cm
21	45 cm	0	0	2	20 cm	25 cm
22	49 cm	0	0	2	20 cm	29 cm
23	51 cm	0	0	2	20 cm	31 cm
24	55 cm	0	0	2	20 cm	35 cm

3.7.1 Intact wave velocity

The compression and shear wave velocities are constant for a given medium. Waves propagate through any given material. Different blocks of various lengths are obtained to understand the longitudinal wave velocity of the samples. Figure 3.17 (a) and (b) shows the wave propagation pattern obtained at the receiver transducer from a 20 cm and 9 cm sample respectively. The intact wave velocity of the sample is found to be 3871 m/s from the tests on different intact blocks. This wave velocity of intact sample (V_i) is used for comparing and understanding the change in longitudinal wave velocity while propagating through samples in which different types of joints exist.

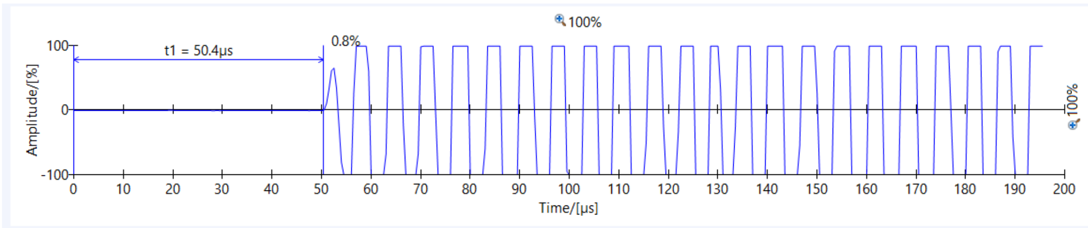

(a)

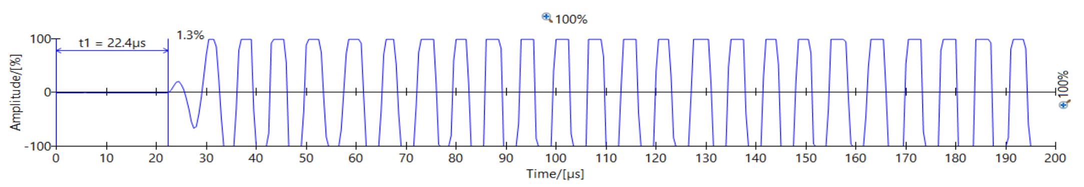

(b)

Figure 3.17: Wave propagation obtained at the receiver transducer for an intact sample (a) 20 cm length (b) 9 cm length

3.7.2 Effect of Joint Angle

Samples of length 20 cm with different joint angles, as shown in Figure 3.5 are studied in the laboratory. The joint angle is varied from 0˚ to 60˚ with respect to normal, as shown in Figure 3.18. Figure 3.19, 3.20 and 3.21 shows the typical wave traces obtained from the UPV tests carried out at different joint angles. Figures 3.19, 3.20 and 3.21, when compared to Figure 3.17, shows a multiple interferences pattern, and the waves undergo multiple reflections. This also indicates an increase in the travel path which leads to an increase in the wave arrival time. The wave arrival time obtained from the testing device is used to obtain the wave velocity, as shown in Table 3.4. A normalised value of wave velocity as the ratio of longitudinal wave velocity through the joint (V_j) with respect to intact wave velocity (V_i) is also provided. From Table 3.4, an increase in wave velocity is observed as the joint angle increases beyond 50˚. The increase in wave velocity with the increase joint angle was also observed by Pyrak Nolte et al. (1990). This increase in wave velocity is described as the change in phase as the wave passes through the joint, which leads to a decrease in travel time with different joint positions.

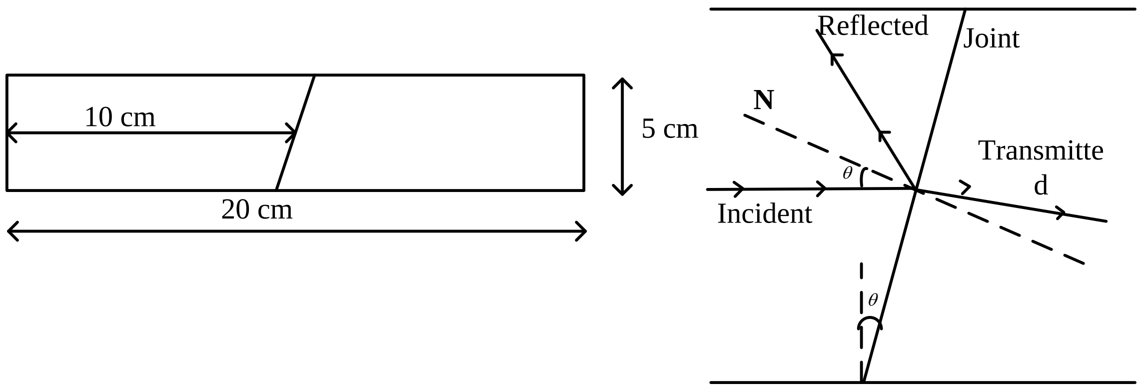

Figure 3.18: Joint and joint angle in the block

Table 3.4: Longitudinal wave velocity values for different joint angles.

Joint Angle (°)	Longitudinal wave velocity (m/s)	$\left(\frac{V_j}{V_i}\right)$
10	3298	0.85
20	2301	0.59
30	2667	0.69
55	3221	0.83
60	3683	0.95

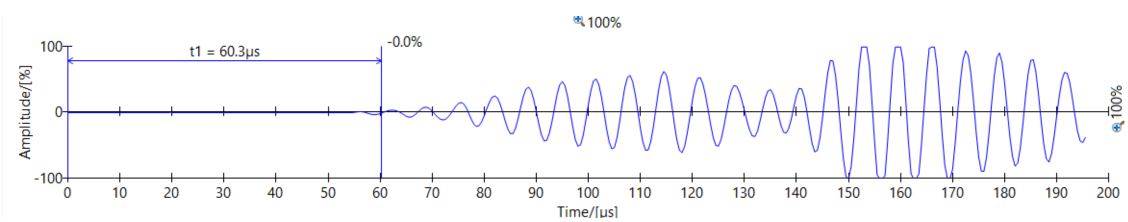

Figure 3.19: Wave propagation obtained at the receiver transducer for 10° angle

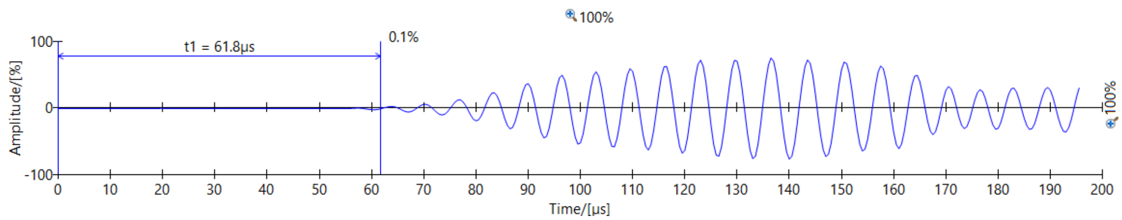

Figure 3.20: Wave propagation obtained at the receiver transducer for 55˚ angle

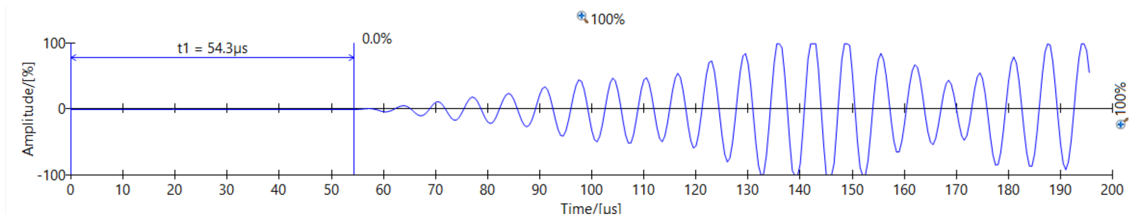

Figure 3.21: Wave propagation obtained at the receiver transducer for 60˚ angle

3.7.3 Effect of Joint Roughness Coefficient

Limited studies have been done by researchers using different experimental methods to understand the effect of roughness on the wave propagation (Kahraman, 2002; Cha et al., 2009, 2013; Mohd-Nordin et al., 2014; Chen et al., 2016). The UPV testing is conducted in blocks of 20 cm, as shown in Figure 3.9. The longitudinal wave velocity obtained for different JRC samples is given in Table 3.5. It can be seen that the longitudinal wave velocity decreases with an increase in joint roughness. The increase of joint roughness increases the total joint surface area and reduces the contact area which in turn reduces the contact stiffness and thus decreases the longitudinal wave velocity. This variation in longitudinal wave velocity with JRC is found to be very small when studied for the high frequency which might be due to its high energy content. Similar results were observed by Kahraman (2002) and Mohd-Nordin et al. (2014).

Table 3.5: Longitudinal wave velocity for blocks with different joint roughness

JRC (Barton, 1982)	Longitudinal wave velocity (m/s)			$\left(\frac{V_j}{V_i}\right)$
	Sample 1	Sample 2	Average	
6.5	3811	3809	3810	0.98
11.5	3799	3793	3796	0.97
17.0	3781	3781	3781	0.96
20.0	3610	3670	3643	0.94

3.7.4 Effect of Block Size and Number of Joints

A seismic wave passing through rock mass encounters multiple joints, and therefore, the effect of joint frequency on longitudinal wave velocity need to be understood. The study has been experimentally conducted for single and double joints. The study also attempted to understand the variation of longitudinal wave velocity with the different joint spacing and block length. Various block size combinations are used for the study. Different block combinations as given in Table 3.3 are used for the study. Longitudinal wave velocity for different joint combinations is presented in Table 3.6 and 3.7 for different block lengths and joint position.

Table 3.6: Longitudinal wave velocity for blocks with single joint

Length of blocks (cm)		Longitudinal wave velocity (m/s)	$\left(\frac{V_j}{V_i}\right)$
Block 1	Block 2		
20	20	3544	0.92
15	20	3529	0.91
11	15	3489	0.90
11	20	3512	0.91
9	20	3434	0.89
1	20	3382	0.87

It can be found from Tables 3.3 and 3.6 that a reduction in longitudinal wave velocity occurs with an increase in the number of joints. However, a clear understanding on the effect of joint spacing could not be obtained from this study as the study is conducted for a single frequency. The variation of joint spacing value with respect to the wavelength of the applied ultrasonic pulse is relatively small. To understand the effect of frequency, a numerical study is done and discussed in the next chapter.

Table 3.7: Longitudinal wave velocity for blocks with two joints

Length of blocks (cm)			Longitudinal wave velocity (m/s)	$\left(\frac{V_j}{V_i}\right)$
Block 1	Block 2	Block 3		
20	1	20	3198	0.83
20	3	20	3118	0.81
20	4	20	3235	0.84
20	5	20	3286	0.85
20	9	20	3221	0.83
20	11	20	3271	0.85
20	15	20	3246	0.84

3.8 SUMMARY

The strains induced by the waves on the rock mass is usually small unless it is very near to the source. The wave propagation through rock mass gets affected by various joint parameters. This chapter attempted to understand the effect of various joint parameters like joint angle, joint roughness and joint frequency on the wave velocity in the ultrasonic range. The UPV tests are conducted in the laboratory with artificially prepared rock specimens. The samples are incorporated with joint angles, namely 0˚, 10˚, 30˚, 55˚ and 60˚. The joint angles are equal to the angle of incidence of the wave. The longitudinal wave velocity is observed to decrease initially from 0˚ to 10˚and as the joint angle is changed from 10˚ to 55˚, no significant change in the wave velocity is observed. However, the wave velocity suddenly increased as the joint angle is 60˚. This is explained to be due to the effect of phase change by Pyrak Nolte et al. (1990). To understand the effect of joint roughness on wave velocity, tests are conducted with different roughness profile corresponding to different joint roughness coefficients (JRC). The longitudinal wave velocity is found to decrease with the increase in joint roughness as the contact area between the joints decreases, leading to a decrease in joint stiffness. The number of joints also affect the velocity of a wave transmitted. The study also attempted to understand the variation in wave velocity with the increase in the number of joints. The longitudinal wave velocity is found to decrease with increasing joints. The study helps to understand the wave velocity through rock mass and the corresponding influence by various joint characteristics. The experimental study is constrained with the frequency and block size ranges.

CHAPTER 4

NUMERICAL ANALYSIS OF WAVE PROPAGATION IN JOINTED ROCKS

4.1 INTRODUCTION

The experimental studies on wave propagation in jointed rock mass have certain limitations, especially while trying to understand the behaviour of jointed rock mass over a wide range of wave frequencies and rock joint parameters. The numerical modelling techniques have gained widespread attention in understanding the behaviour of wave propagation. Different numerical methods namely, finite element method, finite difference method, boundary element method, discrete element method are available. The choice of each modelling tool depends on the problem under consideration.

As seen from the literature, studies on wave propagation along joints are mainly conducted using the discrete element method. The ease in the modelling of joint and joint properties resulted in this popular choice. Universal Distinct Element code (UDEC) (Cai and Zhao, 2000; Zhao et al., 2008; Eitzenberger, 2012), 3-Dimensional Distinct Element code (3DEC) (Sebastian, 2015) and Particle Flow Code (PFC) (Resende, 2010) are the commonly used numerical tools in the studies. Due to its efficient computation of jointed rock mass, Universal Distinct Element code (UDEC) is used in the the present study. This chapter tries to extend the experimental studies from chapter 3 for a wider range of wave frequencies, block size and number of joints. The effect of each of these parameters on wave velocity is studied and relations to predict the longitudinal wave velocity for different joint conditions have been discussed and presented in this chapter.

4.2 MODELLING OF WAVE PROPAGATION OF JOINTED ROCK MASS BY DISCRETE ELEMENT METHOD

The capability of UDEC in successful modelling of jointed rock mass with one-dimensional wave propagation has been established by Chen and Zhao (1998), Cai and Zhao (2000), Zhao et al., (2006, 2008), Zhu et al., 2012, Chai et al., (2016). In the current numerical model, each block is considered to be a continuum and analysed using finite difference method by constant strain triangles and the joints using boundary conditions. For the accurate representation of wave propagation, Kuhlemeyer and Lysmer (1973) recommended the size of the elements to be smaller than 1/10th to 1/8th of the wavelength associated with the highest frequency component of the input wave.

$$\Delta l \leq \frac{1}{10}\lambda \tag{Eq. 4.1}$$

where, Δl is the size of the element and λ is the wavelength associated with the highest frequency. A step by step stress relaxation technique is adopted in the numerical analysis, which alternates between Newton's equation of motion and stress displacement law. The calculation cycle mainly depends on the assumption of the blocks as rigid or deformable (Figure 4.1). In rigid, the force and displacement calculations for the blocks are carried out at the centre of the block. The force and motion is calculated as

$$F_i = \sum F_i^c \tag{Eq. 4.2}$$

$$\ddot{u} = \frac{F_i}{m} \tag{Eq. 4.3}$$

where, F_i^c is the force at the contact interface and m is the mass of the block under consideration. In the case of deformable blocks, the analysis is conducted for each zone element. The motion of each vertex of the triangular zone (gridpoint) is calculated by considering a Gaussian surface along the block

$$\ddot{u} = g_i + \frac{1}{m}\int_s \sigma_{ij} n_j \, ds + F_i \tag{Eq. 4.4}$$

where, s is the surface enclosing the mass, m lumped at the gridpoint, F_i is the resultant of all the external forces applied to the gridpoint (which will be zero in case of static condition), n_i is the unit normal to s, g_i is the acceleration due to gravity.

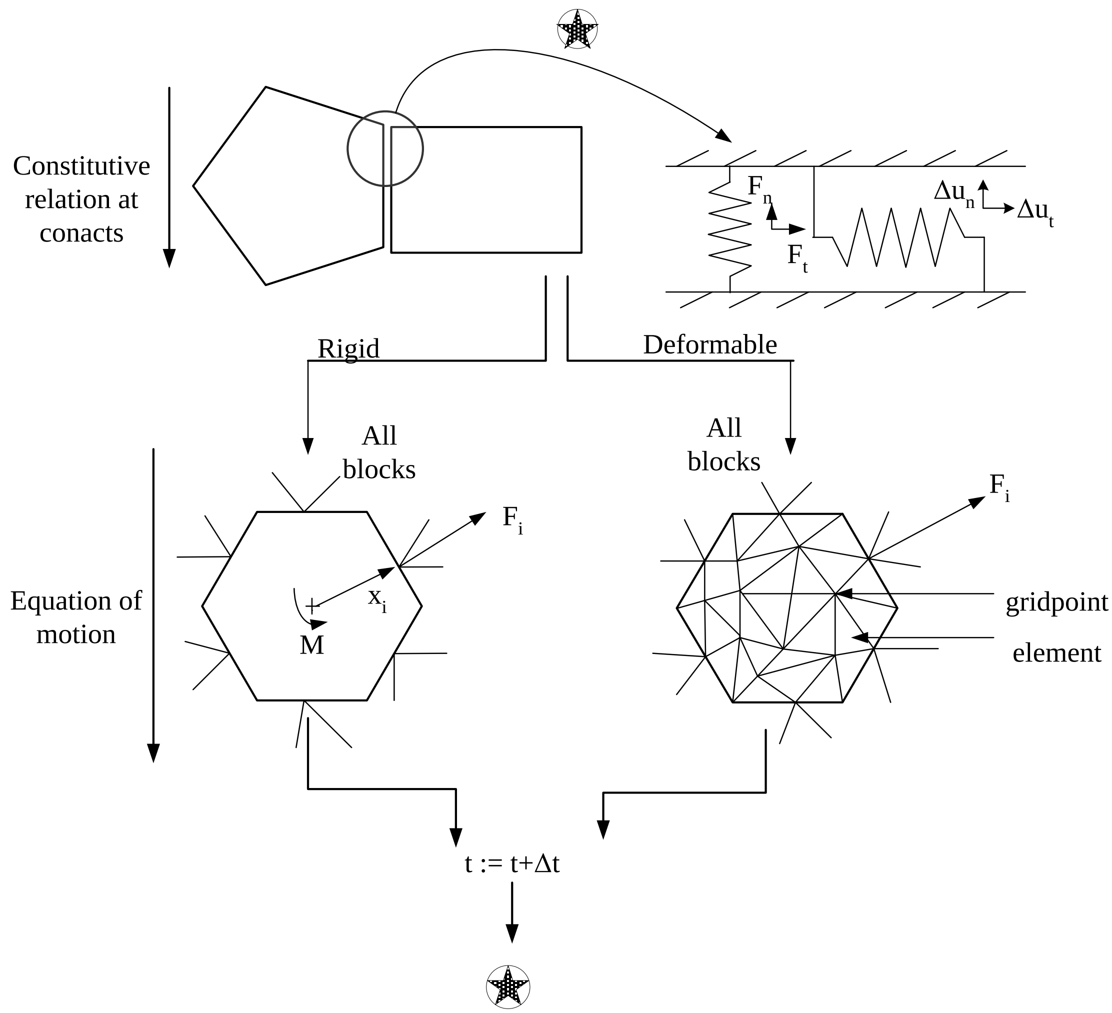

Figure 4.1: Calculation cycle of UDEC (Adopted and redrawn from Hart, 1993)

This modelling method has a shortcoming while calculating the contact overlap and joint contacts, known as contact overlap error. The interaction and the loading between adjacent blocks play a crucial part in the behaviour of joints. These contact interactions are determined by the minimum distance between the adjacent blocks, which is numerically established. The contact type, maximum gap and sliding plane of joints are determined by a contact detection algorithm. The joint stiffness defined between the blocks in normal and tangential directions determine the mechanical calculations done at contacts as in Figure 4.1. The interaction forces developed in the normal and tangential directions (F_n and F_t) at the contact points determine the relative displacements these blocks shall undergo (u_n and u_t).

$$\Delta F_n = K_n \Delta u_n \qquad \text{(Eq. 4.5)}$$

$$\Delta F_t = K_t \Delta u_t \qquad \text{No Slip} \qquad \text{(Eq. 4.6)}$$

$$\Delta F_t = \Delta F_n \tan\emptyset \qquad \text{Slippage} \qquad \text{(Eq. 4.7)}$$

The contact surfaces may be a vertex-to-edge contact or an edge-to-edge contact (combination of numerous vertex-to-edge contacts). A linear or nonlinear constitutive model can express slippage between the contact surfaces such as the Mohr-Coulomb model, the continuously yielding model or the Barton-Bandis model. The stress-displacement relation for simple Coulomb friction for these contacts are established as

$$\Delta\sigma_n = k_n \Delta u_n \qquad \text{(Eq. 4.8)}$$

$$\Delta\sigma_t = k_t \Delta u_t \qquad \text{No Slip} \qquad \text{(Eq. 4.9)}$$

$$\Delta\sigma_t = \Delta\sigma_n \tan\emptyset \qquad \text{Slippage} \qquad \text{(Eq. 4.10)}$$

The term Δu_n represents the interpenetration of the adjacent blocks in the normal direction, known as contact overlap. Cohesion is always assumed to be zero when slippage occurs.

The numerical simulation of any geomechanics problem, requires assigning proper boundary conditions. In dynamic conditions, when wave propagation studies are carried out, boundaries should aid the arrangement of wave reflection or transmission as required. In this study, the boundaries are not supposed to reflect the waves coming on the ends of the block, as this would create mutual interference. Quiet boundaries are adopted as it absorbs all the incoming waves and creates no reflections.

4.3 MODEL VALIDATION STUDY

The theoretical solution of Myer et al. (1990) is used to compare and validate the numerical model. The ratio of the transmitted or reflected wave to the incident wave is called transmission coefficient or reflection coefficient respectively. The magnitude of these coefficients is defined by many researchers (Schoenberg, 1980; Pyrak-Nolte et al., 1990; Cai and Zhao, 2000). Pyrak-Nolte et al. (1990) observed that specific stiffness is the most relevant parameter that determines the seismic properties of the fracture since it gives the quantitative description of mechanical coupling between two fractures affecting wave transmission. Specific stiffness was hence used by most researchers to understand transmission and reflection coefficients. The variation of stiffness value determined the behaviour of the joint as open joint, welded joint or non-welded joint. When the joint stiffness is zero, the joint behaves as an open joint, where the wave incident on the joint is fully reflected, and no transmission takes place. As the joint stiffness increases, the joint behaves like a non-welded joint, where partial transmission and partial reflection occurs. As the stiffness value increases, the transmission increases and the reflection decreases. When the joint stiffness further increases reaches a value equivalent to the elastic modulus, the transmission coefficient reaches a value near one, while the reflection coefficient reaches a value near zero. Myer et al. (1990) defined the equation for seismic coefficients for non-welded joint as,

$$|R(\omega)| = \left[\frac{\omega^2}{4\left(\frac{\kappa}{z}\right)^2 + \omega^2} \right]^{\frac{1}{2}} \qquad \text{(Eq. 4.11)}$$

$$|T(\omega)| = \left[\frac{4\left(\frac{\kappa}{z}\right)^2}{4\left(\frac{\kappa}{z}\right)^2 + \omega^2} \right]^{\frac{1}{2}} \qquad \text{(Eq. 4.12)}$$

Where, $|R(\omega)|$ is the reflection coefficient, $|T(\omega)|$ is the transmission coefficient, ω is the angular frequency, κ is the specific stiffness and z is the joint impedence.

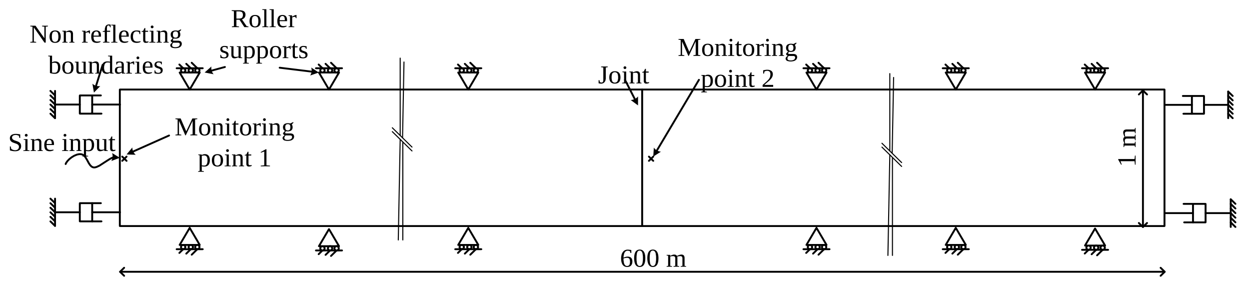

Figure 4.2: Representative numerical model for wave propagation in the block

The numerical model as shown in Figure 4.2 is used to understand the wave propagation across single jointed rock mass. The rock mass considered is 600 m long and 1 m wide with a joint at the centre. The ends of the block are provided with quiet boundaries to avoid wave reflections, and the sides to the direction of propagation are provided with roller supports to assist the propagation of waves. The material model considered is elastic while the joints are assigned to follow the Coulomb slip condition. These material properties will allow in understanding the effect of waves on joints and avoid the consideration of block deformation and plasticity.

The block is assigned with the material properties of Bukit Timah granite of Singapore having density 2650 kg/m^3, bulk modulus 56 GPa and shear modulus 36.9 GPa (Zhao et al., 2008). The joint shear stiffness and friction angle are 1 GPa and 45º, respectively. The joint normal stiffness is varied from 1 GPa/m to 15 GPa/m. The stress input of 1 MPa is applied as a longitudinal wave along the length of the block. A sine wave with frequency 50 Hz is applied as input at one end of the block, as shown in Figure 4.2.

The monitoring points are fixed to obtain the wave propagation pattern at 10 m from the start point and at 10 m from the joint location as shown in Figure 4.2. As the stress wave travels through the block and the joint, a part of the wave is transmitted while a part of the wave is reflected when it is incident on the joint. Figure 4.3 shows the incident, transmitted and reflected waves for joint stiffness 2 GPa/m and 15 GPa/m, respectively. It can be seen that with the increase in joint stiffness, the amplitude of the transmitted wave increased and the reflected wave decreased. When the joint stiffness is 2 GPa/m, the value of transmitted and reflected waves are similar. As the joint stiffness is increased to 15 GPa/m, the transmission increases and reaches a value equivalent to the incident wave while the amplitude of reflected wave decreases.

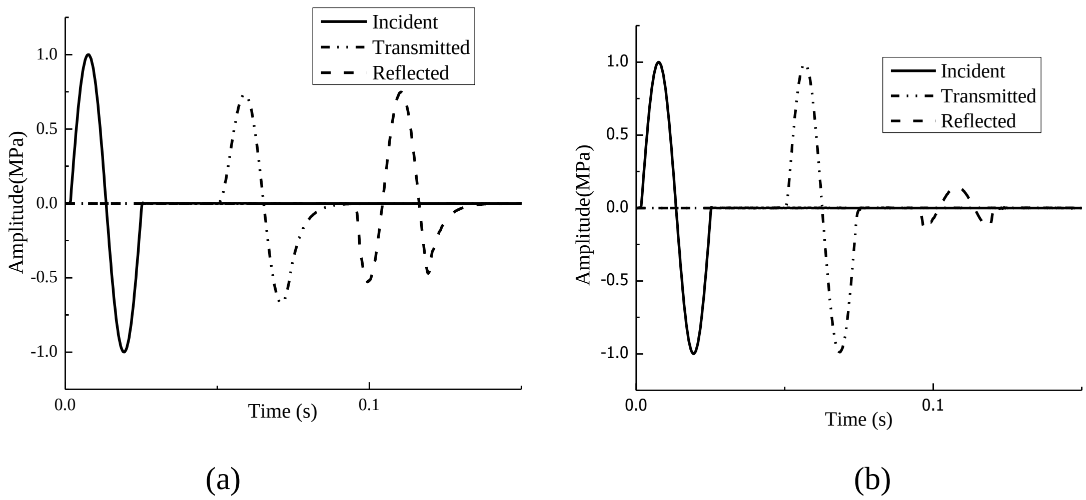

Figure 4.3: Incident, transmitted and reflected wave for joint normal stiffness as obtained from numerical analysis (a) 2 GPa/m (b) 15 GPa/m

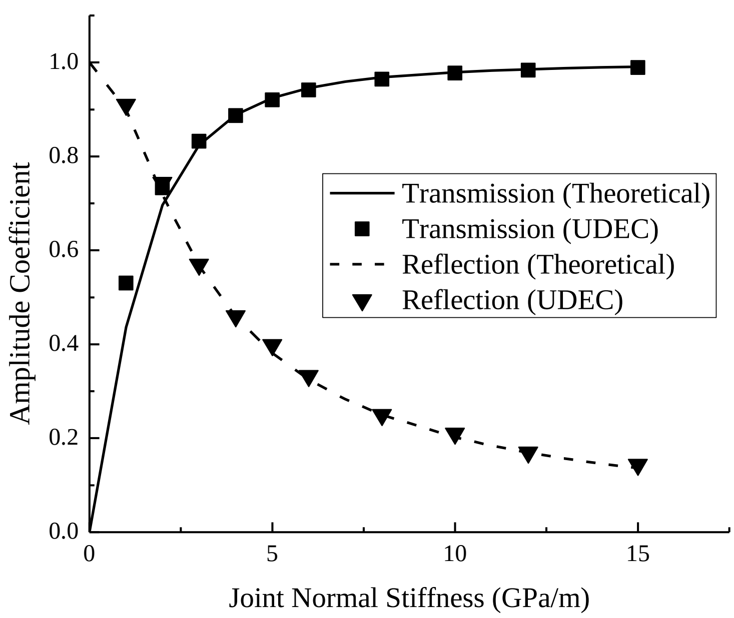

Figure 4.4: Theoretical and numerical results for transmission coefficient and reflection coefficient

Figure 4.4 shows the variation of transmission and reflection coefficient for different joint stiffness values by theoretical solution (Eq. 4.11 and 4.12) as well as from the numerical model. This curve represents the variation in transmission and reflection coefficients from an open joint to the welded joint through a non-welded joint as the stiffness value changes. It can be seen that the transmission coefficient increases with an increase in joint stiffness. At zero joint stiffness, the joint behaves as an open joint; the whole waves are reflected while no portion of the wave transmits. When the reflection coefficient is unity; the transmission coefficient is zero. As the joint stiffness is increased, an exponential increase in the transmission coefficient and an exponential decrease in reflection coefficient can be seen. After an exponential increase, the joint starts acting like a welded joint and the increase in transmission coefficient is negligible. The transmission coefficient reaches near unity while reflection coefficient is near zero.

4.4 PARAMETRIC STUDY USING NUMERICAL MODEL

The numerical model is also validated using the experimental studies on joint angle and joint roughness from chapter 3. Further to carry out parametric studies a distinct element model with 20 cm length and 5 cm in width as shown in Figure 4.5 is considered. The material, joint and boundary conditions used in the study is similar to that of the validated model. The properties of Capping Gypsum found using laboratory experiments are used in numerical modelling, and the corresponding joint properties are obtained using Eq. 4.11 and 4.12 (Table 4.1). A longitudinal wave is applied as a stress input, with the wave amplitude much less than the strength of the block. Monitoring points are assigned at both ends of the block to understand the wave propagation time and arrival time. Damping is not considered in the study, assuming that most of the wave attenuation happens at the joint, and no attenuation happens when the wave propagates through the block. The analysis with intact blocks are performed, which is found to compare well with the experimental results. No variation in the longitudinal wave velocity is occurring with frequency change in an intact block.

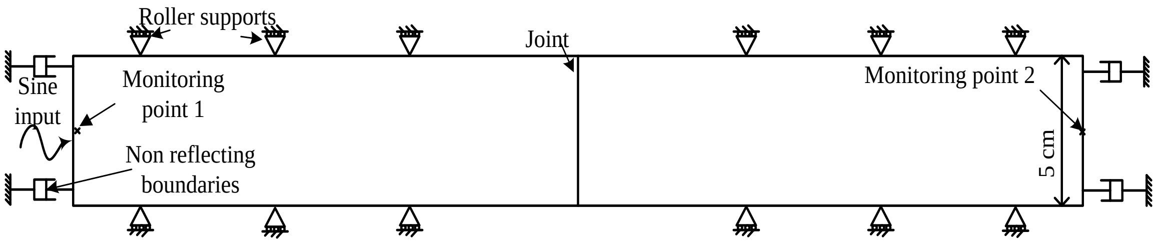

Figure 4.5: Numerical model configuration

The effect of frequency during dynamic loading is studied within the elastic range. In earlier studies, the effect of cut off frequency was described based on normalised joint stiffness parameters (Pyrak-Nolte et al., 1990). Most of the earlier studies focussed on the variation in longitudinal wave velocity with respect to the variation in the ratio of joint stiffness to impedance (k/z). In the present study, the joint stiffness and impedance are considered constant to keep the study focussed on the effect of wavelength, joint orientation, joint roughness, joint position and block size.

Table 4.1: Joint Properties considered in numerical modelling

Property	Value
Joint Friction	35°
Joint Cohesion	0.5 MPa
Joint Normal Stiffness	10 GPa
Joint Shear Stiffness	2.25 GPa

4.4.1 Joint Angle

The effect of joint angle on the longitudinal wave velocity test has been described in the experimental study using ultrasonic pulse velocity test. The study using ultrasonic pulse velocity test for various joint angles are done on a block of 20 cm length. Angle measurement is such that 0˚angle is the normal incidence of the wave. The joint angle is measured such that it is equal to the angle of incidence. The joints are positioned such that the centre of the joint passes through the centre of the block. The study on the effect of angle is analysed using experimental and numerical analysis. For the experimental study, a block of 20 cm is used, and spacers are introduced at the centre of the block at angles 0˚, 10˚, 30˚, 45˚and 60˚. The numerical study is done on a numerical model, as in Figure 4.5. The joint angle θ is varied from 0˚ to 70˚ for the numerical study for every 10˚ change. The 90˚ angle of incidence will represent a horizontal (parallel) joint and is not considered for analysis.

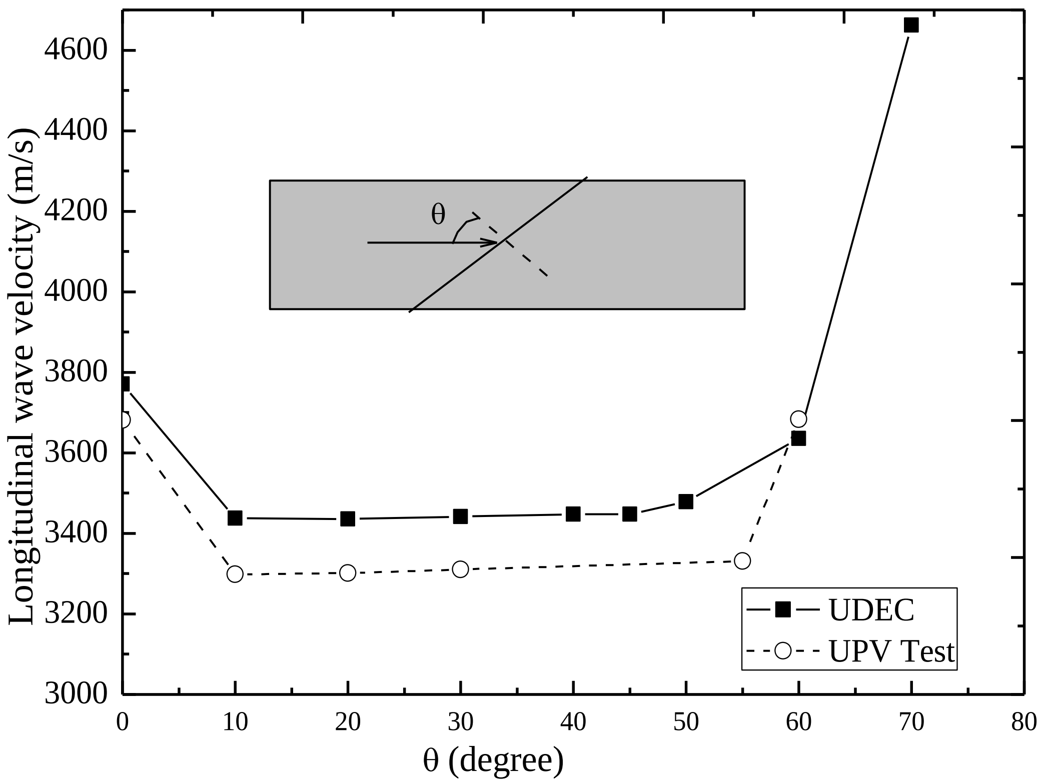

Figure 4.6: Comparison of longitudinal wave velocity from UPV test and UDEC for 150 kHz frequency

Figure 4.6 shows the comparison of the change in longitudinal wave velocity over different joint angles in 20 cm blocks for experimental and numerical studies. A sudden decrease in the wave velocity is observed as the angle is changed from 0˚ to 10˚. With ta further increase in joint angle from 10˚ to 50˚, the longitudinal wave velocity is found to be a constant. For angles greater than 50˚, a steady increase in the longitudinal wave velocity is seen, which is greater than the intact wave velocity. This increase is because the angle of incidence reaches the critical angle of refraction which leads to a phase difference in the transmitted waves. Pyrak-Nolte et al. (1990) observed similar results for longitudinal wave velocity for a set of joint inclinations from 0º to 90º and different normalised joint stiffness values. The sudden decrease in longitudinal wave velocity is justified as a result of the increase in travel length. Based on their study, the increase beyond the intact wave velocity was due to the change in the phase of the wave which leads to a decrease in the time delay.

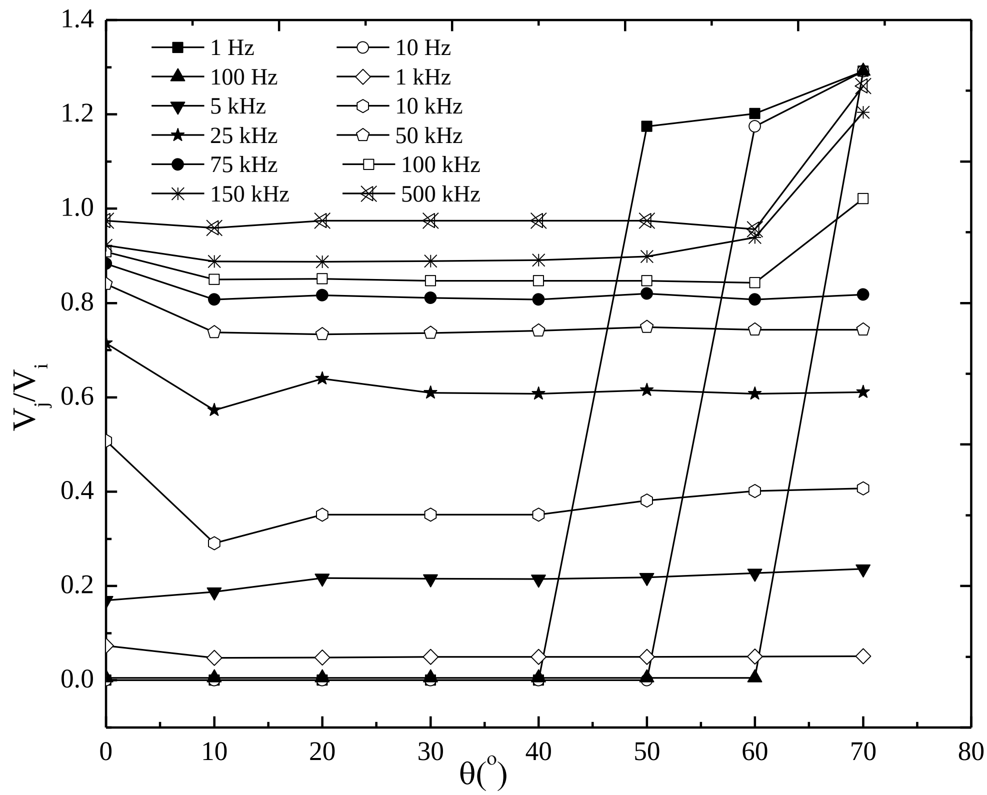

Figure 4.7: Variation of V_j/V_i with the change in joint angle for a frequency range of 1 Hz to 500 kHz

The study is further extended using numerical model to understand the variation in longitudinal wave velocity for other frequencies. Figure 4.7 shows the variation in the ratio of longitudinal wave velocity through joints and longitudinal wave velocity through intact blocks $\left(\frac{V_j}{V_i}\right)$ as the joint angle is varied from 0º to 70º for the frequency range from 1 Hz to 500 kHz. The initial decrease in longitudinal wave velocity as the joint angle changes from 0º to 10º occurs when the incident wave frequency is in the ultrasonic range. The increase in longitudinal wave velocity with an increase in joint angle can be attributed to the multiple reflections and interferences the wave undergoes. The analysis observes a change in the variation of $\left(\frac{V_j}{V_i}\right)$ according to the Eq. 4.13, for a jointed block. Table 4.2 shows the values of dimensionless constants A_1, A_2 and constants B_1 and B_2 with the degree as the unit for each frequency range.

$$\frac{V_j}{V_i} = A_2 + \frac{(A_1 - A_2)}{(1 + e^{(\frac{\theta - B_1}{B_2})})} \qquad \text{(Eq. 4.13)}$$

Table 4.2: The value of constants for different frequency range

Frequency	A_1	A_2	B_1	B_2
>20 kHz	0.89	1.12	67.71	0.47412
20 Hz-20kHz	0.1652	0.2229	11.9066	4.7187
<20 Hz	5.45x 10^{-5}	1.269	54.63	0.723

The variation in the longitudinal wave velocity is found to follow Eq. 4.13 with the constants varying according to the frequency range, as shown in Table 4.3. For v frequencies above 100 kHz, there is an increase in longitudinal wave velocity when the joint angle is greater than or equal to 60º. Similar response of longitudinal wave velocity is observed at lower frequencies in the range of 1 Hz to 100 Hz also. However, it is noticed that as the frequency decreases from 100 Hz to 1 Hz, the effect of the joint angle is more critical. An increase in wave velocity can be observed even below 60º for 1 Hz and 10 Hz. However, for intermediate frequency, a sudden increase in the longitudinal wave velocity is not observed after 60º. An increase of longitudinal wave velocity for a higher frequency ranges is also observed by Pyrak Nolte et al. (1990) and Sebastian (2015).

4.4.2 Joint Roughness Coefficient

The study by UPV testing conducted on blocks of 20 cm is extended with numerical modelling. The roughness profiles are extracted from the digitized images of gypsum blocks used in the experimental studies and corresponding numerical models are also developed. Figure 4.8 shows the image of numerical model for a joint roughness in the range 6-8. Figure 4.9 shows the variation of $\left(\frac{V_j}{V_i}\right)$ with an increase in joint roughness value. It can be seen that the longitudinal wave velocity decreases with an increase in joint roughness.

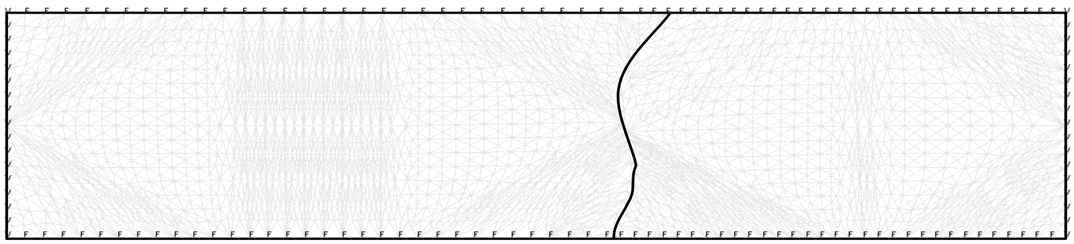

Figure 4.8: Numerical model with JRC value 6-8

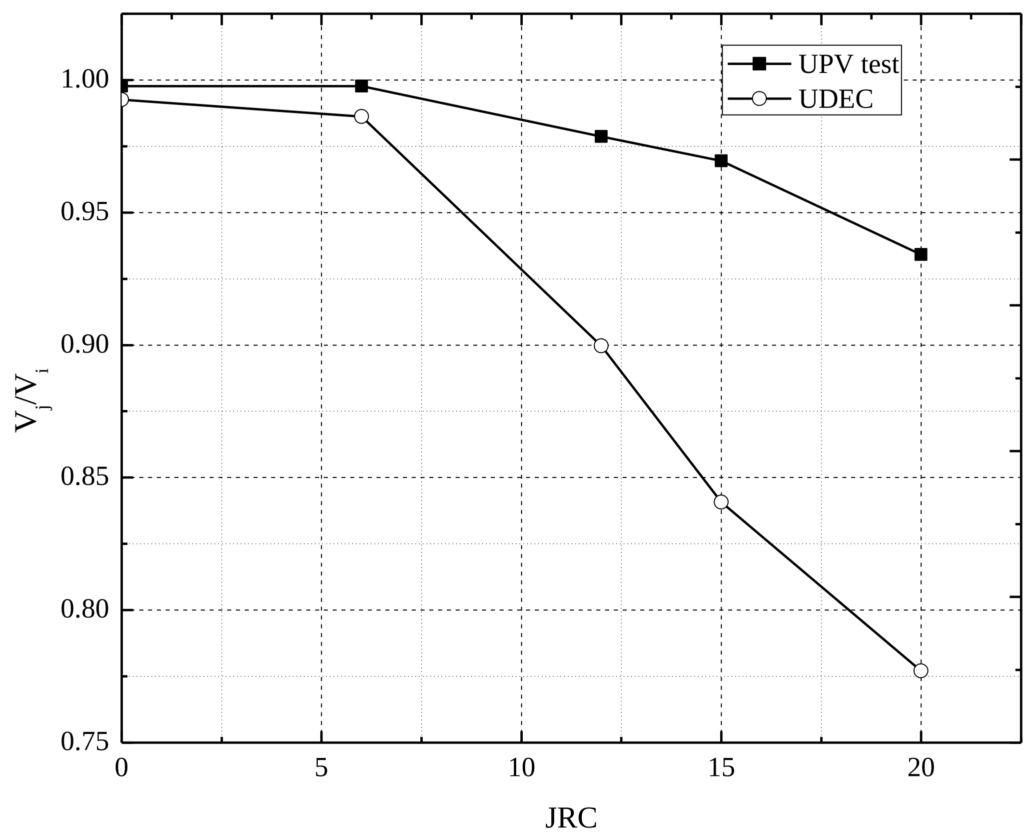

Figure 4.9: Variation of $\left(\frac{V_j}{V_i}\right)$ with increase in JRC values by UPV test and UDEC studies

The increase of joint roughness leads to an increase in the total joint area. Therefore, the decrease in longitudinal wave velocity can be attributed to the increase in the contact area, which leads to a reduction in contact stiffness. The variation $\left(\frac{V_j}{V_i}\right)$ for the frequency of 150 kHz is found to decrease slightly with increase in JRC according to the quadratic equation

$$\left(\frac{V_j}{V_i}\right) = 0.998 + 0.0013JRC - 0.00022(JRC)^2 \qquad \text{(Eq. 4.14)}$$

This variation in longitudinal wave velocity with JRC is found to be very small when studied for the high frequency which might be due to its high energy content. A similar result in the reduction of wave velocity with an increase in JRC value was observed by Kaharman (2002) and Mohd-Mordin et al. (2014). A parabolic relation between longitudinal wave velocity and joint roughness is observed by Kahraman (2002).

4.4.3 Block Length

Although the wave propagation pattern across different sample sizes has been studied by various researchers independently, the actual effect of the sample size is hardly analysed (Cai and Zhao, 2000; Sebastian, 2015). In the present study based on the numerical model, the effect of the block length, L_B with a centrally located joint is studied for a longitudinal wave propagating through the joint. Different blocks of length 0.2 m, 0.4 m, 1 m, 1.5 m, 2 m, 10 m, and 600 m are used in the study. For each block length, the variation of longitudinal wave velocity for a range of frequencies ranging from 1 Hz to 150 kHz is analysed. Figure 4.10 and 4.11 shows the variation of longitudinal wave velocities with frequency and wavelength for all block sizes. It can be noticed from Figure 4.10 that at lower frequencies, the effect of block length is predominant. As the block length increases, the longitudinal wave velocity increases. From Figure 4.11, it can be seen that this variation is an effect of block size and wavelength λ of the longitudinal wave.

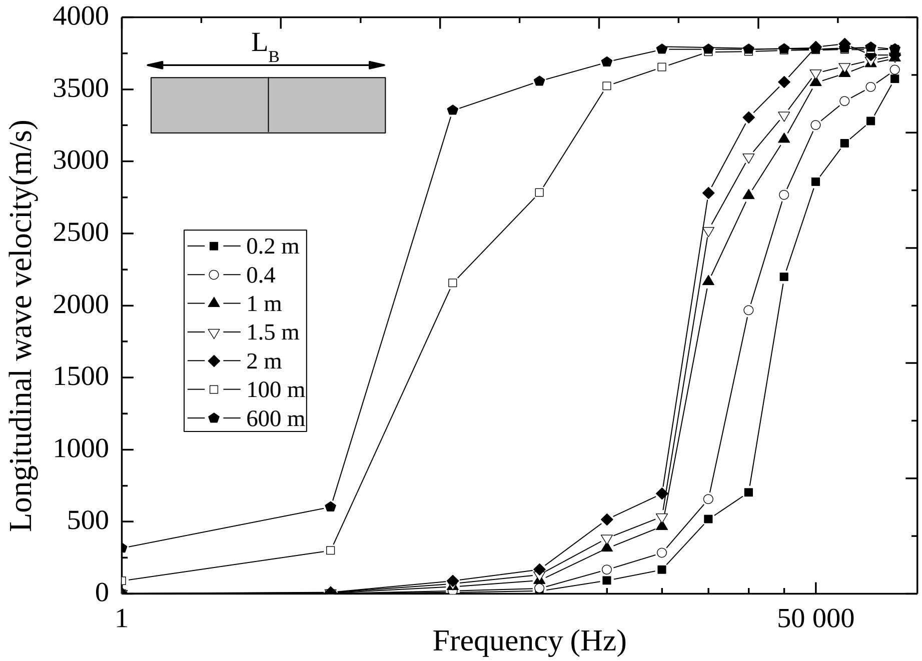

Figure 4.10: Variation of longitudinal wave velocity with frequency for different block sizes

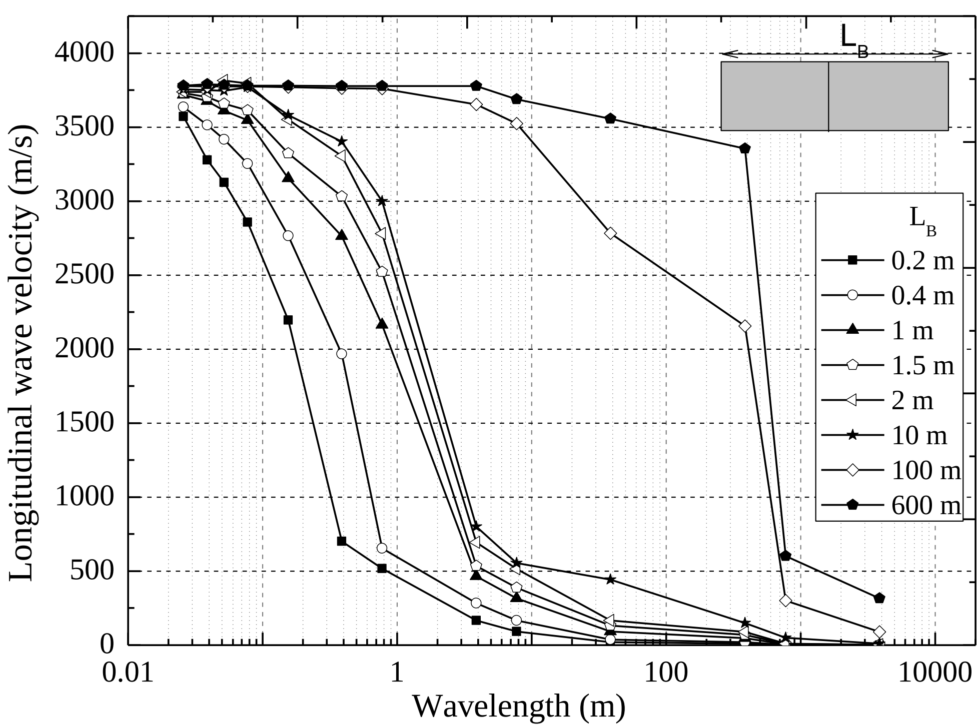

Figure 4.11: Variation of longitudinal wave velocity with wavelength for different block sizes

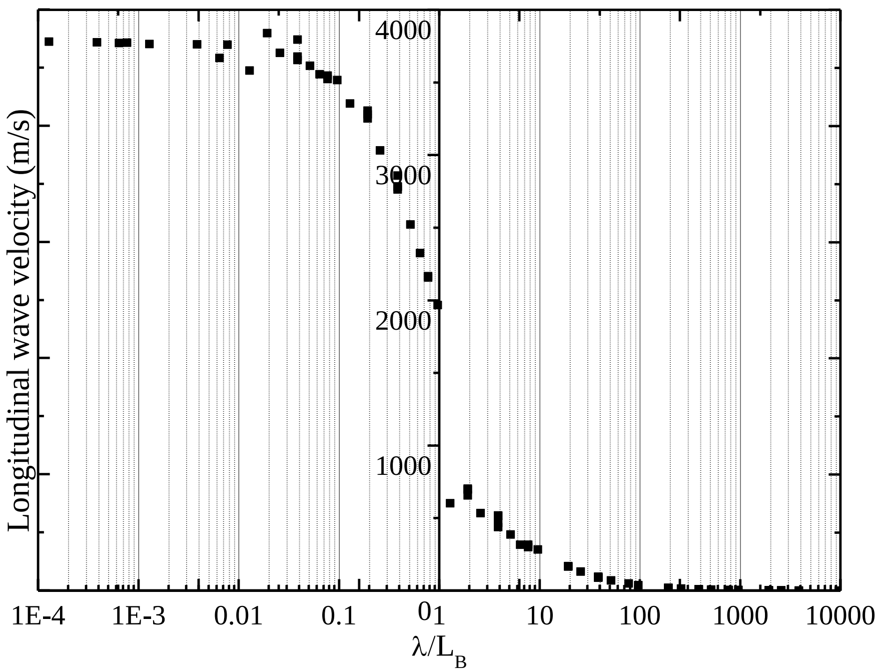

Figure 4.12: Variation of longitudinal wave velocity with change in wavelength to block length ratio

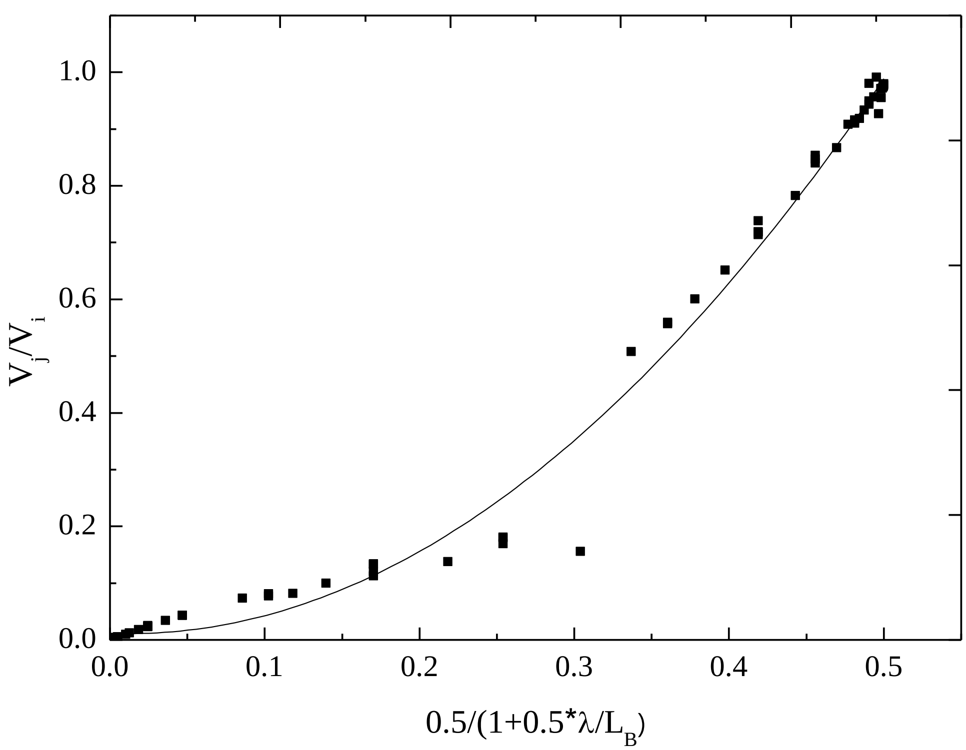

Figure 4.13: Variation of $\left(\frac{V_j}{V_i}\right)$ as a function of wavelength and block length

Figure 4.12 shows the variation of longitudinal wave velocity with a change in the ratio of wavelength to block length. A sudden change in longitudinal wave velocity can be seen when the ratio of wavelength to block length is equal to one. The value of the longitudinal wave velocity is higher and comparable to intact wave velocity when the ratio of λ/L_B is less than one. And a sudden decrease in wave velocity by 75% happens when the ratio λ/L_B is more than 1. This creates an important effect in the study with the measurement of longitudinal wave velocity especially through a joint. If the block length of the measured sample is not higher than the wavelength, then the value of longitudinal wave velocity will be much lower than the longitudinal wave velocity of the intact sample. A function of block length and wavelength is observed to follow an exponential relation, as shown in Figure 4.13. For a given block size and wavelength, $\left(\frac{V_j}{V_i}\right)$ is found to follow the relation,

$$\frac{V_j}{V_i} = 0.002 + 0.09 e^{\left(\frac{-\lambda}{30.27 L_B}\right)} + 0.9 e^{\left(\frac{-\lambda}{1.0362 L_B}\right)} \qquad \text{(Eq. 4.15)}$$

4.4.4 Joint Position

The effect of joint position on the longitudinal wave velocity has been studied by using numerical study for two block lengths of 2 m and 10 m. The joint position is varied over the length of the block. For the 2 m block, the joint position is changed from 0.2 m to 1.8 m with an increment of 0.2 m for each analysis. Similarly, 10 m block is analysed at joint positions 2 m, 5 m, 7m and 9 m. Figure 4.14 and 4.15 shows the variation of longitudinal wave velocity with the change in frequency for different joint positions. It is seen that at higher and lower frequencies, the positions of the joint play minimal effect. However, at intermediate frequencies of 100 Hz to 10 kHz, the variation of longitudinal wave velocity for the various joint positions are evident.

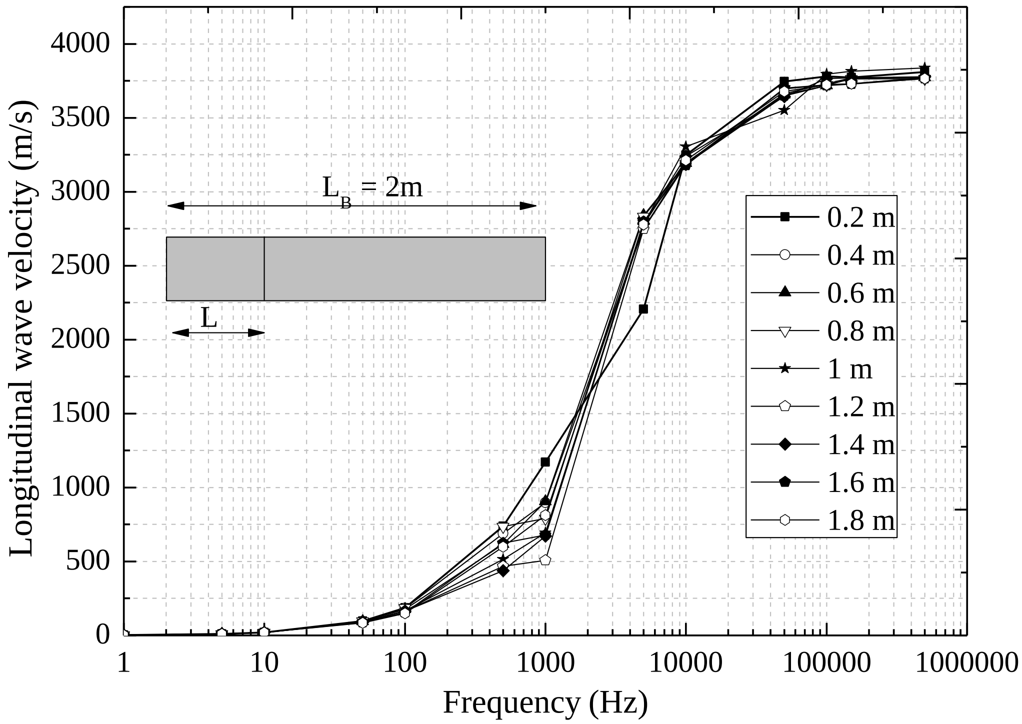

Figure 4.14: Variation of longitudinal wave velocity for 2 m block with change joint positions from 0.2 m to 1.8 m

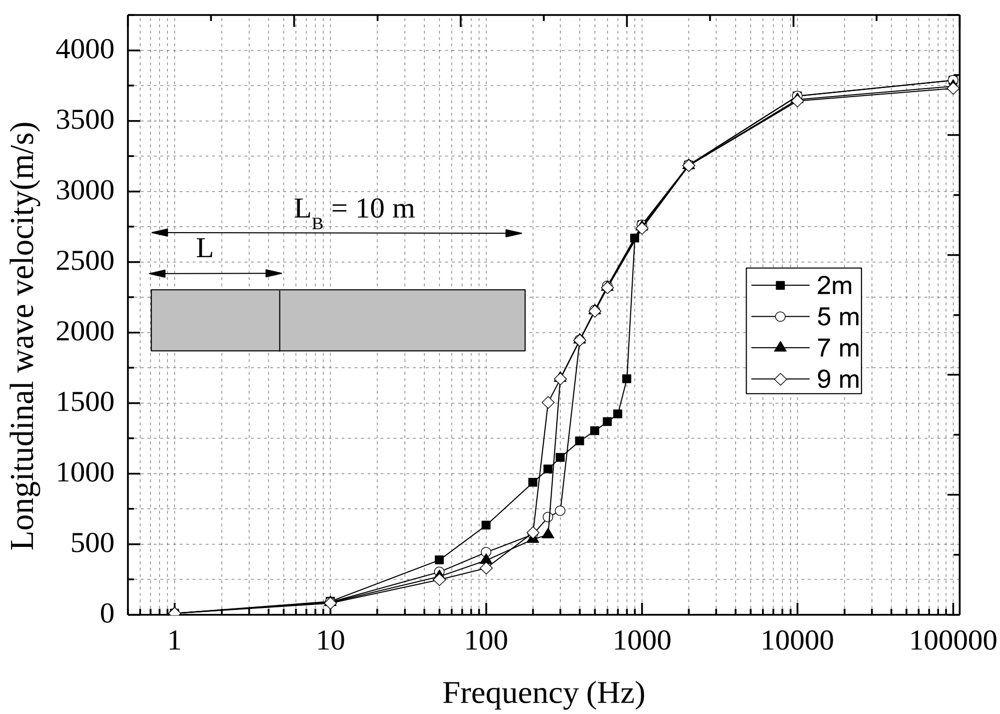

Figure 4.15: Variation of longitudinal wave velocity for 10 m block with change in joint position from 2 m to 9 m

A sudden shift in longitudinal wave velocity occurs when the joint position is half the wavelength of the applied longitudinal wave velocity. Longitudinal wave velocity of the transmitted wave shows a sudden decrease when the joint position is equal to half the wavelength. However, once the wavelength is more than the position of the joint from the source, the longitudinal wave velocity pattern is reversed. This might be due to the surpassing of a complete crust/ trough of the wave at the joint position. The longitudinal wave velocity pattern is reverted. The steep change of longitudinal wave velocity in the joint is a function of the wavelength and joint position. At high frequency, when the wavelength is smaller than joint position, longitudinal wave velocity is lowest for the nearest joint and increases with distance. However, this is reversed when the wavelength is smaller than the joint position. When λ is greater than L, the longitudinal wave velocity will be slightly higher for higher (L / L_B) ratio. However, when λ is less than L, longitudinal wave velocity of higher (L / L_B) will be comparatively lower. This can be observed in Figures 4.14 and 4.15. The distance to the joint in comparison with longitudinal wave velocity through joint and through intact rock for various wavelength can be given as:

$$\frac{V_j}{V_i} = 0.0481 + \frac{0.944}{0.561\left(1+10^{(1.634-\ln(\frac{2\lambda}{L})}\right)} \qquad \text{(Eq. 4.16)}$$

4.4.5 Number of joints

The presence of rock mass with just one joint is scarce. The behaviour of the wave changes as it propagates through each joint. So understanding the effect of multiple joints in wave velocity will help us in determining the wave behavior in a rock mass and also estimating the number of joint sets. Assuming here that the joints are all evenly spaced, the effect of wave propagation with the number of joints are studied. In this section, the effect of an increasing number of equally spaced joints on the longitudinal wave velocity is analysed for different wave frequencies. For this, a numerical study is conducted on a block of length 10 m. The number of joints is increased from 1 to 99, as shown in Figure 4.16.

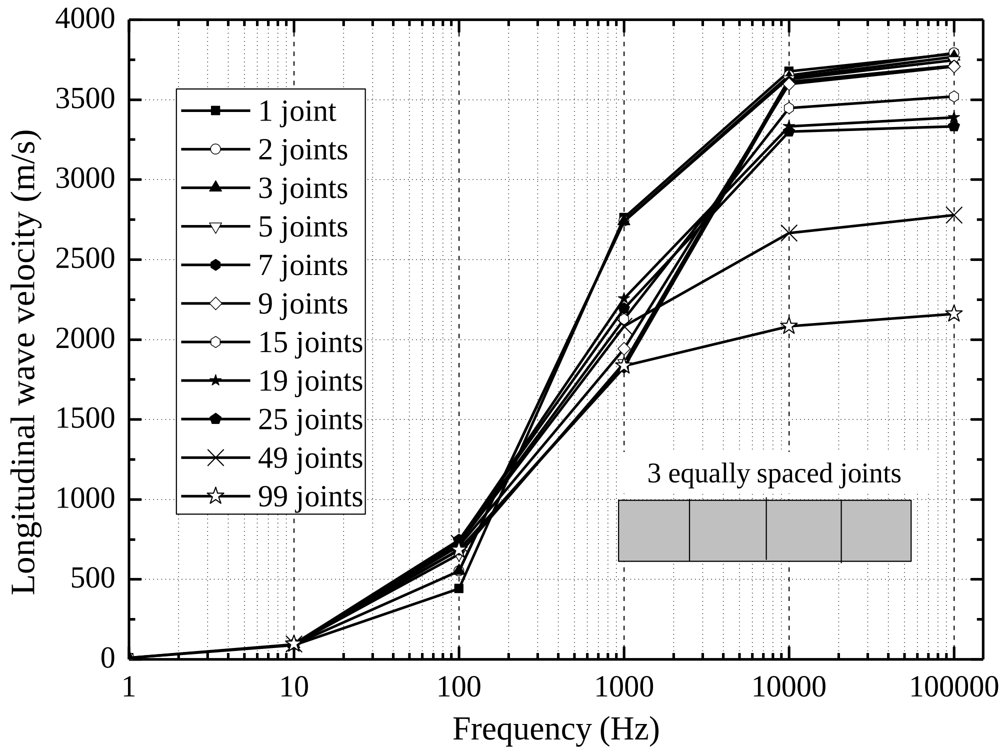

Figure 4.16: Variation of longitudinal wave velocity with the increase in number of equidistant joints

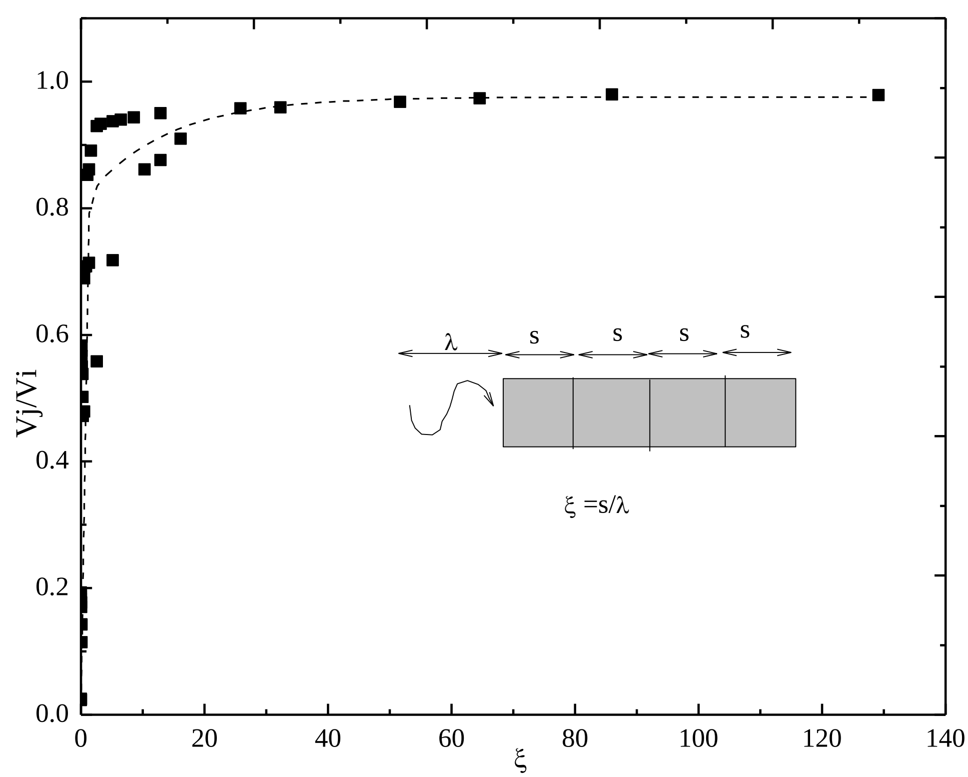

Figure 4.17: Variation of Vj/Vi with ξ

It can be seen from Figure 4.17 that at very high frequencies with an increase in number of joints, longitudinal wave velocity decreases. However, the effect of number of joints at low frequencies is not significant as λ/s value at low frequency will be higher than 1 under most circumstances. The reduction of longitudinal wave velocity for an increase in λ/s value is also observed by Sebastian and Sitharam (2016).

A parameter ξ is used to represent the spacing to wavelength ratio by Cai and Zhao (2000), where the spacing between the joints are equal. An exponential increase in the ratio of longitudinal wave velocity to intact wave velocity for change in spacing to wavelength ratio for equally spaced joints is found (Figure 4.17). The relation can be represented as

$$\frac{V_j}{V_i} = 0.97 - 68447.68e^{-\left(\frac{\xi+0.2}{0.016}\right)} - 0.88e^{-\left(\frac{\xi+0.2}{0.45}\right)} - 0.17e^{-\left(\frac{\xi+0.2}{13.11}\right)} \qquad \text{(Eq. 4.17)}$$

4.4.6 Multiple Parameters

The variation of longitudinal wave velocity as a function of the multiple parameters has been analysed to obtain a unified relation. Different functions correlating different parameters have been introduced. Cai and Zhao (2000) explained the importance of a critical and threshold value in the variation pattern of transmission coefficient in joints with multiple fractures with a change in the ratio of fracture spacing to wavelength. The value of transmission coefficient was found to decrease with an increase in the number of joints. A decrease and constant value followed an increase in the magnitude of transmission coefficient after attaining an individual peak transmission coefficient, which depended on the joint spacing to wavelength ratio.

Similarly, for each frequency, a critical and threshold value for joint spacing to block length is observed, as shown in Figure 4.18. A minimum value of longitudinal wave velocity exists for the given normalised joint stiffness at each frequency, which is called the critical spacing to block length ratio. And for each frequency, a certain ratio of joint spacing to block length exists after which the longitudinal wave velocity is a constant called the threshold value. An increase in longitudinal wave velocity occurs initially with an increase in spacing to length ratio. This increase is prominent for higher frequencies and negligible for lower frequencies.

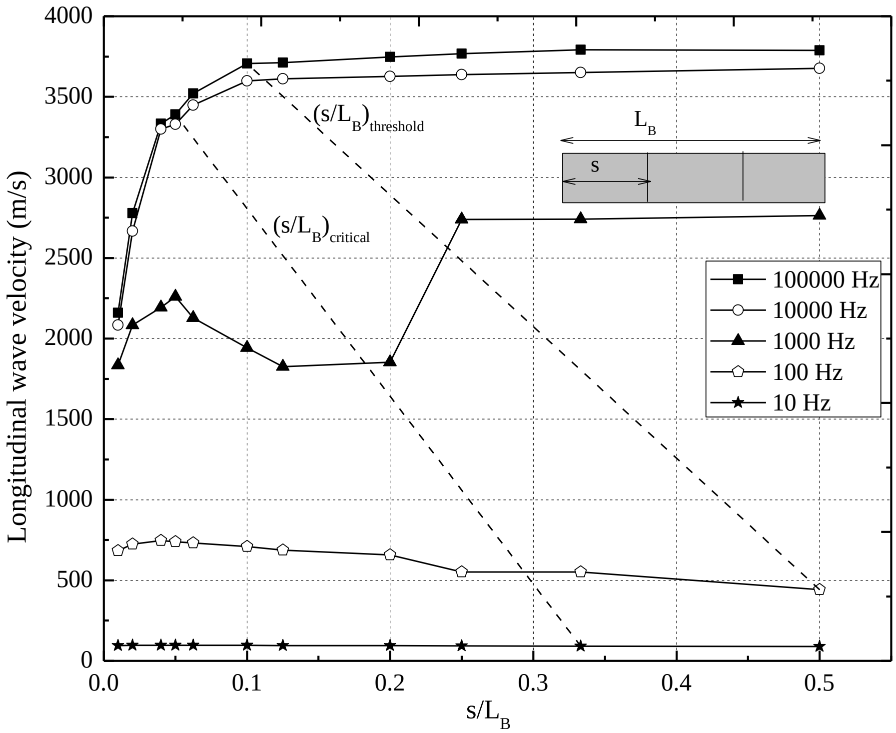

Figure 4.18: Variation of longitudinal wave velocity with spacing to block length ratio for each frequency

A function connecting joint position, block length and wavelength has been introduced and represented as ς

$$\varsigma = \frac{1}{\left(\frac{L}{L_B} + \frac{\lambda}{L}\right)} \quad \text{(Eq. 4.18)}$$

An exponential variation between $\left(\frac{V_j}{V_i}\right)$ and ς is obtained, as shown in Figure 4.19. The dimensionless function ς is found to have an exponential relation with the ratio of wave velocity through jointed rock to intact wave velocity. The effect of joint position, block length and wavelength on longitudinal wave velocity is mutually dependent, and it can be represented as

$$\frac{V_j}{V_i} = 0.993 - 0.49 e^{-\left(\frac{\varsigma - 5.166x10^{-5}}{0.635}\right)} \qquad \text{(Eq. 4.19)}$$

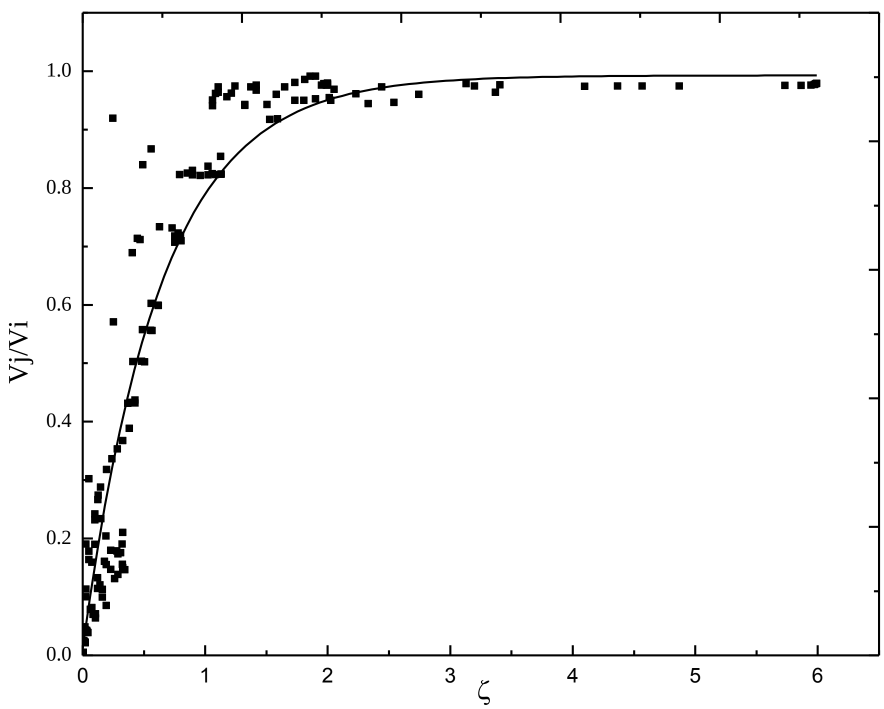

Figure 4.19: Variation of $\left(\frac{V_j}{V_i}\right)$ with change in ς

4.5 SUMMARY

A discontinuum approach is adopted for wave propagation study in jointed rocks. A numerical model is developed to analyse the longitudinal wave propagation by adopting properties similar to the experimental study. The material is modelled as elastic while the joints are assigned to follow the Coulomb slip condition. The numerical model is systematically validated with the experimental results along with analytical solution. It is found that the joint parameters affect a specific range of wave frequencies and not all ranges. A distinct variation in the wave velocity is observed for different frequency ranges.

Different joint parameters like angle, spacing, block length and corresponding roughness are found to play significant roles and dictate the wave characteristics in the rock mass. An increase in the longitudinal wave velocity occurs when the joint angle is more than $60^\circ$and can attain a velocity more than that of an intact rock. This is observed for very high and low frequency ranges but not for the intermediate frequency ranges. As the joint roughness coefficient increases, a non-linear decrease in longitudinal wave velocity occurs. The effect of block length is found to be dependent on the ratio of block length to the wavelength. A sudden decrease in the longitudinal wave velocity is found to occur when the ratio of block length to wavelength is less than one. For very long blocks, the longitudinal wave velocity in ideal condition is much higher than that of a small block in the same frequency. A definite shift in the velocity can be found when $\lambda/L_B=1$. The joint position affects the longitudinal wave velocity at intermediate frequencies, ranging from 10 Hz to 10000 Hz. The change in longitudinal wave velocity is significant at ultrasonic frequencies with an increase in the number of joints. Empirical correlations are also developed to predict the wave velocity with respect to joint characteristics.

CHAPTER 5

NUMERICAL MODELLING OF A TUNNEL IN JOINTED ROCKS SUBJECTED TO SEISMIC LOADING

5.1 INTRODUCTION

The dynamic load produced from sources like impact load, blasting, earthquake or any other, propagate through rocks in the form of waves. These waves travel through the media and affect different parts of the rock mass. Any structure built in/on the rock will be affected by the propagating wave. Thus a need in the analysis of tunnels or other underground structures in rock susceptible to the dynamic load. Many of the infrastructural projects are closely linked with the underground structures, such as utility tunnel, MRTS, hydropower cavern or a nuclear repository. This leads to the susceptibility of damage in the underground structure being a cause of major concern. The idea of underground structures being resistant to dynamic loading, especially earthquake, is commonly believed in the design community. However contrary to this belief, many underground structures have undergone damage under the action of earthquakes (Dowding and Rozen,1978; Owen and Scholl,1981; Sharma and Judd,1991; Power et al.,1998; and Kaneshiro et al.,2000).

Model studies have been performed by researchers to identify the performance of tunnels under dynamic loading conditions (Adyan et al., 1994; Kana et al., 1996; Genis and Adyan, 2002). In most of these studies, damages in rock tunnels occurred via a pre-existing discontinuity, that acted as a guiding medium for further damage. The discontinuity may occur in the form of faults, joints, folding, infilling or any other kind of anisotropy, which gives rise to weakness. Among these, joints are the most common and unavoidable, with high uncertainty regarding its properties, giving rise to highly complex behaviour in rocks. A jointed rock tunnel stable under static conditions, may or may not show the same behaviour under the action of dynamic loads. So, it becomes important to study the performance of rock jointed tunnels under seismic action. In this chapter, details of numerical modelling carried out on unsupported jointed rock tunnels under the action of earthquake loading are presented. The study extends to understand the effect of different stress conditions and joint properties like joint dip angle, joint stiffness and joint friction on the tunnel stability. The chapter highlights the strength degradation and instability in tunnels under seismic loads due to the presence of joints.

5.2 NUMERICAL ANALYSIS OF JOINTED ROCK TUNNEL UNDER SEISMIC LOAD

In order to understand the behaviour of the joints around a tunnel under earthquake loads, dynamic analysis of tunnel in jointed rock is carried out using distinct element code UDEC. A scaled model test of a case study by CNWRA to understand the behaviour of joint rock tunnels under seismic condition is considered. The experimental study was based on Lucky Friday Mine, USA. The site was scaled to 1/15 to understand the performance of those joints. The shake table was rigid in nature supported by rollers at the bottom, which help in initiating the shear displacements.

The numerical model is provided with dimensions same as that of the laboratory study reported by Ahola (1996) (Figure 5.1 and 5.2). The model dimensions are 122 cm length, breadth 122 cm and extending to a depth of 61 cm. Two joint sets of 5 cm spacing dipping 45º in the clockwise and anticlockwise direction with the horizontal are present. A tunnel of 15.2 cm diameter is introduced at the centre of the model. The top of the model is free and the bottom of the block, as well as sides of the block, are fixed to simulate a rigid shake table apparatus (Figure 5.1). The ingots used in the shake table experiment is similar to long beam element, continuous in the lateral direction. This agrees well with the numerical model in plane strain assumption. An insitu stress of 4.695 MPa and 10.941 MPa is applied in the horizontal and vertical directions, respectively. The material model is elastic to facilitate block displacements to be strictly by joint deformations and the joints adhere to Coulomb slip condition to allow the blocks to slide past each other. The properties of the model are given in Table 5.1 (Ahola et al.,1996 and Kana et al.,1997). Each of the blocks are meshed to triangular zones of size 1 cm. The joint properties used in numerical modelling were obtained from the psuedostatic and cyclic shearing tests conducted on the joints by Kana et al. (1997) and Ahola et al. (1996).

Table 5.1: Material properties of the rock and joints (Ahola et al.,1996)

Property	Values
Density	1682 kg/m^3
Bulk modulus	0.145 GPa
Shear modulus	0.129 GPa
Joint normal stiffness	0.7 GPa
Joint shear stiffness	0.5 GPa
Joint friction angle	25.56°

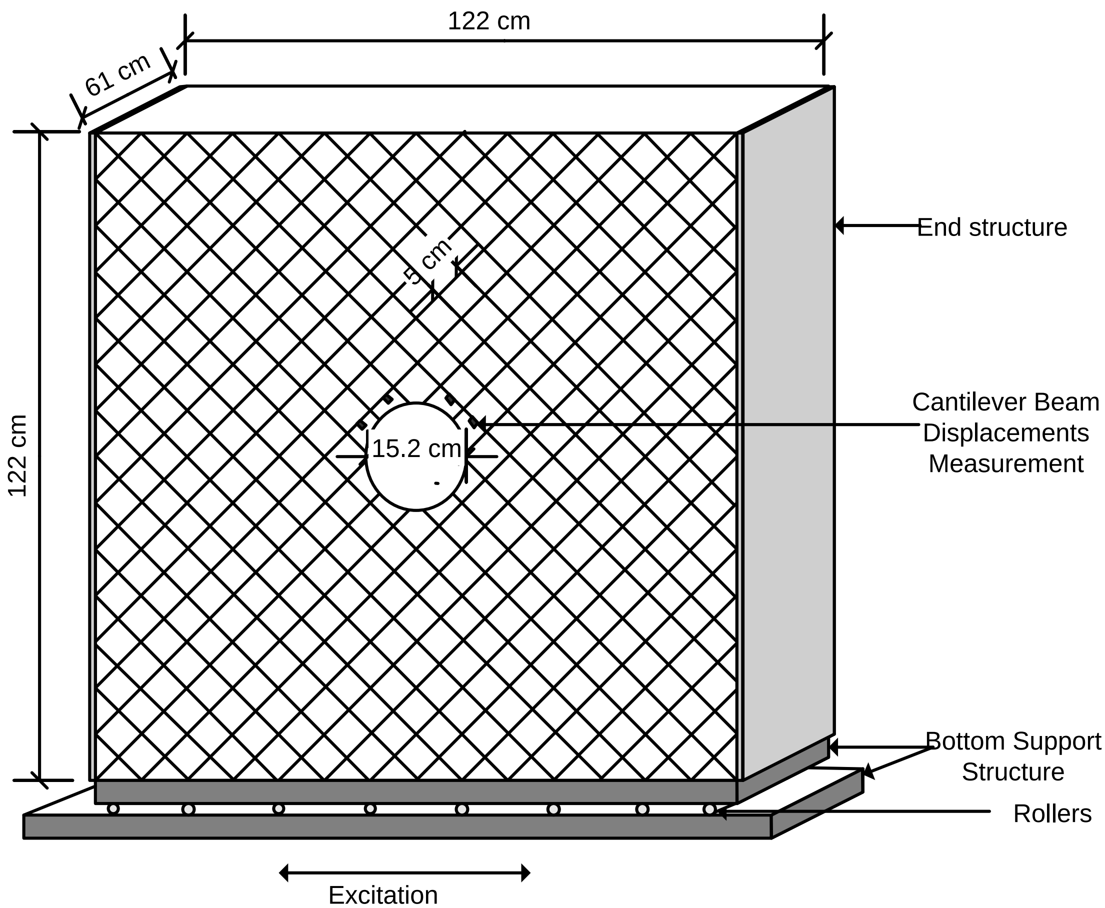

Figure 5.1: Representative image for the shake table experiment (Adopted and redrawn from Ahola et al.,1996)

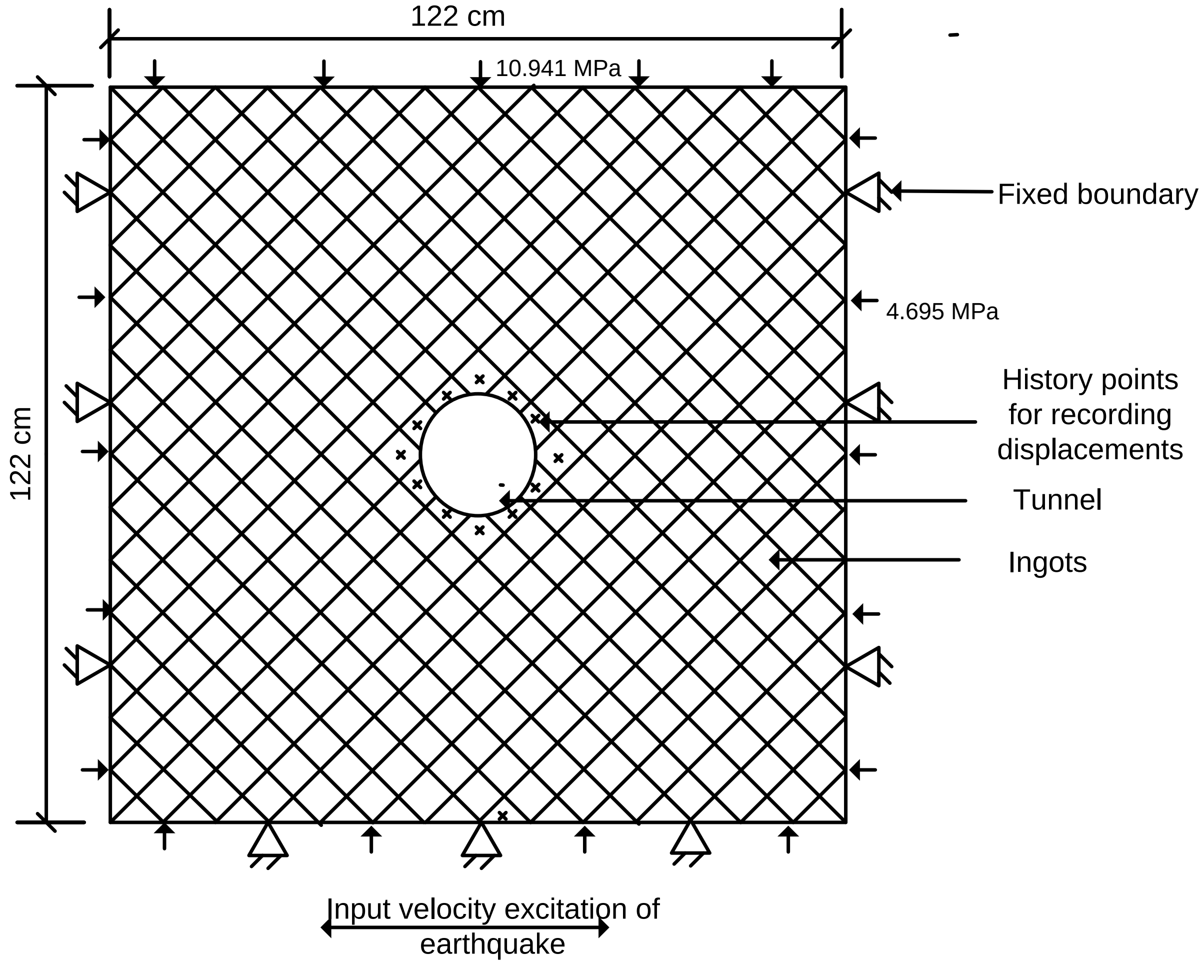

Figure 5.2: The numerical model for the scaled tunnel

5.2 SEISMIC INPUT

Seismic loading has been provided as a scaled value of September 1985, Mexico City earthquake on the bottom and sides of the model to validate it with the experimental study. The recorded accelerogram of 1985 Mexico earthquake is shown in Figure 5.3. The acceleration time history for the earthquake motion is obtained from accelerograms of the Guerrero array, and the motion in the south direction as published by COSMOS website is considered for the study. The acceleration time history is converted to velocity time history (Figure 5.4) and displacement time history (Figure 5.5). To understand the frequency content of the earthquake motion, Fourier spectra is obtained from the time history of acceleration, which is shown in Figure 5.6. It is found from the Fourier spectra that the frequency content of the input motion varies from 0.1 to 10 Hz and the Fourier amplitude predominately concentrates between 0.2 to 2 Hz. The fundamental frequency of rocky terrain in general ranges between 3 Hz to 5 Hz as Zulficar et al. (2012). However, for a jointed slope, the fundamental frequency is found to be about 2 Hz, according to Noorzad et al. (2008). Hence, the predominant frequency of the input motion is found to be close to the fundamental frequency of a typical jointed rocky terrain, which makes the considered model highly susceptible to the 1985 Mexico earthquake. The earthquake data was taken for a bracketed duration starting from 15 s to 45 s when the earthquake was predominant. Since the study is conducted on a scaled model and not field size model, the earthquake data for the bracketed duration is scaled down. The scaling down is done according to the similitude ratio for 1 g by Iai (1989). The scaling for velocity is calculated as

$$(\text{Scaled velocity})=(\text{Distance scaling factor})^{1.5} \text{ x } (\text{Actual velocity})$$

The scaled down value of the velocity and displacement for the bracketed duration are shown in Figure 5.7 and Figure 5.8, respectively. The earthquake loading was applied as velocity input. The scaled down velocity time history, as shown in Figure 5.7 is applied as the input for the numerical analysis. The shake table displacement obtained during this input is the same as in Figure 5.8. This is similar to the shake table displacement given as input in the laboratory experiment. The frequency of the original earthquake velocity is 0.464 Hz while the frequency of the scaled input velocity used for numerical model automatically increases to 1.798 Hz and follows the similitude ratio.

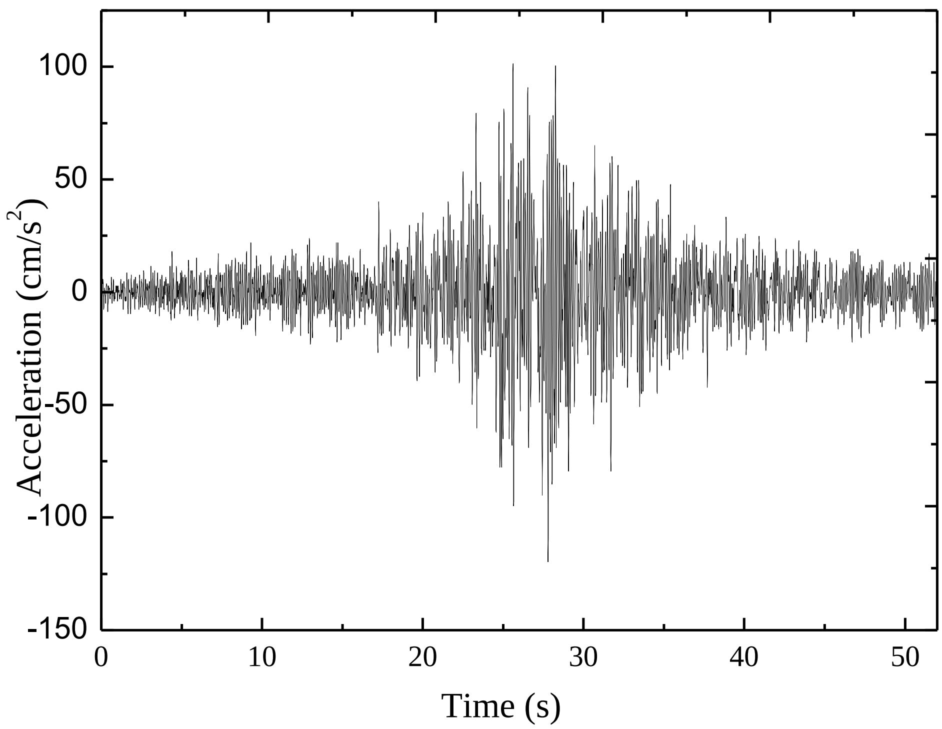

Figure 5.3: Time history of acceleration

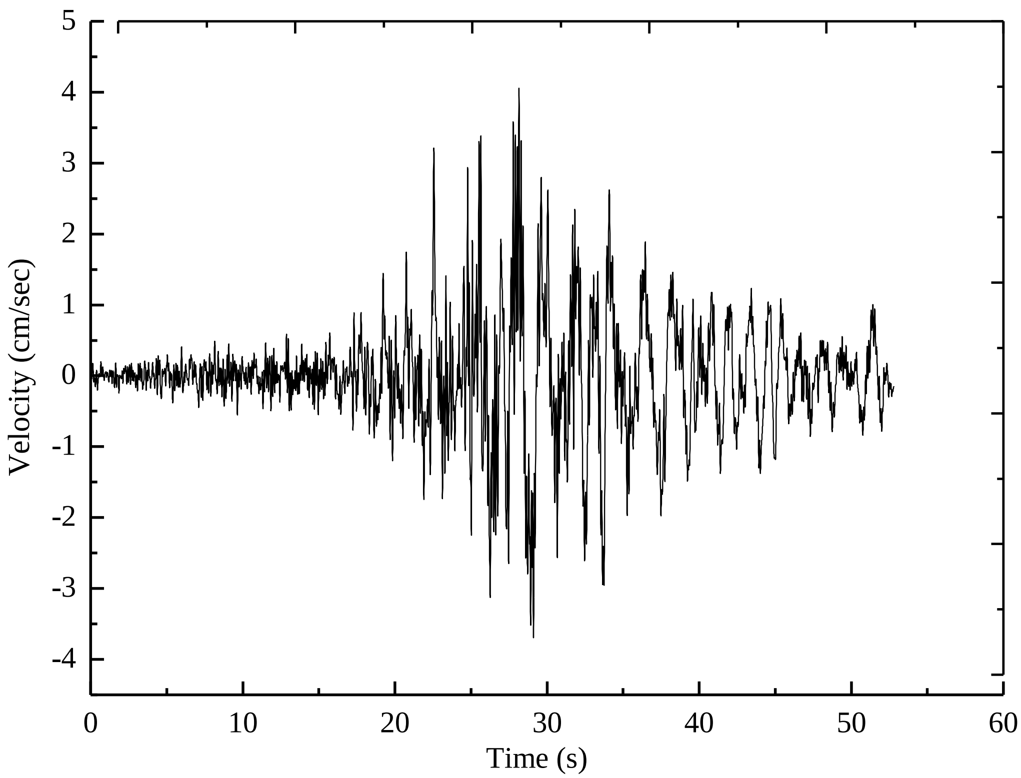

Figure 5.4: Velocity time history of the 1985 Mexico earthquake

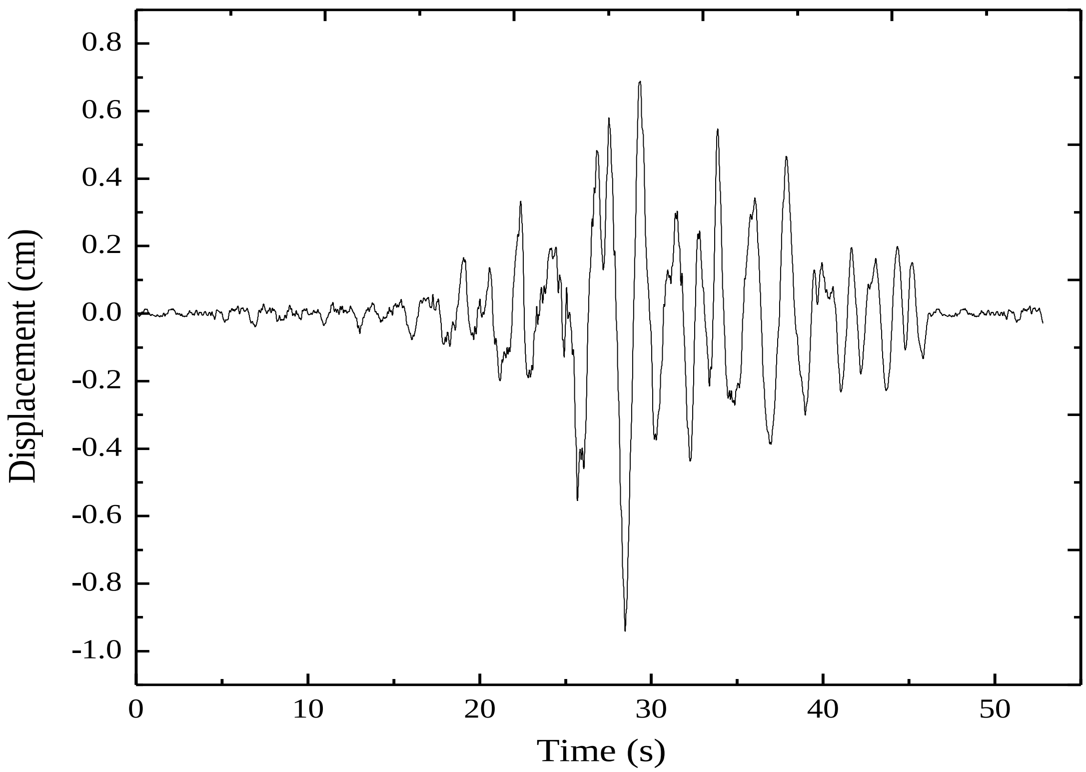

Figure 5.5: Displacement time history of the 1985 Mexico earthquake

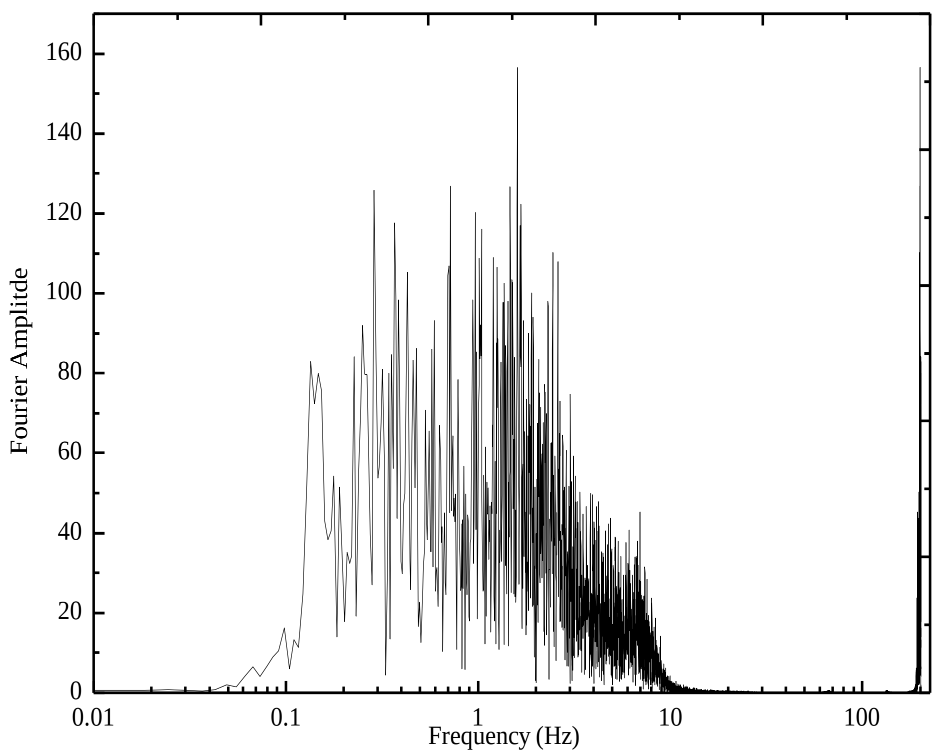

Figure 5.6: Fourier Spectra of recorded 1985 Mexico earthquake

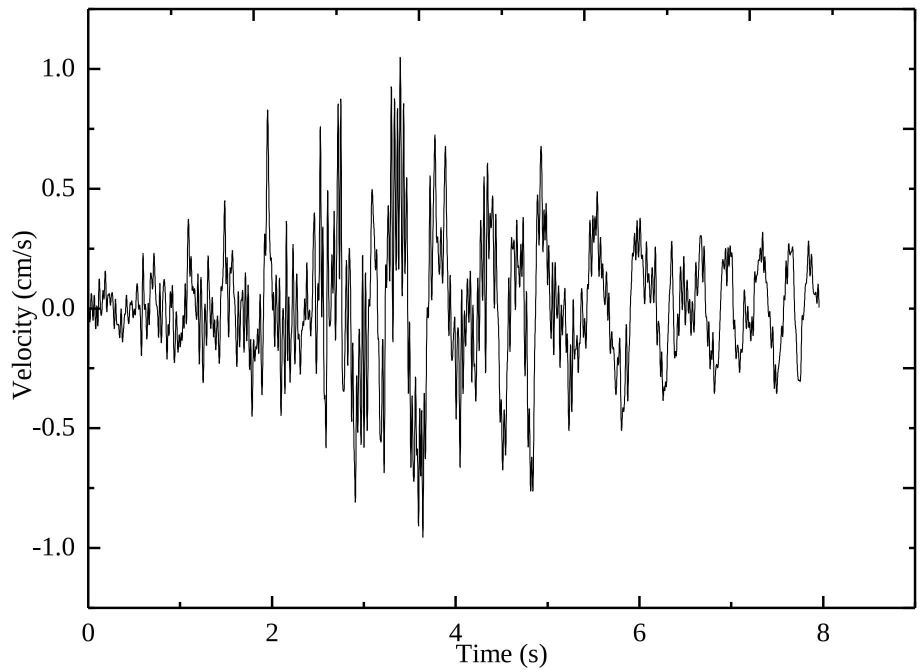

Figure 5.7: Scaled down velocity time history of the 1985 Mexico earthquake

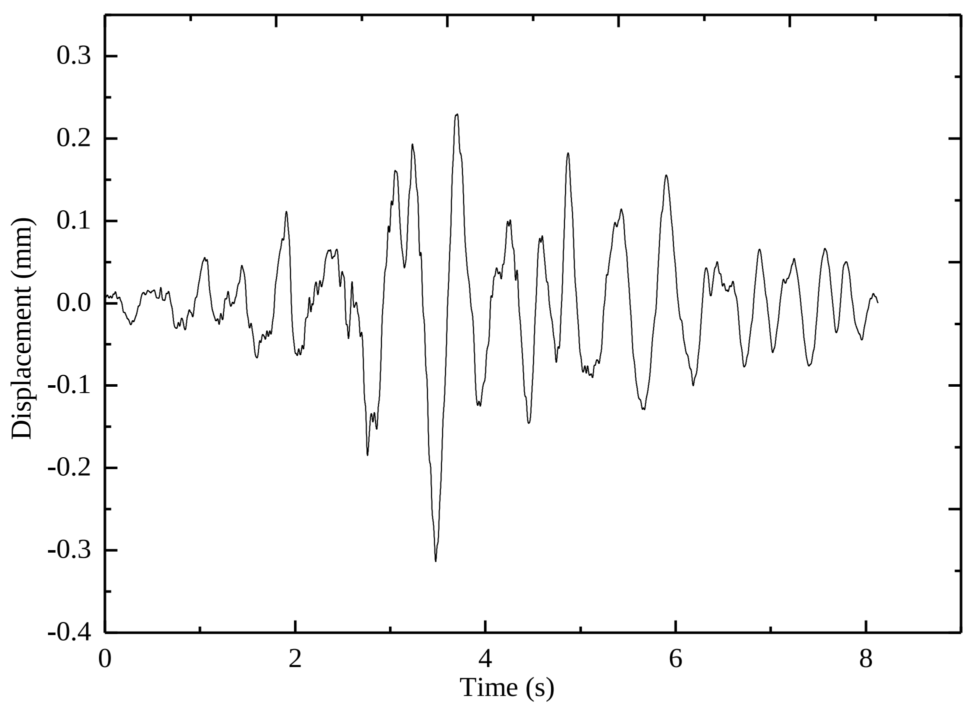

Figure 5.8: Scaled down displacement time history of the 1985 Mexico earthquake

5.4 VALIDATION WITH EXPERIMENTAL STUDY

The model is first analysed under static conditions before applying the earthquake input. To understand the threshold input displacement at which the block sliding initiate, several loading cycles are given with different scaled input motion. Each value repeated for four cycles. The maximum displacement of the shake table from the original position is increased to 3.8 mm, 7.6 mm, 11.7 mm and 15.5 mm. The deformations caused by sliding along the joints are found to be cumulative, and a threshold seismic displacement amplitude is identified. The deformations occurring around the tunnel are high above this threshold value. It is found to be 15.5 mm displacement of the shake table in crossing the threshold. During the application of earthquake loading, the deformations of the blocks in the tunnel periphery are recorded. Figure 5.9 shows the tunnel at the end of all loading cycles as obtained from the numerical analysis. The displacement of the top left ingot as marked in Figure 5.9 is compared with the displacement of the same ingot during experimental study is shown in Figure 5.10 It is found from Figure 5.10 that blocks on the top-left of the tunnel are found to slip down 4.5 mm after the 15th cycle of loading with the displacement amplitude to be 15.5 mm. The overall pattern of displacement is found to be similar, but the peak displacement value in UDEC is underestimated by 13%. But the numerical simulation is able to achieve the same threshold input value as the laboratory experiment.

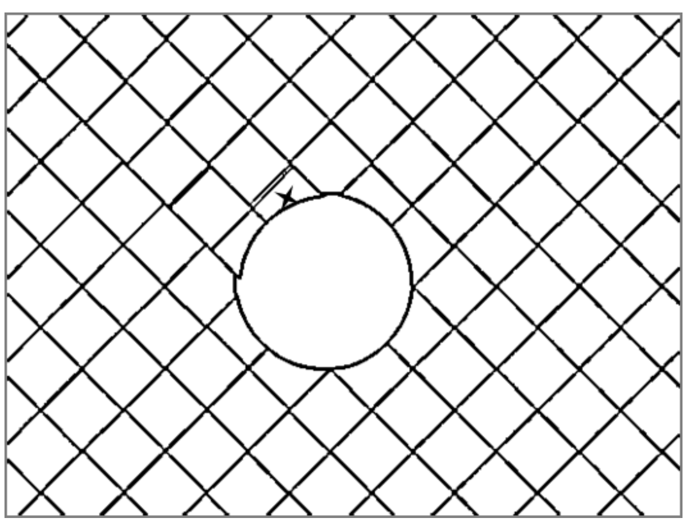

Figure 5.9: The ingot considered for validation

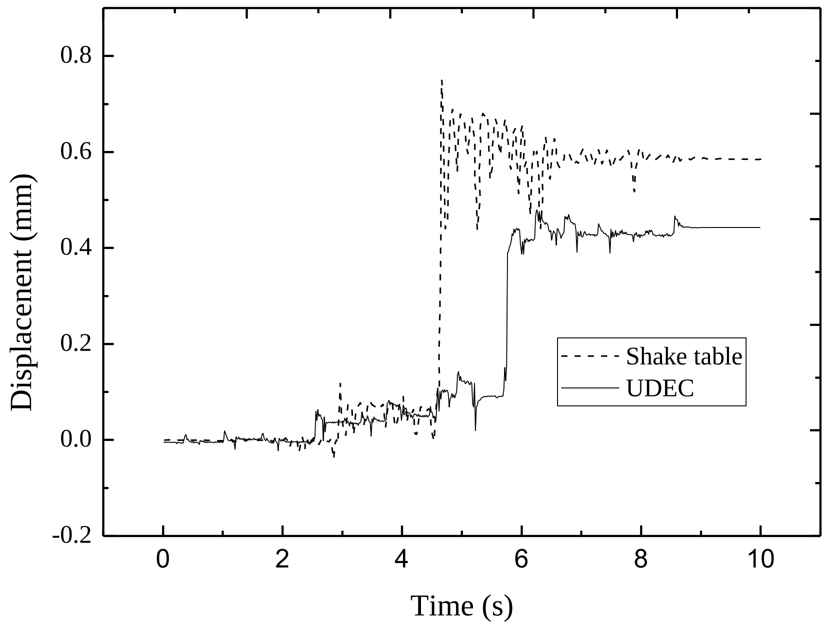

Figure 5.10: Comparison of displacements in the top left ingot from the experimental and the numerical analysis for the 13th cycle

5.5 TUNNEL DEFORMATION UNDER SEISMIC LOADING

Behaviour of the joints is highly dependent on the properties of the medium as well as the joints. So, understanding the effect of the seismic loads under different conditions are necessary. This numerical study is extended to understand the effect of different combinations of insitu stress, joint dip angle, joint stiffness and joint friction angle on this circular tunnel. In this study, the numerical analysis of a tunnel in jointed rock is carried out for a single cycle of the scaled Mexico earthquake loading lasting 10 s with a threshold displacement of 15.5 mm. The validated model has two joints, both having dip angle 45˚ with the horizontal, one clockwise and other anticlockwise direction, insitu stress of 10 MPa and 4 MPa in the vertical and horizontal direction, joint normal stiffness of 0.7 GPa/m and joint shear stiffness 0.5 GPa/m. So, all the parameters are kept same as the validated model, and only the parameter under consideration is changed. In the study, a tunnel is considered to fail if a block undergoes destressing or joint slip occurs. The tunnel is considered to be unsupported in nature due to its high stability under static conditions

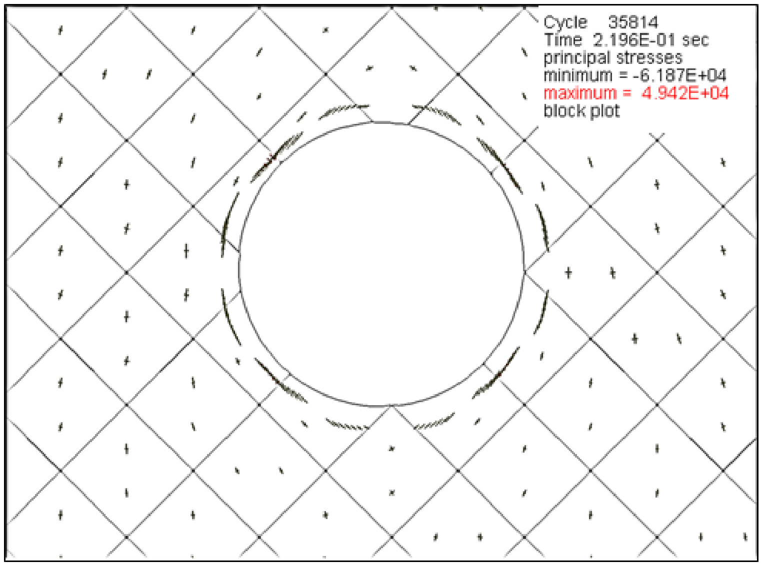

Figure 5.11: Stress concentration around the tunnel under static loading

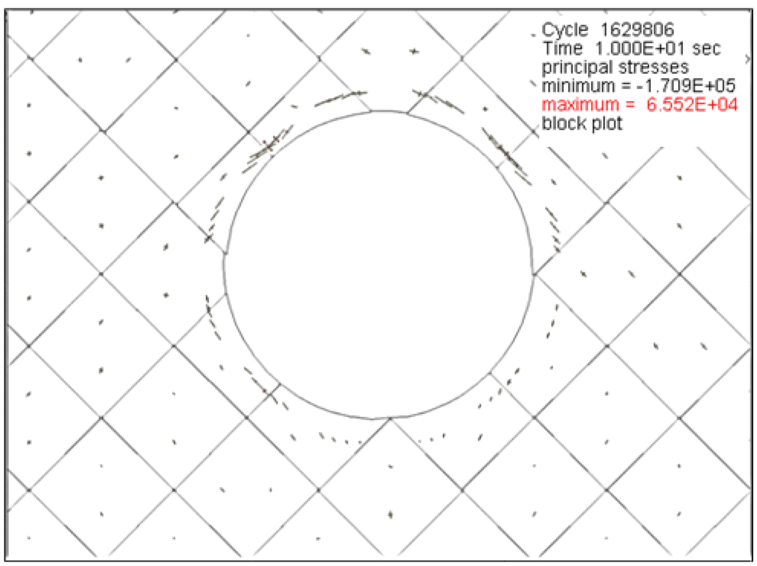

Figure 5.12: Stress concentration around the tunnel under seismic loading

Figure 5.11 and 5.12 shows the change in stress around the tunnel due to static and seismic loading. The joint slip and displacement can be observed on the sides of the crown block. This is due to the presence of the shear zone around the tunnel in an X shape as reported by Shen and Barton (1997) based on their study under static loading conditions. Under the static condition, stresses can be observed to be concentrated equally around the tunnel. However, additional stress concentrations around the tunnel after the application of earthquake load leads to stress redistribution. But the main stress concentrations still follow the X shape. It is evident from the destressing which occurred by displacements in the ingot (Figure 5.12). This destressing is due to the increase in tensile stresses, which leads to an increase in the principal stress values after dynamic loading.

5.5.1 Effect of Insitu Stress

The experimental study by Ahola et al. (1996) was done for a scaled model representing high insitu stress in the field. But under the urban scenario, where the tunnels are shallow, the insitu stresses acting on the tunnels are low. To understand the behaviour of jointed rock tunnels for all depths, the models are analysed for different combinations of insitu stresses. For shallow depth, the horizontal stress may be high compared to vertical stress. In other conditions, the horizontal stress may be lower than vertical stresses, when there is a structure above the ground. So the importance of the effect of insitu stress on the joints and the portion of the tunnel experiencing problems can be understood by considering the insitu stress effects. The study is done with different combinations of horizontal and vertical stresses. The ratio of horizontal stress to vertical stress is called lateral stress coefficient. Since the variation of change in lateral stress coefficient is a representation different of stress combinations, the results are given in terms of lateral stress coefficient.

Figure 5.13 shows the tunnel deformations under seismic loading when the lateral stress coefficient is varied from 0.1 to 1 for various horizontal stress conditions. It is found that, as the lateral stress coefficient increases, the tunnel deformations increase. Though the pattern of stress variation is similar for all horizontal stress values, at lower stresses, the blocks are found to undergo maximum deformation. This might be due to the fact that the blocks are relatively loose at lower confinement. For higher lateral stress coefficient, the deformations are lower for a given horizontal stress. Thus the destressing would be more prominent under higher lateral stress coefficient. But as the horizontal stress increases, the total stresses acting on the blocks will be higher for the same lateral stress coefficient value, hence producing less displacement and more stress concentration. The decrease in displacements around tunnel with the increase in insitu stress can be explained by the fact that the effect of stresses due to seismic loading has a smaller influence on the tunnel if it is approximately equal to or less than the existing stresses around the tunnel. Deng et al.

(2014) also obtained similar findings for tunnel deformation under blast loading under different insitu stress conditions. This implies that a tunnel at shallow depth is having more risk of failure than a deep seated tunnel. This result agrees well with Hashash (2002) and Deng et al. (2014). Maximum deformation with the present combination of stresses is found to be around 21 mm under the scaled earthquake load, whereas for static case, it is less than 0.3 mm. This accounts for 14% strain under seismic loads and is a very high value.

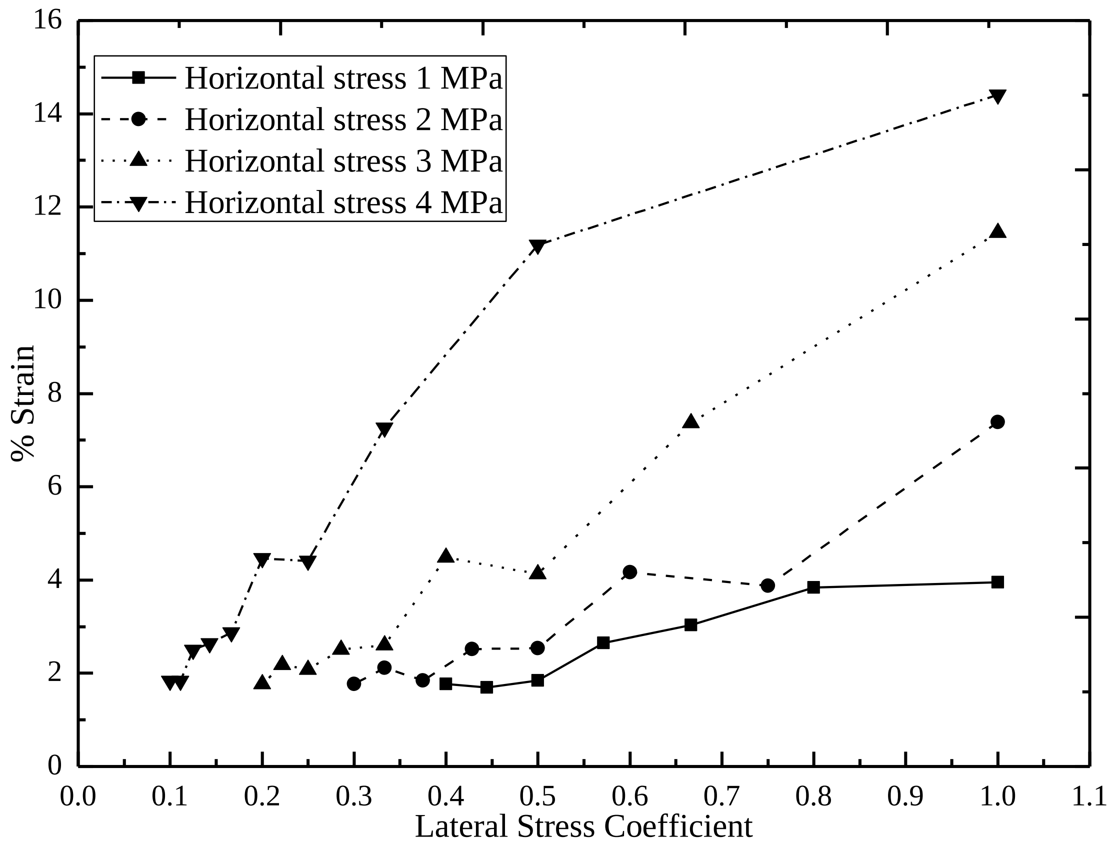

Figure 5.13: Effect of lateral stress coefficient on tunnel seismic deformation at different horizontal stress

5.5.2 Effect of Joint Properties

5.5.2.1 Joint Angle

The joint angle is varied to understand the effect of joint dip on the tunnel deformation and its effect at the surface. The study is conducted for all possible joint combinations by keeping the first joint angle constant and varying the second joint angle from 0º to 90º in the anticlockwise direction from horizontal. The first joint angle is varied from 0º to 90º clockwise with horizontal. The joint angle variations from 0 to 90˚ are only considered as the tunnel is circular and symmetric nature. Many blocks which are stable under static condition, loosened and failed on the application of seismic load. Figure 5.14, 5.15, 5.16 and 5.17 shows various joint combinations under static and seismic loading where the tunnels are stable under static loading (Figure 5.14a, 5.15a, 5.16a, 5.17a) while it failed under the application of a seismic load of scaled 1985 Mexico earthquake (Figure 5.14b, 5.15b, 5.16b, 5.17b). Figure 5.14 shows a tunnel in a joint set with one angle of 40º and the other 0º. The tunnel stable under static conditions had two key blocks from the side which move out during earthquake loading. In Figure 5.15(b) shows the tunnel with joint angle 40º and 10º stable under static loading in Figure 5.15(a) have a large part of the tunnel from left sidewall move into the tunnel. Figure 5.16(b) shows the failure of the tunnel with joint angles 50º and 0º under seismic loading compared to a stable tunnel under static condition. The blocks on the left bottom adjoining the tunnel periphery are found to undergo destressing and move into the tunnel during the application of seismic load. Figure 5.17(b), the tunnel in joint angles 50º and 10º has a key block from the left tunnel wall slide into the tunnel under the action of seismic load.

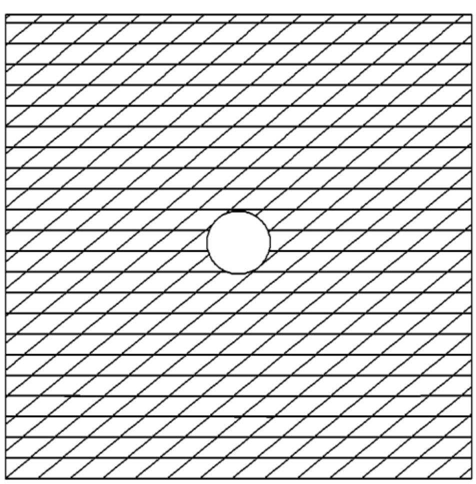

(a)

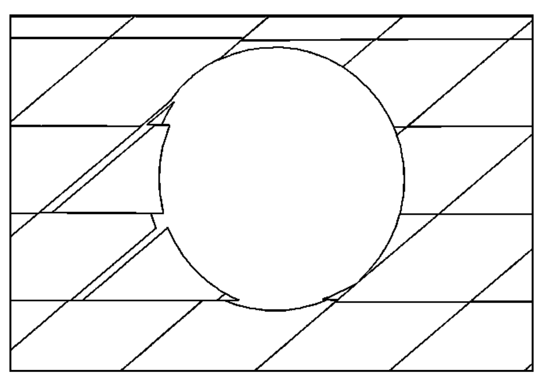

(b)

Figure 5.14: Model for first joint angle 40º and second angle 0º after (a) static loading (b) seismic loading as obtained from the numerical model

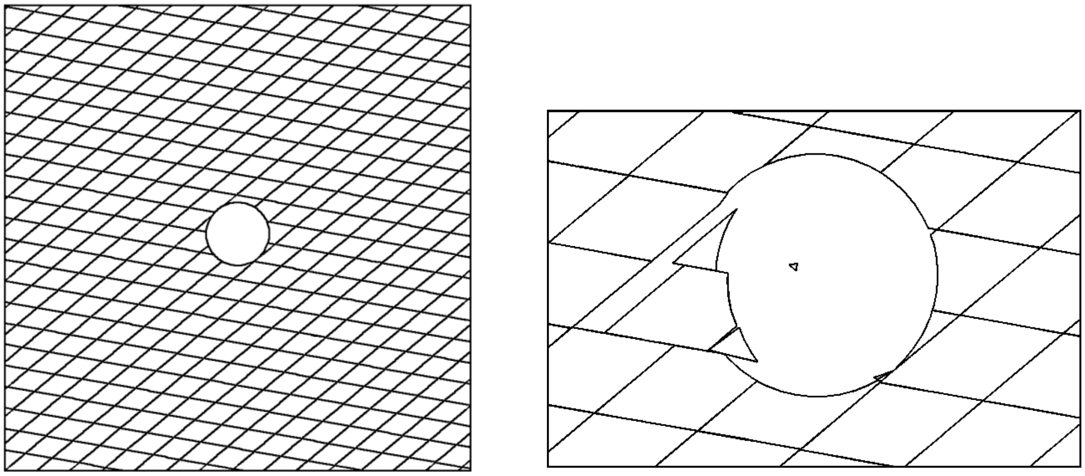

(a) (b)

Figure 5.15: Model for first joint angle 40º and second angle 10º after (a) static loading (b) seismic loading as obtained from the numerical model

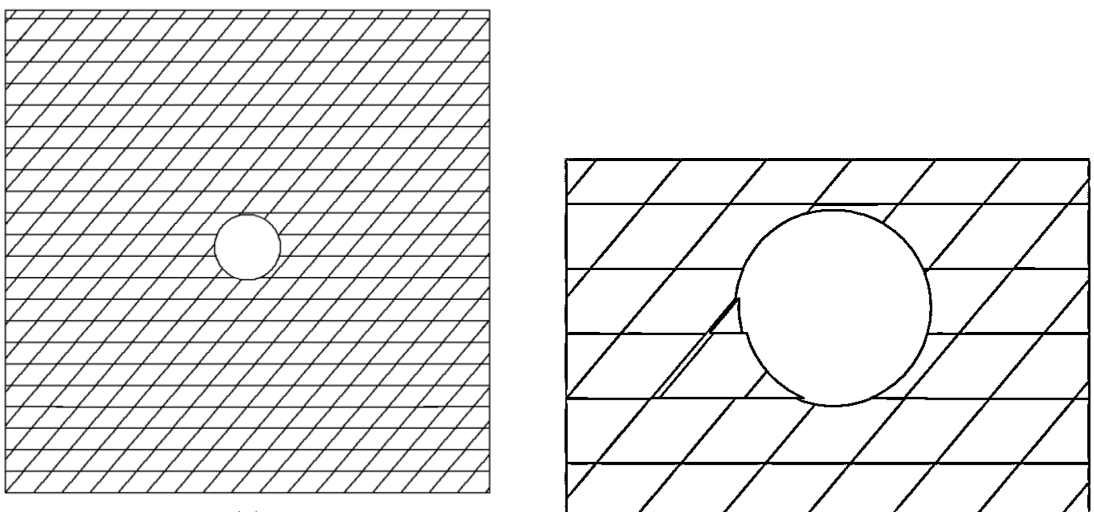

(a) (b)

Figure 5.16: Model for first joint angle 50º and second angle 0º after (a) static loading (b) seismic loading as obtained from the numerical model

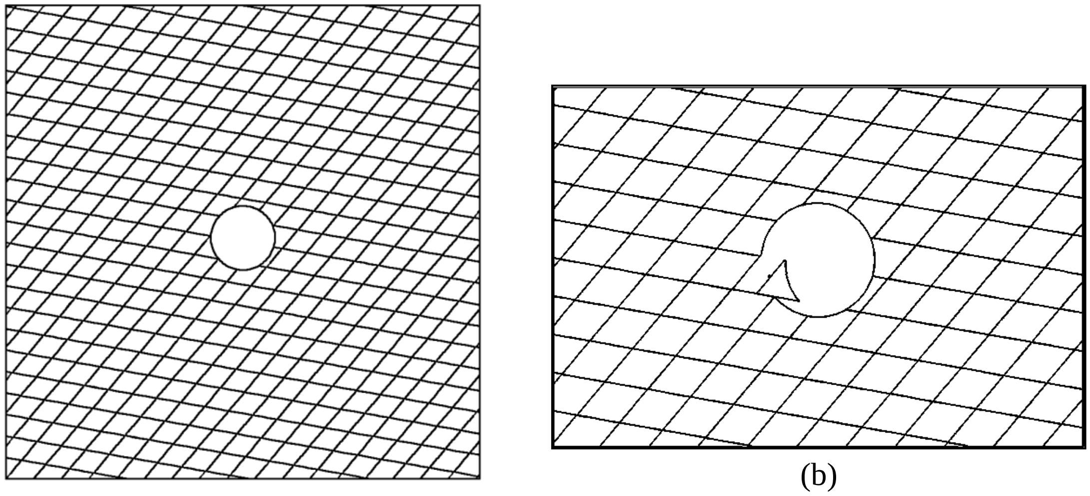

(b)

(a)

Figure 5.17: Model for first joint angle 50º and second angle 10º after (a) static loading (b) seismic loading as obtained from the numerical model

In most cases, the simulation stops because of joint overlap error, which occurs during UDEC analysis. This occurs as the overlap between the two blocks is higher than the permissible limit. In actual field condition, this collision of blocks may also lead to breakage of blocks. In the study, the joint angles are found to undergo loosening or separation, if one of the joint angles are around 40º and 60º with the horizontal. The maximum failure happens when one angle is between 0º and 20º while the second joint set at an angle between 40º and 60º, creating a wedge for the block to slide. It may be because the slips along joints are difficult when the angle created between the joints is less than the interjoint friction angle, which is equal to 35˚ in this case. Under these joint combinations, all the four angles in the blocks are greater than the joint friction angle. It is found that the left roof and sides of the tunnel experienced maximum deformation. Similar results are observed by Deng et al. (2014) in their study to understand the maximum peak particle velocity occurring at different parts of the tunnel for a blast occurring at the surface. Results from the study by Boon (2013) for his doctoral thesis also put light into the stability of unsupported tunnels with joint sets of varying dip. The study considered sliding failure for small joint spacings. With the list of joint angles adopted for the study and the toppling conditions obtained from it, the results of failure from the study for multiple joint combinations showed stability when the angles created by the joints are less than joint friction angle. Though this result is from a static condition, the seismic approach can be considered to be of a similar trend.

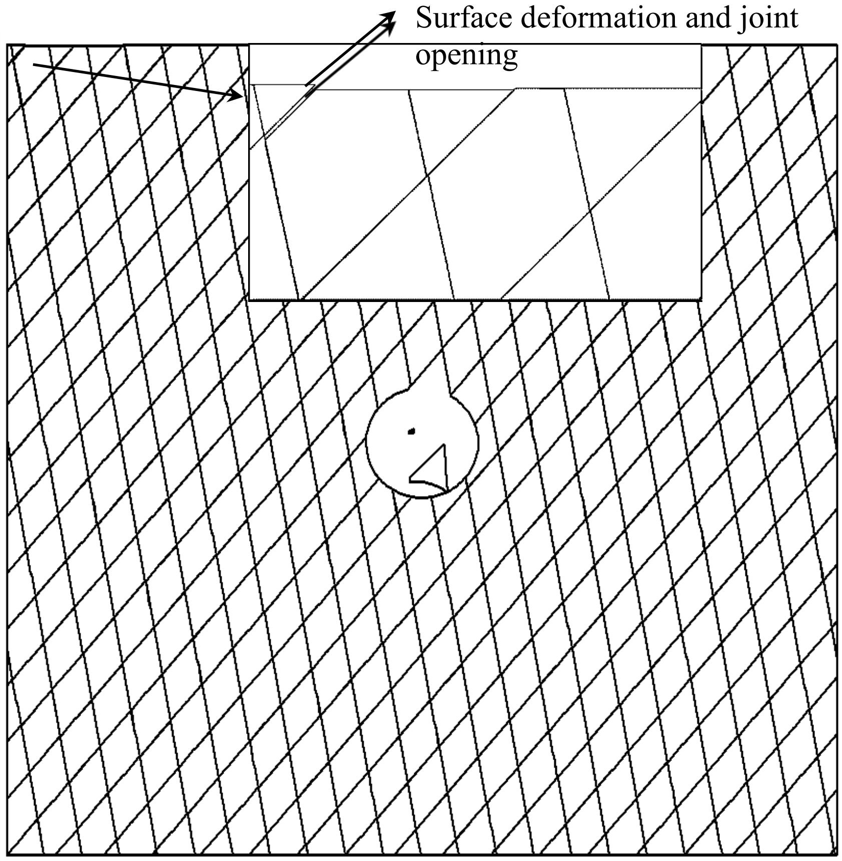

Figure 5.18: Surface deformation and joint opening under the action of seismic load when joint first joint angle is 50º and second is 80º as obtained from the numerical model

The joint angle variation from 0 to 90˚ has only been considered as the tunnel is circular and symmetric nature. Figures 5.18 and 5.19 show the surface settlement occurring under the action of the earthquake load. Surface settlements are found to occur in most cases due to readjustment of blocks even though the displacement at the tunnel periphery is negligible. Readjustment in the blocks happens as a part of the opening and closing of joints under the action of the earthquake load, as shown in Figure 5.18. It can be seen from Figure 5.18 and 5.19 that, the maximum surface displacement may not always occur above the crown as it is dependent on the joint angle. The surface settlements and the opening of joints at different portions of the model occurs due to the rearrangement and slippage of blocks, even if no specific damage is observed around the tunnel. The settlement near the boundary was noticed in most of the joint conditions. This is an effect of boundary conditions and a drawback with laboratory or numerical modelling. Under field conditions, this boundary settlements will be continuous or stepped.

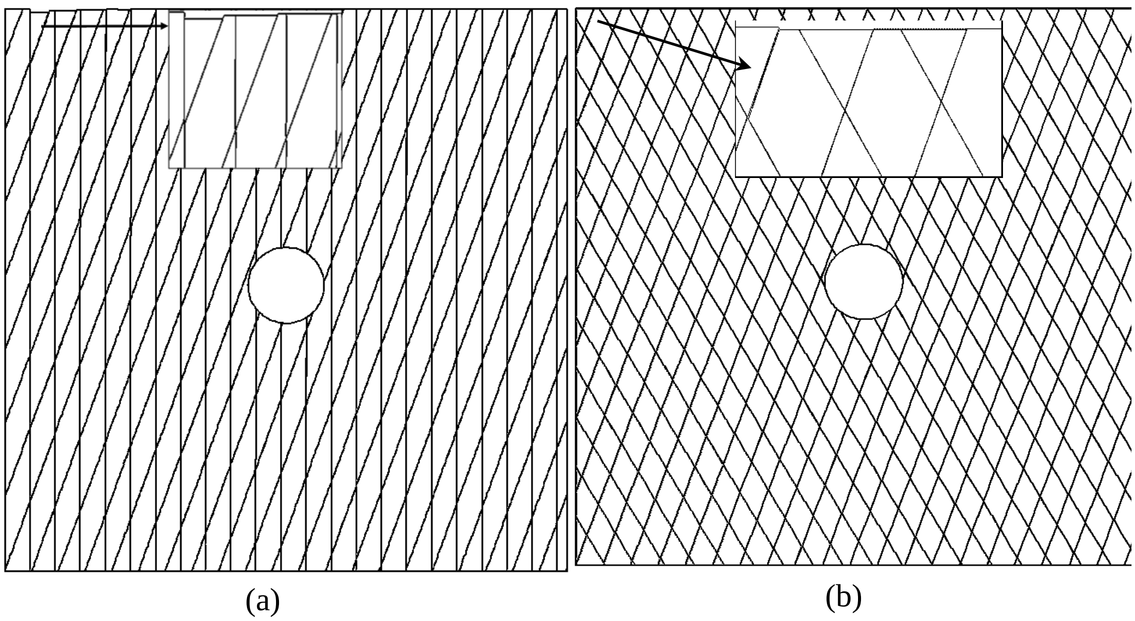

Figure 5.19: Surface settlement with no tunnel deformation as obtained from UDEC (a) first joint angle 90º and second 70º (b) first joint angle 70º and second angle 60º

5.5.2.2 Joint Stiffness

Joint stiffness is an important aspect which determines the slippage between joints. The value of joint stiffness adopted in the numerical study is often higher than the elastic modulus of the intact rock itself. But it is reasonable to use such a value, as the joint infilling material affects the joint stiffness value in the field which is not incorporated in the numerical model as indicated by Deng et al. (2014). In this study, the effect of deformation with the variation of joint normal stiffness and joint shear stiffness is studied. The joint normal stiffness is varied from 0.3 GPa/m to 1 GPa/m without changing the original joint shear stiffness value of 0.5 GPa/m. Figure 5.20 shows the variation of tunnel deformation with various joint normal stiffness values, both for static and seismic conditions. It is found from Figure 5.20 that, as the joint normal stiffness increases, tunnel deformation decreases. The variation in joint normal stiffness shows a direct relation with tunnel deformation. In the static case, the variation is mostly linear, but when the seismic load is applied, the deformation values decrease exponentially with the increase of joint stiffness, both at tunnel periphery and surface. As the normal stiffness value is varied from 0.6 GPa/m to 1 GPa/m, the variation is comparatively small for static and seismic loading. But for the variation from 0.3 GPa/m to 0.6 GPa/m, the effect on maximum deformation is drastic under seismic loading. A peak displacement of 5 mm is observed under the seismic condition for normal stiffness of 0.3 GPa/m compared to 0.5 mm deformation for the same stiffness under static condition. The studies by Park and Yoo (2014) also showed a great influence of joint stiffness on moment and shear forces acting around a jointed rock tunnel. Pyrak-Nolte (2016) explains the importance of fracture stiffness as one of the most important joint properties.

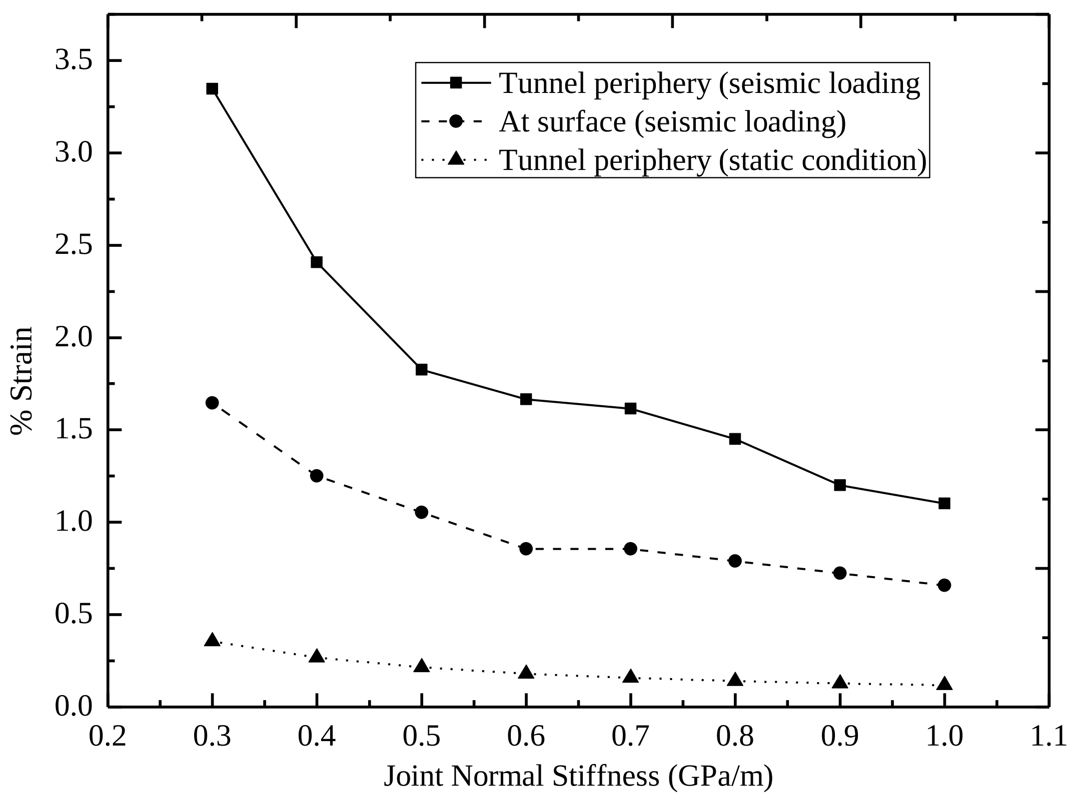

Figure 5.20: Effect of joint normal stiffness on static and seismic deformation of tunnels

Figure 5.21 shows the variation of deformation corresponding to changes in joint shear stiffness. Then joint shear stiffness is varied from 0.1 GPa/m to 1 GPa/m with a constant joint normal stiffness value of 0.7 GPa/m. But the variation of joint shear stiffness shows no considerable differences in the tunnel deformations both in static as well as in seismic situations. This result corresponds to the UDEC theory of interaction forces and displacements (Eq. 4.2 and 4.4) during joint slippage. According to the theory, shear forces on the contact are influenced by normal stiffness and friction angle. Similar results are reported by Yoo et al. (2017) for a single set of joints. Though the tunnel deformations have comparatively small effect with a change in shear stiffness, the increase in deformation under seismic loading conditions shows an increase of 5 mm from 0.25 mm under static conditions around the tunnel. This accounts for around 3% strain with reference to the tunnel diameter. Though these displacements look negligible in the scaled model, it corresponds to large displacements in the field. For the seismic loading a tunnel of 10 m diameter, for 3% strain, it will have 30 cm displacement of the blocks in seismic loading from 1.6 cm under static conditions. This clearly shows the instability of the tunnel under earthquake loading.

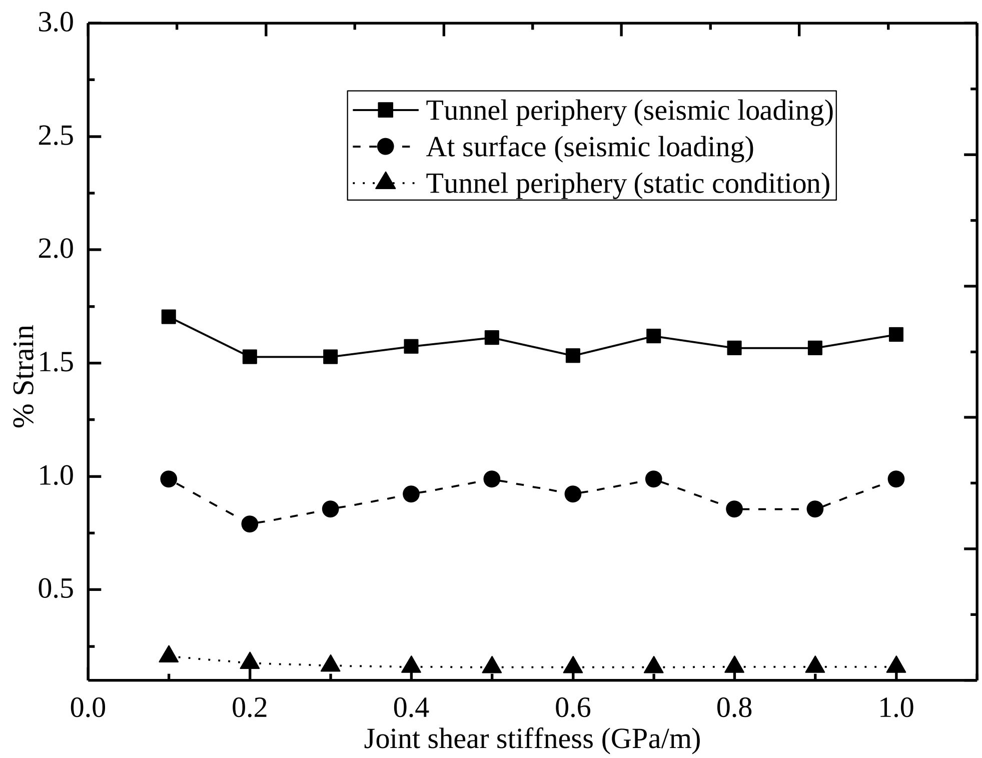

Figure 5.21: Effect of joint shear stiffness on static and seismic deformation of tunnels

5.5.2.3 Joint Friction Angle

The study is based on the tunnel deformation by interjoint slip, where the interjoint friction plays an important role. The variation of joint friction depends on the smoothness or roughness of the joints and the presence of infilling material. As the roughness decreases, the joint friction decreases and the effect of this change in joint friction on the joint slip has been studied. The joint friction angle was changed from 18˚ to 38˚assuming that the joint stiffness properties are not significantly affected in the above ranges of friction angle values. Figure 5.22 represents the variation in tunnel deformation with a change in friction angle for static and seismic cases.

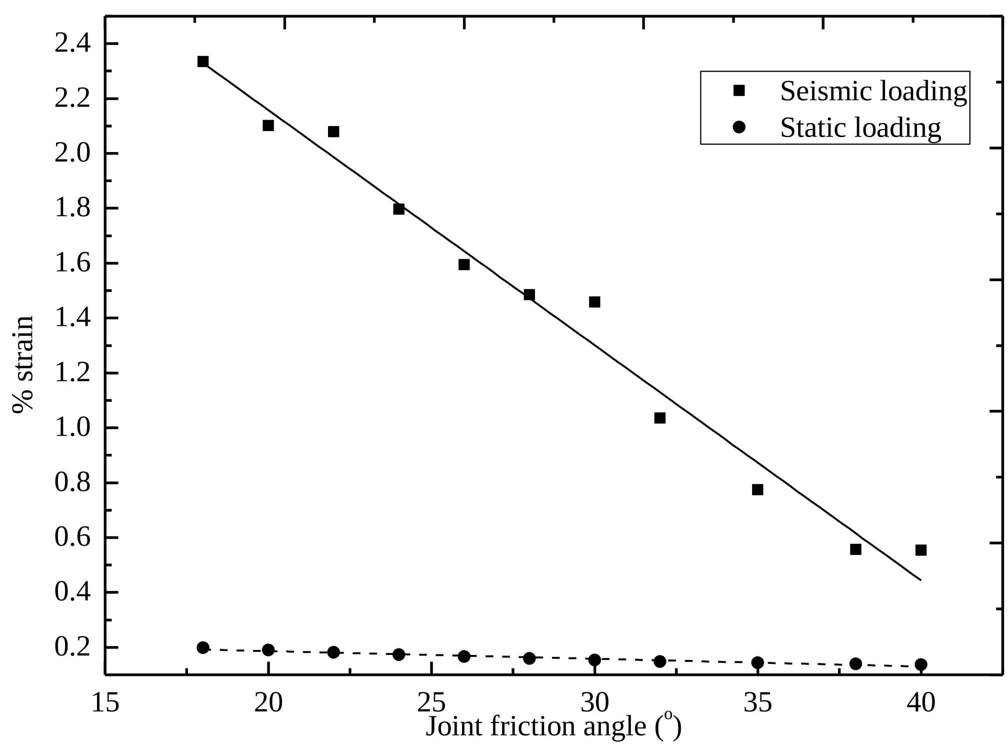

Figure 5.22: Tunnel deformation under seismic and static loading for various joint friction angles

From Figure 5.22, it can be observed that under static and seismic conditions, tunnel deformation linearly decreases with the increase in the joint friction angle. Since the deformation and failure allowed in the present study is only by joint slip, this directly reflects the effect of joint slippage with a change in joint friction angle. This decrease is much predominant in the case of seismic loading compared to static loading conditions. The slope of deformation in the case of seismic loading is much higher compared to that of static loading, indicating a steep increase of deformation with a decrease in angle of joint friction. The linear decrease is because the slippage is directly proportional tan φ. It can also be seen that the effect becomes more pronounced with the application of seismic load. The joint slip difference between static and seismic case is relatively less at higher friction angles.

5.6 SUMMARY

This chapter tries to understand the performance of unsupported tunnels in jointed rocks. A laboratory scale model of a tunnel is simulated in UDEC. The tunnel is subjected to scaled input motion of the 1985 Mexican earthquake. The numerical results are validated with the findings of the shake table experiment. Further, the developed numerical model is used to carry out parametric studies to understand the effect of insitu stress, joint orientation, joint stiffness and joint friction angle on the deformation and stability of the tunnel under the same earthquake input motion.

The tunnel was subjected to a series of repetitive loading to understand the threshold amplitude for deformations to occur. Displacements of joints are found to be cumulative under earthquake loads, and the tunnel fails after a series of repetitive loading. Increase in tunnel deformations under seismic loading shows that tunnels in jointed rocks are highly susceptible to earthquake loads. The tunnel deformation under static conditions is less than 0.1%, but under the action of seismic load, a considerable increase in tunnel deformations is observed, leading to complete failure in some cases. Deformations around the tunnel are found to increase with increasing lateral stress coefficients. For the same lateral stress coefficient, lower horizontal stress produces higher deformations. This implies that a tunnel at shallow depth is having a higher risk of failure than the deep tunnels. The joints that are stable under static conditions are found to fail under seismic loading, especially for some specific joint angle combinations. The joint angles are found to undergo loosening or separation if one of the joint angles are around 40º and 60º with the horizontal. The maximum failure happens when one angle is between 0º and 20º, while the second joint set is at an angle between 40º and 60º, forming a wedge for the block to slide. Under the action of seismic loads, with an increase in joint normal stiffness, the tunnel deformations are found to decrease exponentially unlike a linear decrease under the static case. The difference in tunnel deformation under seismic loading and static loading decreases as the joint stiffness value increases. Joint friction was also found to have a direct effect on the deformation patterns. With a decrease in joint friction angle, the joint slip is found to increase linearly. This increase is steep under seismic conditions compared to static conditions. The difference in tunnel deformation under static and seismic condition reduces for higher friction angles. Since the current chapter does not consider any support system, the next chapters incorporates the effect of the supports in the tunnel analysis under dynamic condition.

CHAPTER 6

PERFORMANCE OF ROCKBOLTS UNDER SEISMIC LOAD

6.1 INTRODUCTION

Support for the tunnel excavation is done using various methods. Kaiser et al. (1996) define the purpose of support as reinforcement, maintenance and retention. Commonly used support systems for underground openings are rockbolts, cables, steel mesh, shotcrete, strap lacing, tin liners, steel sets, shotcrete arches and concrete liners. Although the purpose of each of these systems is the same, its functions are fundamentally different. Amongst the specified methods, bolting is an economical and effective support technique. Its versatile nature and adaptability to the changing rock conditions make it the most commonly used support system for ground excavations. The basic design of the rockbolt is by following the simple structural mechanics principle of providing a strength higher than the weight of the unstable block. Well-designed rockbolts installed with grouting helps to strengthen its bond with the surrounding blocks and prevent corrosion.

Rockbolt designs are normally done for static conditions. Therefore, understanding their performance under dynamic conditions becomes necessary, especially when the purpose includes stabilisation of a joint. A continuous differential displacement between the blocks due to dynamic loading will lead to a change in performance of the bolts. Some studies have been carried out to understand the behaviour of underground openings supported with rockbolts in mining areas under 'rockburst' conditions (Kaiser and Cai, 2012; Stacey, 2011; Li et al., 2014) and under the effect of blast loading (Brummer et al., 1994; Li et al. 2016). However, these studies were done for very deep mines under high stress where failure can be catastrophic. Though many case studies focused on the effect of earthquake on a support system (Yu et al., 2013; Do et al., 2015; Yu et al., 2016; Lukic et al., 2017; Miao et al., 2018) and the performance of rockbolt under blasting or rockburst conditions (Goodman and Dubious, 1971; Tannant et al., 1995; Ortlepp and Stacey, 1998; Ortlepp, 2001; Mortazavi and Alavi, 2013; Wang et al., 2018; Zhang et al., 2018), study on the performance of rockbolt passing through joints under earthquake conditions is very limited. This understanding is vital in cases of rock structures posing a high risk and located in areas of seismicity. The study aims to understand the performance of rockbolts under different earthquake loads and its comparison with static conditions. The chapter highlights the stress and deformation behaviour of rock bolts and its efficiency while passing through joints.

6.2 ROCKBOLTING IN TUNNELS

The design of rockbolts based on empirical approaches mostly takes the depth of loosened rock and bolt parameters into consideration. In order to offer the necessary support, rockbolts are supposed to anchor beyond the loosened/ tension zone. The following factors are considered in the design of rockbolts (Panek, 1964; Barton et al., 1974; Lang and Bischoff, 1982; Hoek and Moy, 1993; Statens vegvesen, 2000; Ramamurthy, 2014; Li, 2017). As suggested by various researchers,

- Bolt length should be at least half of the blasting round length or one-third of the tunnel opening.
- The length of the rockbolt can be taken as

  $$L=B^{(2/3)} \quad \text{(Eq. 6.1)}$$

  The required length of rockbolt for various tunnel positions

Roof	$L=2+0.15B$	or	$L\leq 0.5H$	(Eq. 6.2)
Walls	$L=2+0.15H$	or	$L \leq 0.5B$	(Eq. 6.3)

  For relatively small failure zone, length of the rockbolt should be 1 m longer than the depth of the failure zone.
- The spacing of the bolts (distance between the bolts) should not be more than half to two third of the blast round length.
  or

  $$\text{Spacing. } S<L/2 \quad \text{(Eq. 6.4)}$$
- For untensioned rockbolts in the central span of a blocky rockmass excavation,

  $$L=1.4+0.184\ B \quad \text{(Eq. 6.5)}$$

  and rockbolt spacing is three to four times the mean joint spacing.
- Failure load per bolt in a laminated roof is calculated as

  $$T=S_1.S_2.t.\gamma.F \quad \text{(Eq. 6.6)}$$

Where, L is the length of the rockbolt, B is the span of the opening, H is the height of the opening, F is the factor of safety, γ is the density, S is the rockbolt spacing, and S_1 and S_2 are bolt spacings in two perpendicular directions.

6.3 ROCKBOLT FORMULATION IN THE NUMERICAL MODEL

The rockbolts are used to support an excavation against inelastic deformation along a discontinuity. UDEC considers rockbolts as two-dimensional elements with 3 degrees of freedom at each node (two displacements and one rotation). The rockbolts are installed and grouted using a bonding agent or grout to support it. Each rockbolt is divided into nodes of equal segmental length. The rockbolt is a linear elastic material until the yield stress is attained both in compressive and tensile directions. Figure 6.1(b) represents the material behaviour. Once the plastic moment is reached, the bolt starts yielding without further resistance. The mass of each segment is lumped at the nodes. The analysis of the nodes in response to axial, transverse and flexure loads with reference to Figure 6.1(a) is represented in matrix form as

$$\begin{bmatrix} T_1 \\ S_1 \\ M_1 \\ T_2 \\ S_2 \\ M_2 \end{bmatrix} = \frac{E}{L} \begin{bmatrix} A & 0 & 0 & -A & 0 & 0 \\ 0 & \frac{12I}{L^2} & \frac{6I}{L} & 0 & -\frac{12I}{L^2} & -\frac{6I}{L} \\ 0 & \frac{6I}{L} & 4I & 0 & -\frac{6I}{L} & 2I \\ -A & 0 & 0 & A & 0 & 0 \\ 0 & -\frac{12I}{L^2} & -\frac{6I}{L} & 0 & \frac{12I}{L^2} & -\frac{6I}{L} \\ 0 & -\frac{6I}{L} & 2I & 0 & -\frac{6I}{L} & 4I \end{bmatrix} \begin{bmatrix} u_1 \\ v_1 \\ \theta_1 \\ u_2 \\ v_2 \\ \theta_2 \end{bmatrix} \qquad \text{(Eq. 6.7)}$$

The defined plastic moment capacity controls the limit of internal moments. And beyond the user-defined tensile failure strain limit, the bolt breaks and separate at the nodes. The total plastic strain at every node is calculated according to the equation,

$$\varepsilon_{pl} = \sum \varepsilon_{pl}^{ax} + \sum \frac{d}{2} \frac{\theta_{pl}}{L} \qquad \text{(Eq. 6.8)}$$

where, d is the bolt diameter, L is the bolt segment length, θ is the average angular rotation over the rockbolt, ε_{pl} is the total plastic tensile strain and ε_{pl}^{ax} is the axial plastic strain accumulated based on the average strain acting on the rockbolt segment. Once the strain exceeds the limiting plastic strain, rockbolt is assumed to have failed, and the forces and moments on the bolt become zero.

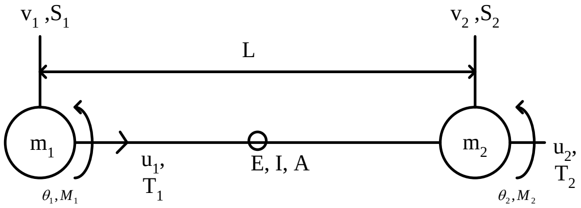

Figure 6.1(a): Structural element sign convention

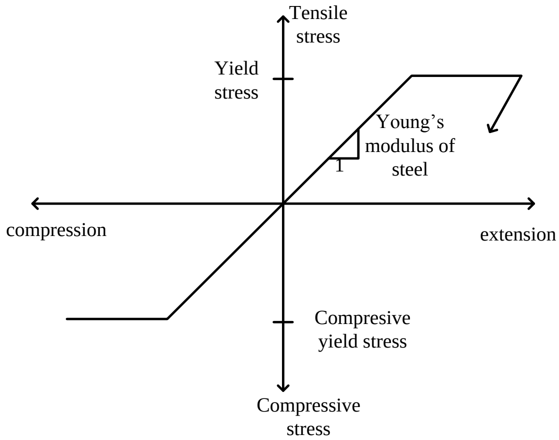

Figure 6.1(b): Material behaviour for rockbolts

The resistance is calculated between structural nodes and block zones by spring connections, as shown in Figure 6.2. The connector springs are nonlinear elements used to transfer motion and forces between rockbolt and gridpoint in the block zone. The coupling spring shear stiffness numerically describes the shear behaviour of the interface while coupling spring normal stiffness describes the normal behaviour. Figure 6.3 shows the working on shear stiffness and normal stiffness.

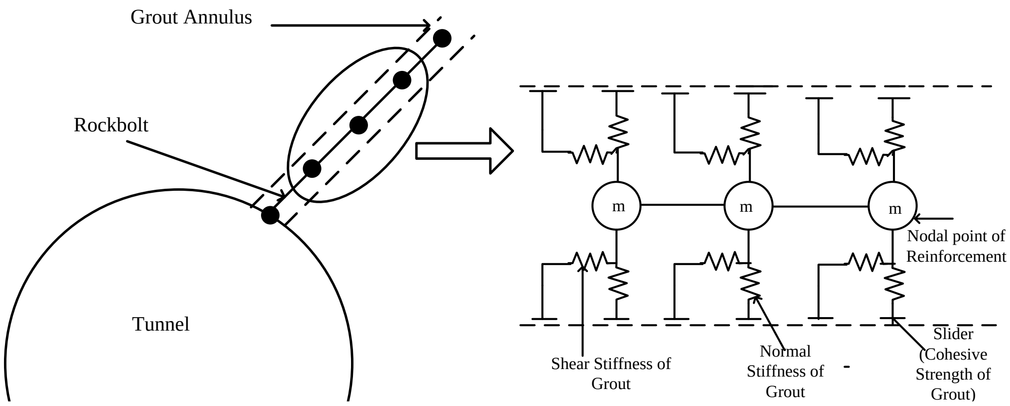

Figure 6.2: Conceptual mechanical representation of fully bonded reinforcement

The normal and shear forces acting on the spring elements are given by the equation

$$\frac{F_s}{L} = cs_{sstiff}\left(u_p - u_m\right) \qquad \text{(Eq. 6.9)}$$

$$\frac{F_n}{L} = cs_{nstiff}\left(u_p^n - u_m^n\right) \qquad \text{(Eq. 6.10)}$$

Where, F_s and F_n = the shear and normal forces developing on the respective springs

L= contributing element length

cs_{sstiff} and cs_{nstiff} = shear and normal stiffness on respective coupling springs

u_p = axial displacement of rockbolt

u_m =axial displacement of the rock

u_p^n =displacement of rockbolt normal to the axial direction of rockbolt

u_m^n =displacement of the rock normal to the axial direction of rockbolt

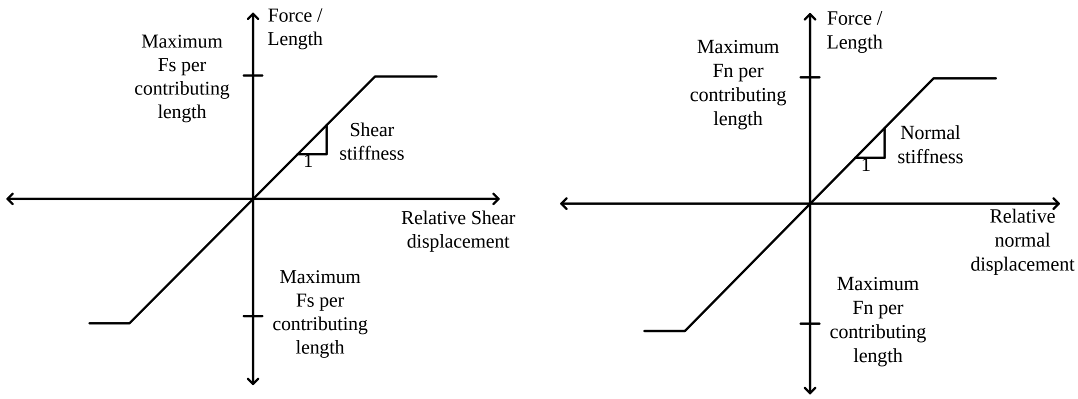

(a) (b)

Figure 6.3: Mechanical behaviour of (a) shear and (b) normal coupling springs in rockbolt

6.4 CASE STUDY

A tunnel case study from Tehri hydroelectric project in Uttarakhand, India is considered, which falls close to aMegathrust that separates the Indian and Eurasian plates. In this convergent tectonic zone, the major thrusts are Main Mantle Thrust (MMT), Main Central Thrust (MCT) and Main Boundary Thrust (MBT). They extend from the northwest of the Himalayas to southeast of the Himalayas. These fault lines being active has experienced many earthquakes in the past few decades including the recent Nepal 2015 earthquake with Richter scale magnitude 8.1. Besides, an earthquake of more than 8.5 Richter scale magnitude is anticipated in the near future, according to many scientists (Parija et al.,2018). The region also accommodates some important infrastructural projects like the bridges, tunnels and dams. Many important projects like the tallest arch bridge in the world and the longest tunnel are located in this region. Most of these projects are designed to be safe for seismic activity from 8 to 9 on the Richter scale and considered to be safe (Iyengar, 1993). The study of a rockbolt used as a support system in this area is considered to be beneficial. With these safety considerations, the performance of the tunnel support systems under earthquake conditions is proposed. Hence, an analysis of a head race tunnel hosted on a rockmass condition of two joint sets from Tehri dam site has been adopted for the study. The dam is placed in the seismic zone V of the Himalayan region. This dam project is under critical surveillance because of its position and ecological impact.

The Tehri dam owned by Tehri Hydro Development Corporation (THDC) India limited, is one of the highest hydroelectric dams in the world. It is located at Tehri in Uttarakhand, India, built over Bhagirathi river, with a capacity of 1000 MW. The dam consists of 4 headrace tunnels, of which one head race tunnel through region D is situated in a jointed rock bed as shown in Figure 6.4 (Final report on three-dimensional stress analysis of cavern at Tehri hydro dam project, U.P., 1999).

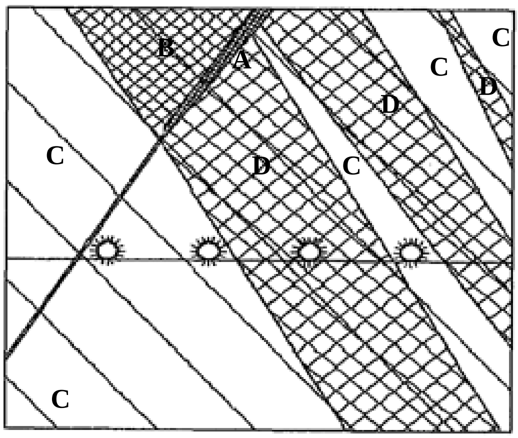

Figure 6.4: Geological region of the headrace tunnel

Table 6.1 : Properties of material in zone D

Parameter	Value
Density (kg/m^3)	2770
Modulus of Elasticity (GPa)	27
Poisson’s ratio	0.22
Joint Friction Angle (˚)	40
Cohesion (MPa)	0

The head race tunnels which help in conducting water from the reservoir to the power station, are 8.5 m in diameter built according to IS 5878 (1972). The head race tunnel 3, assumed for the current study in Zone D is built in aggrillaceous-phyllite (10-20%), phyllite (45-55%), quartzite phyllite (10-35%) and consists of 2 joints sets of 8 m spacing and 45˚ dip. The properties of the rockmass in zone D is as given in Table 6.1Each tunnel is supported using 16 rockbolts equally spaced around the tunnel.

Shotcrete and concrete liners are used for extensive support in addition to the rockbolts. The effect of the tunnel when only placed with rockbolts, is analysed using UDEC assuming plane strain condition. In the present study, the performance of rockbolts, shotcrete and tunnel structures are analaysed without considering the effect of the water flow or the dynamic load acting on the tunnel due to running water.

6.5 SEISMIC LOADS

The performance of the tunnel is studied using actual data from Uttarkashi earthquake (1991) and Nepal earthquake (2015) based on its location and magnitude respectively. The Uttarkashi earthquake (1991), also known as the Garhwal earthquake, had a Ritcher scale magnitude of 6.8 and is considered a violent earthquake in the Mercalli scale. The Tehri area is at a distance of 54 km from the epicentre of the earthquake. Jain et al. (1993) classified the earthquake as very strong of Mercalli magnitude VII for the Tehri area. This placed the earthquake at a critical point with respect to the Tehri dam. The 2015 Nepal earthquake, also known as Gorkha earthquake had its epicentre at Gorkha district of Nepal at a depth of 8.2 km. The earthquake had a magnitude of 8.1 in the Richter scale and a maximum on the Mercalli scale of VIII. The earthquake was also followed by many aftershocks at the intervals of 15-20 minutes, with two major aftershocks within days having a magnitude of 6.7 and 7.3 on the Ritcher scale. 2015 Nepal earthquake being the highest recorded earthquake in the Mega Thrust over the past few decades and the 1991 Uttarkashi earthquake with its vital position to Tehri dam is considered for the study. The acceleration time history, velocity-time history, displacement time history and predominant frequency of the earthquakes are shown in Figures 6.5 to 6.12.

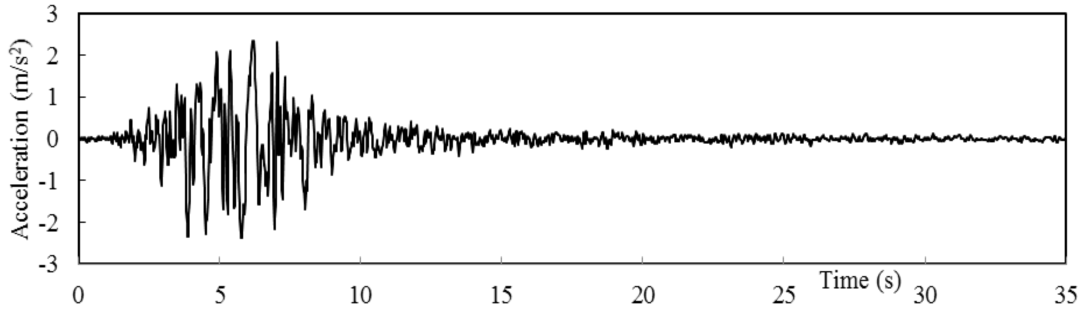

Figure 6.5 : Accelration time history of Uttarkashi earthquake, 1991 (M_w=6.8)

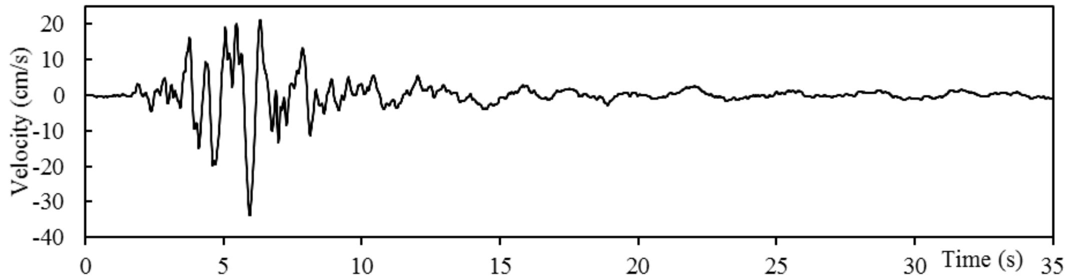

Figure 6.6: Velocity time history of Uttarkashi earthquake, 1991 (M_w=6.8)

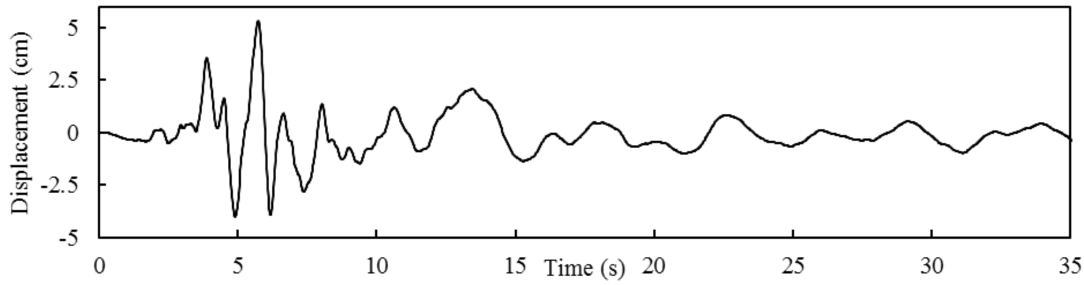

Figure 6.7: Displacement time history of Uttarkashi earthquake, 1991 (M_w=6.8)

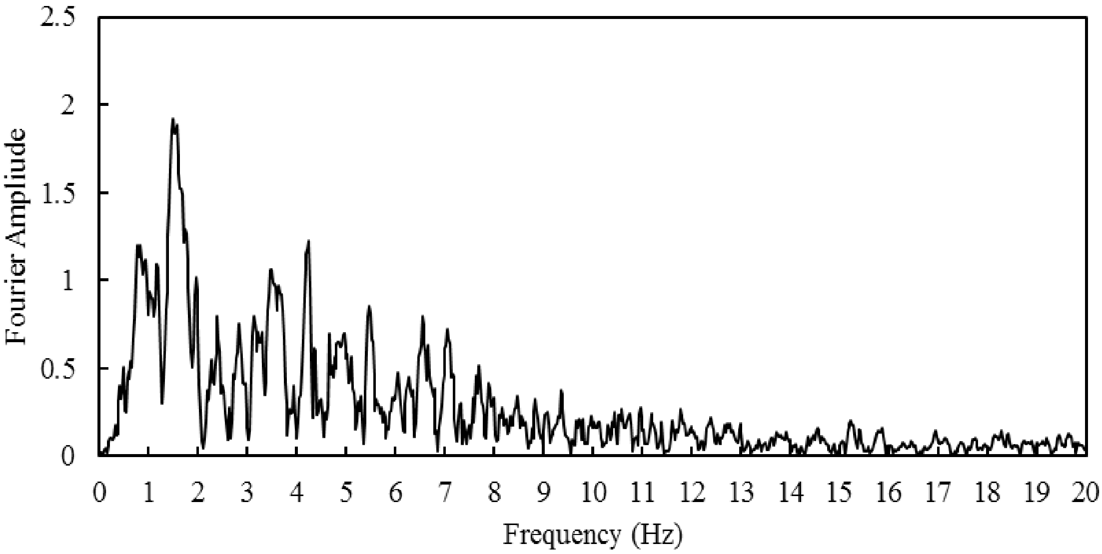

Figure 6.8: Fourier spectra of recorded Uttarkashi earthquake, 1991(M_w=6.8)

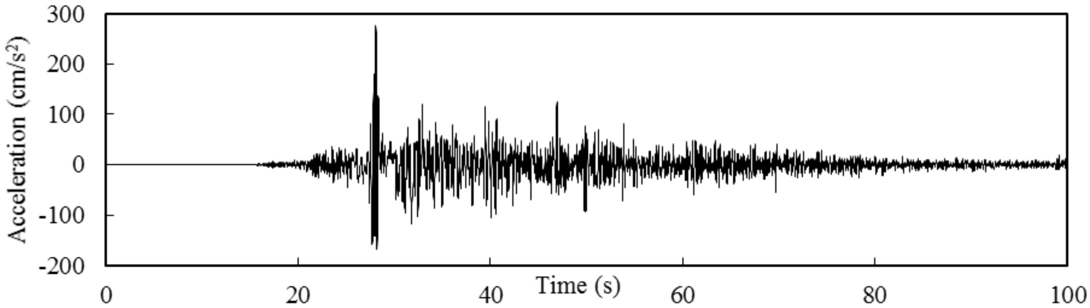

Figure 6.9: Acceleration time history of Nepal earthquake, 2015 (M_w=8.1)

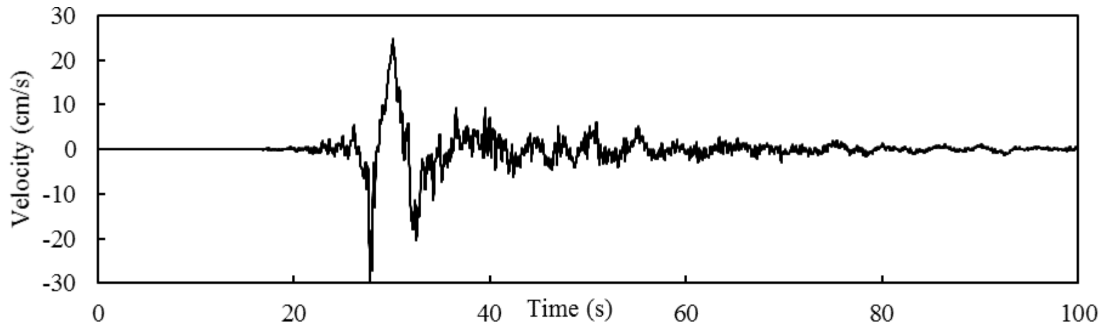

Figure 6.10: Velocity time history of Nepal earthquake, 2015 (M_w=8.1)

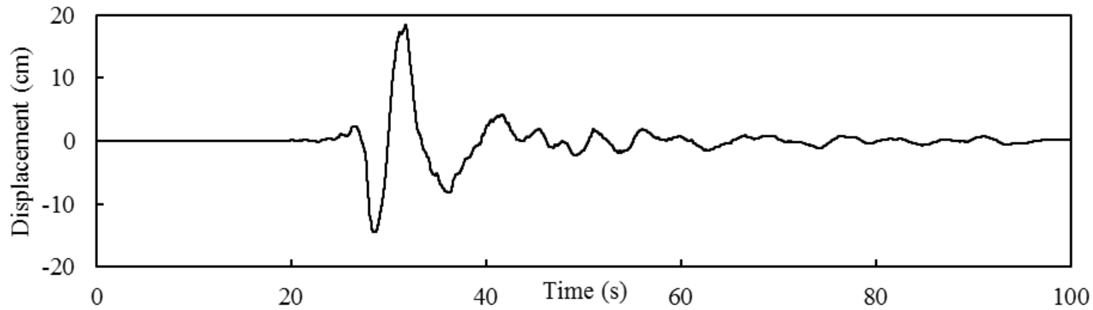

Figure 6.11: Displacement time history of Nepal earthquake, 2015 (M_w=8.1)

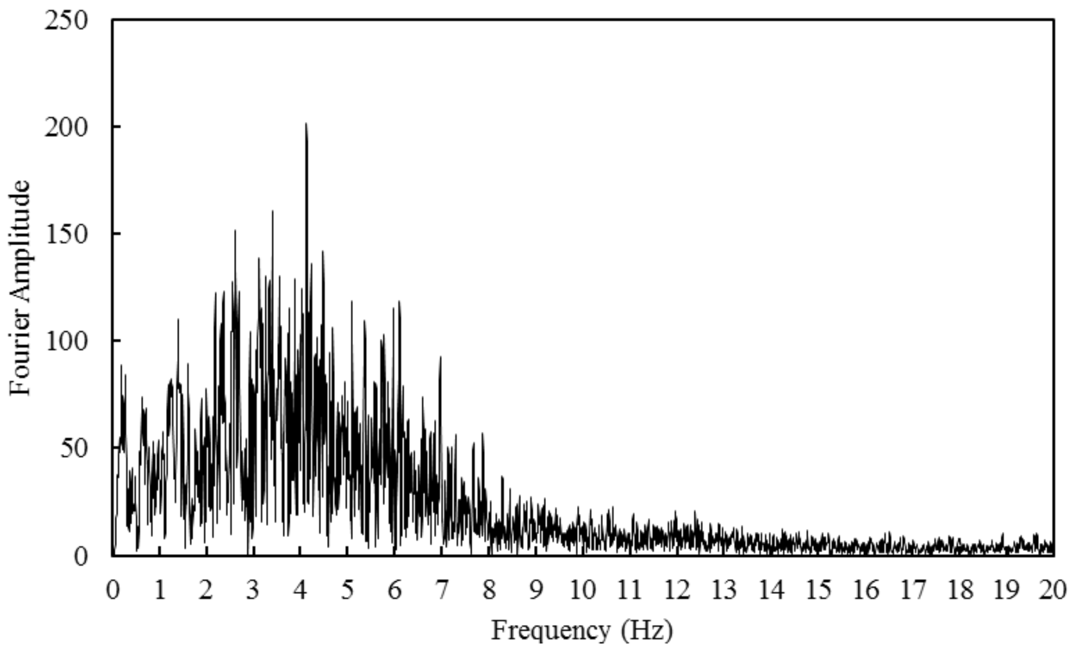

Figure 6.12: Fourier spectra of recorded Nepal earthquake, 2015 (M_w=8.1)

The acceleration time history for the earthquake motions is obtained from the COSMOS, USGS website. The Uttarkashi earthquake (1991) data is obtained from Bhatwari station in India with a peak acceleration of 2.89 m/s^2. The Nepal earthquake (2015) is obtained from Kirtipur Municipality station with a peak acceleration of 2.63 m/s^2 in the East-West direction. A Fourier analysis is done to obtain the frequency content of the earthquake motion from the time history of acceleration, which is shown in Figure 6.8 and 6.12. The Fourier spectra show the frequency content of the earthquake to vary from 0.1 Hz to 10 Hz for the Nepal earthquake (2015) with a predominant frequency concentration between 1 to 10 Hz. The Uttarkashi earthquake (1991) has a frequency concentration between 0.2 Hz and 10 Hz, while the predominant frequency concentrates between 1 and 3 Hz. The velocity-time histories (Figure 6.6 and 6.10) are used as input for the current study.

6.6 NUMERICAL MODELLING OF THE TUNNEL

A numerical model is developed to simulate the effect of the tunnels. The tunnels under analysis are of 8.5 m in diameter. To minimize the boundary effects, the size of the numerical model is adopted to be 200 m x 140 m. Two joint sets of 45˚ and 135˚ dip at 8 m spacing are provided. The tunnel of 8.5 m diameter is located at a depth of 115 m. The top surface of the model is kept free while the other sides of the block are provided with free field boundary so that no wave reflections are affecting the study. The stresses around the tunnel are assumed to be hydrostatic. Rock blocks are modelled as elastic while the joints follow Coulomb slip (Eq. 4.2) model, to concentrate on the failure by joint slip and not by the block failure. The properties of the rockmass are as provided in Table 6.2. Rockbolts of 3 m length is placed around the tunnel at every 22.5˚ with a spacing of 3.3 m. Each rockbolt contains five nodes over which the mass of the rockbolt is concentrated. The reinforcing material follows the elastoplastic model where the material yields and when the yield stresses are generated. The rockbolt and the blocks are bonded by shear and normal springs as in Eq. 6.1 and 6.2. The properties of the rockbolt are as given in Table 6.2.

Hence, the Nepal earthquake (2015) and Uttarkashi earthquake (1991) histories are converted to velocity histories. The velocity histories (Figure 6.6 and 6.10) are applied as shear input at the base of the model. Figure 6.13 shows the numerical model. Figure 6.14 shows the position of the tunnel in the jointed rockmass. It can be seen that rockbolts number 3, 9, 13, 14 and 15 pass through a joint. So the effect of earthquake on these bolts in comparison with the bolts passing through the intact block is done in the following sections.

Table 6.2: Rockbolt properties

Parameter	Rockbolt
Characteristic strength (MPa)	415
Factor of safety	1.15
Density (kg/m^3)	7850
Modulus of elasticity (GPa)	200
Poisson’s ratio	0.3
Thickness (mm)	
Diameter (mm)	28
Spacing (m)	3.5
Length (m)	3
Interphase Normal Stiffness (Pa/m)	1×10^{10}
Interphase Shear Stiffness (Pa/m)	1×10^{10}
Interphase Friction Angle (degrees)	40
Interphase Cohesion	0

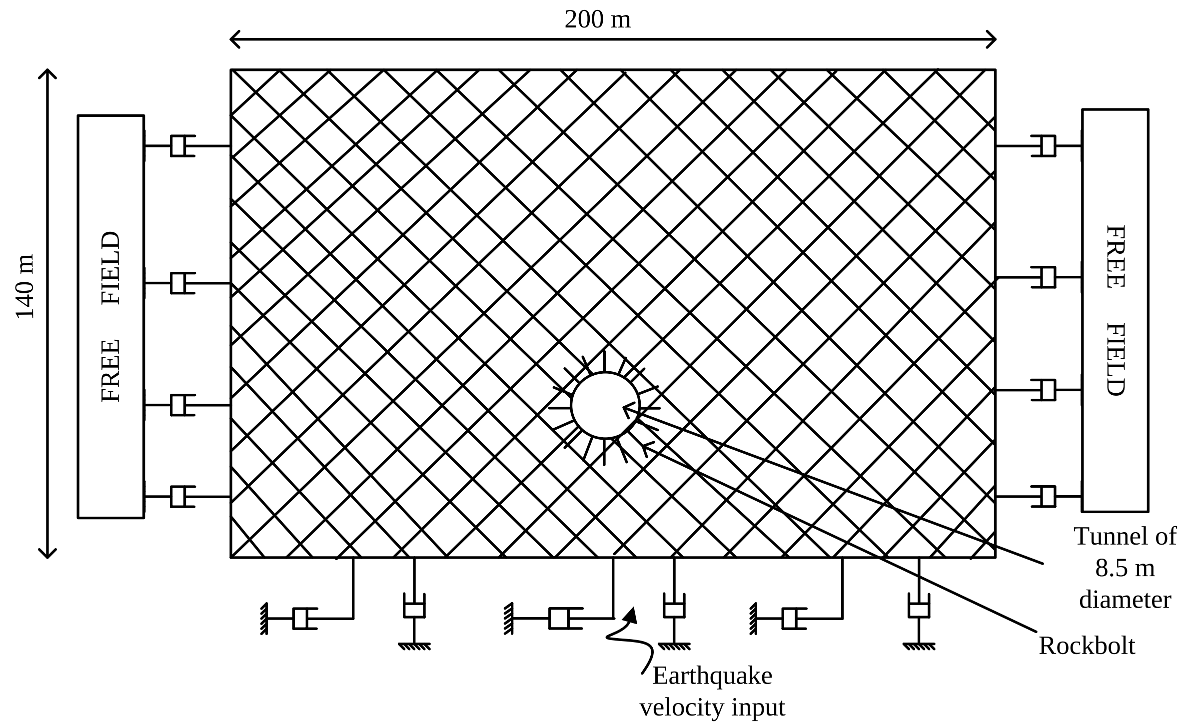

Figure 6.13: Numerical model for the Tehri dam tunnel

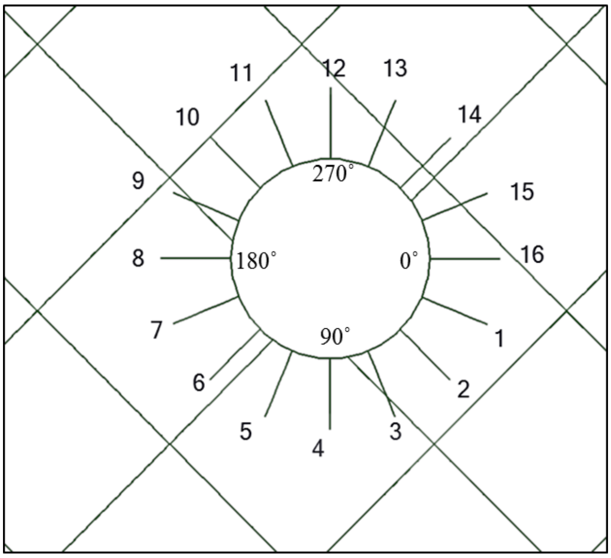

Figure 6.14: Rockbolt numbering and orientation around the tunnel

6.7 FORCE ACTING ON ROCKBOLTS

The maximum force acting on each rockbolt varies according to its position. Figures 6.15 to 6.30 show the maximum force acting on each rockbolt for Nepal earthquake (2015) and Uttarkashi earthquake (1991). The maximum force acting on the bolt and the number of cycles over which the force acts also varies with each rockbolt. Figure 6.15 to 6.30 shows the cycles of force acting on each rockbolt for applied earthquake histories of Nepal earthquake (2015) and Uttarkashi earthquake (1991).

The ultimate strength of the rockbolt is 415 MPa, and the maximum force acting on the 28 mm rockbolt is 100 kN on rockbolt number 4. This is lower than the rockbolt strength, and the failure of the rockbolt is unlikely. But, with several cycles of loading, a reduction in the strength of the rockbolt is anticipated. Rockbolts 5, 6, 7, 8, 9, 10, 11, 12, 13, 14 and 15 undergo many cycles with a force of 40 kN force and higher. All rockbolts undergo at least one cycle with a force more than 45 kN. This is almost one-fifth of the ultimate strength of the rockbolt. Tistel et al. (2017) and Wu et al. (2019) verified with their experimental studies for the loss of ultimate strength with an increase in the number of cycles of loading. Wu et al. (2019) found a reduction of 50% from maximum strength in the steel after five cycles of loading. Thus with a number of peak dynamic forces, its magnitude is varying for each rockbolt. The possibility of rockbolt failure can be anticipated when the tunnel is subjected to multiple earthquakes even of lower magnitude. This leads to the requirement of constant monitoring and analysis of tunnel support system in regions of high seismicity.

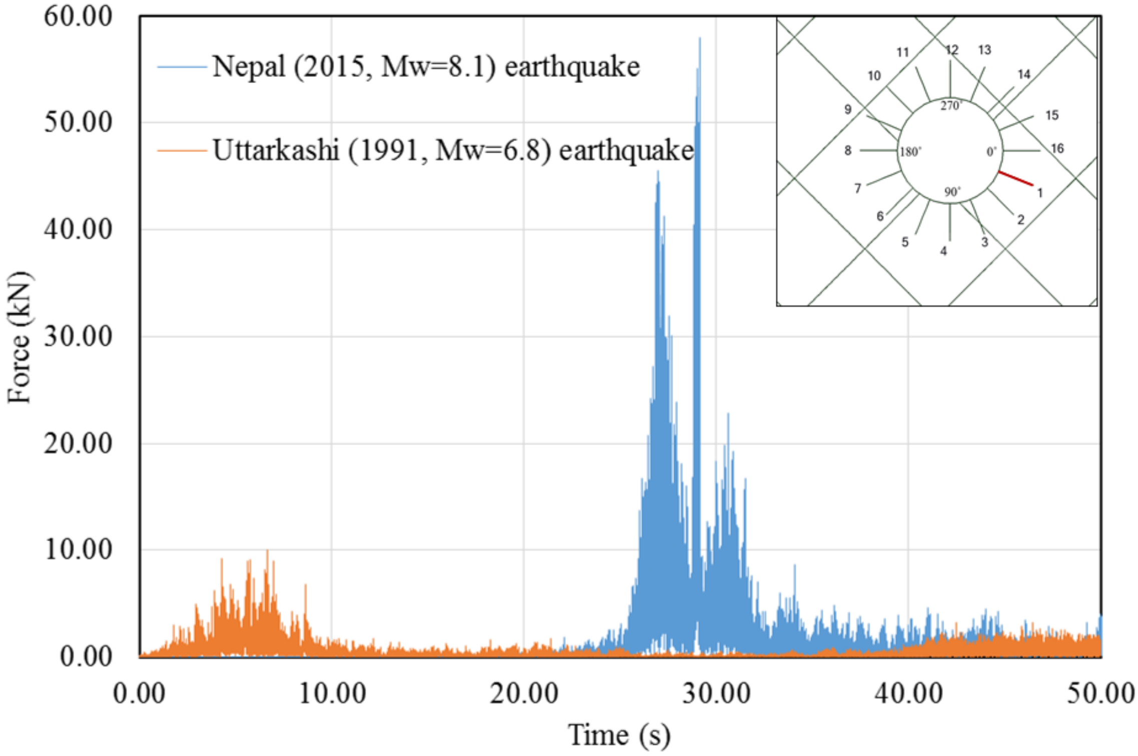

Figure 6.15: Force acting on Rockbolt 1

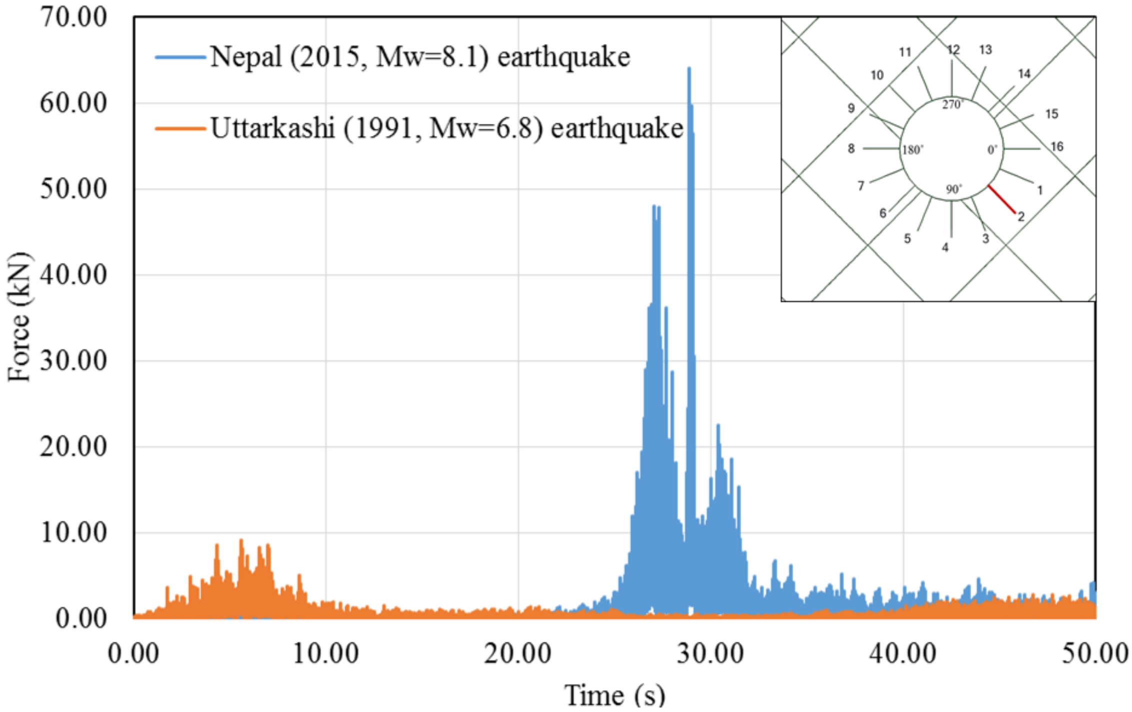

Figure 6.16: Force acting on Rockbolt 2

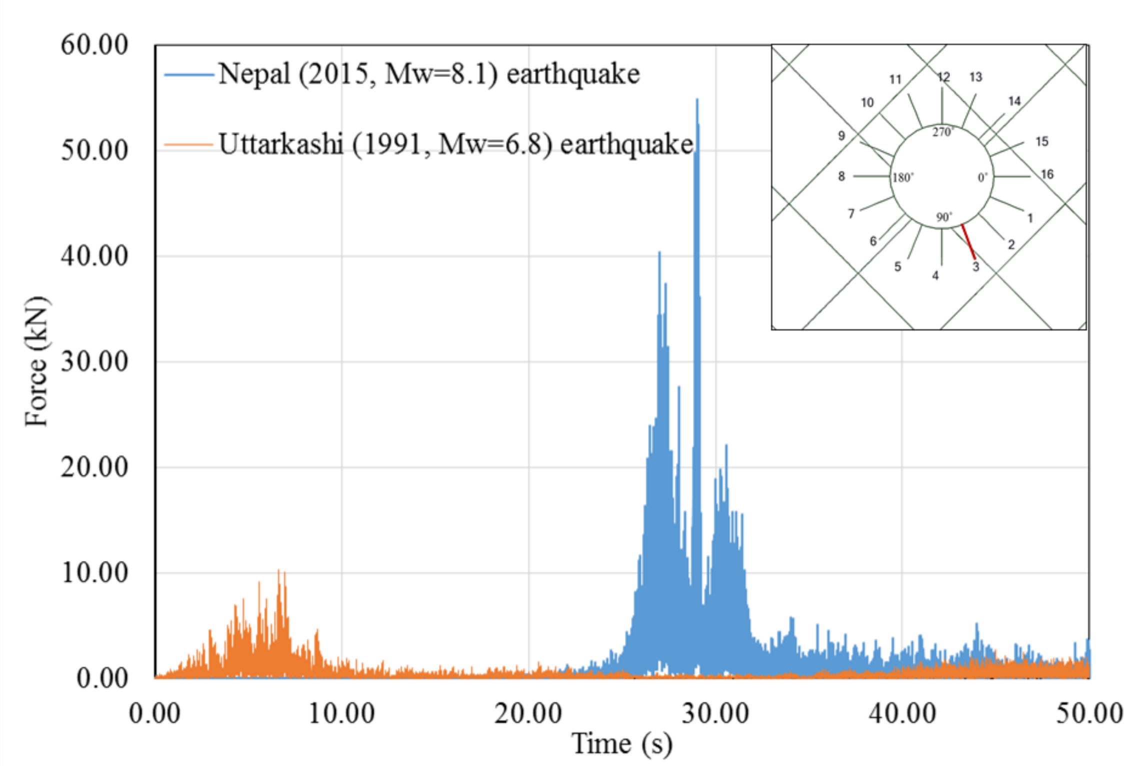

Figure 6.17: Force acting on Rockbolt 3

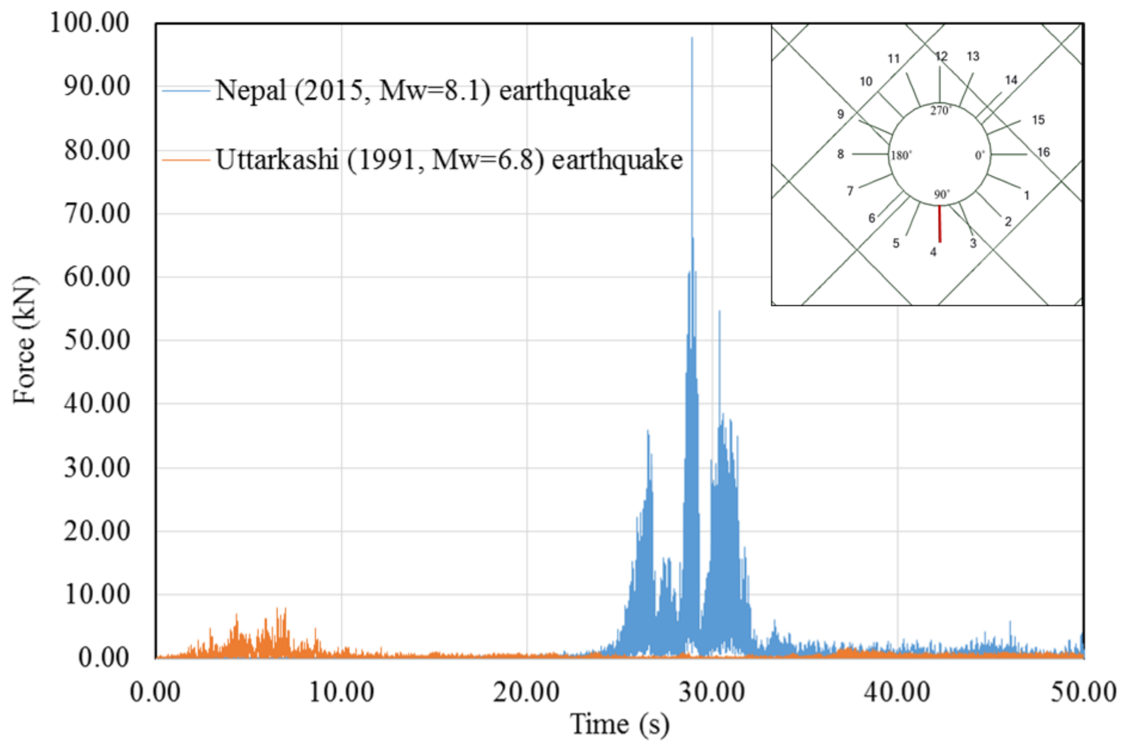

Figure 6.18: Force acting on Rockbolt 4

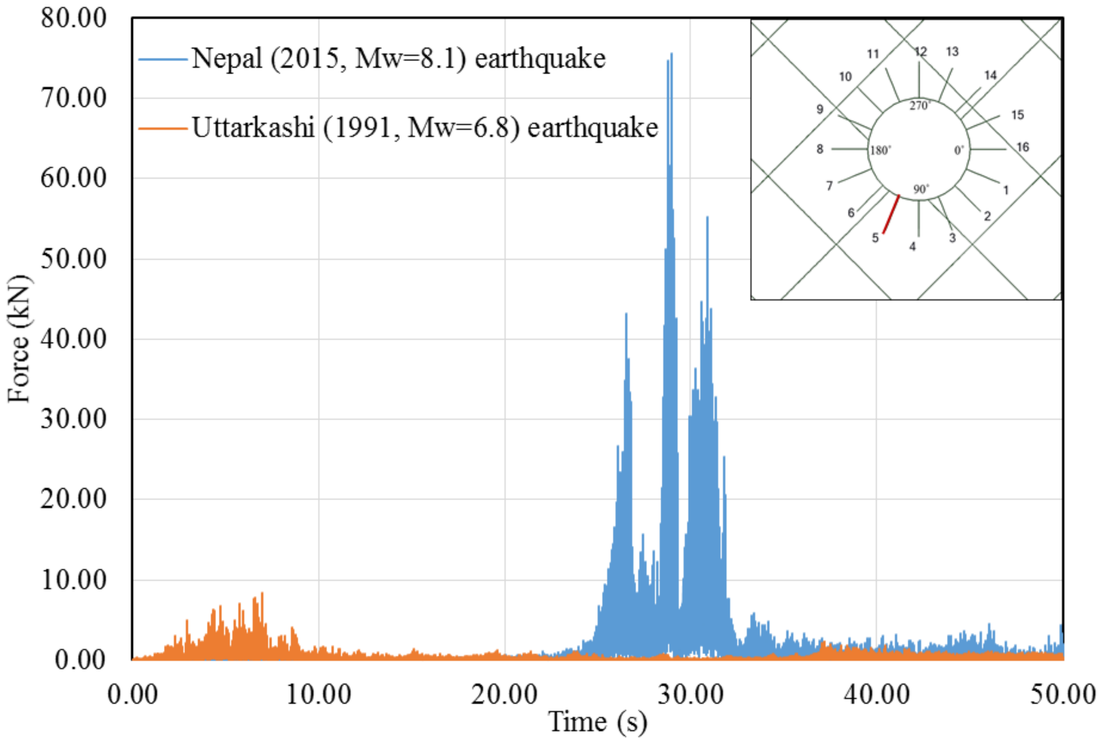

Figure 6.19: Force acting on Rockbolt 5

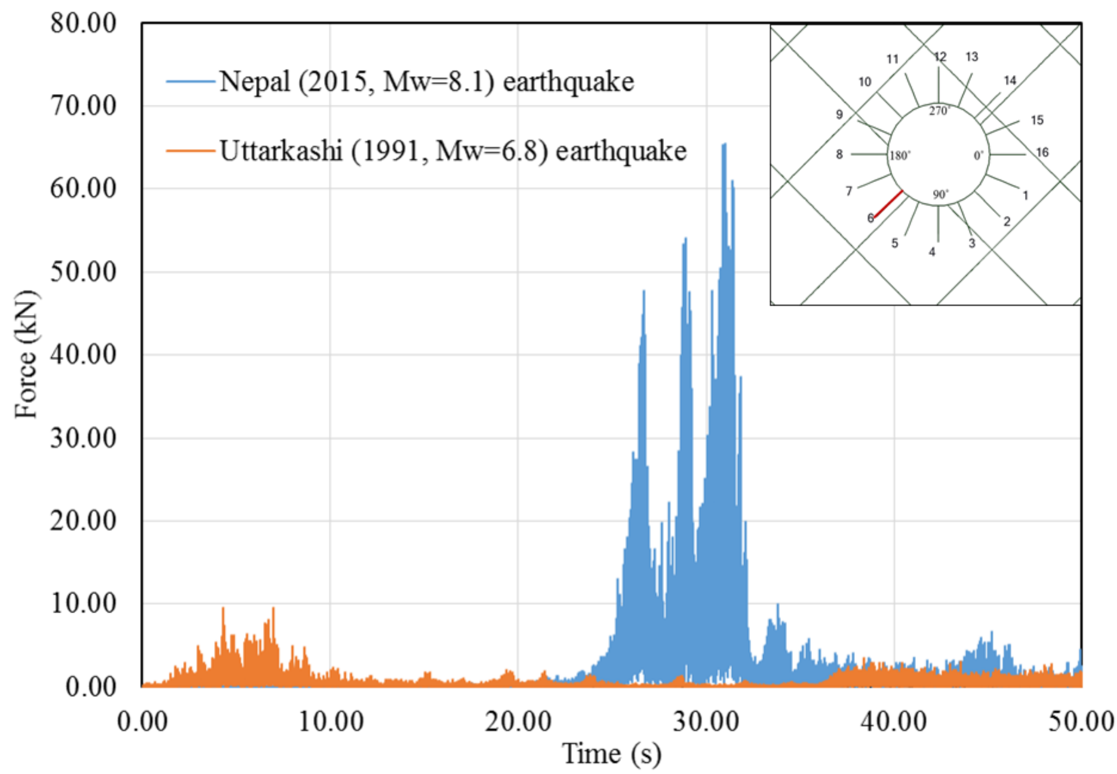

Figure 6.20: Force acting on Rockbolt 6

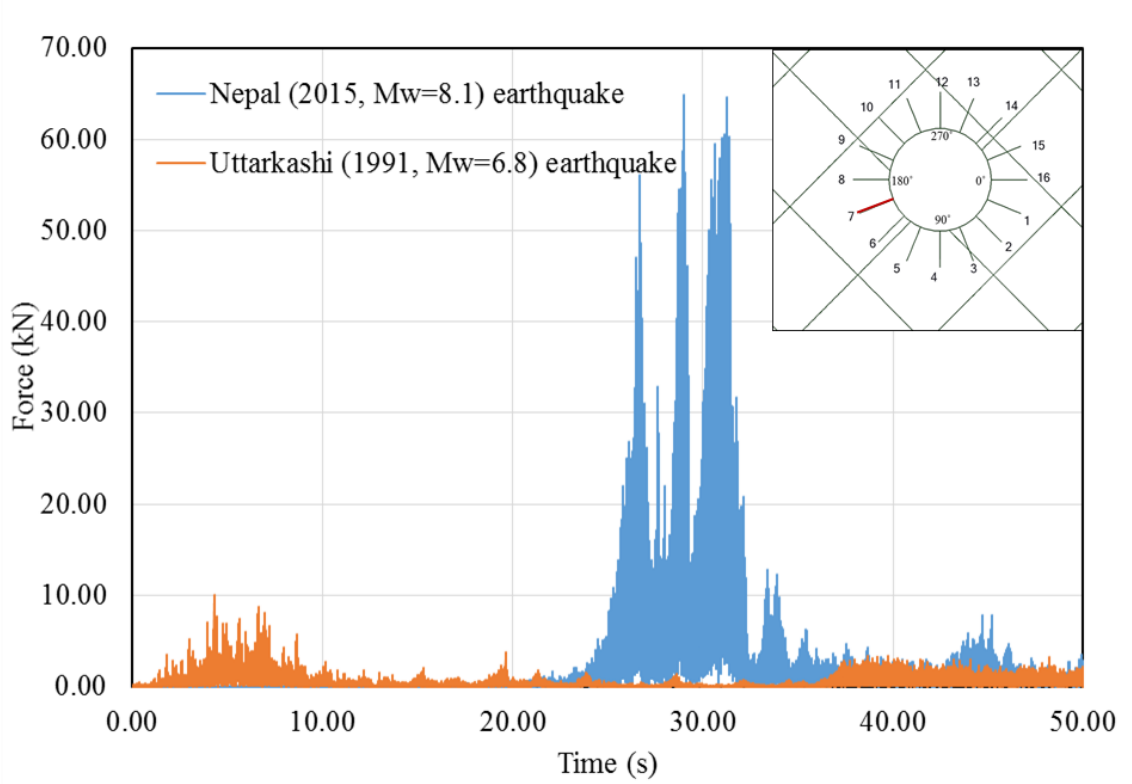

Figure 6.21: Force acting on Rockbolt 7

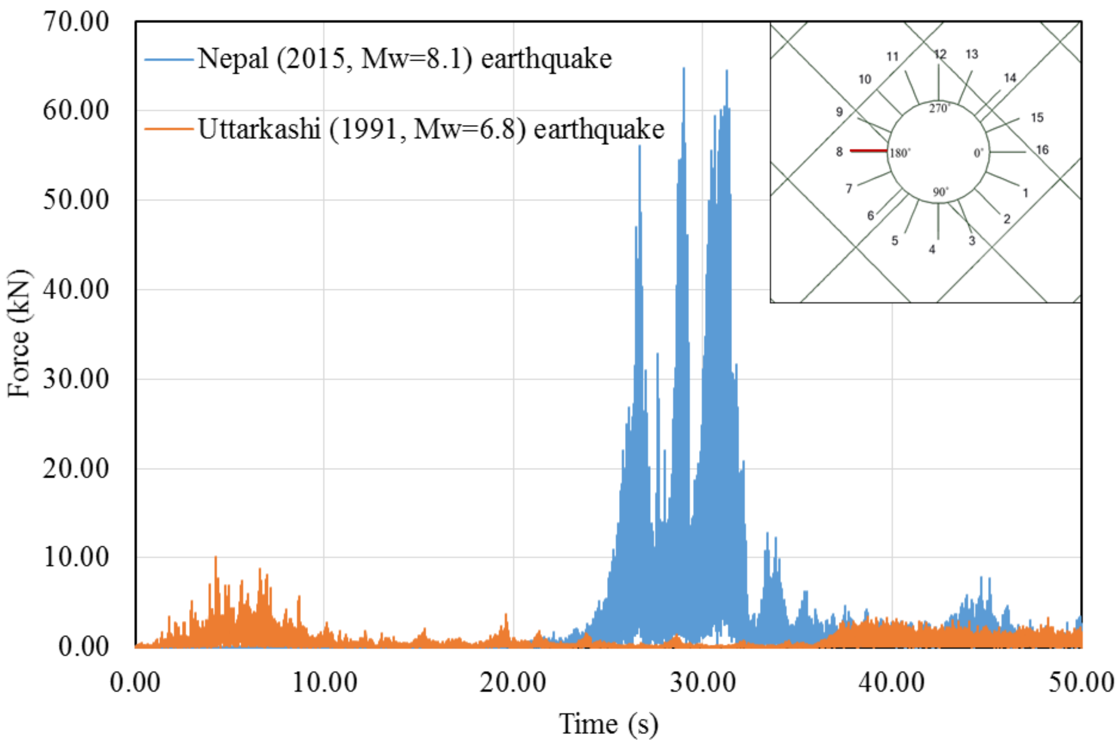

Figure 6.22: Force acting on Rockbolt 8

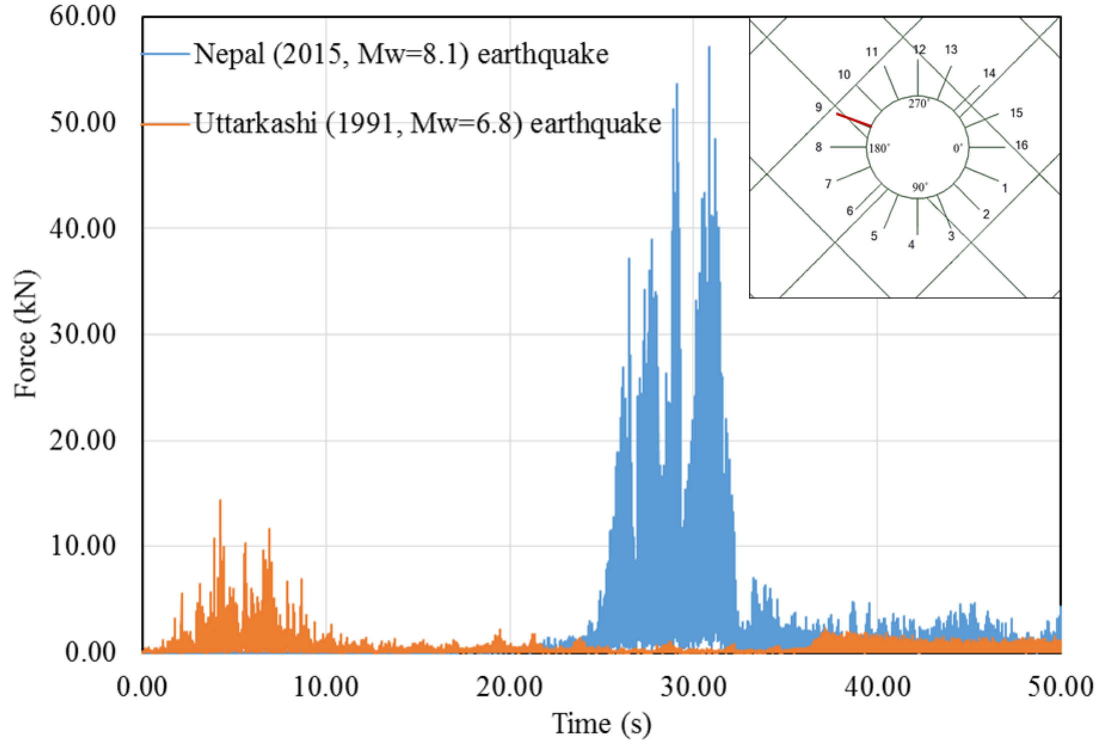

Figure 6.23: Force acting on Rockbolt 9

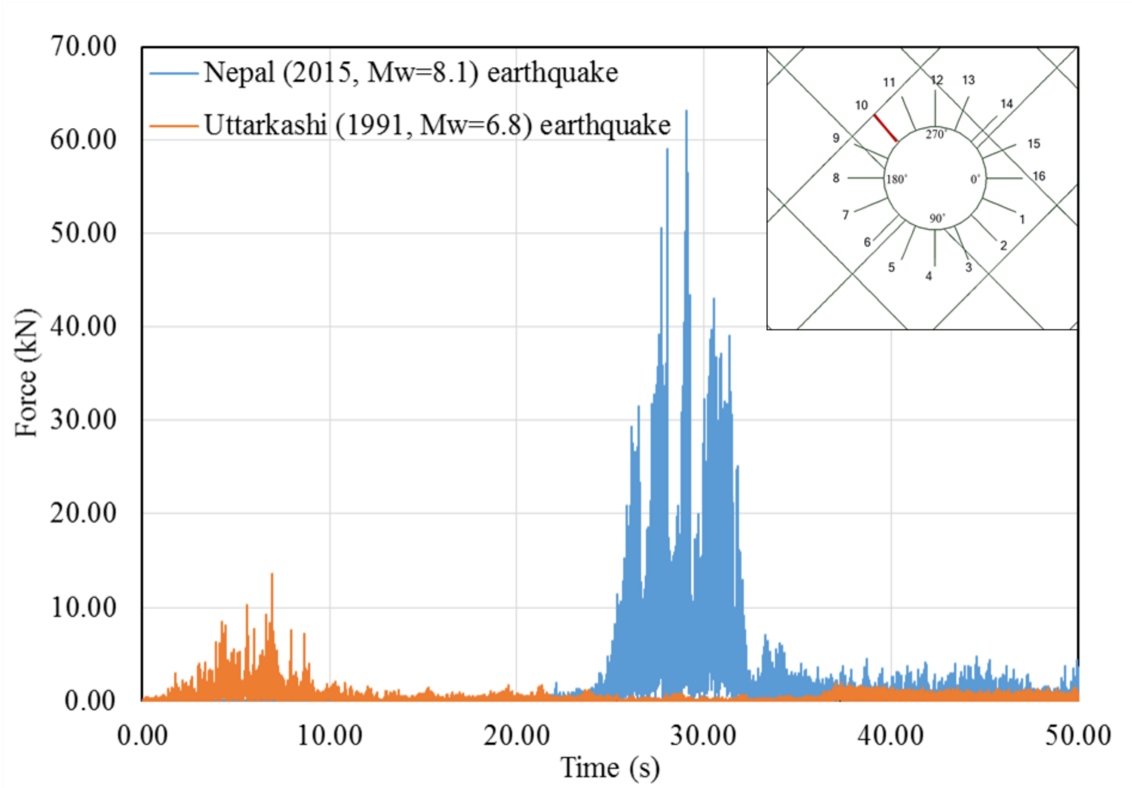

Figure 6.24: Force acting on Rockbolt 10

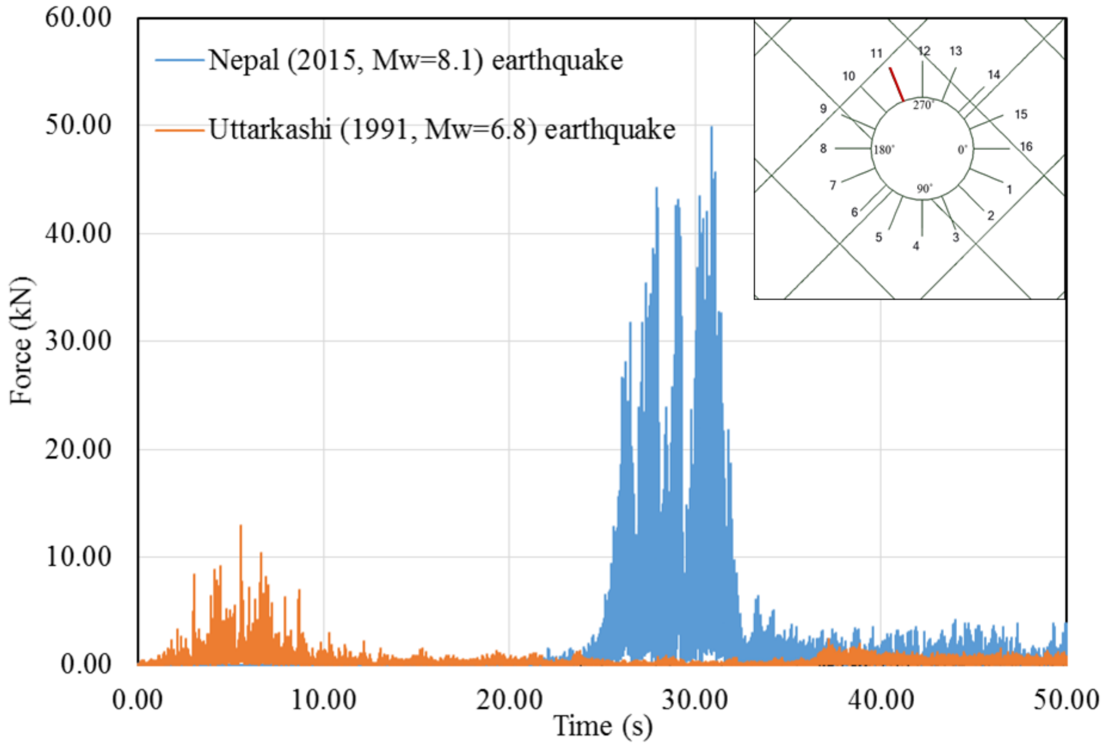

Figure 6.25: Force acting on Rockbolt 11

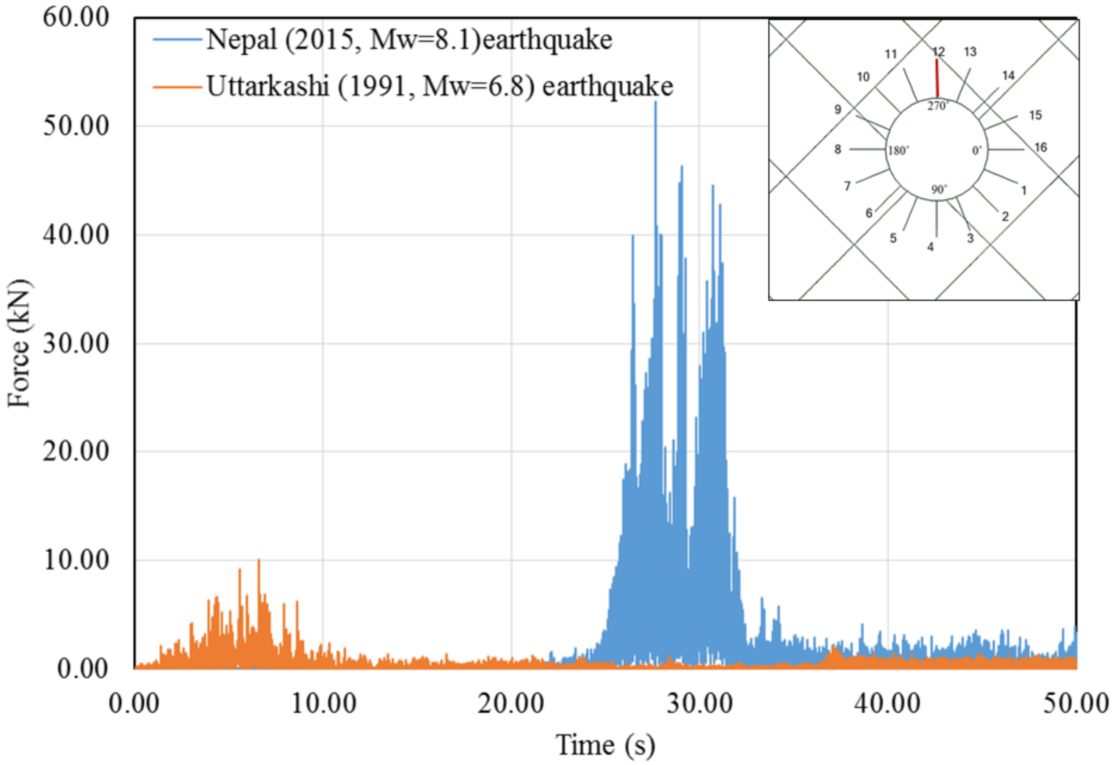

Figure 6.26: Force acting on Rockbolt 12

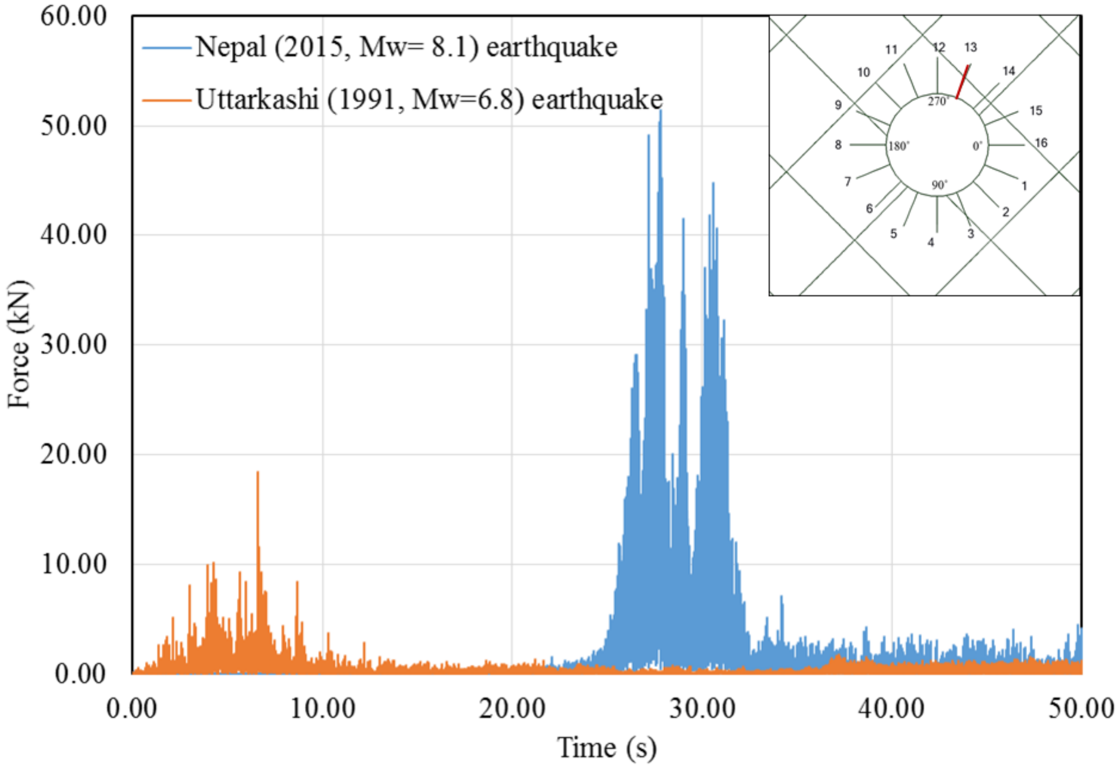

Figure 6.27: Force acting on Rockbolt 13

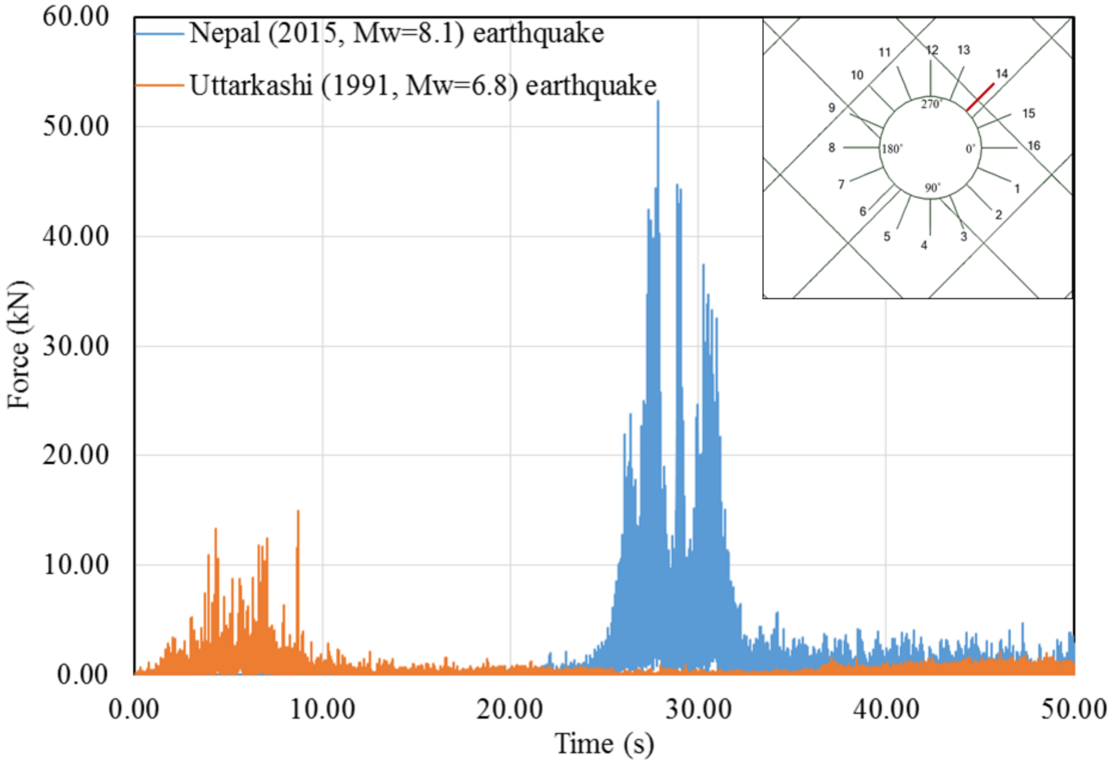

Figure 6.28: Force acting on Rockbolt 14

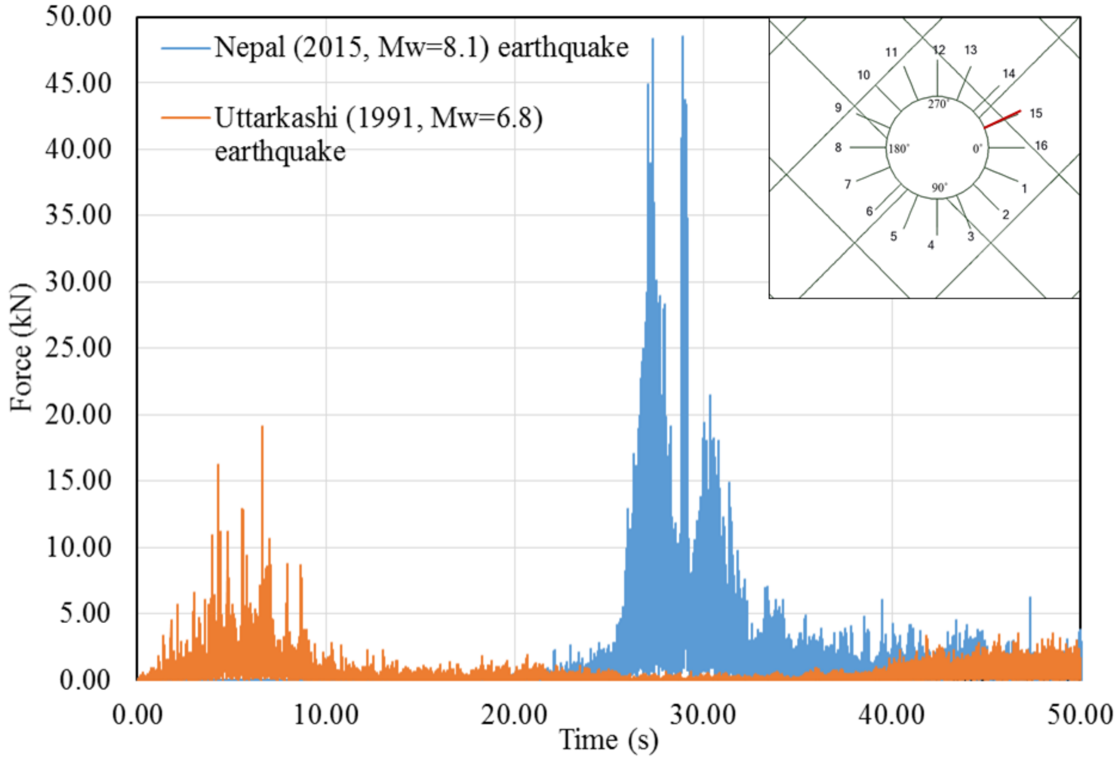

Figure 6.29: Force acting on Rockbolt 15

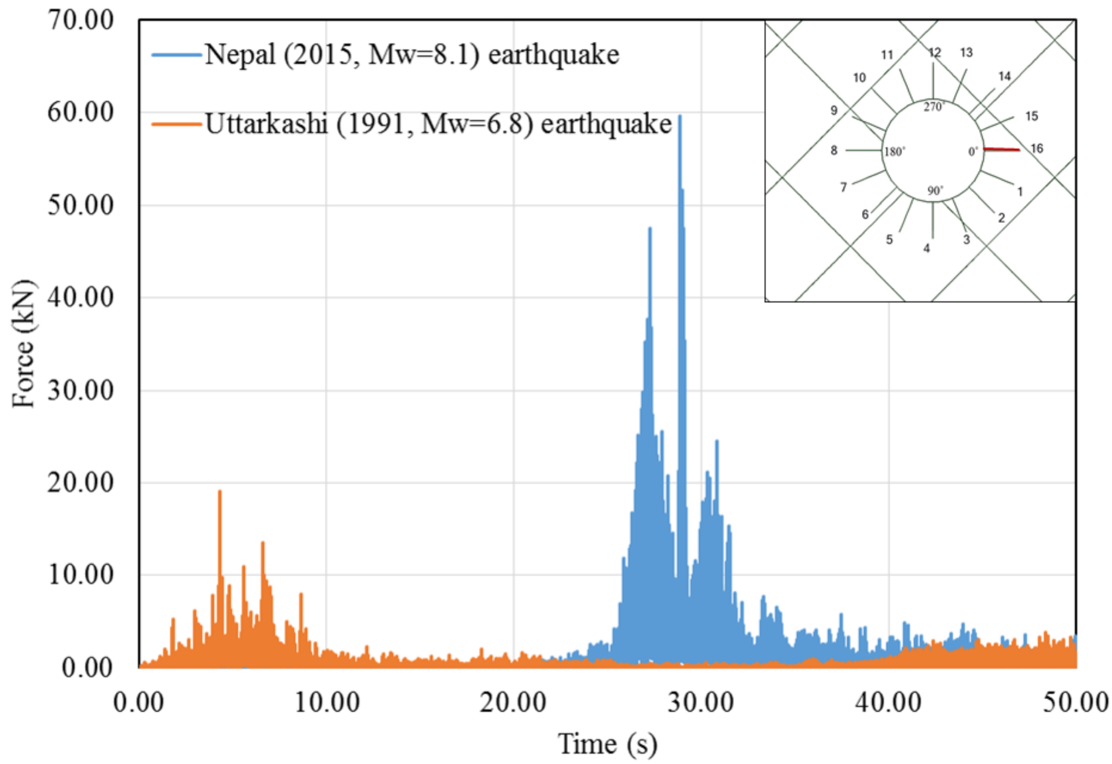

Figure 6.30: Force acting on Rockbolt 16

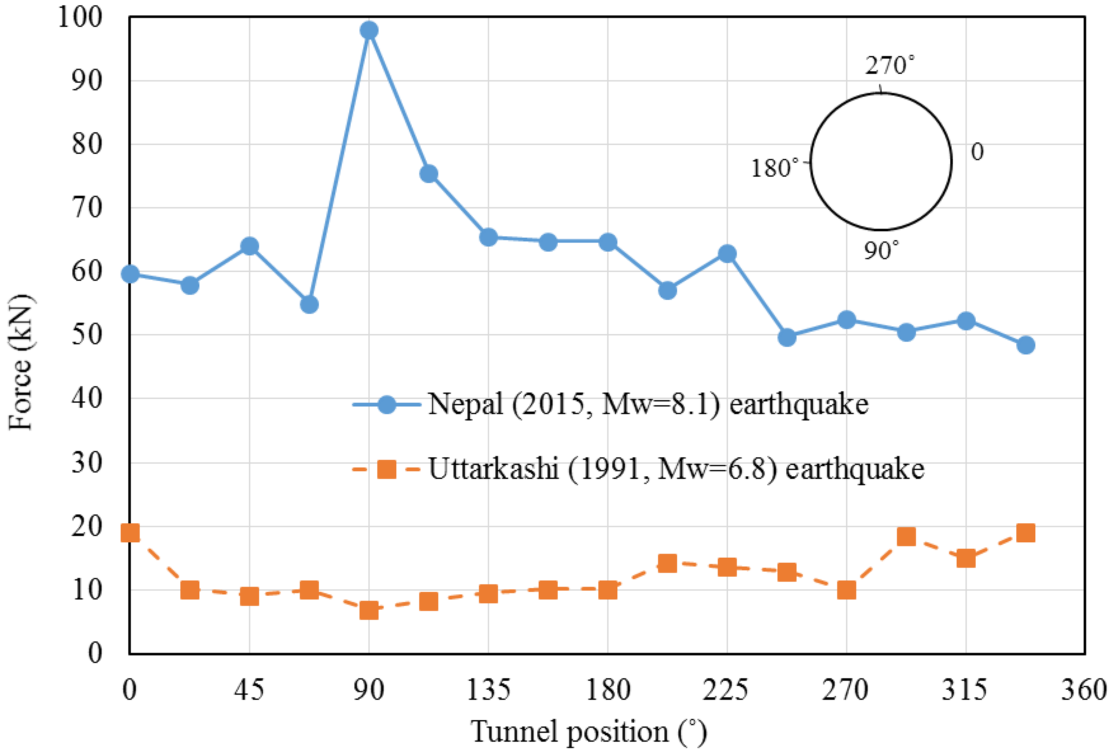

Figure 6.31: Force acting on different rockbolt according to the position.

Figure 6.31 shows the maximum force acting on each rockbolt. It shows that the maximum force acting on the rockbolt is not the same in the case of both the earthquakes. For Nepal earthquake (2015, M_w=8.1), the rockbolt 4 undergoes maximum force of 97.4 kN while rockbolt 15 receives a minimum force of 48.51 kN. For Uttarkashi earthquake (1991, M_w=6.8) rockbolts 15 and 16 suffer maximum force of 19.13 and 19.09 kN while rockbolt 4 undergoes a minimum of 6.96 kN. This implies that the effect of the incoming seismic waves on rock bolts are different for different earthquakes.

The understanding of maximum normal forces acting on each bolt is necessary to understand the effect of the earthquake. Figure 6.32 shows the maximum normal force acting on each rockbolt during Nepal (2015, M_w=8.1) and Uttarkashi (1991, M_w=6.8) earthquakes. From Figure 6.32, it can be seen that the normal force acting on rockbolts passing through intact portion does not have much effect with the action of the earthquake. However, rockbolts passing through joints experience a sudden increase in the normal force. The increase in normal force under seismic condition is found to be at least twice the normal force acting on the bolt under static condition. Similar results were also observed by Owada and Adyan (2012), Owada et al. (2004) while conducting few shake table tests to understand the behaviour of rockbolts under earthquake. Adyan (2017) confirmed the increase in stresses on the bolts to be twice the initial value.

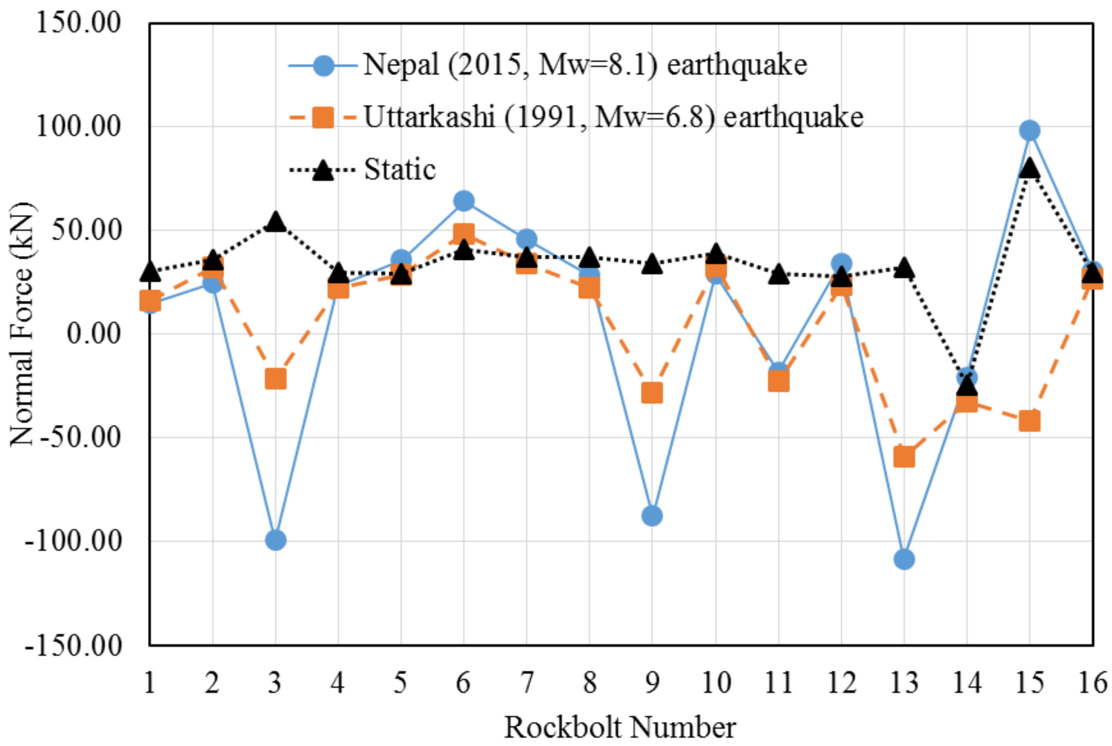

Figure 6.32: Maximum normal force acting on each rockbolt during Nepal (2015) and Uttarkashi (1991) earthquakes

From these results, it is clear that all rockbolts undergo normal forces, even if they do not pass through a joint. Figure 6.33 shows that shear forces act on rockbolts only if they pass through a joint. Maximum shear force acts on rockbolt number 13, 14 and 15. This might be because the bolts experiences loosening of the blocks. It can also be seen that the shear force acting on a rockbolt is very small compared to the normal force on the rockbolt. The ultimate strength of the rockbolt being much higher than the shear stress, the chances of a rockbolt to fail in shear is very less. The maximum normal force acting on the bolts during earthquake loading is 2 to 3 times the force under static conditions. Adyan (2017) also reports similar results where the possibility of the support system to fail under dynamic loading is by the failure of the grouting material and not by bolt deterioration.

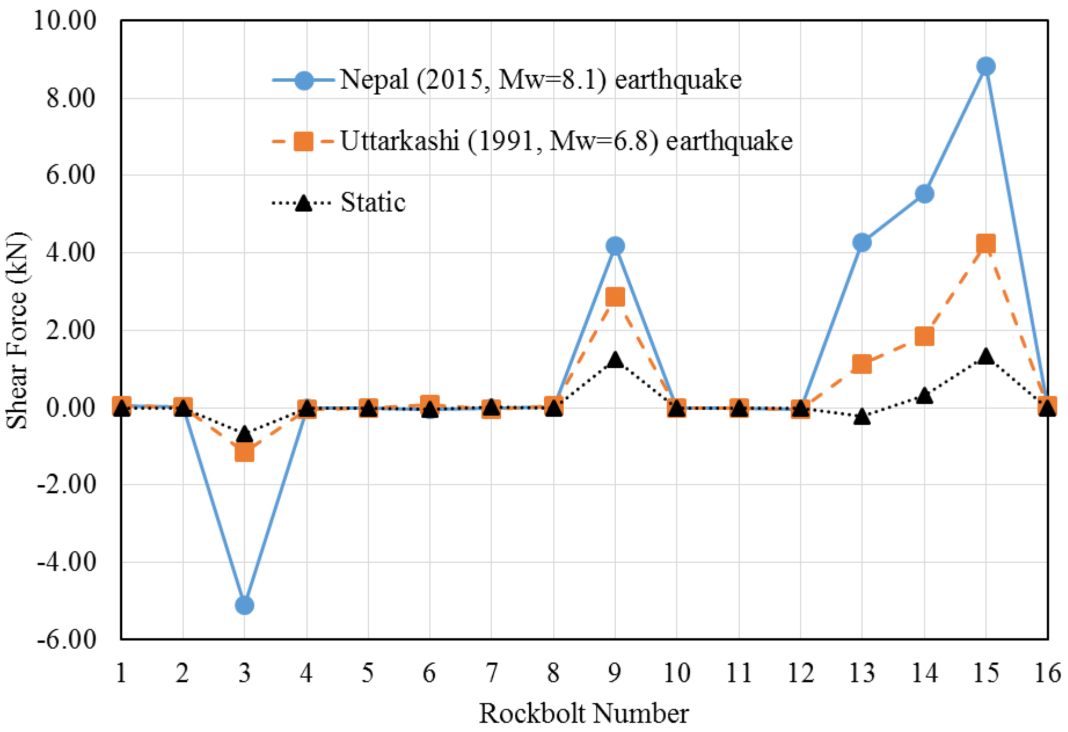

Figure 6.33: Maximum shear force acting on each rockbolt during Nepal (2015) and Uttarkashi (1991) earthquakes

6.8 ROCKBOLT DISPLACEMENT

The displacements of the rock and rockbolts due to an earthquake can be categorised into two 1) the displacements during the earthquake motion and 2) the residual displacements. The displacements occurring as a part of the earthquake will have a motion similar to the displacement time history of the earthquake. According to the position and the forces acting on the rockbolt, the residual displacement in each rockbolt varied from one rockbolt to another. Figure 6.34 shows the displacements in rockbolts due to Nepal (2015) and Uttarkashi (1991) earthquakes. Figure 6.35 shows the rockbolt displacements occurring at different tunnel position during static and seismic conditions with Nepal (2015, M_w=8.1) and Uttarkashi (1991, M_w=6.8) earthquake. It can be seen that rockbolts in the upper and lower half of the tunnel behave differently even in the case of static load. The upper rockbolts from 202.5˚ (Rockbolt 9) to 337.5˚ (Rockbolt 15) have higher displacements in the static condition. This is due to the destressing of the blocks due to gravity, which tends to increase the displacements acting on the rockbolts. Amongst these rockbolts, rockbolt number 9 (202.5˚), 12 (270˚) and 14 (315˚) are found to undergo maximum displacements. The displacement in these rockbolts can be attributed to the destressing of the blocks, according to the shear zone formation reported by Shen and Barton (1997).

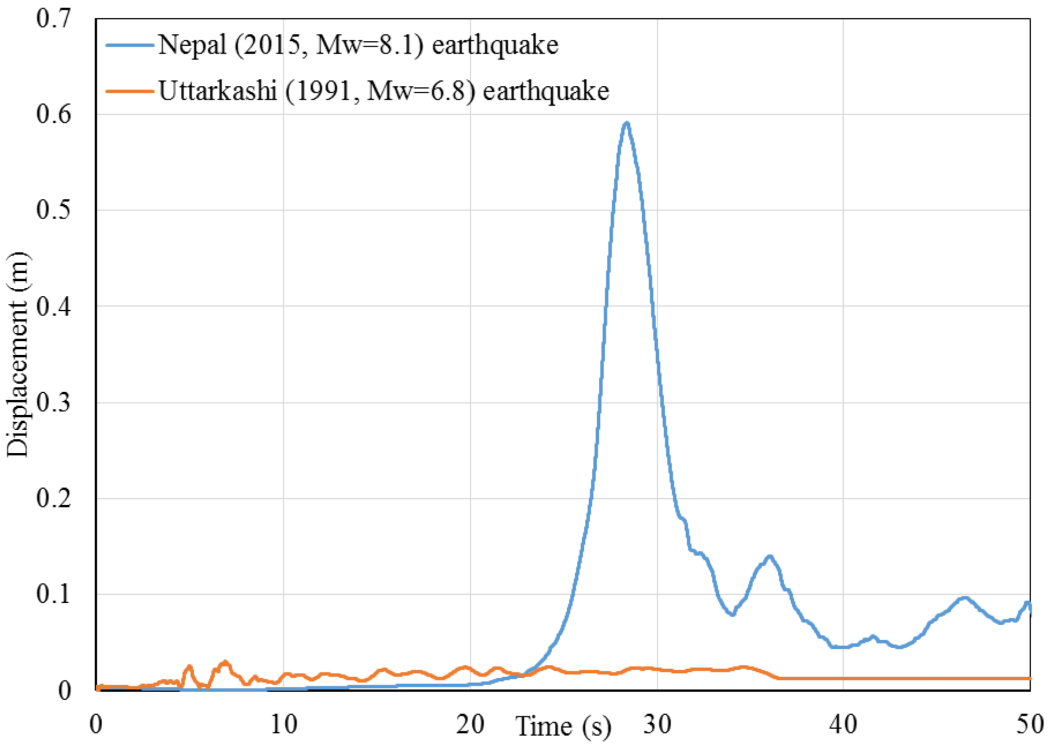

Figure 6.34: Displacement in rockbolt during Nepal earthquake (2015, M_w=8.1) and Uttarkashi earthquake (1991, M_w=6.8)

The behaviour of these rockbolts under the action of earthquakes is different from static conditions. The rockbolt displacements are also observed to be dependent on the type of earthquake. Both the earthquakes produced different displacements on the rockbolts (Figure 6.35). The displacements due to Nepal earthquake (2015, M_w=8.1) is more than Uttarkashi earthquake (1991, M_w=6.8) for all rockbolts and the pattern of displacement is also found to be different. The deformations in rockbolt due to Uttarkashi earthquake (1991, M_w=6.8) is similar to the static condition. The maximum deformations are found to occur on the crown of the tunnel. During the Nepal earthquake (2015, M_w=8.1), rockbolts on the lower part of the tunnel are found to undergo more displacements compared to the rockbolts on the upper hemisphere. This might be due to the high force acting on the bottom of the tunnel from earthquake shaking. Moreover, this force will be less than the force transmitted to the top of the tunnel. Amongst these, rockbolt number 3 (102.5˚) is found to undergo maximum deformation. This might be due to the fact that rockbolt 3 passes through a joint. The earthquake makes a separation between the blocks causing the blocks to undergo differential movement with respect to the rockbolts. The permanent displacements were also found to occur post shake table loading (Adyan, 2017). An increment in permanent deformation is also observed with an increase in the magnitude of acceleration level. The strains on rockbolts crossing discontinuities are referred to as very high by Adyan et al. (2017).

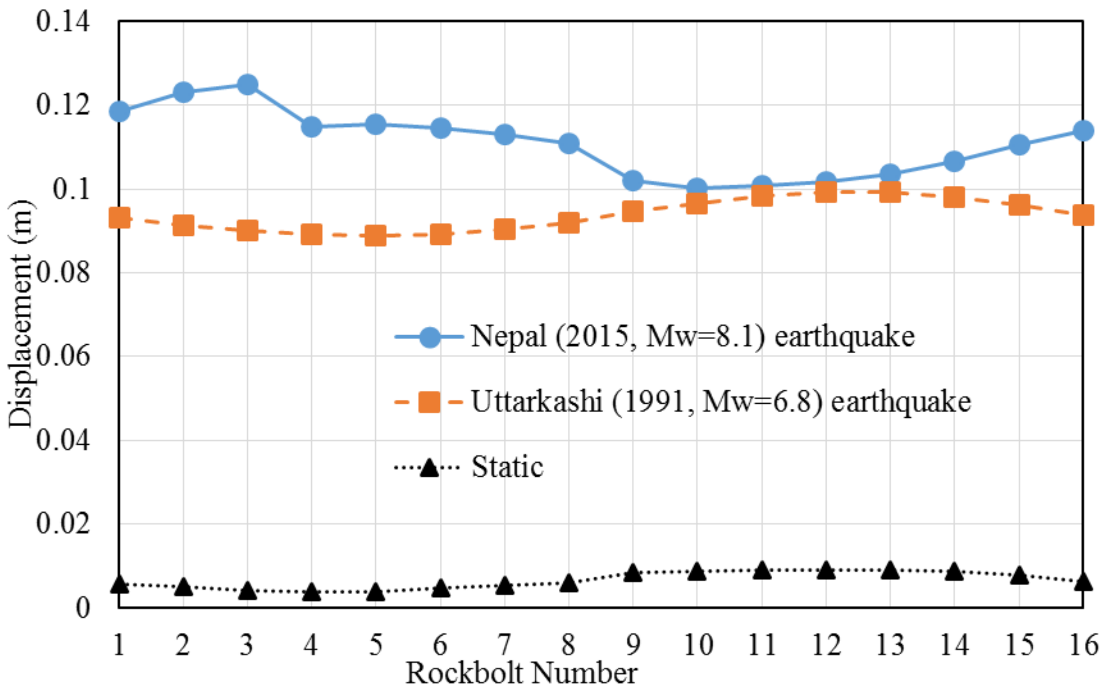

Figure 6.35: Maximum displacements on rockbolts at different tunnel postions due to Nepal (2015, Mw=8.1), Uttarkashi (1991, Mw=6.8) earthquakes and static conditions

6.9 BENDING MOMENT ACTING ON THE ROCKBOLTS

Rockbolts provide bending resistance, which leads to the formation of bending moment on the bolts. Bending resistance is important under conditions of jointed rocks so that relative displacements between the blocks can be minimised. Figure 6.36 shows the unbalanced moment on rockbolt 3 during Nepal (2015, M_w=8.1) and Uttarkashi (1991, M_w=6.8) earthquake. The peak moments in the rockbolt are found to correspond with the peak ground acceleration of the earthquakes. The maximum bending moment acting on the rockbolt with Uttarkashi earthquake (1991, M_w=6.8) is corresponding with the peak of the earthquake input. The negative and positive values of unbalanced moment correspond to moments in a clockwise and anticlockwise direction. Several cycles of unbalanced moment are found to be acting on the rockbolt. These number of cycles leads to loss of strength in rockbolt over a considerable period.

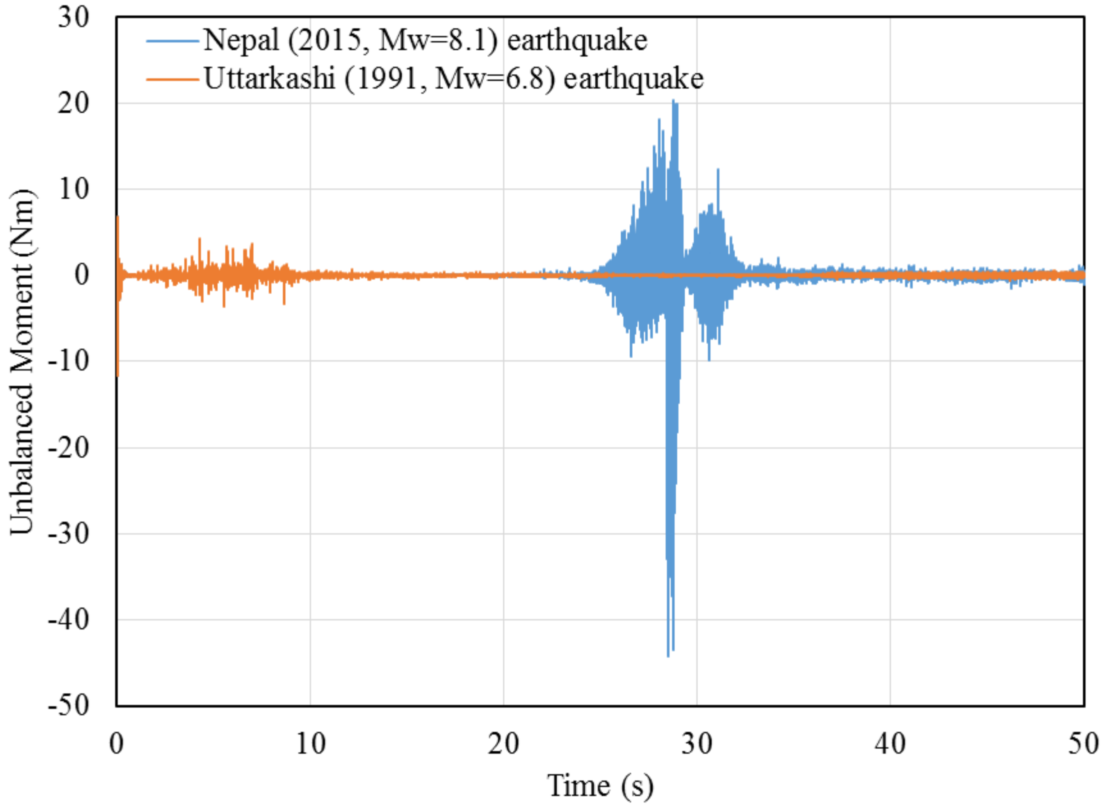

Figure 6.36: Time history of unbalanced moment acting on the rockbolt during Uttarkashi earthquake (1991) and Nepal earthquake (2015)

Figure 6.37 shows the maximum total moment acting on each rockbolt during Nepal (2015, M_w=8.1) and Uttarkashi (1991, M_w=6.8) earthquake. The maximum moment is found to be acting on rockbolts passing through joints while on other bolts, the moment is near zero. Maximum bending moment is found to act on rockbolt 15 (337.5˚). A substantial increase in the moment value is observed compared to static condition. All rockbolts passing through joints generated a moment in static condition except Rockbolt 3. This might be due to the fact that rockbolt 3 undergoes no deformation under gravity. The moment due to Nepal earthquake (2015, M_w=8.1) is higher than the Uttarkashi earthquake (1991, M_w=6.8) due to its higher magnitude.

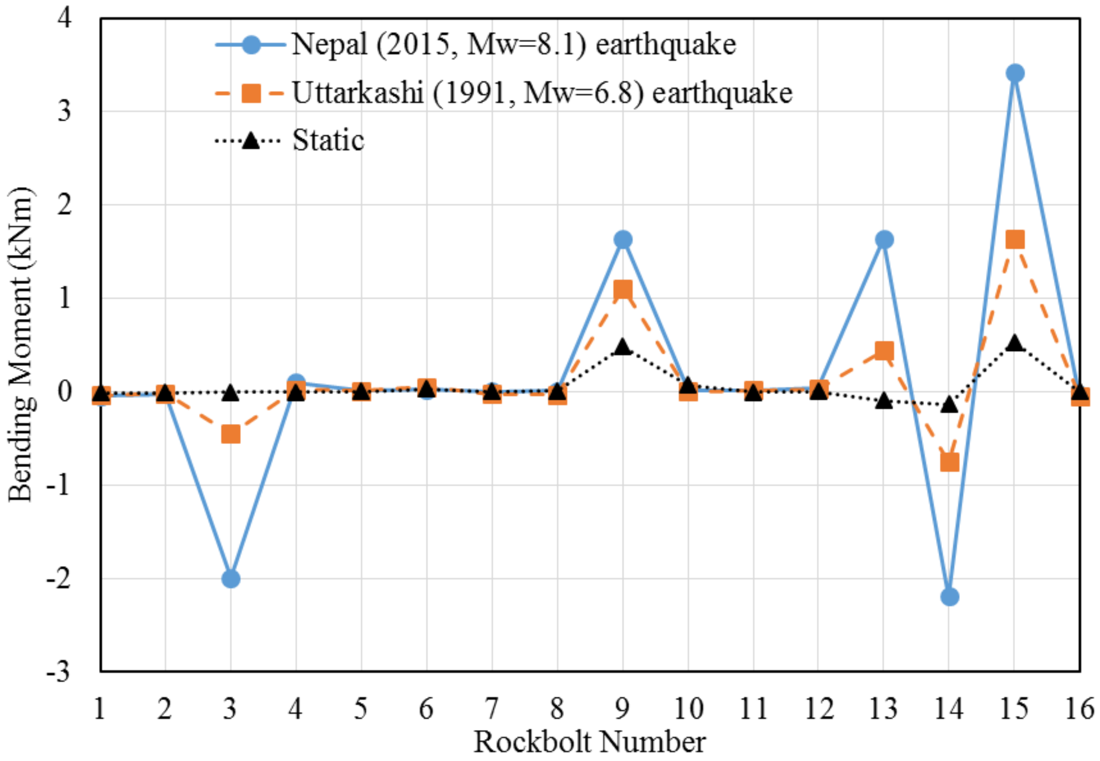

Figure 6.37: Maximum bending moment acting on rockbolts located at different tunnel position for Nepal earthquake (2015) and Uttarkashi earthquake (1991)

6.10 THE PERFORMANCE OF ROCKBOLT – PARAMETERIC STUDY

The performance of rockbolt may be affected according to different parameters under consideration. This variation can be according to rockbolt properties, the wave properties or the rockmass properties. Analysis of the performance of the rockbolts under dynamic loading condition for various properties is done in the current section. The model used in the parametric study is the same as that of the Tehri dam site. One input parameter at a time is varied for the study while keeping the others constant. Input is a sinusoidal wave with a frequency of 1 Hz acting for a duration of 20 s. The amplitude of the input is selected to be 1 m/s corresponding to the minimum peak particle velocity affecting any tunnel structure. The variation in normal force, shear force and bending moment acting on the rockbolt corresponding to varying properties are studied.

6.10.1 Rockbolt Diameter

Rockbolts of different diameters are available in the market and size used in a tunnel ranges typically between 20 mm to 24 mm. It is important to know the performance of rockbolt diameter under dynamic load. The effect of rockbolt diameters variation from 20 mm to 34 mm is studied. This will allow in providing the required diameter rockbolt or designing a specific rockbolt for critical projects. Figure 6.38 shows the change in normal force on each rockbolt with the change in diameter. The effect on rockbolt performance highly depended on the position of the rockbolt. The variation in normal force in the rockbolts for the upper (tunnel position 180° to 360°) and lower half (22.5° to 157.5°) of the tunnel is different. Normal force on bolts passing through joints is comparatively unaffected by the change in diameter. However, bolts through intact block experience an increase in normal force as the diameter increases. This change is more pronounced in the rockbolts on the lower half, rockbolt numbers 1, 2, 4, 5, 6 and 16 (0˚ to 135˚) of the tunnel. In the upper half of the tunnel also, rockbolts undergo higher normal force for larger diameter rockbolts, but the effect is comparatively low. Even with these changes, the maximum normal force still acts on rockbolt numbers 3 and 9 with a force of 112.3 kN and 112.5 kN respectively. However, at 32 mm and 34 mm diameters, rockbolts 2 and 6 also approach a normal force of 106.7 kN and 109.2 kN.

The shear force on bolts through intact rock is negligible compared to jointed rocks as seen in Figure 6.33. An increase in shear force occurs as the diameter of the rockbolt increases from 20 mm to 34 mm (Figure 6.39). Increase in shear force occurs on all bolts with the increase in diameter, but it is negligible for rockbolts through intact blocks. As the rockbolt diameter increases, strength and modulus of the rockbolt also increase, producing higher resistance. Jalalifar et al. (2005), in their study on rockbolt shear, noticed a higher resistance is offered by rockbolt with bigger diameter. Shear force is maximum in rockbolt 15 as it produces 17.42 kN for 34 mm rockbolt diameter. The maximum ratio of shear force increase is on rockbolt number 13 as shear force increases from 0.87 kN for a 20 mm rockbolt to 8.21 kN at 34 mm. The increase in shear force in rockbolts 13 and 14 are also comparably high, producing a maximum value of 11.08 kN and 11.95 kN respectively for 34 mm diameter rockbolts. However, with the increase in diameter from 20 mm to 34 mm, the change in shear force is lowest for rockbolt 3, where it increases from 1.92 kN to 5.14 kN. This indicated a predominant increase in shear force on the rockbolts in the upper half of the tunnel compared to the lower half. This might be due to the additional force acting on the blocks due to gravity.

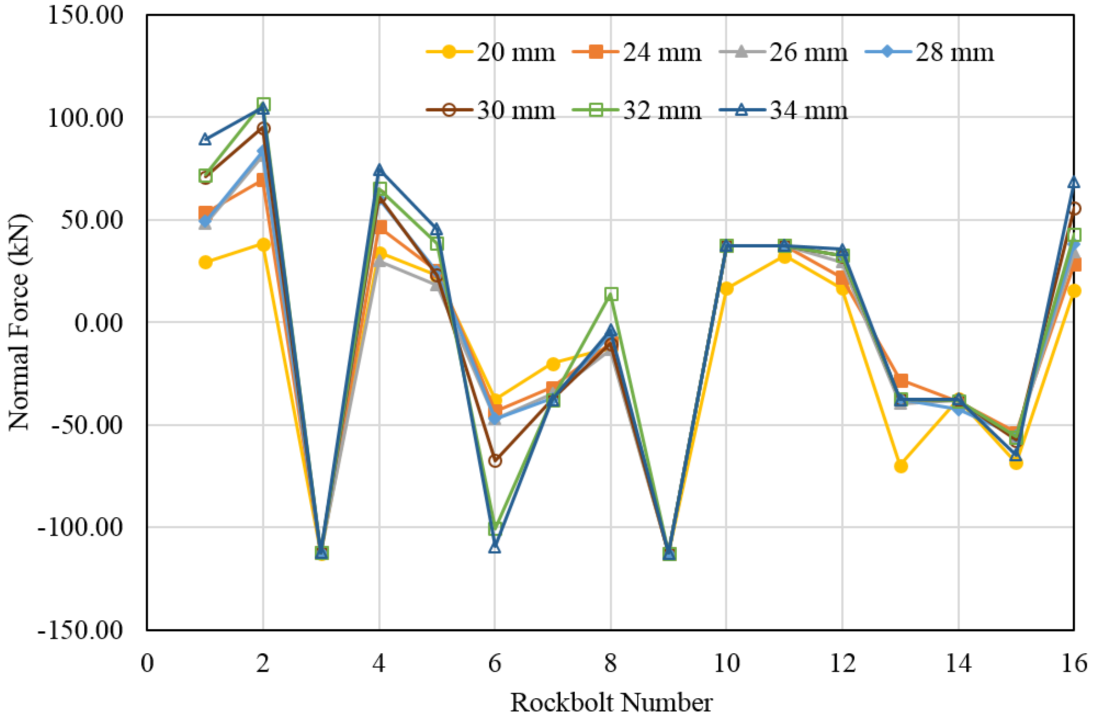

Figure 6.38: Normal force acting on each rockbolt with variation in rockbolt diameter

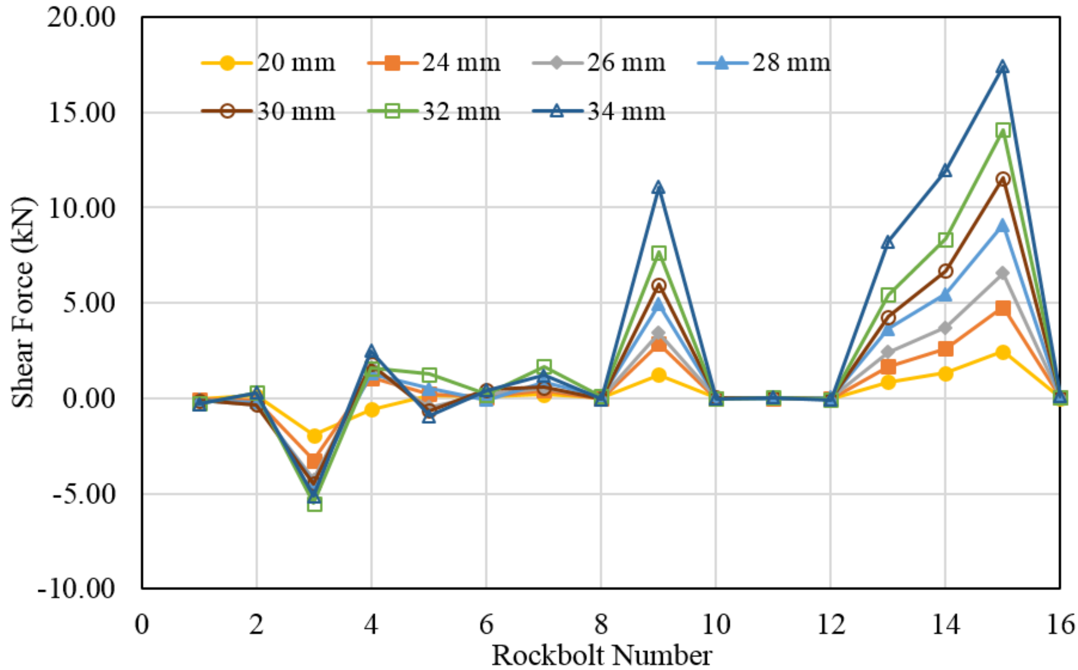

Figure 6.39: Shear force acting on each rockbolt with the change in rockbolt diameter

The angle between the rockbolt and joint is different for each rockbolt. Rockbolts 3 and 9 are at angles 23˚ and 20˚ to the joint, while rockbolts 13, 14 and 15 are at angles 62˚, 84˚ and 73˚ respectively with the joint. Though there might be an effect on the angle of rockbolt placement, these results point out that the position of the bolt plays a much significant role.

As the shear force increases, the bending moment also increases as in Figure 6.40. The bending moment acting on rockbolts passing through joints increases as the diameter of the rockbolt increases. The increase in bending moment for rockbolts through joints is shown in Figure 6.41. Bending moment acting on rockbolt 15 is 7.38 kNm for 34 mm diameter and is the maximum among all the rockbolts. But the increase in bending moment is lowest for rockbolt 3 from 0.82 kNm to 3.08 kNm as the diameter increases from 20 mm to 34 mm.

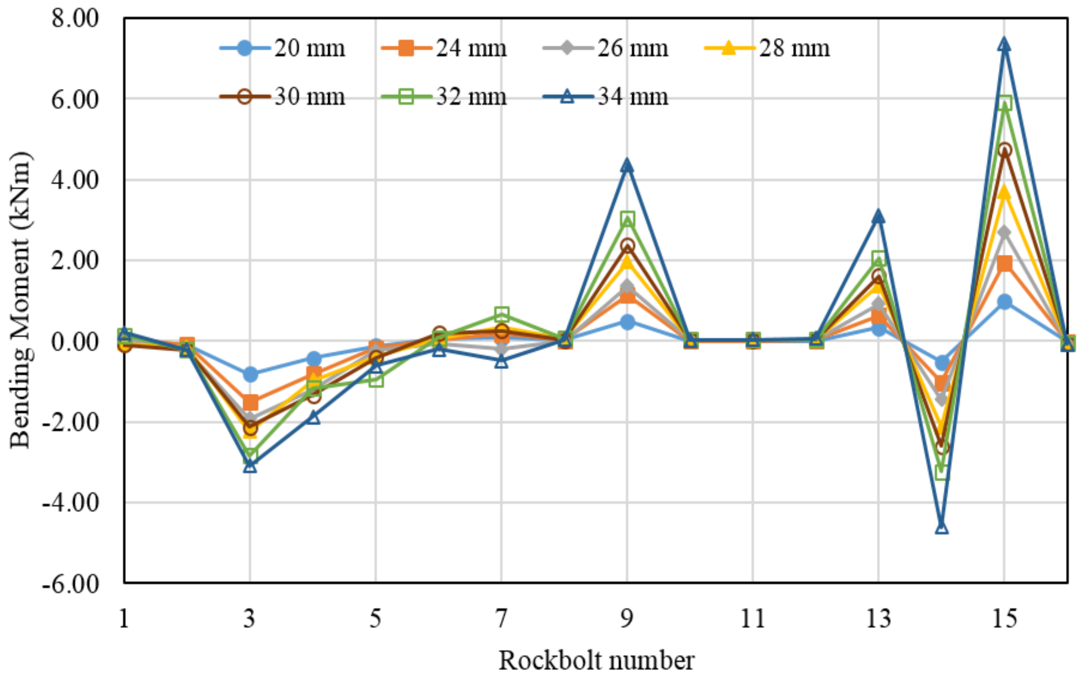

Figure 6.40: Bending moment acting on each rockbolt with the change in rockbolt diameter

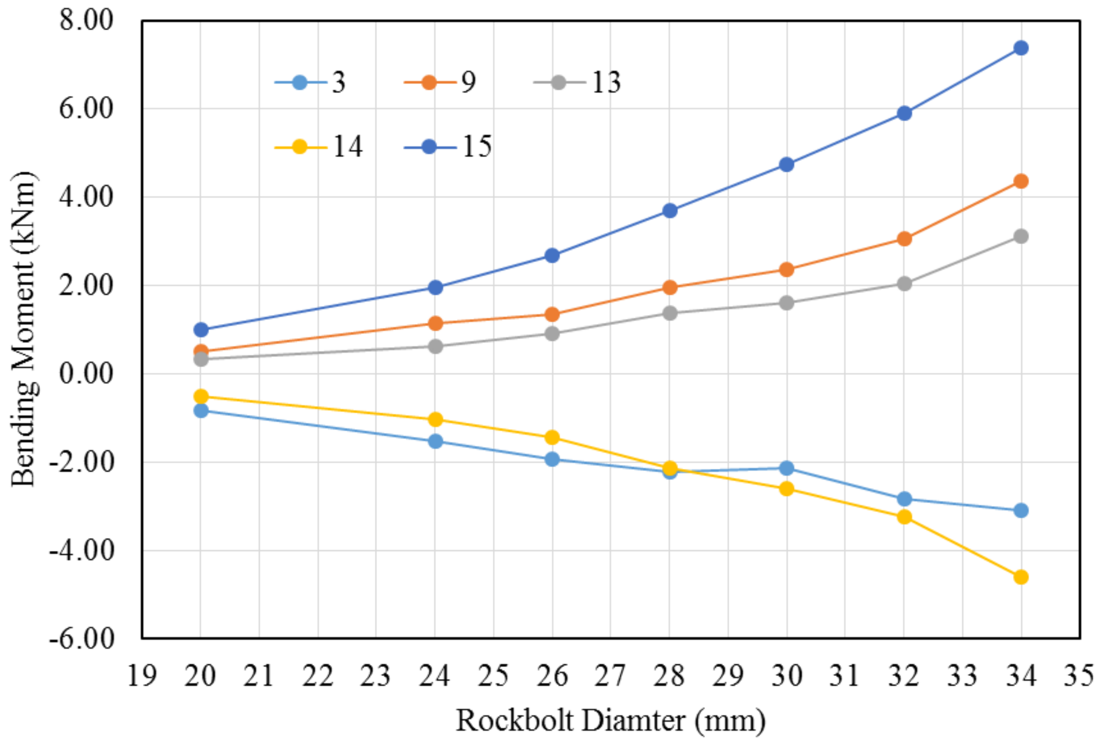

Figure 6.41: Effect of diameter on bending moment for rockbolts passing through joints

6.10.2 Length of the Rockbolt

The embedment length of all bolts is greater than one meter and as per standards. Figure 6.42 shows the rockbolt orientation in rockmass for lengths 4 m and 5 m. The orientation of 3 m bolt is the same as that of Figure 6.14. With the increase in rockbolt length, the embedment length of the existing bolts increases. However, the new intersections may not follow the minimum embedment length rule. Bolt numbers 10, 11, 12 and 16 which passed through intact blocks earlier, now passes through joints for increased bolt length of 4m. When the bolt length is increased to 5m, rockbolt number 2 also gets intersected by joints. Additionally, as the bolt length is increased to 4 m and 5 m, rockbolt number 9 intersects a second pair of joint. The study will give us an understanding on the effect of embedment length on rockbolts under dynamic conditions. This also gives an insight into the difference in the forces acting on rockbolt under the intact and jointed condition.

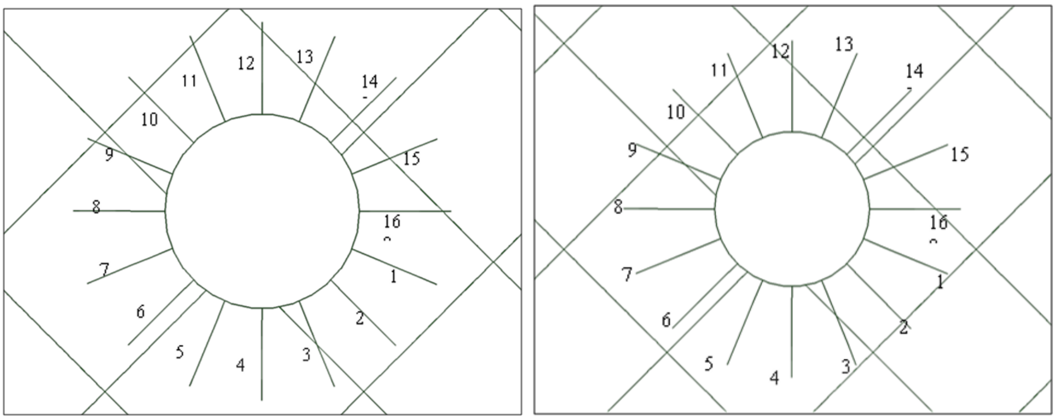

(a) (b)

Figure 6.42 : Rockbolt orientation for bolt lengths (a) 4 m (b) 5 m

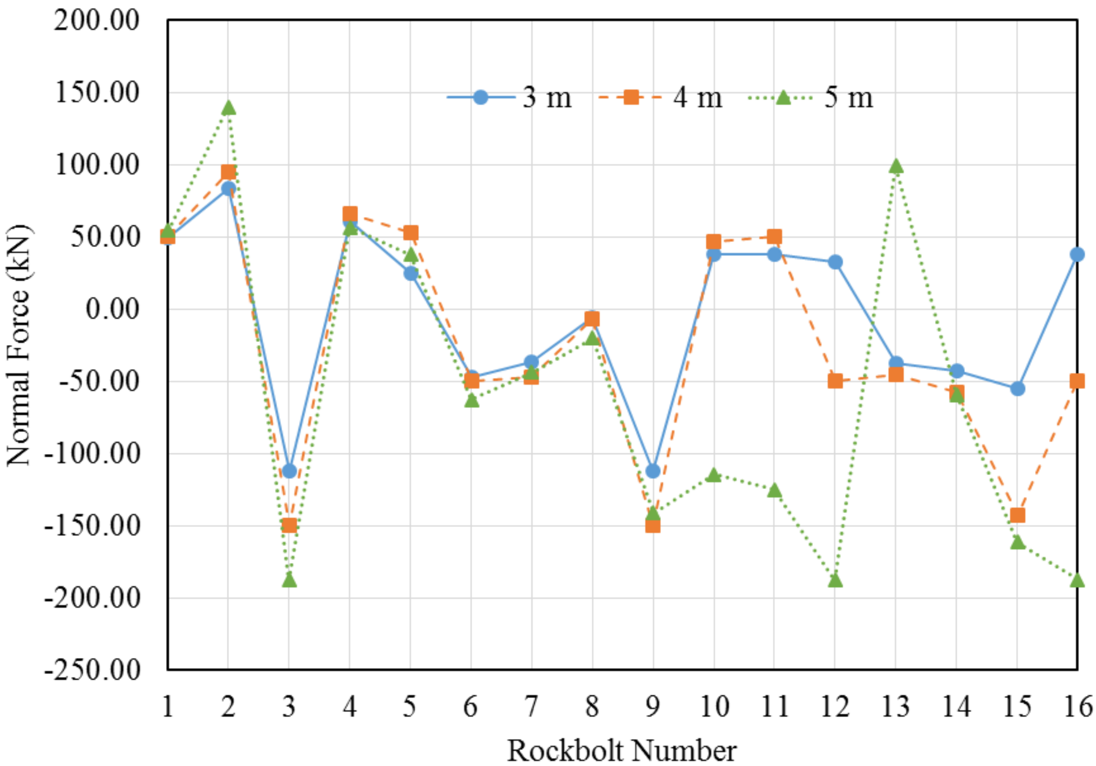

Figure 6.43: Normal force acting on rockbolt for different bolt lengths

Figure 6.43 shows the variation of normal force with the increase in bolt length. Under all bolt, a maximum normal force acts on rockbolt 3. It can be noticed that the normal force on the bolt increases as the bolt length increases. As the bolts pass through a joint, an increase in normal force is observed. The normal force acting on the bolt further increases as the embedment length increases. Rockbolt 9 on the increase of length passes through a second set of joint. This leads to an increase in the normal force acting on the bolt. However, as the bolt length is further increased to 5m, a better embedment is obtained, and the normal force slightly decreases. Rockbolt 16 undergoes a large change in normal force with the increase in bolt length. Sato et al. (2004) stated that embedment length has no effect on bond strength under dynamic loading condition but does not give any details about the change in force acting on the bolt. An increase embedment length leads to a decrease in shear force (Figure 6.44) and bending moment (Figure 6.45) on the rockbolts. The bolts already passing through joints have slightly lower bending moment. However, for new intersections, an increase in shear force and bending moment occurs at 4m, which later decreases when bolt length increases to 5 m. For bolts which do not have a joint intersection, the increase in bolt length is found to bring little or no difference in normal force, shear force and bending moment.

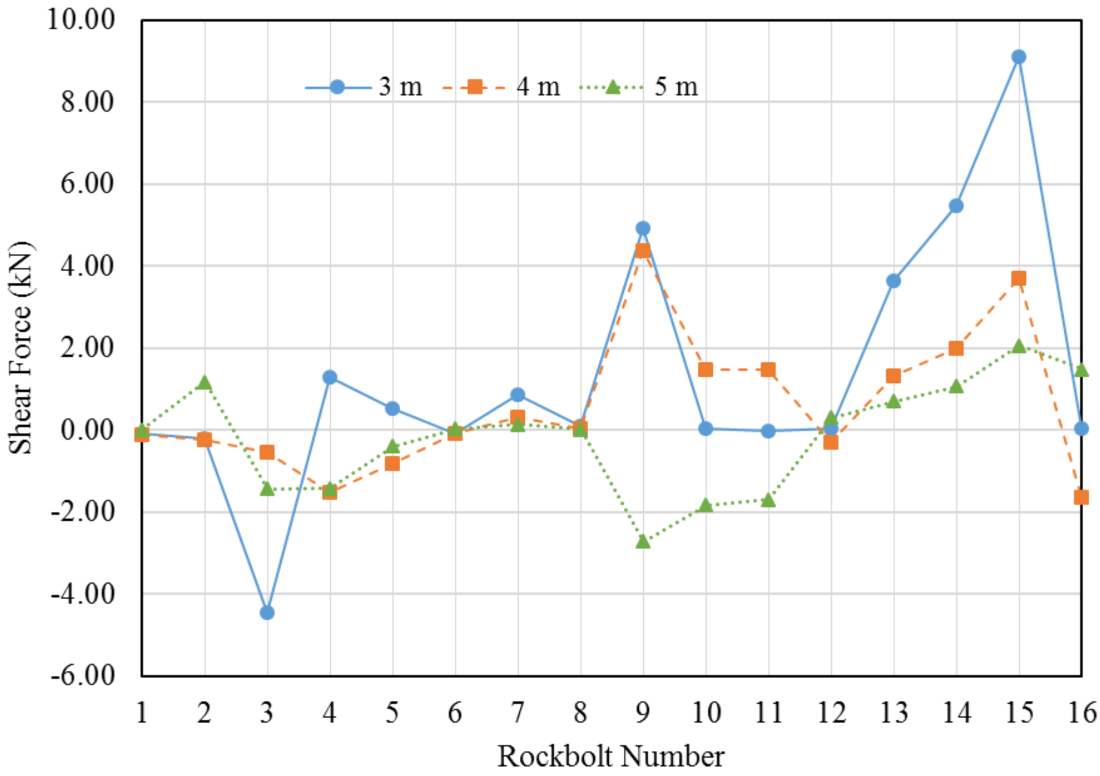

Figure 6.44: Shear force acting on rockbolt for different bolt lengths

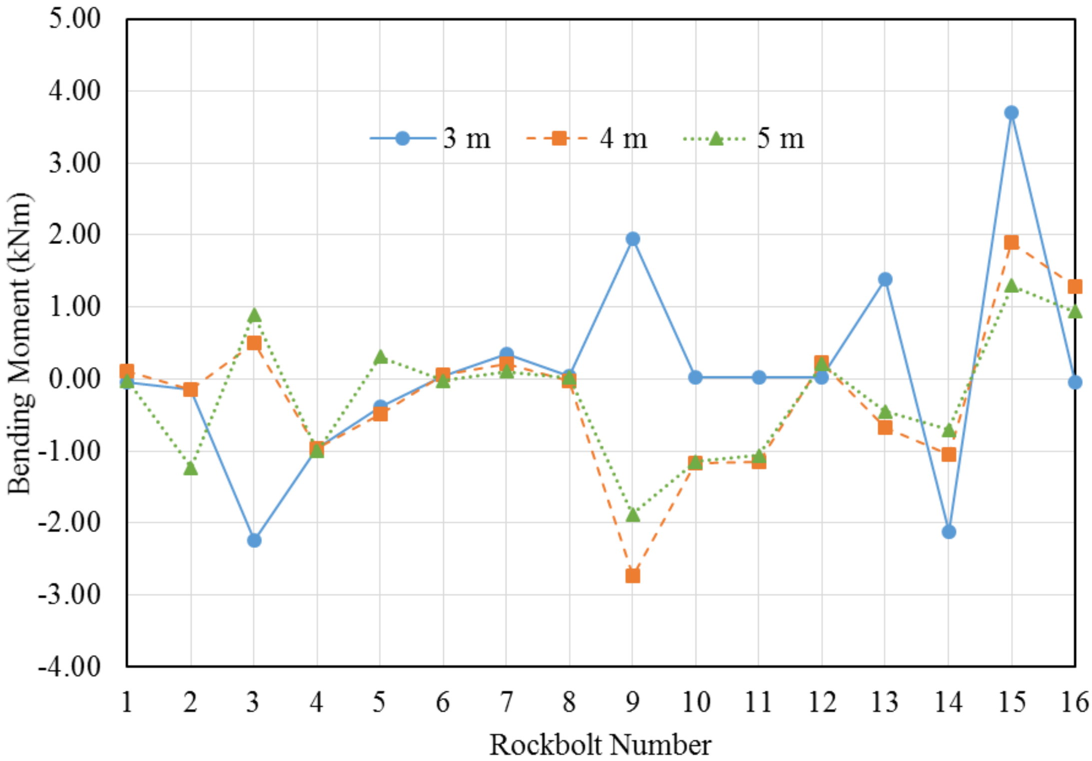

Figure 6.45: Bending moment acting on rockbolt for different bolt lengths

6.10.3 Joint Friction

Joint friction determines the strength of joint to a large extent. For bolts not passing through joints, no effect is visible. Figure 6.46 to Figure 6.48 shows the effect of increasing joint friction on normal force, shear force and bending moment. The joint friction is varied from 28˚ to 40˚ Figure 6.46 shows the variation of normal force acting on the bolts with varying joint friction. Normal force is unaffected by the change in joint friction. However, shear force and bending moment acting on rockbolts decreases with an increase in joint friction as shown in Figure 6.47 and Figure 6.48. As the joint friction increases, the relative displacement between the blocks reduces, which leads to a decrease in shear force and bending moment acting on the bolts. Since the shear displacements being mainly affected by joint friction, the normal force is largely unaffected.

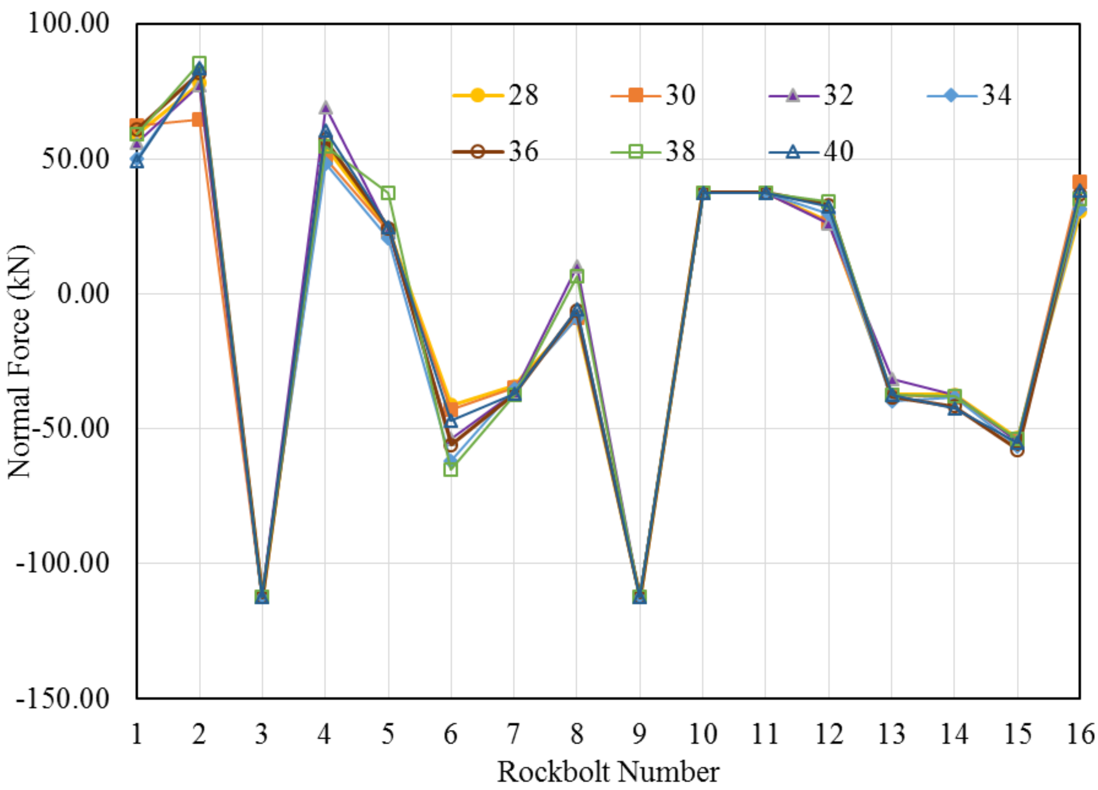

Figure 6.46 : Effect of joint friction on rockbolt normal force

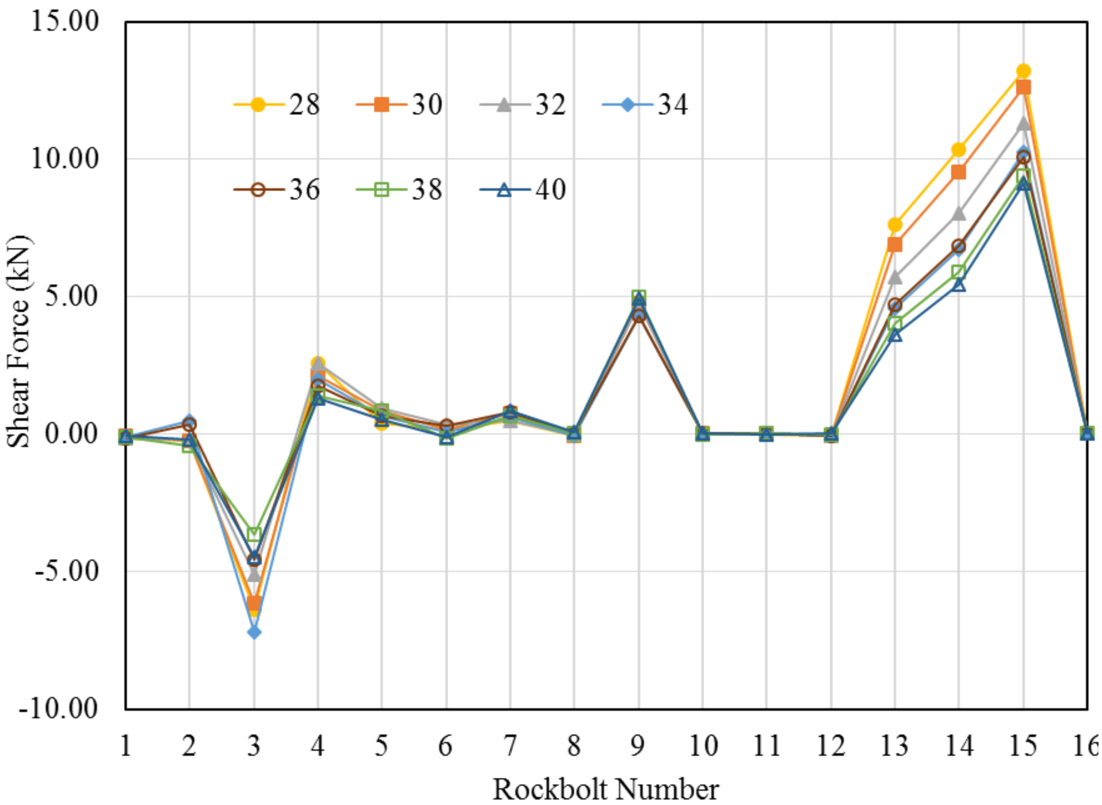

Figure 6.47 : Effect of joint friction on rockbolt shear force

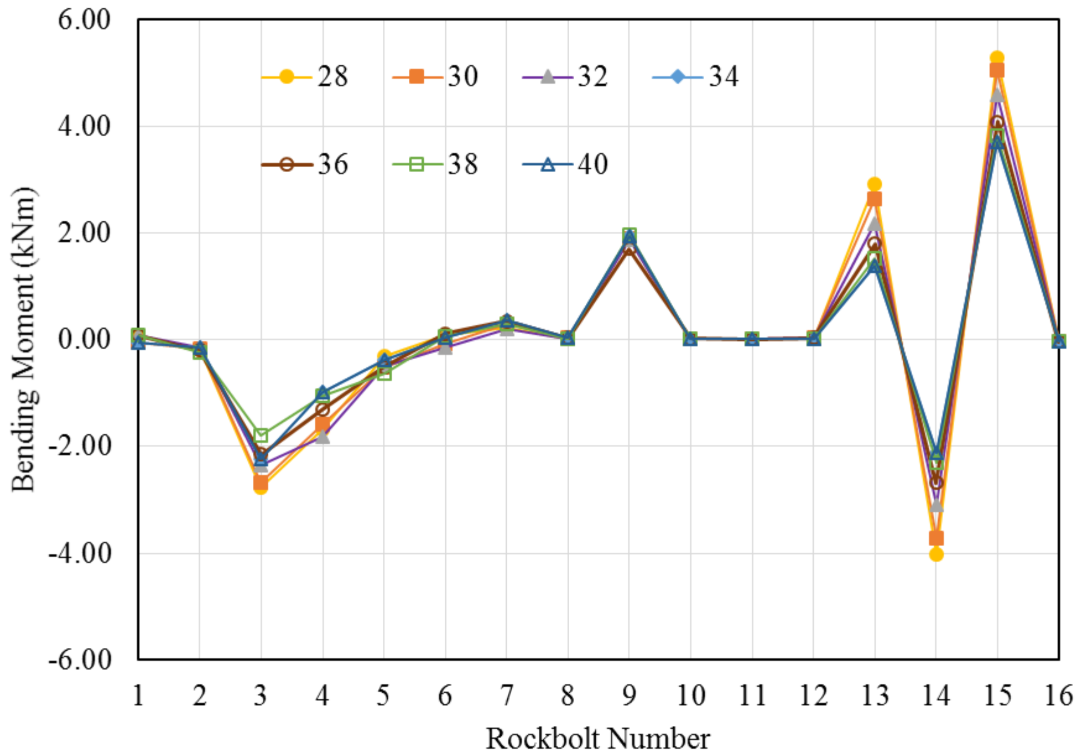

Figure 6.48: Effect of joint friction on rockbolt bending moment

6.10.4 Frequency of the Dynamic Input Motion

Under dynamic loading, the frequency of the incoming wave is identified to have a high influence on the tunnel. Frequencies between 1 Hz to 6 Hz found to have impact on the tunnel or tunnel structure (Roy and Sarkar, 2018). For the current study, the frequency is varied from 1 Hz to 6 Hz to understand its effect on different rockbolts. The normal force acting on rockbolts varies with frequency. Figure 6.49 shows that maximum normal force exerted by each frequency is on different rockbolt. The maximum normal force of 112.6 kN acts on rockbolt 9. Other frequencies also exert the similar magnitude of normal force on rockbolt number 9. Rockbolt numbers 3 also experience the almost equal normal force of 112.3 kN at all frequencies. Next highest normal force acts on rockbolt number 13 of 110 kN at 3 Hz. Individually each rockbolt experiences different maximums for different frequencies. For rockbolts through intact blocks, the maximum normal force is mostly exerted by 1 Hz frequency.

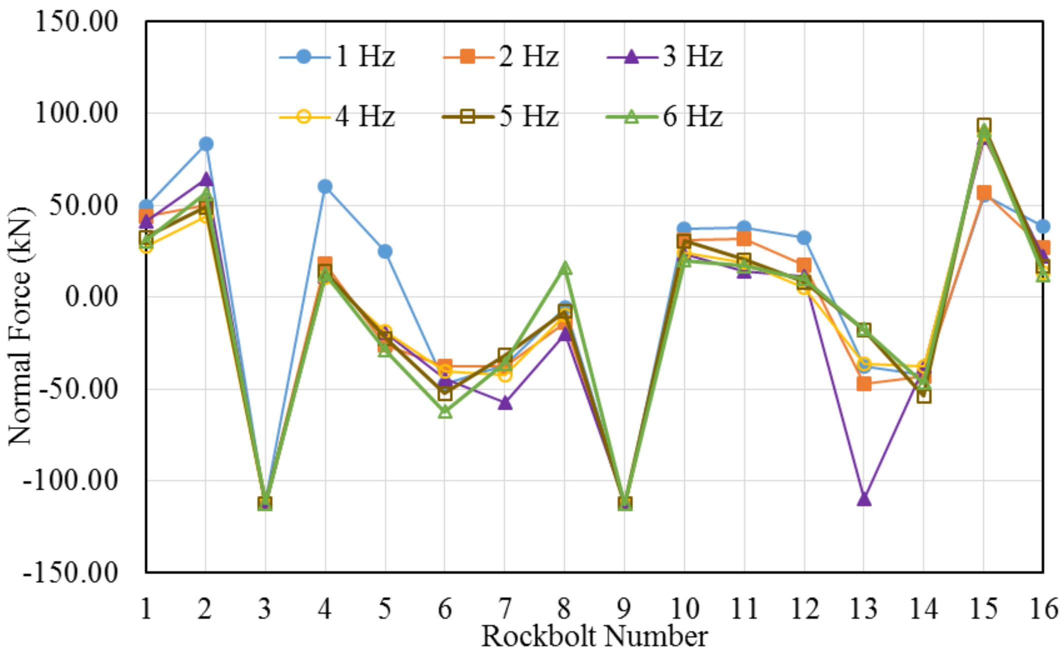

Figure 6.49: Variation in normal force with change in frequency

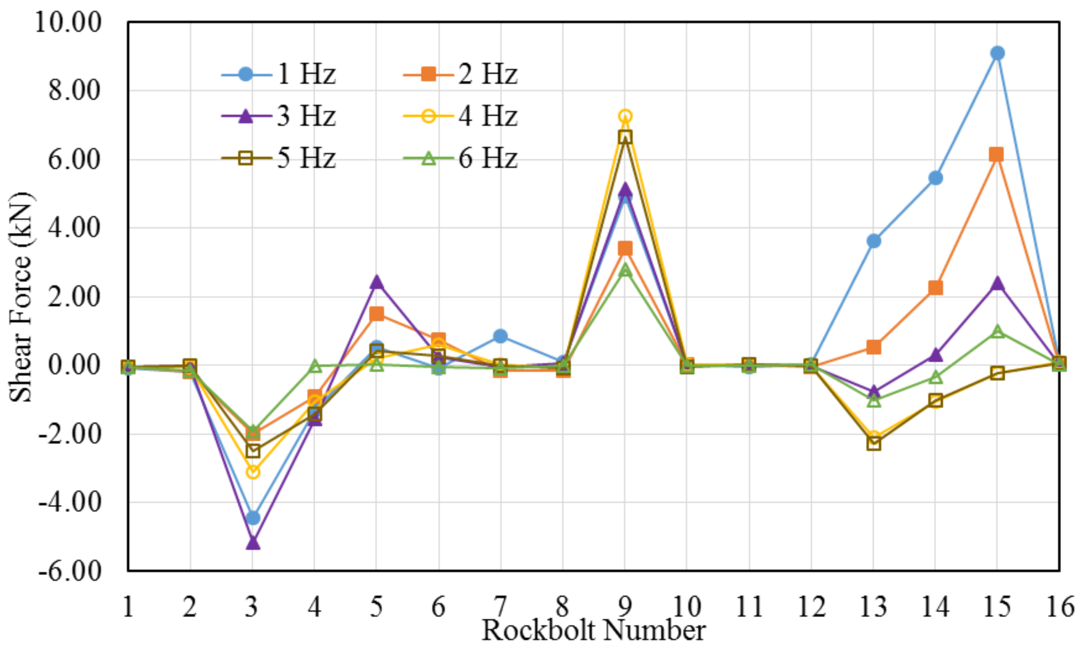

Figure 6.50: Variation in shear force with the change in frequency

The shear force (Figure 6.50) and bending moment (Figure 6.51) acting on all the rockbolts passing through joints are considerably affected by frequency. However, the maximum shear force and bending moment do not occur for the same frequency in all the rockbolts. This shows that each frequency wave affects different points in the tunnel. The upper half of the tunnel is mainly affected at a frequency of 1 Hz. The effect by the other frequencies are small and one-fourth of that of1 Hz, in rockbolts 13, 14 and 15. For rockbolt 3, the frequencies 1 Hz and 2 Hz exerts maximum moment whereas in rockbolt 9 frequencies 4 Hz and 5 Hz exerts maximum moment. This implies that the damage or stress occurring in a tunnel depends on the frequency of the incoming stress wave. An incoming wave of different frequencies affects different parts of the tunnel. The influence of frequencies higher than 5 Hz is found to be negligible on shear force and bending moment.

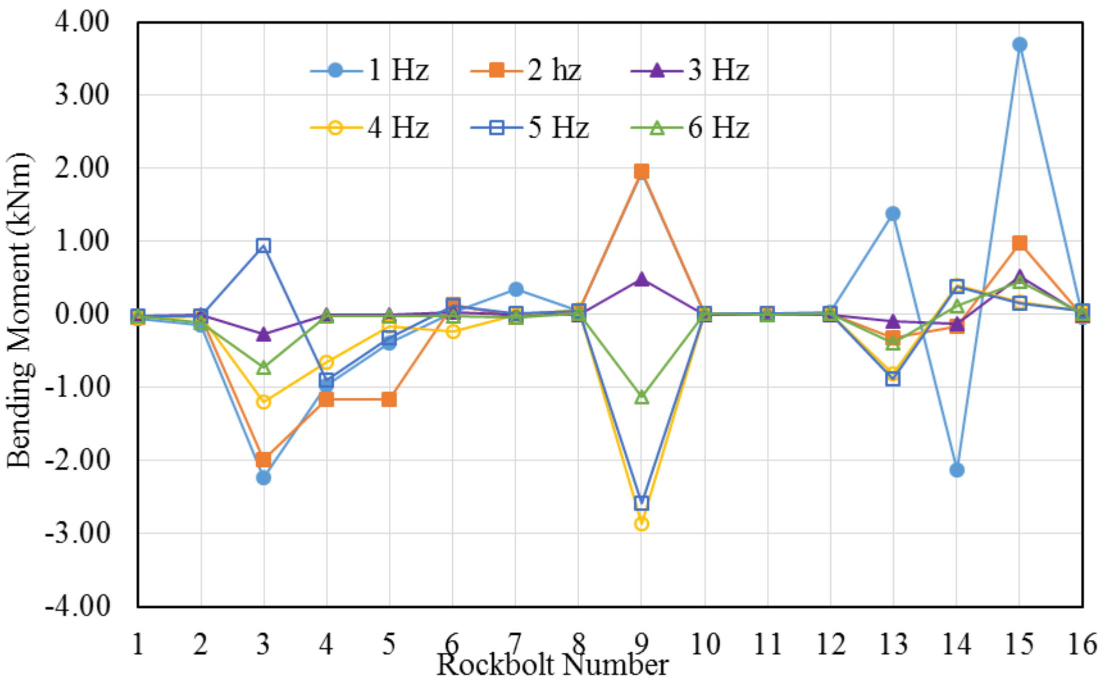

Figure 6.51: Variation in bending moment with change in frequency

6.10.5 Duration of Dynamic Input Motion

Time duration over which the dynamic load acts affects the forces acting on the rockbolts. The duration of dynamic input is varied from 5 s to 20 s. However, it is noticed that the effect of duration on normal force, shear force and bending moment (Figure 6.52, Figure 6.54 and Figure 6.55 respectively) relatively small. Similar findings are presented in the study by Ahola et al. (1996) where the tunnel displacements were found to have very little variation with amplitudes less than the threshold.

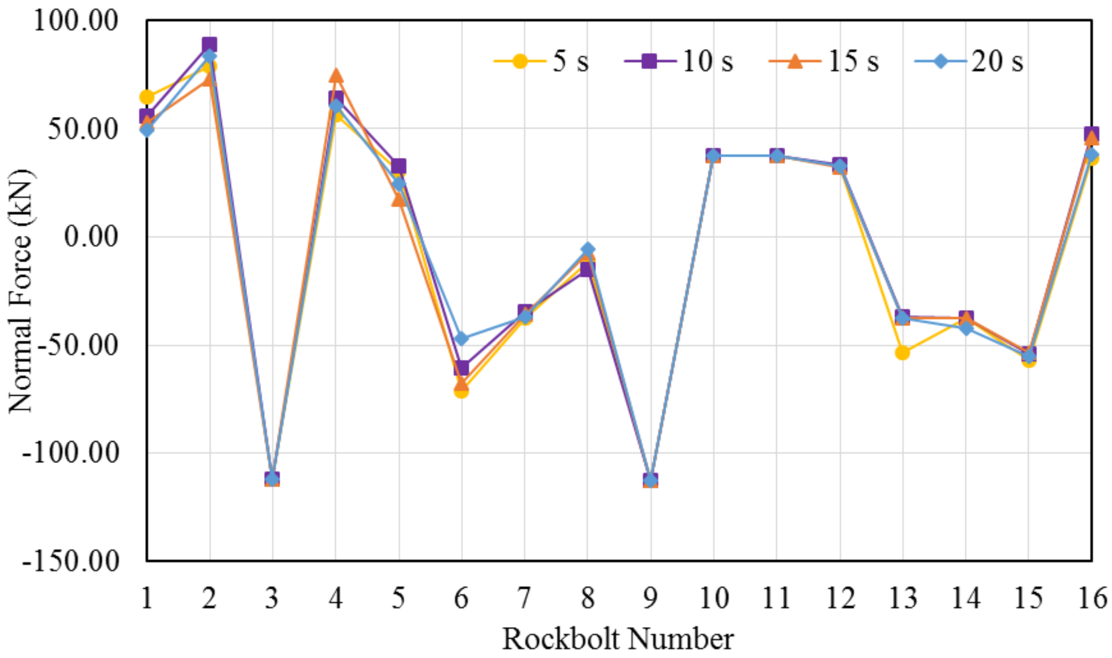

Figure 6.52: Effect of duration on normal force

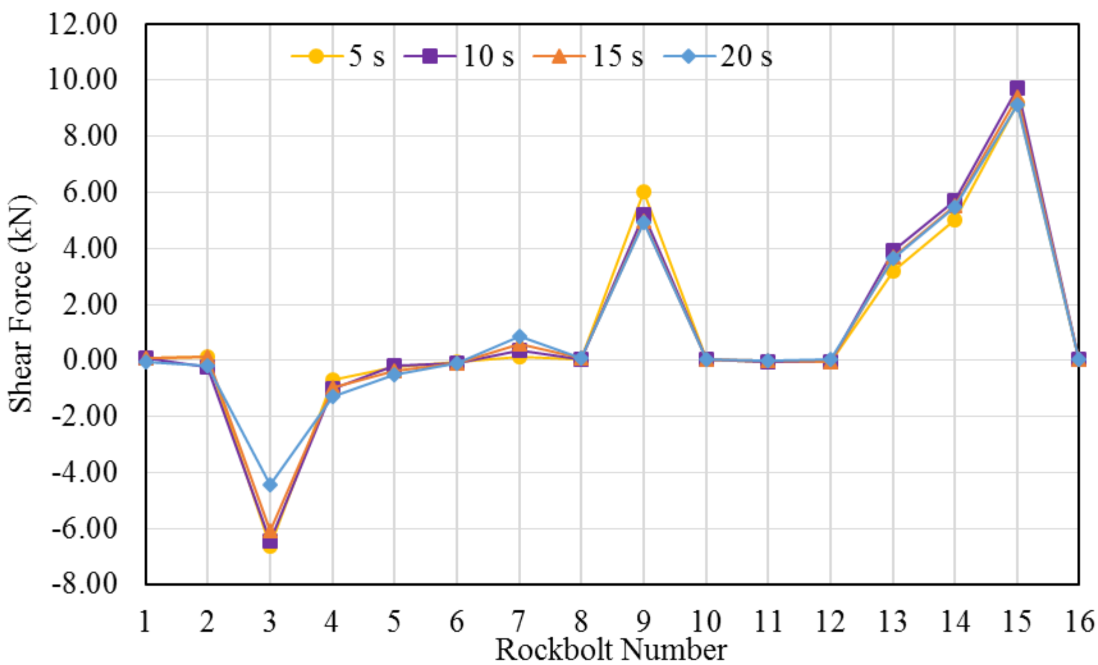

Figure 6.53: Effect of duration on shear force

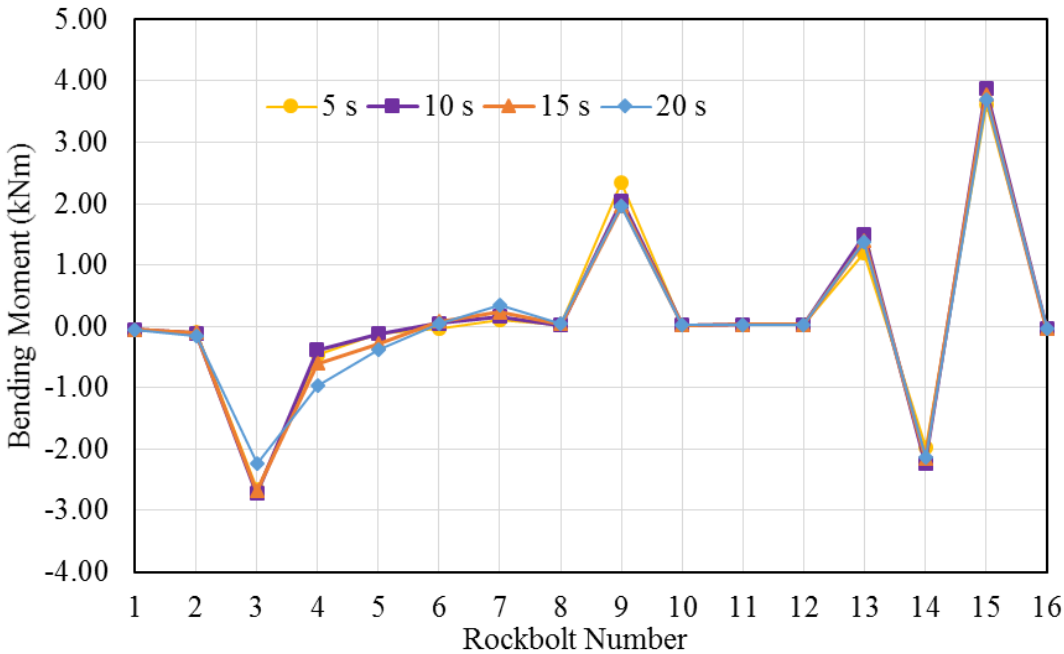

Figure 6.54: Effect of duration on bending moment

6.10.6 Amplitude of the Dynamic Input Motion

Failure of any structure depends on the maximum force acting on it. The studies from Chapter 5 also highlights the presence of a threshold amplitude beyond which the dynamic loads trigger the tunnel deformation. Researchers point out that a peak particle velocity below 800 mm/s produces a negligible effect on a rockbolt. In the current research, the wave amplitude is varied from 400 m/s to 1200 m/s. Figure 6.55, Figure 6.56 and Figure 6.57 show the maximum normal force, shear force and bending moment acting on each rockbolt at different load amplitudes respectively. The effect of change in amplitude is different in the upper half of the tunnel and lower half of the tunnel. The normal force acting on rockbolts 3 and 9 which passes through joints are comparatively unaffected by the increase in amplitude. However, the bolts through intact block are affected, and an increase in normal force occurs with an increase in amplitude. For the upper half of the tunnel, normal force increases with an increase in amplitude. This is most significant in rockbolt 13. Normal force acting on rockbolt 13 increases to 113 kN from 23.7 kN as amplitude changes from 0.4 m/s to 1200 m/s. Maximum normal force acts on rockbolts 3, 9 and 13 at 1.2 m/s.

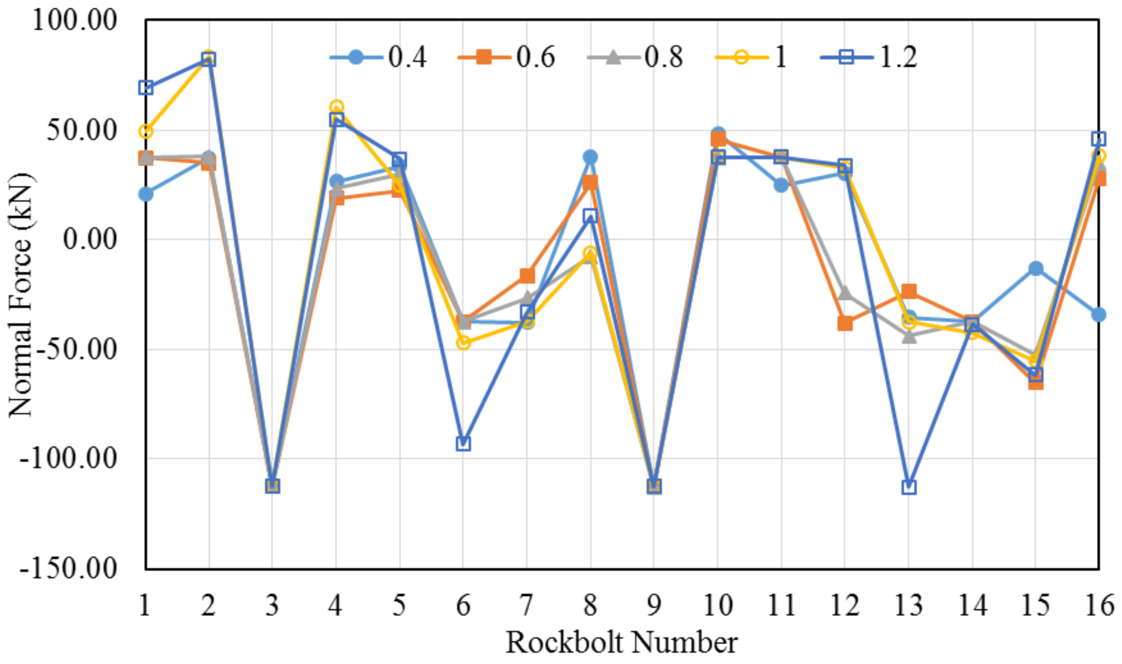

Figure 6.55: Effect of load amplitude on normal force

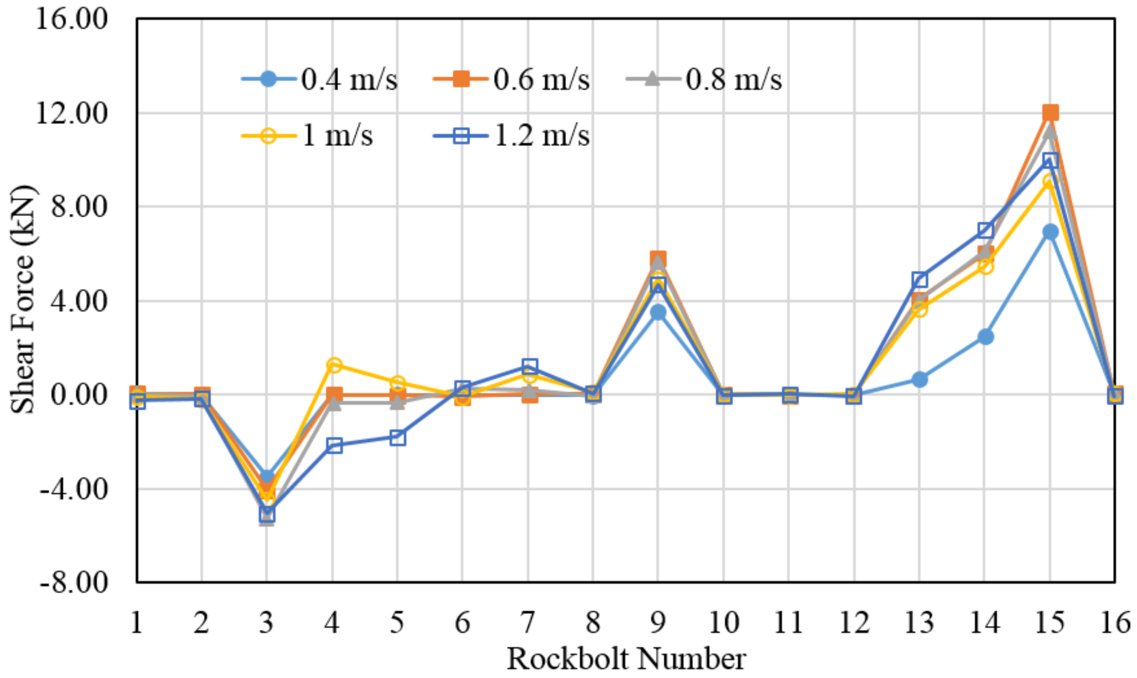

Figure 6.56: Effect of load amplitude on shear force

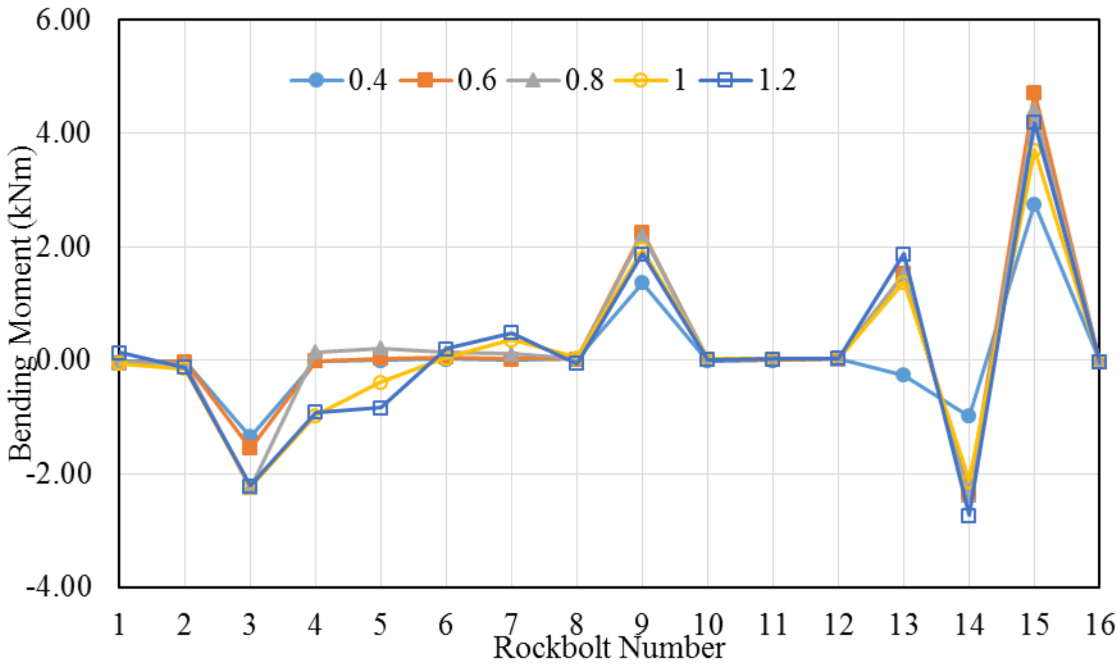

Figure 6.57: Effect of load amplitude on bending moment

The shear force and bending moment increase in all rockbolts as amplitude increases. The increase is more significant in the upper half of the tunnel compared to the lower half. Rockbolt 15 experiences a maximum shear force and bending moment at 0.6 m/s wave amplitude. The bending moment and shear force for rockbolt 15 further decreases with an increase in amplitude. Similar variation occurs on rockbolt 9 as well. This suggests a difference in the magnitude of shear loads acting on bolts adjacent to the walls of the tunnel.

6.11 SUMMARY

The present chapter attempts to understand the performance of rockbolts under seismic conditions. A headrace tunnel of Tehri dam site in seismic zone V is considered. Rockbolts are considered to be the only support system around the tunnel and its response under the action of two earthquakes. The study is then extended to understand the effect of different parameters on the rockbolts.

The normal force, shear force, bending moment and deformations acting on the rockbolts are analysed to understand the performance of the rockbolts. The behaviour for rockbolts passing through joints and intact blocks are compared under static and seismic conditions. The pattern of maximum forces acting, and the position of maximum force acting also differs. Normal force is found to act on all rockbolt under static and seismic conditions. The maximum normal force acts on rockbolts passing through joints. Shear force and bending moment act only on rockbolts intersecting joints. The magnitude of shear force and bending moment increases under the action of earthquake load, and the effect is predominant in the bolts passing through joints on tunnel shoulders. The deformation of rockbolts is higher under the action of seismic load compared to static load. The displacement patterns for Uttarkashi earthquake (1991, M_w=6.8) and Nepal earthquake (2015, M_w=8.1) showed different trends. Hence giving light to the fact that pattern of failure affected by the earthquake characteristics.

A parametric study is carried out to understand the performance of the tunnel under different rockbolt, earthquake and rock mass conditions. Rockbolts are found to have an increase in the forces, as the rock bolt diameters are increased. This increase is most predominant in the upper half of the tunnel compared to the lower half. The rockbolts passing through joints are found to produce maximum force. The embedment length is found to decrease the shear force and bending moment acting on the rockbolt. When a rockbolt initially in intact block coincides with a joint, an increase in shear force and bending moment occurs. Shear forces and bending moment subsequently decreases with the increase in embedment length. The relative displacement between blocks being influenced by the joint friction leads to a decrease in relative displacement with increase in the joint friction value. This leads to a decrease in shear force and bending moment as the joint friction increases. Normal force acting on the rockbolts remain comparatively unaffected by the change in joint friction.

The earthquake properties are found to have considerable influence as seen from the results of Uttarkashi earthquake (1991, M_w=6.8) and Nepal earthquake (2015, M_w=8.1). Hence, the effect of frequency and duration of an incoming earthquake is studied. With the variation of incoming wave frequency, different parts of the tunnel behave differently. The normal force acting on each rockbolt differs for different frequency and is found to follow no uniform pattern. The increase in the duration of loading is found to increase the forces acting on the rockbolt. However, these changes are comparatively small since the duration makes a negligible influence on the rockbolt for lower earthquake magnitude. The forces acting on each rockbolt is also found to be affected by the amplitude of the incoming wave. Increase in the forces are also observed with an increase in amplitude.

CHAPTER 7

PERFORMANCE OF SHOTCRETE UNDER SEISMIC LOAD

7.1 INTRODUCTION

Shotcrete, also known as sprayed concrete lining (SCL), is extensively being used as a temporary or permanent support system in rock tunnels. Rabcewicz (1969) identified shotcrete to be a material well suited for tunnelling due to 1) Shotcrete can be used as a permanent support structure 2) provides the characteristics of a good support system and allows small deformations due to stress redistribution along with resistance to large strains 3) provides support to all types of geometry. The use of shotcrete has allowed the construction of tunnels of various size and cross-section quickly and economically. This is especially true for the excavations of blocky rock, where the method and shape of excavation depends on the strength of the rock and type of jointing. The sprayed concrete helps in providing support to the blocks. A layer of shotcrete used in tunnels is of 50 mm to 150 mm thickness with requirement for reinforcement with steel fibres or wire mesh depending on the load acting.

The performance of shotcrete is supposed to be very good under the action of seismic loads due to its flexible nature and their lower vulnerability under its inertia (Thomas, 2009). However, a lack of good understanding on the performance of shotcrete under the action of an earthquake is persistent. The present study attempts to identify the performance of shotcrete during earthquakes when it is acting as the only supporting member in a tunnel. For the study, the headrace tunnel of Tehri dam as discussed in Chapter 6 is considered with shotcrete as the support system. The earthquake histories of Uttarkashi (1991, M_w=6.8) and Nepal (2015, M_w=8.1) as described in the previous chapter, is considered for analysis. A parametric study is carried out as in the case of rockbolt to understand the performance of shotcrete under various conditions of seismic loading.

7.2 SHOTCRETE FORMULATION AND CALCULATIONS IN NUMERICAL MODEL

The analysis of the shotcrete in UDEC is similar to rockbolt, where the structure discretised first into nodes over which the mass concentrated. The axial, shear and rotational forces acting are calculated on these nodes by the matrix equation,

$$\begin{bmatrix} T_1 \\ S_1 \\ M_1 \\ T_2 \\ S_2 \\ M_2 \end{bmatrix} = \frac{E}{L}\begin{bmatrix} A & 0 & 0 & -A & 0 & 0 \\ 0 & \frac{12I}{L^2} & \frac{6I}{L} & 0 & -\frac{12I}{L^2} & -\frac{6I}{L} \\ 0 & \frac{6I}{L} & 4I & 0 & -\frac{6I}{L} & 2I \\ -A & 0 & 0 & A & 0 & 0 \\ 0 & -\frac{12I}{L^2} & -\frac{6I}{L} & 0 & \frac{12I}{L^2} & -\frac{6I}{L} \\ 0 & -\frac{6I}{L} & 2I & 0 & -\frac{6I}{L} & 4I \end{bmatrix}\begin{bmatrix} u_1 \\ v_1 \\ \theta_1 \\ u_2 \\ v_2 \\ \theta_2 \end{bmatrix} \qquad \text{(Eq.7.1)}$$

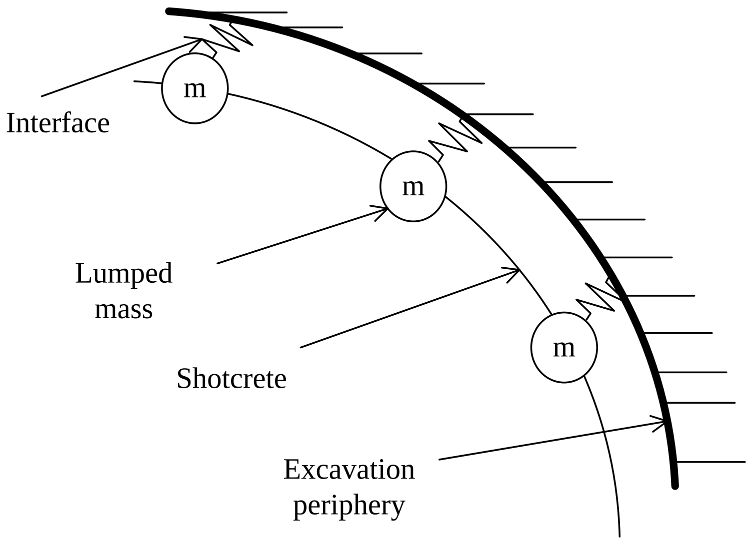

Figure 7.1: The segmental division of shotcrete as lumped mass.

The desirable characteristics of the formulation are the slip between support and excavation, which can be modelled similar to the slip along discontinuities and that large displacements and nonlinear behaviour of the material are adjusted inherently. The material model used in this surface lining can simulate inelastic behaviour. It can exhibit ductile or brittle behaviour, but the material model does not support shear failure. Moment thrust interaction values are used for calculations and corresponding failure. The axial forces and bending moments acting on the shotcrete are calculated as

$$P = \frac{F_c + F_t}{2} A \qquad \text{(Eq. 7.2)}$$

$$M = I \frac{(F_c - F_t)}{h} \qquad \text{(Eq. 7.3)}$$

where, P is the axial force, M is the bending moment, F_c and F_t are compressive and tensile strength of the material, I is the moment of inertia and h is the thickness of the shotcrete. At every calculation step, the axial force and moment are compared to the ultimate capacity. When any node reaches the ultimate value, the node is assigned with a fracture flag, which ensures that the future evaluations for the particular node will use "cracked" failure envelope and residual strength capacity. For unreinforced concrete and shotcrete, cracking is permissible with crack depth ratio ($\frac{h_c}{h}$) upto 0.5. The axial force and moment under this condition is represented as,

$$P_{crack} = \frac{1}{2} F_c A \left(1 - \frac{h_c}{h}\right) \qquad \text{(Eq. 7.4)}$$

$$M_{crack} = \frac{1}{12} F_c A h \left(1 + \frac{h_c}{h} - 2\left(\frac{h_c}{h}\right)^2\right) \qquad \text{(Eq. 7.5)}$$

7.3 NUMERICAL MODELLING OF THE TUNNEL

A UDEC model of Tehri dam head race tunnel as discussed in chapter 6 (sections 6.4 and 6.6) is used in the current study. Keeping the rock mass and tunnel structure same, the tunnel support system is replaced with shotcrete. The tunnel is supported by shotcrete of 10 cm thickness, which is uniformly sprayed around the tunnel. This shotcrete is discretised into 60 nodes over which the mass is distributed. The velocity histories (Figure 6.6 and 6.10) are applied as shear input at the base of the model. The properties of the shotcrete are as provided in Table 7.1 and Figure 7.2 shows the schematic UDEC model. The rockmass properties are as in Table 6.2. The tunnel position mentioned in the chapter is similar to the

Table 7.1: Shotcrete properties considered for the numerical analysis

Parameter	Value
Characteristic strength (MPa)	20
Factor of safety	1.5
Density (kg/m3)	2500
Modulus of elasticity (GPa)	21
Poisson's ratio	0.15
Thickness (mm)	100
Interphase Normal Stiffness (Pa/m)	1×10^{10}
Interphase Shear Stiffness (Pa/m)	1×10^{10}
Interphase Friction Angle (degree)	40

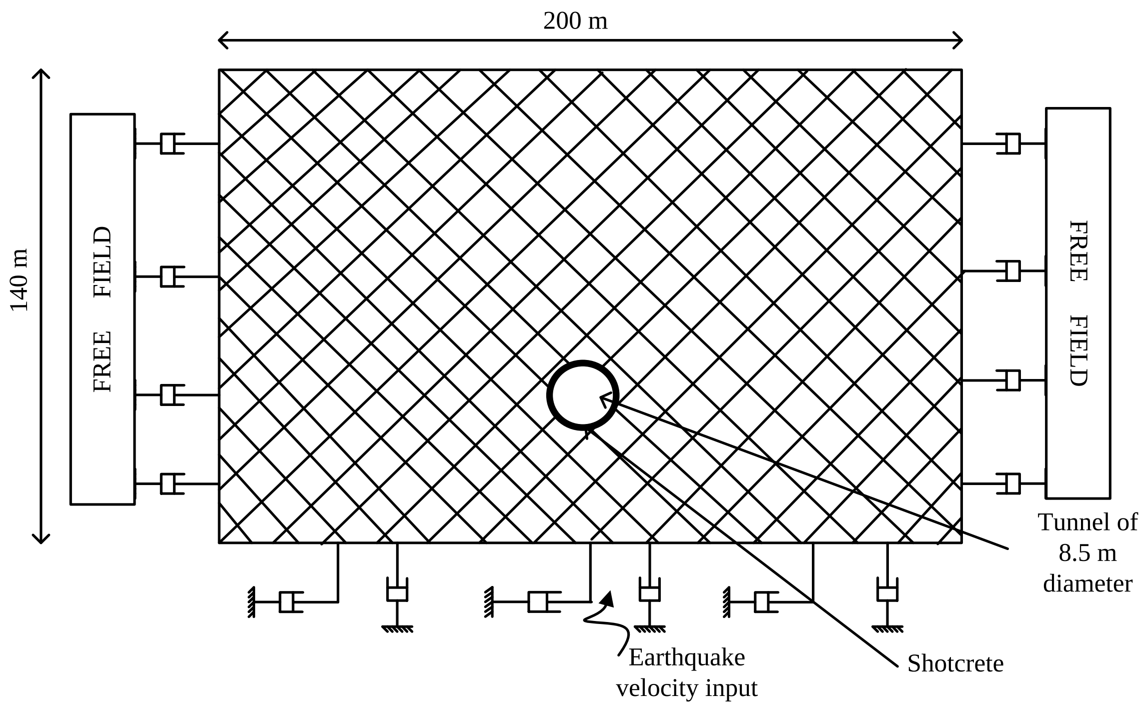

Figure 7.2: Numerical model for the Tehri dam tunnel

7.4 PERFORMANCE OF SHOTCRETE UNDER EARTHQUAKE LOAD

The tunnel supported by shotcrete is initially analysed under static loading condition. To the structure stable under static condition, the earthquake signals of Uttarkashi (1991, M_w=6.8) and Nepal (2015, M_w=8.1) are provided. Figure 7.3 shows the cross section of the tunnel under the action of a) static load b) seismic load with Uttarkashi (1991, M_w=6.8) and c) seismic load with Nepal (2015, M_w=8.1).

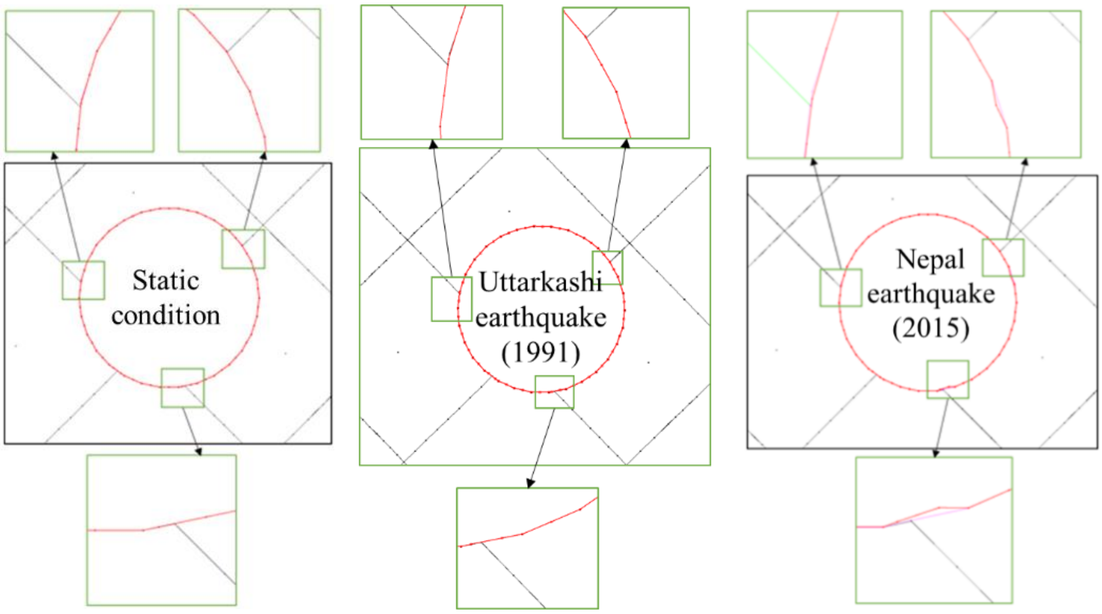

Figure 7.3: Shotcrete deformation (a) static loading (b) Seismic load (Uttarkashi earthquake, 1991, M_w=6.8) (c) Seismic load (Nepal earthquake, 2015, M_w=8.1)

Figure 7.4: Failure on tunnel shoulders No. 1 San-I railway tunnel after Chi-Chi earthquake (Wang et al., 2001)

The response of the shotcrete under static load in Figure 7.3 (a) shows that it is safe and intact. It also shows that the shotcrete is strong enough to be used as a support structure for the tunnel under static conditions. Under the action of Uttarkashi earthquake (1991, M_w=6.8), no deformation (Figure 7.3(b)) is observed and the shotcrete does not show any signs of spalling or breakage. However, under the action of Nepal earthquake (2015, M_w=8.1) (Figure 7.3 c), the shotcrete undergoes spalling at 3 locations, one near the invert and the other two on the shoulders of the tunnel. These locations are points of intersection between the rock joint and shotcrete. The spalling of shotcrete at these points are assumed to be directly related to the movement of joints and the force exerted on the shotcrete by the relative displacement of rock blocks. The literature also shows the presence of cracks at the shoulders as a common failure mechanism as shown in Figure 7.4.

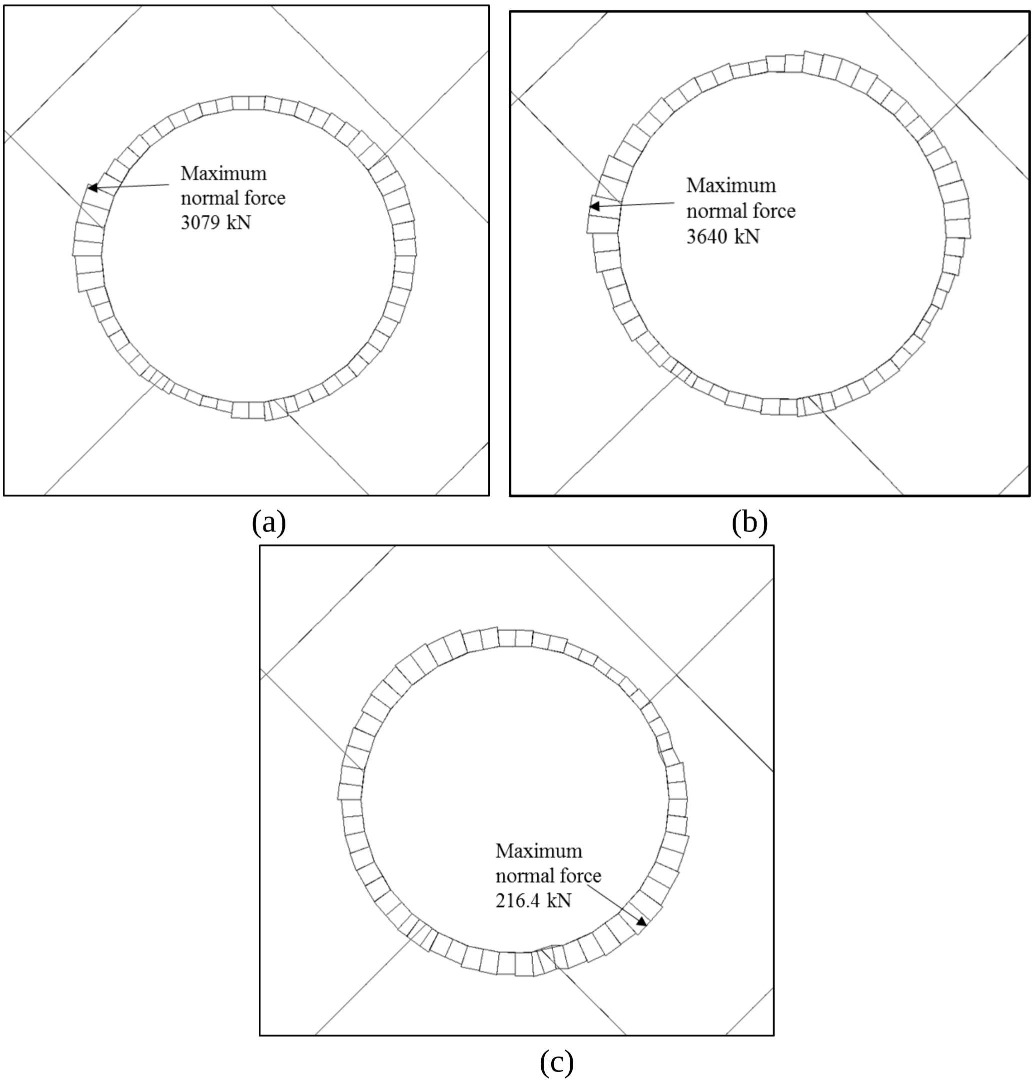

(c)

Figure 7.5: Normal Force acting on shotcrete (a) Static load (b) Seismic load (Uttarkashi earthquake, 1991, M_w= 6.8) (c) Seismic load (Nepal earthquake, 2015, M_w= 8.1)

Figure 7.5 shows the maximum normal force acting on each part of the shotcrete. Under static conditions, the rock joint and shotcrete interface between the sidewall and shoulder (180° and 220°) experiences a maximum normal force of 3079 kN. The maximum normal force acting on the shotcrete increases under the action of Uttarkashi earthquake (1991, M_w=6.8) when compared to the normal force acting on the shotcrete under static condition. The position of maximum normal force concentration happens on the sidewall with a magnitude of 3640 kN. However, this normal force decreases under the action of Nepal earthquake (2015, M_w=8.1) and the position of the maximum force also changes. The maximum normal force acts on the haunch with a maximum of 216.4 kN. This decrease is assumed to be due to the spalling of shotcrete at positions of maximum normal force under the static conditions, as shown in Figure 7.5. This also leads to loss in contact between shotcrete and rockmass.

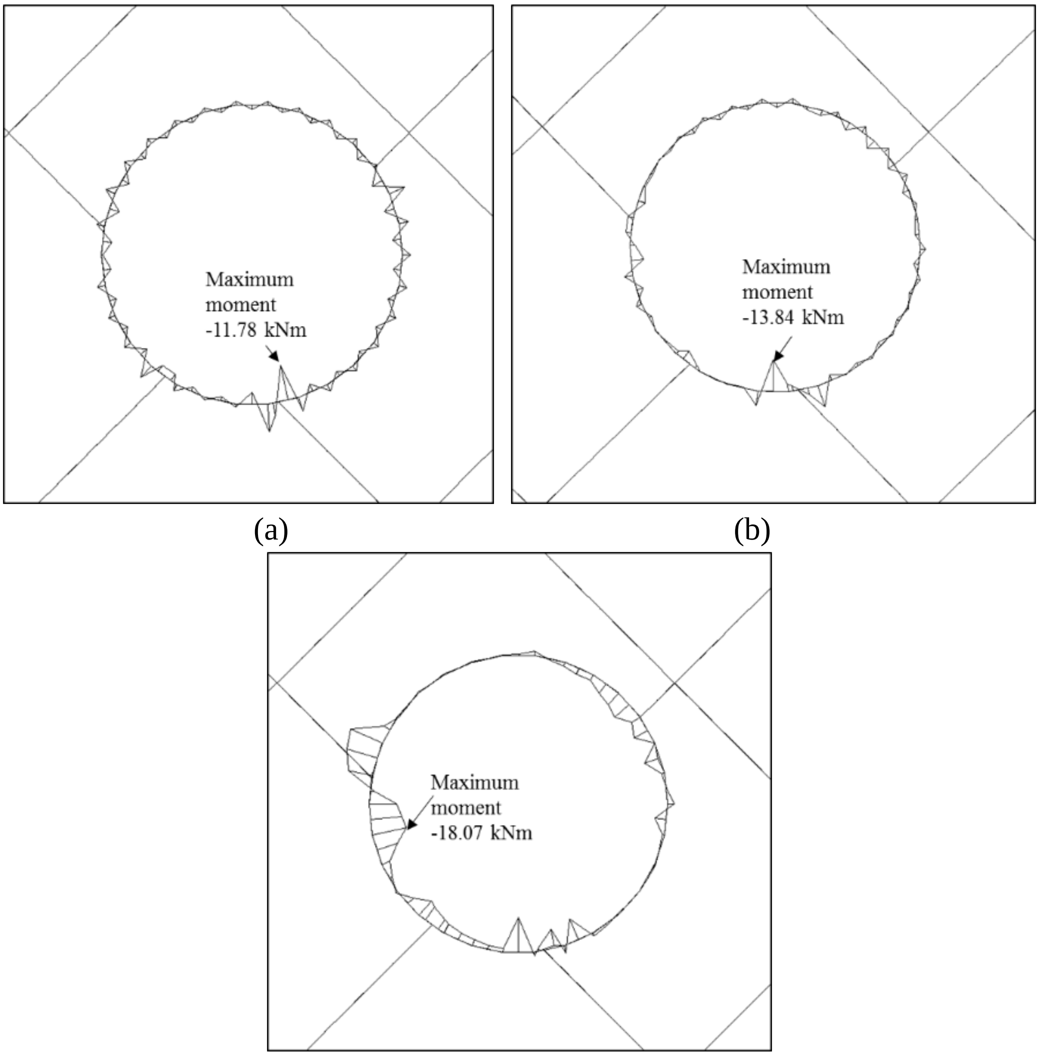

(c)

Figure 7.6: Bending moment acting on shotcrete (a) Static load (b) Seismic load (Uttarkashi earthquake, 1991, M_w=6.8) (c) Seismic load (Nepal earthquake, 2015, M_w=8.1)

Figure 7.6 shows the maximum bending moment acting on the shotcrete. Under static conditions, the maximum bending moment acting on the shotcrete is -11.78 kNm on the tunnel invert close to a rock joint intersection. The value increases to -13.84 kNm on the tunnel invert during Uttarkashi earthquake (1991, M_w=6.8), though certain additional zones of bending moment concentration could be observed. However, under the action of Nepal earthquake (2015, M_w=8.1), the position of bending moment changes to the tunnel sidewall along with additional concentrations. Interestingly these positions of bending moment concentrations are also points of rock joint and shotcrete intersection. This shows that there is a significant effect of rock joints on shotcrete structure. It can be noticed that, with an increase in the intensity of the earthquake, bending moment on the shotcrete also increases.

7.5 PERFORMANCE OF SHOTCRETE - PARAMETRIC STUDY

The performance of shotcrete largely depends on the properties of the surrounding medium, shotcrete or the incoming stress wave. Researchers have conducted extensive studies on the performance of concrete liners under the action of earthquake load for various tunnelling conditions (Zou et al., 2012; Do et al., 2015; Roy and Sarkar, 2018; Miao et al., 2018). This section tries to analyse the effect of various parameters on shotcrete behaviour. The model used in the parametric study is the same as that of Figure 7.2. One of the parameters is varied for the study while keeping the others constant. Input is a sinusoidal wave with a frequency of 1 Hz acting for a duration of 20 s. The amplitude of the input is selected to be 1000 mm/s corresponding to the minimum peak particle velocity affecting any tunnel structure. The variation of shotcrete deformation, normal force and bending moment is considered in the subsequent sections.

7.5.1 Joint Friction

The slippage between blocks is highly influenced by interjoint friction. At higher friction angles, the joints undergo lesser relative motion between the blocks and are according to Coulomb slip model (Eq. 4.7). To understand the behaviour of shotcrete under different joint friction values, it is varied from 28º to 40º. Figure 7.7 shows the spalling occurring on the shotcrete under the action of seismic load for different joint friction. Under the static condition, the effect of joint friction is negligible. It can be seen from Figure 7.7 that for 28º joint friction, the spalling occurring on the shotcrete is relatively high. Here, the blocks are relatively loose with higher sliding. This is especially true for the crown and the shoulders of the tunnel. At tunnel haunch, shotcrete close to rock joint also undergoes spalling. As the joint friction value increases, the spalling reduces. This is evident at the crown, where only intermittent spalling is visible compared to complete spalling at the crown and shoulder. Spalling of the crown is visible due to the compressive forces acting due to overlying load similar to what Roy and Sarkar (2018) also observed.

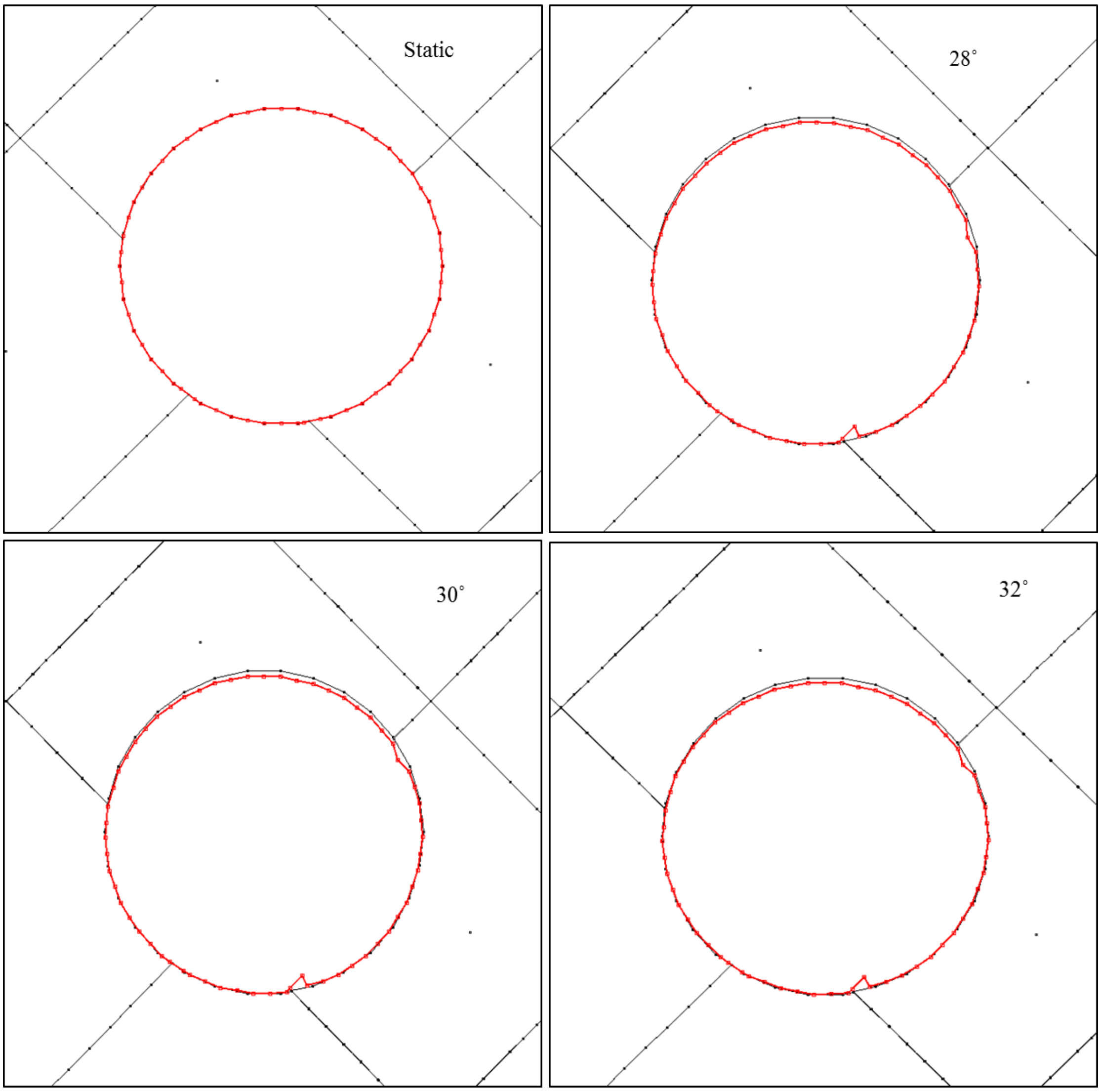

Figure 7.7: Performance of shotcrete under different joint frictions (contd.)

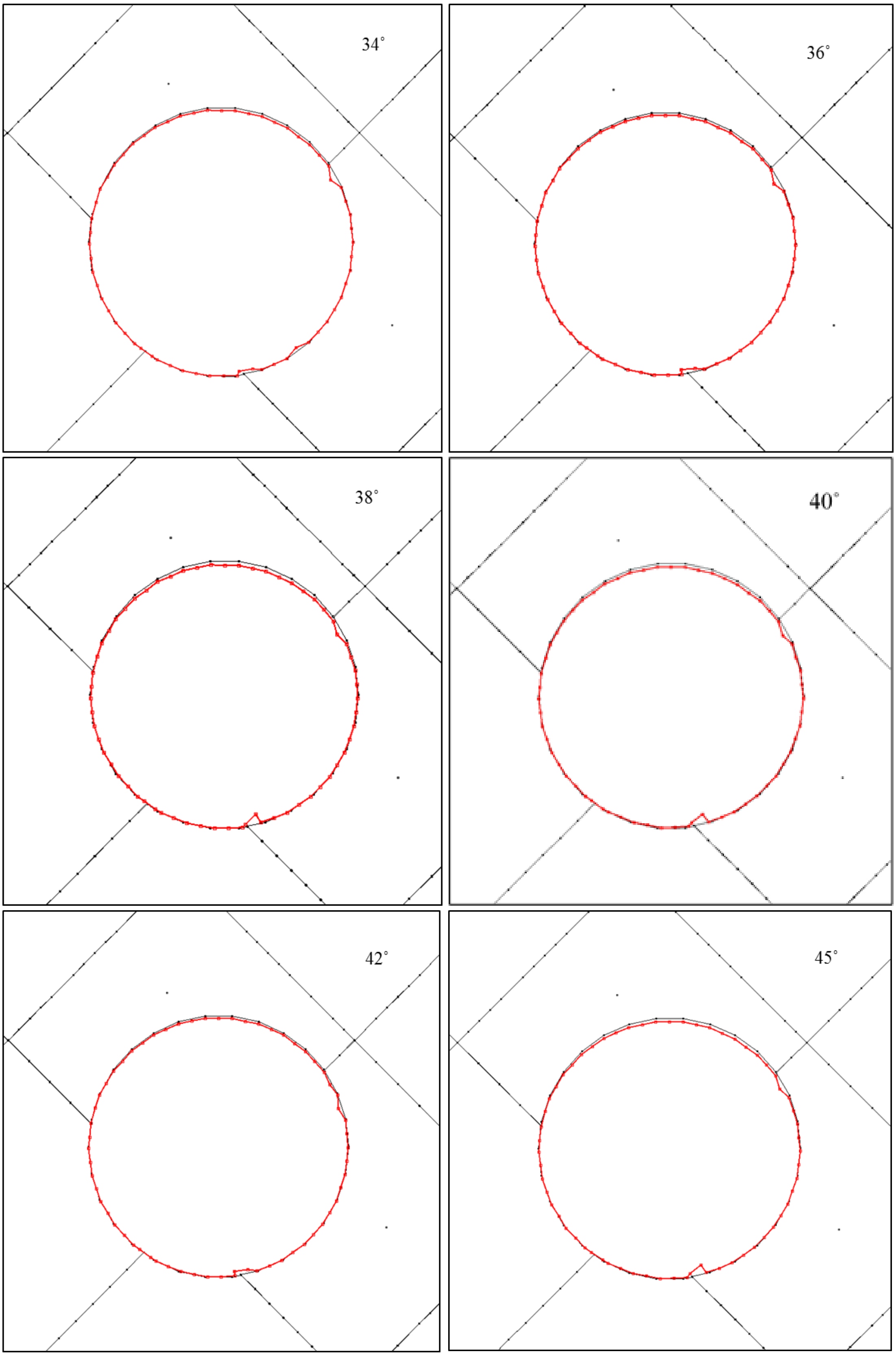

Figure 7.7: Performance of shotcrete under different joint frictions

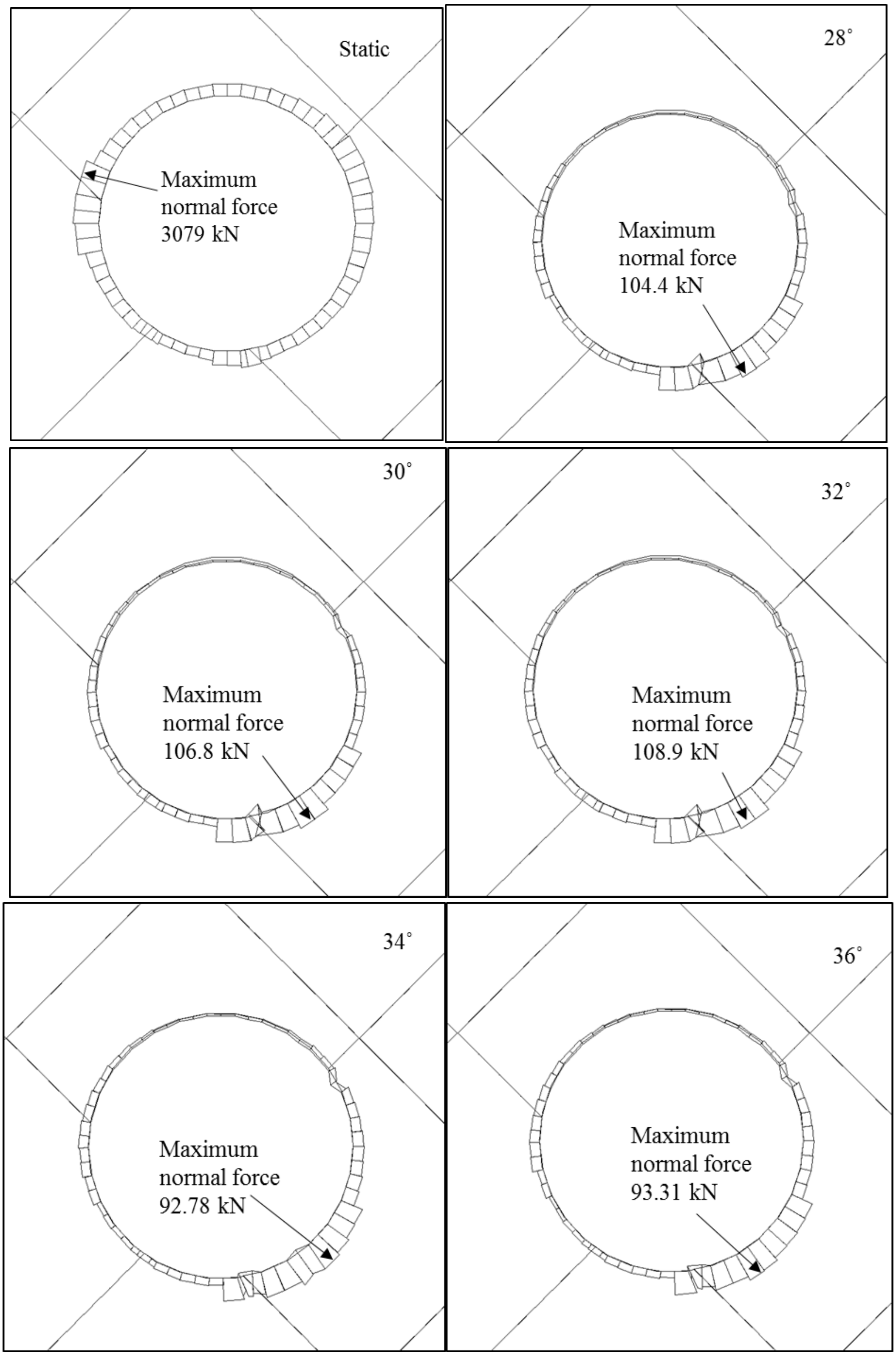

Figure 7.8: Normal force acting on the shotcrete for different joint friction (contd.)

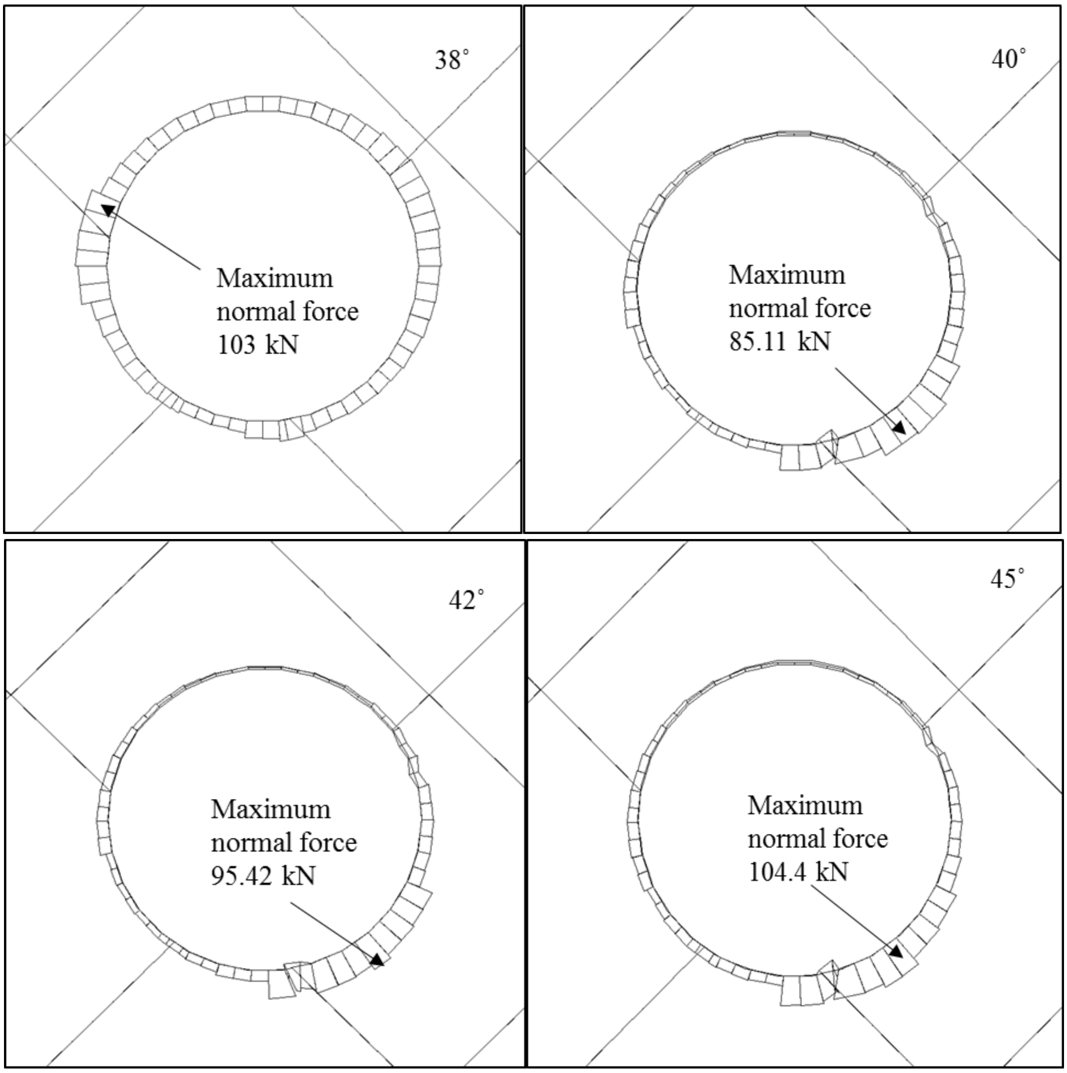

Figure 7.8: Normal force acting on the shotcrete for different joint friction

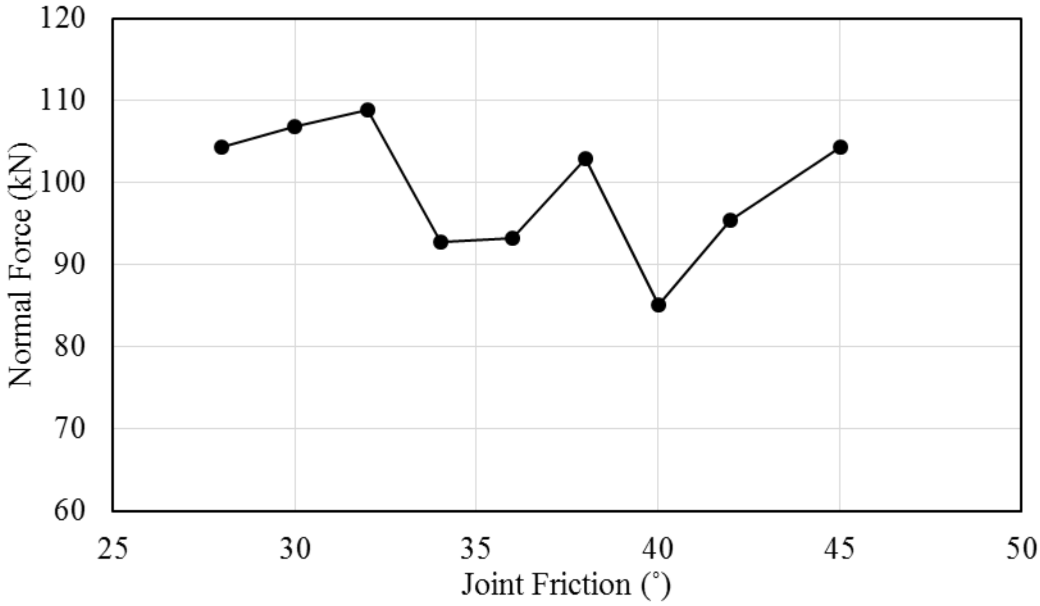

Figure 7.9: Variation in maximum normal force with variation in joint friction

Figure 7.7 shows a decrease in spalling with an increase in joint friction. This decrease leads to increased contact between the shotcrete and rockmass, leading to the higher normal force on the shotcrete (Figure 7.8). However, after the initial increase in the normal force, a sudden reduction followed by an increase is observed. The maximum normal force under static condition is between the sidewall and shoulder of the tunnel. This is also a zone through which a joint is passing. However, under the action of earthquakes, the shotcrete at this zone is no longer in contact with the tunnel. The decrease is not continuous with the variation of joint friction. Figure 7.9 shows the variation of maximum normal force acting on the shotcrete for different joint friction values. The normal force increases from 104.4 to 108.9 kN, as joint friction increases from 28˚ to 32˚. This pattern is found to be repeated at every 6˚ rise of joint friction. This change is assumed to be due to the change in spalling pattern and movement of the rock block. The slight change in position of the maximum normal force resonates with the pattern. Figure 7.10 shows the pattern of bending moment acting on the shotcrete under static and different joint friction conditions. Maximum bending moment is found to act near the invert of the tunnel. An increase in bending moment occurs under the action of the seismic load when compared to static conditions. This variation in the maximum moment is similar to that of the normal force. The maximum bending moment under static conditions is -11.79 kNm which increases to -28.25 kNm under for seismic loading with joint friction of 28˚. The bending moment further increases to -32.38 kNm and then decreases to -23.43 kNm. Figure 7.11 shows this variation pattern of maximum bending moment.

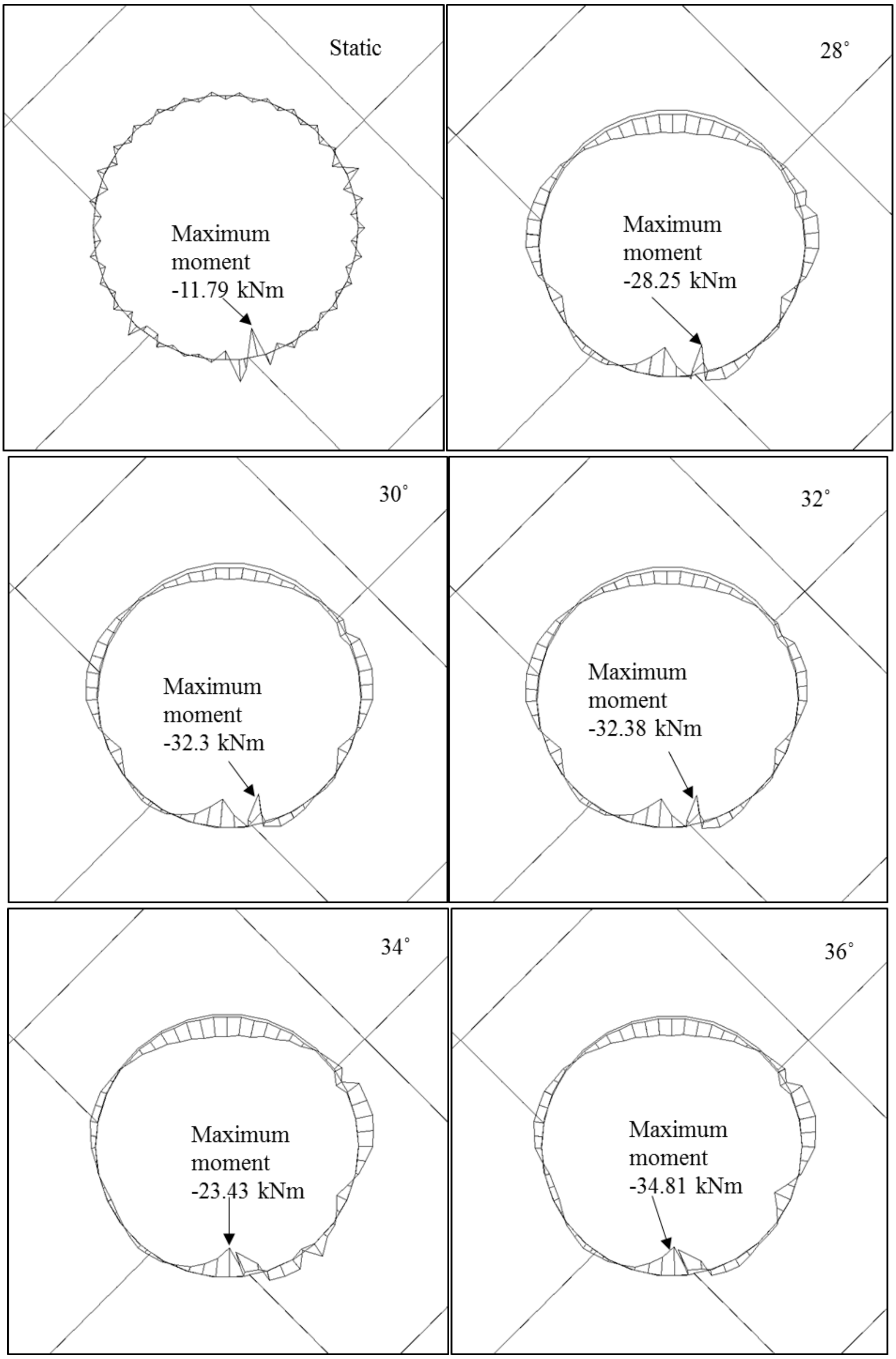

Figure 7.10: Bending moment acting on the shotcrete for different joint friction (contd.)

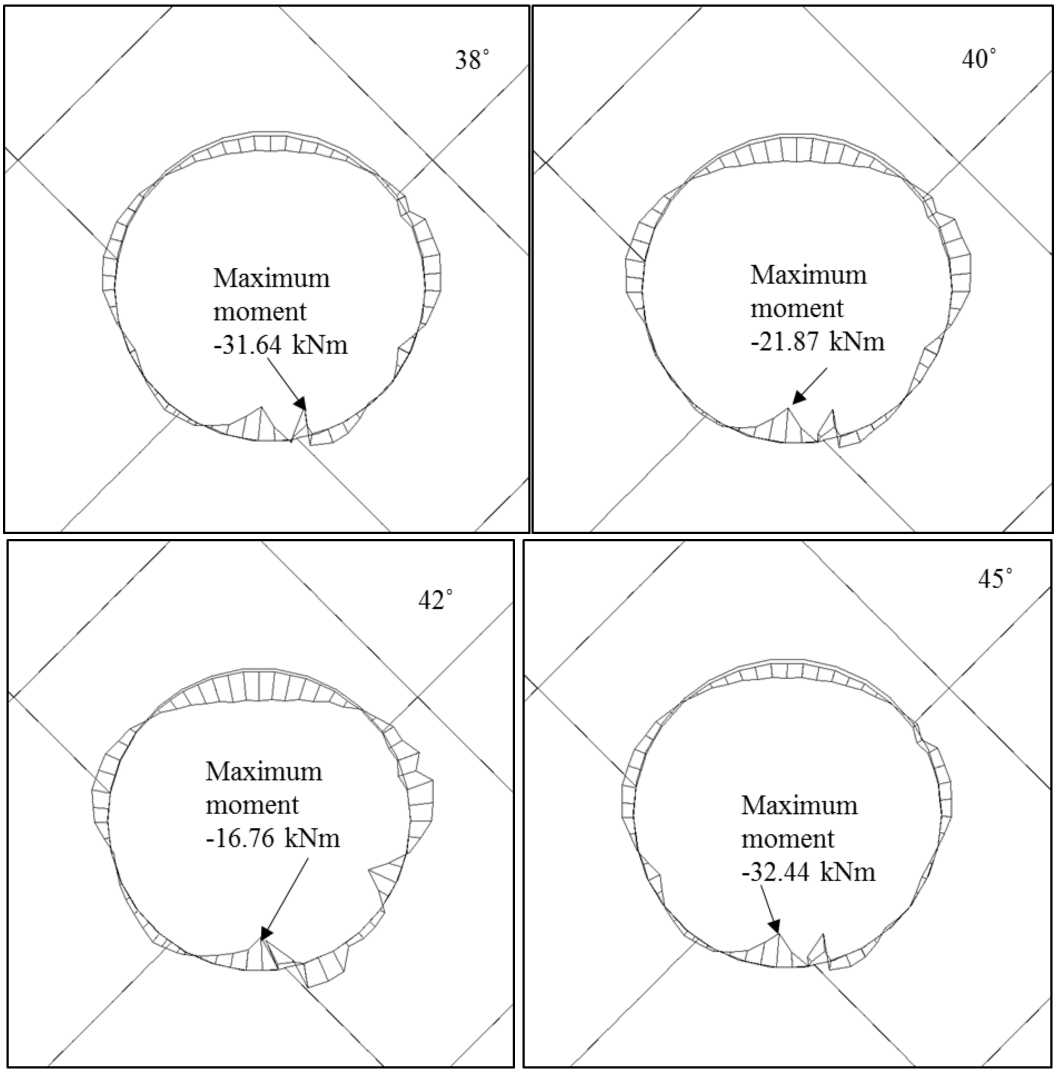

Figure 7.10: Bending moment acting on the shotcrete for different joint friction

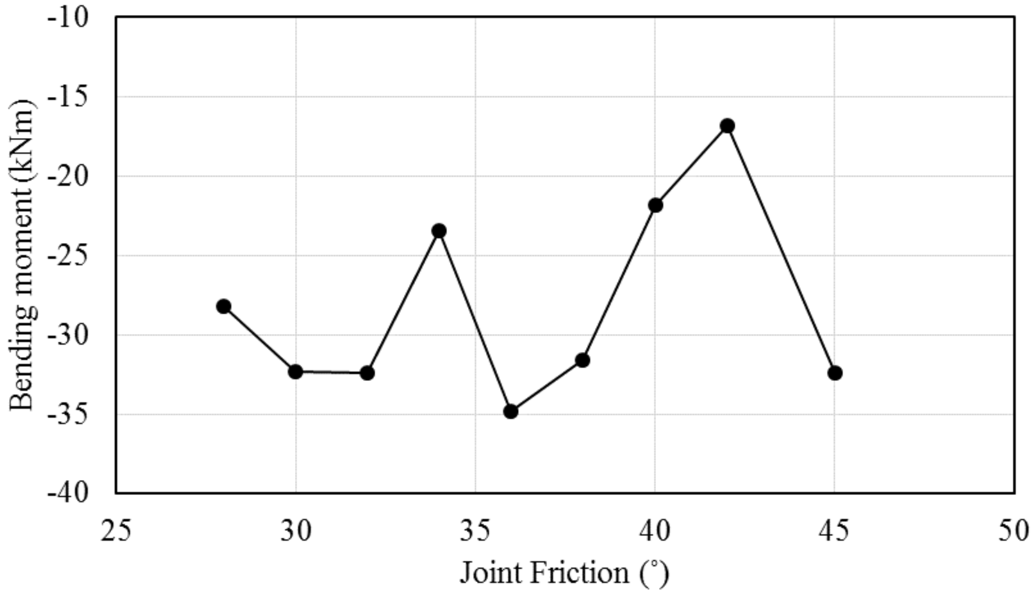

Figure 7.11: Variation in maximum bending moment with change in joint friction

7.5.2 Shotcrete Thickness

Design of shotcrete thickness is normally based on experience and rule of thumb. The thickness can be irregular as per the excavation need. The required shotcrete thickness is correlated to Rock Structure Rating (RSR) by Wickham et al. (1972). With 10 m span of opening and Rock Mass Rating (RMR) under consideration, Biewanski (1989) gave recommendations on shotcrete thickness. However, these recommendations and studies are for openings under static conditions only and the action of dynamic loads is not considered therein. The variation in shotcrete deformation, normal force and bending moment under the action of seismic load for different shotcrete thickness is analysed in this section. The shotcrete thickness is increased from 0.05 m to 0.5 m (5 cm to 50 cm) to understand the change in the forces acting at all points in the shotcrete. Figure 7.12 shows the shotcrete deformation for different shotcrete thickness. According to the deformation pattern, the shotcrete spalling is found to increase with the thickness of the shotcrete. The maximum spalling position also varied as the shotcrete thickness varied. The spalling at the tunnel roof is more with increased thickness. This increase in roof spalling must be due to the additional concrete weight, which increases the effect of the already spalled area. Spalling also occurs on the tunnel invert and shifts towards sidewalls as the thickness increases. This shows the change in force concentration with an increase in shotcrete thickness. The numerical simulations consider the shotcrete as beam elements and the weight acting expected to be higher as the thickness increases.

Figure 7.13 shows the normal force distribution on the shotcrete for different thickness. The maximum normal force acting on the shotcrete is found to act between the invert and the sidewall and shifts towards the sidewall as the shotcrete thickness increases. The maximum normal force acting on the shotcrete is found to decrease with increasing thickness, as shown in Figure 7.14. This decrease might be due to the higher depths for load distribution. And the shift in the position of maximum normal force is due to the extra deformations in shotcrete that exert force on the nearest point of contact.

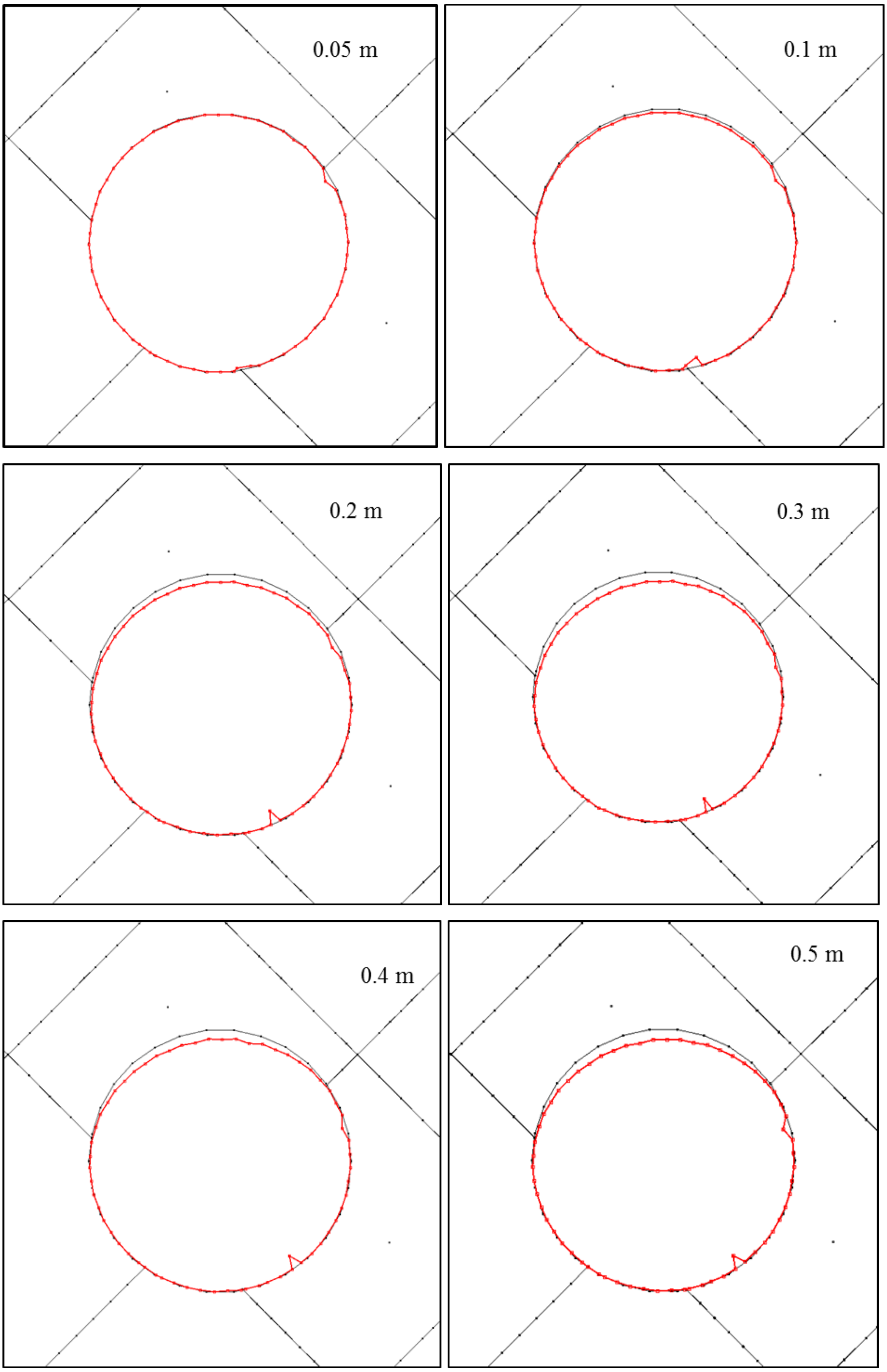

Figure 7.12: Performance of shotcrete under different shotcrete thickness

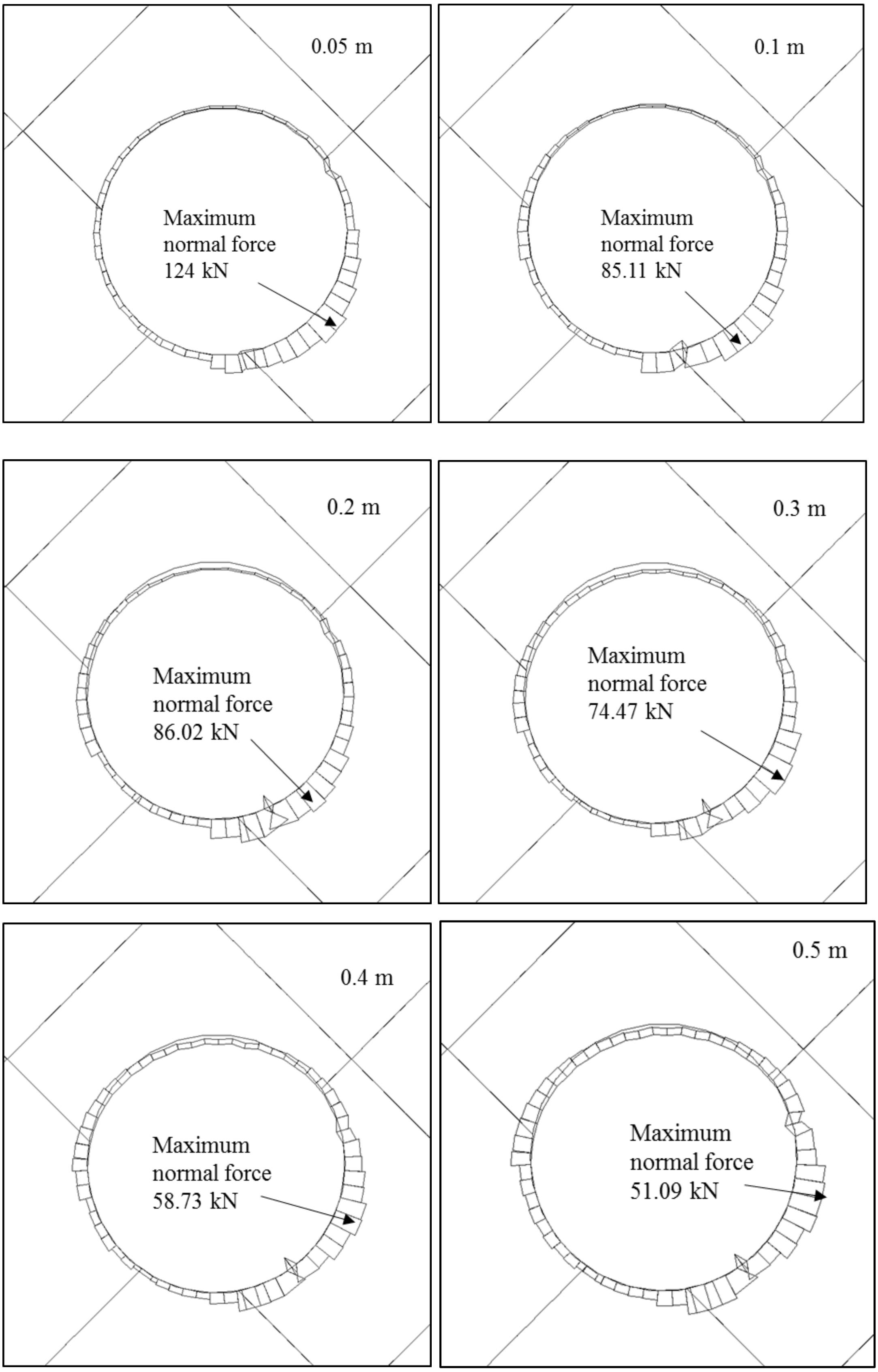

Figure 7.13: Normal force acting on the shotcrete for different shotcrete thickness

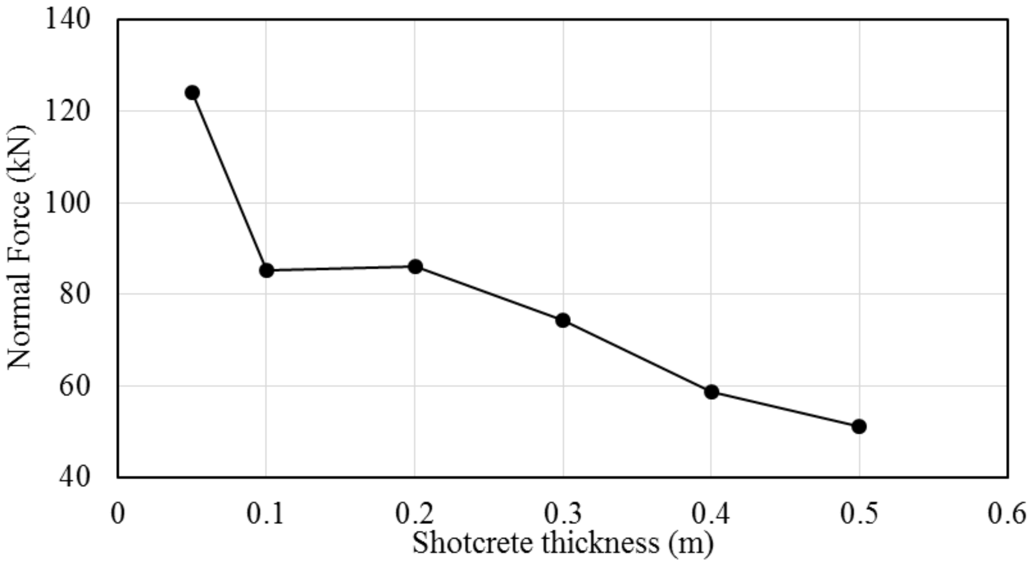

Figure 7.14: Maximum normal force for different shotcrete thickness

Figure 7.15 shows the variation in bending moment distribution around the shotcrete. The shotcrete thickness is varied from 50 mm to 500 mm. High bending moments are also experienced by shotcrete layer on the tunnel roof that underwent spalling. Zones with spalling are under the influence of the high bending moment. The maximum bending moment acting on the shotcrete is usually concentrated around the tunnel invert where spalling occurs. Figure 7.16 shows the variation in maximum bending moment with an increase in shotcrete thickness.

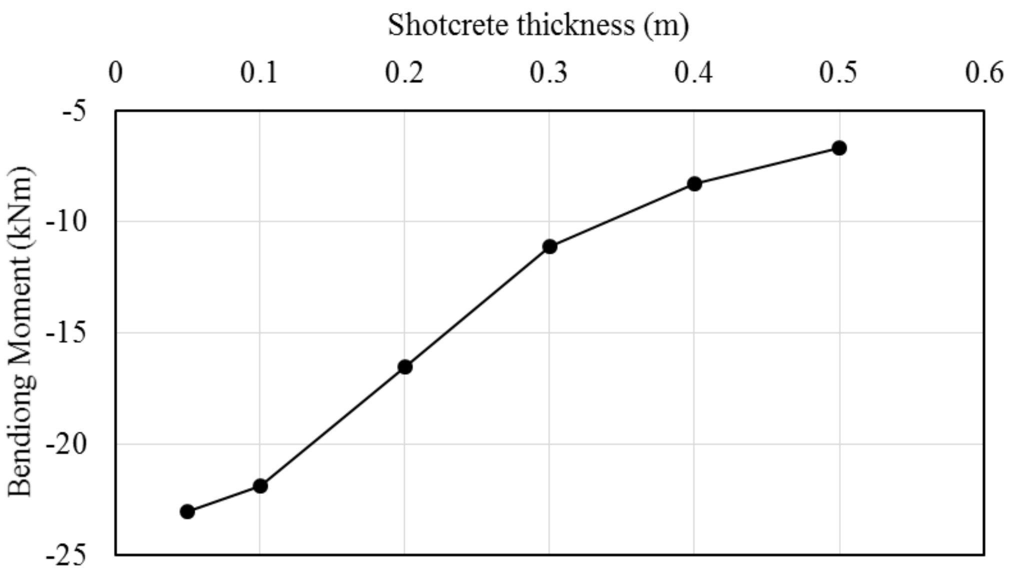

Figure 7.16: Maximum bending moment for different shotcrete thickness

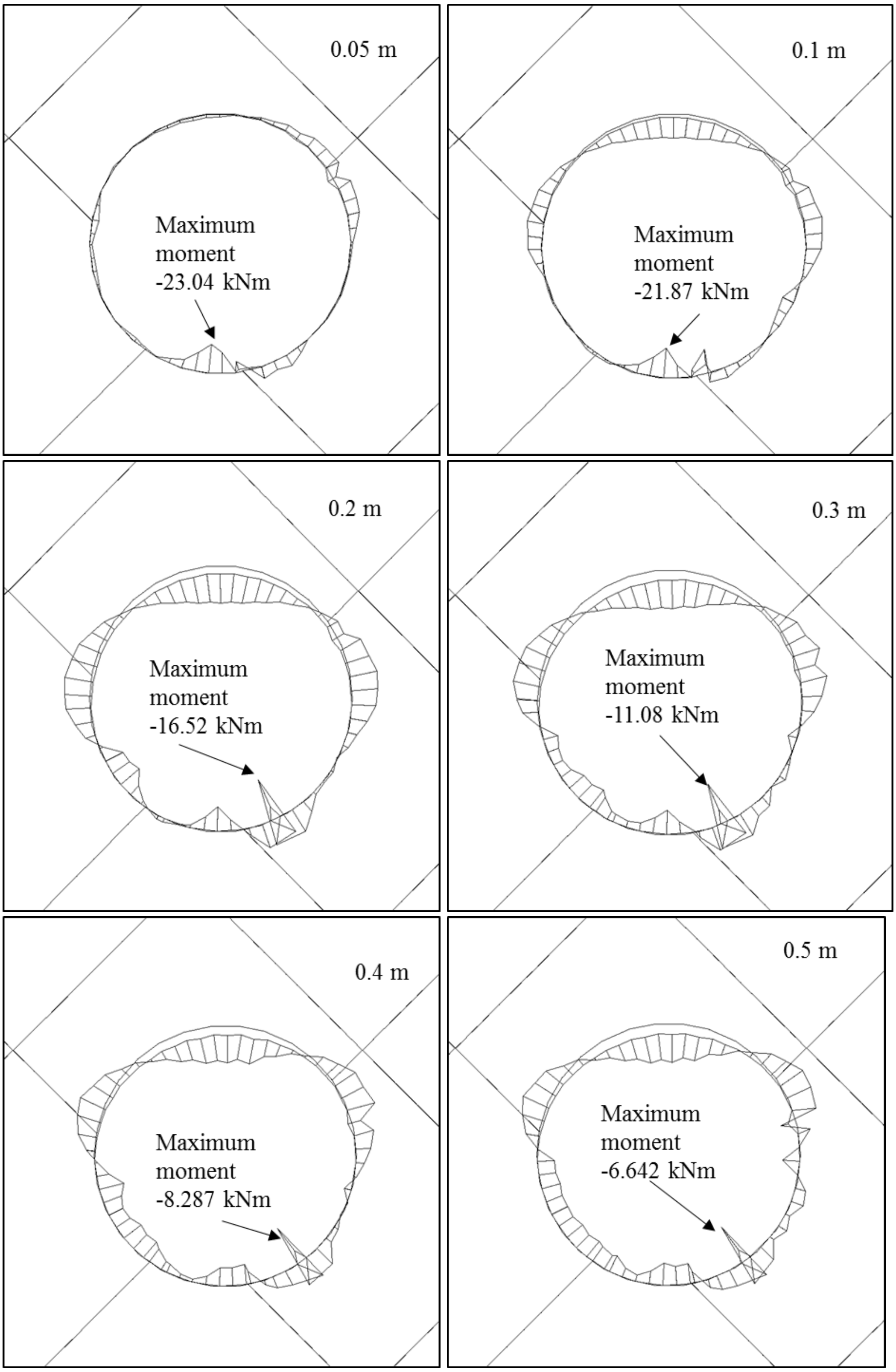

Figure 7.15: Bending moment acting on the shotcrete for different shotcrete thickness

7.5.3 Wave Frequency of Dynamic Input Load

The effect of incoming wave frequency on the shotcrete/concrete liner structure is investigated by various researchers (Zou et al., 2012; Roy and Sarkar, 2018). Zulficar et al. (2012) found that the effect of seismic loading on rock structures is predominant when the frequency ranges from 1 to 6 Hz. So this study concentrates on the variation in this lower frequency ranges. Figure 7.17 shows the change in shotcrete deformation for different frequencies. It can be seen that, each of the frequencies affect the shotcrete differently even when the applied seismic amplitude is the same. For 1-2 Hz frequency, spalling of concrete occurred at the tunnel invert as well as on the roof. At 3-4 Hz, frequency, even though slight spalling is observed, the magnitude is less, especially on the tunnel roof. Also a shift from the tunnel shoulder to the tunnel crown is visible for frequencies 1 Hz to 3 Hz. The spalling at the crown is not present for frequencies greater than 3 Hz. At all frequencies, the area between the sidewall and the invert is found to have a certain amount of spalling. However, the position of this bending is found to change under each frequency. The position of the spalled portion of shotcrete shifts from the invert towards sidewall with an increase in frequency.

Figure 7.18 shows the variation of normal force on the shotcrete. The maximum normal force is commonly found to act adjacent to the zone of bending and spalling of shotcrete on the tunnel invert. The maximum normal forces of 103.2 kN and 103.7 kN is experienced at 3 Hz and 6 Hz frequencies respectively. The maximum normal force is found to be acting on the points of contact next to the area of spalling. The value of maximum normal force is found to follow a pattern of increase with frequency.

Figure 7.19 shows the change in bending moment acting on the shotcrete under the influence of various frequencies. The maximum bending moment is always found to act on the point of spalling between the tunnel invert and sidewall, as shown in Figure 7.20. The maximum bending moment is -28.34 kNm and -21.87 kNm for 2 Hz and 1 Hz frequencies respectively. The decrease in bending moment with increasing frequency is visible, which might be due to the decrease in deformation with increasing frequency. This shows that the portion of the tunnel being affected under the action of seismic load largely depends on the incoming wave frequency.

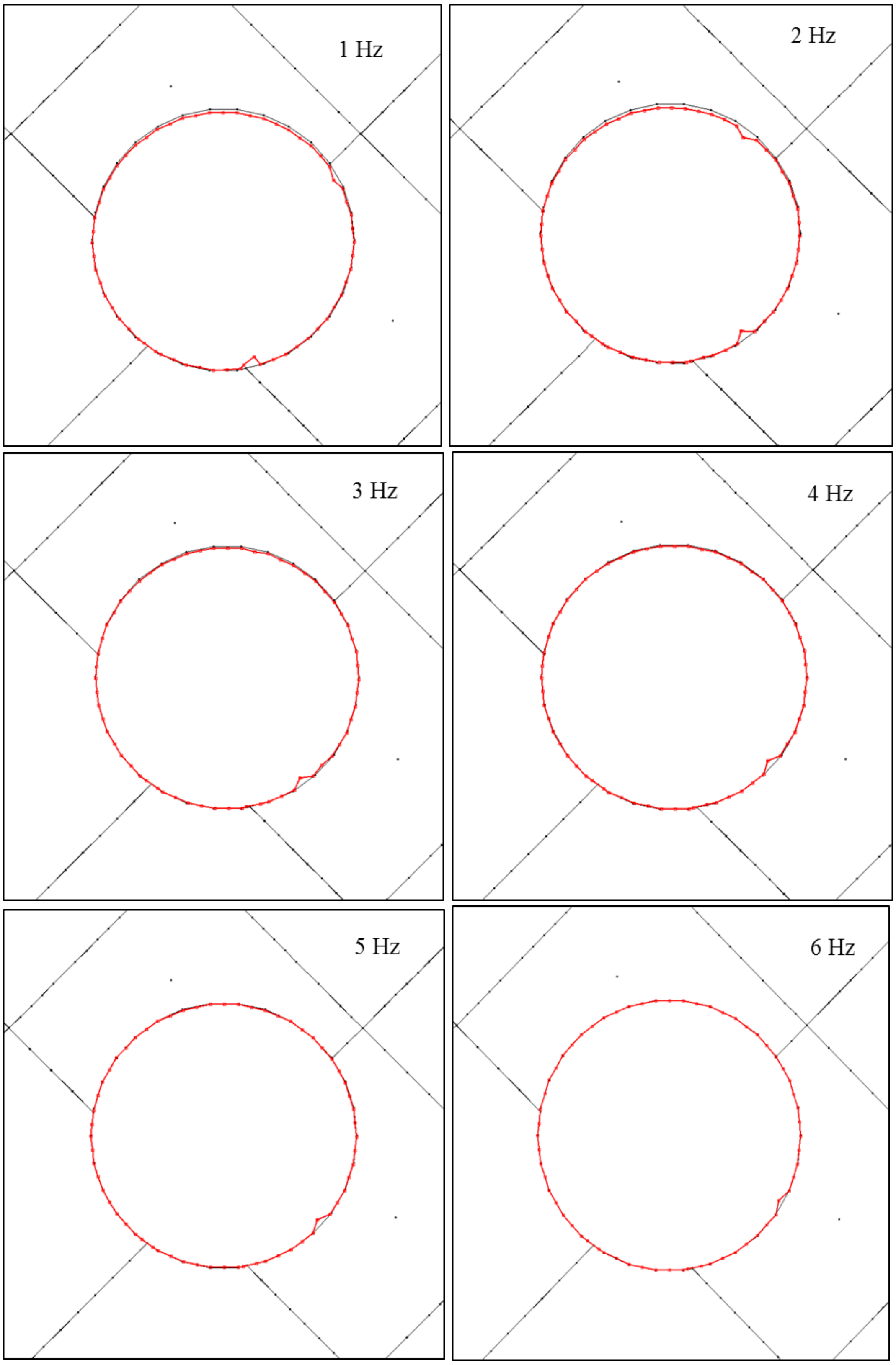

Figure 7.17: Performance of shotcrete under different incoming wave frequencies

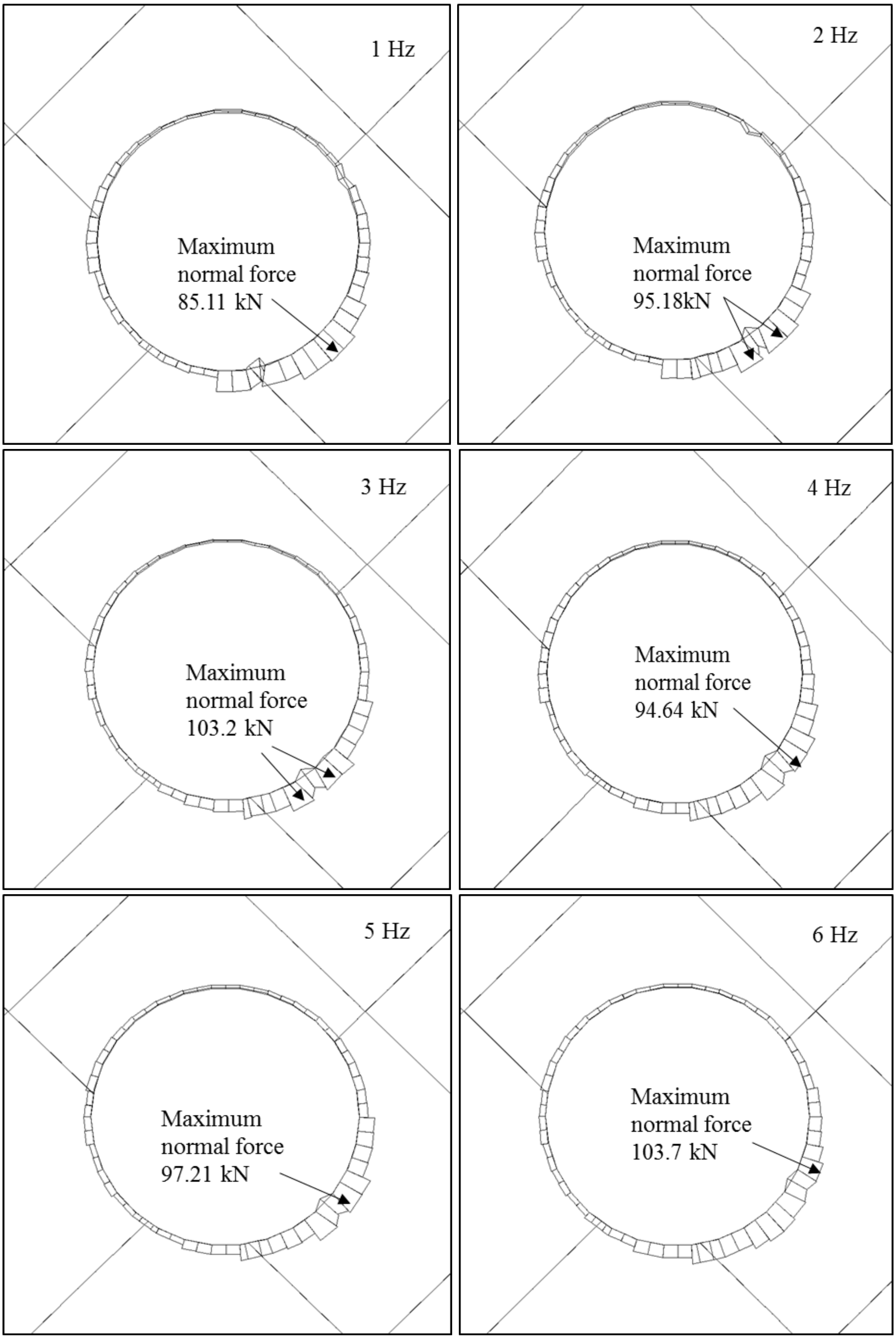

Figure 7.18: Normal force acting on the shotcrete for different incoming wave frequencies

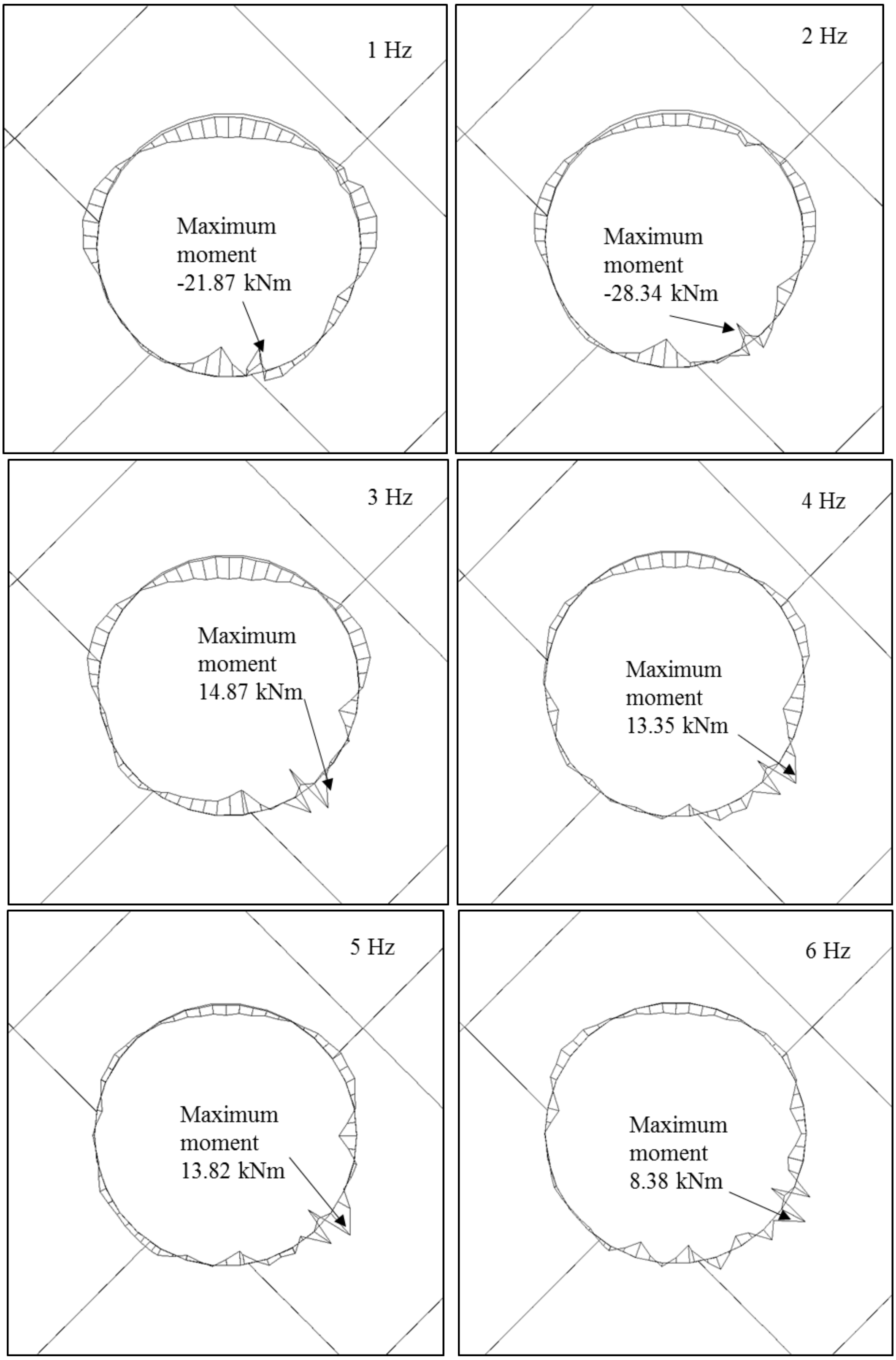

Figure 7.19: Bending moment acting on the shotcrete for different incoming wave frequencies

7.5.4 Duration of Dynamic Input Load

The impact of longer durations of earthquake loads has always found to be more devasting in nature. The variation in the forces acting on the shotcrete under different durations are analysed. This helps in understanding the changes in shotcrete with loading duration. The duration of loading for the sinusoidal wave is varied from 5 s to 20 s. Figure 7.20 shows the variation in shotcrete deformation under different loading durations. It shows that the spalling occurring on shotcrete increases with increase in loading duration. The spalling is concentrated only near two location of rock joint and shotcrete intersection for a loading duration of 5 s and 10 s. But as the loading duration is increased to 15 s and 20 s, the spalling on the roof of the tunnel is very evident. This shows that the increase in loading duration increases the effects on shotcrete.

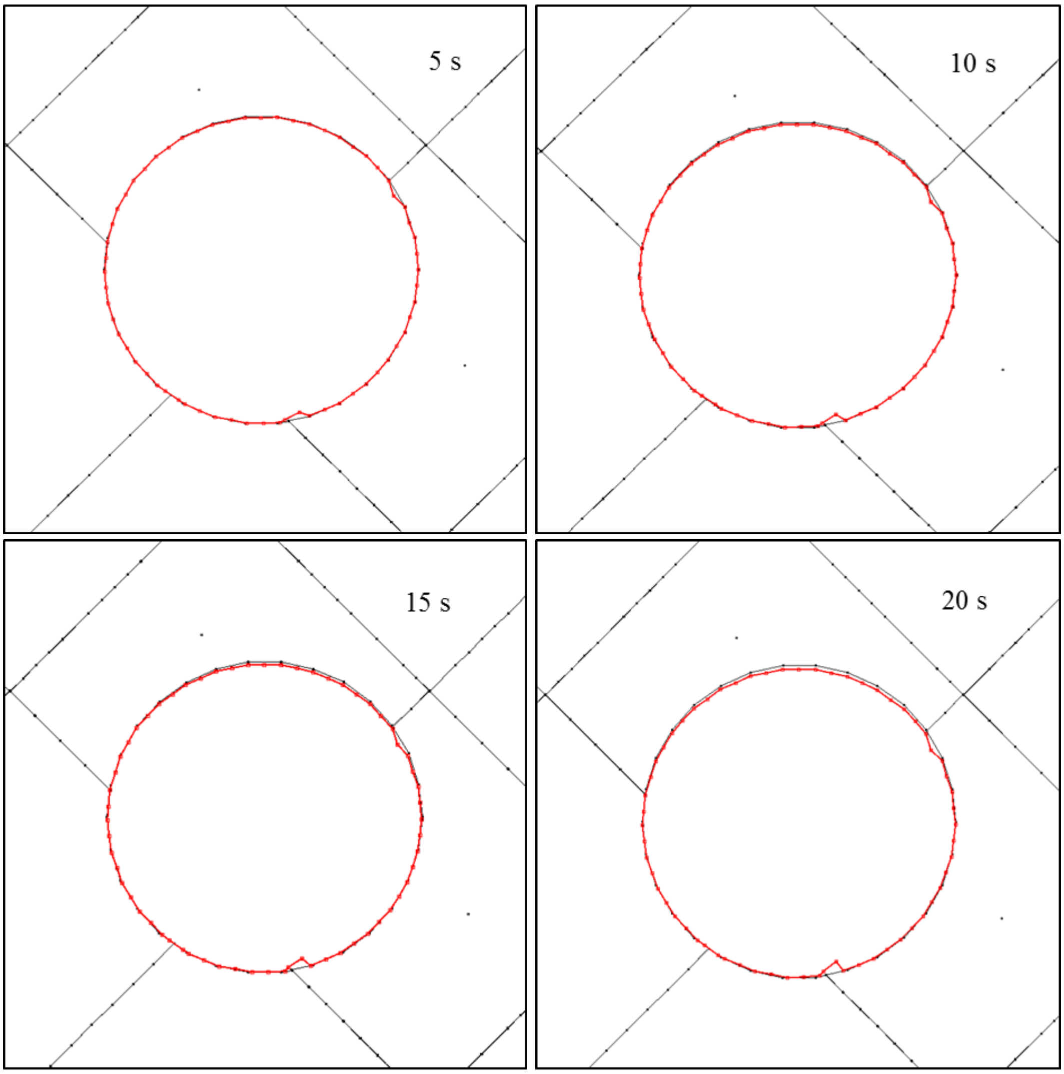

Figure 7.20: Performance of shotcrete under different incoming wave duration

Figure 7.21 shows the variation of normal force on the shotcrete under different loading duration. A decrease in maximum normal force is observed with increase in duration. This could be due to the loss in contact at different points between the shotcrete and the tunnel walls. Figure 7.22 shows the variation of bending moment along the shotcrete for various loading durations. With the increase in loading duration, the bending moment acting on the shotcrete is found to increase. The maximum bending moment acting on the shotcrete is found to be -31.84 kNm at 15s duration.

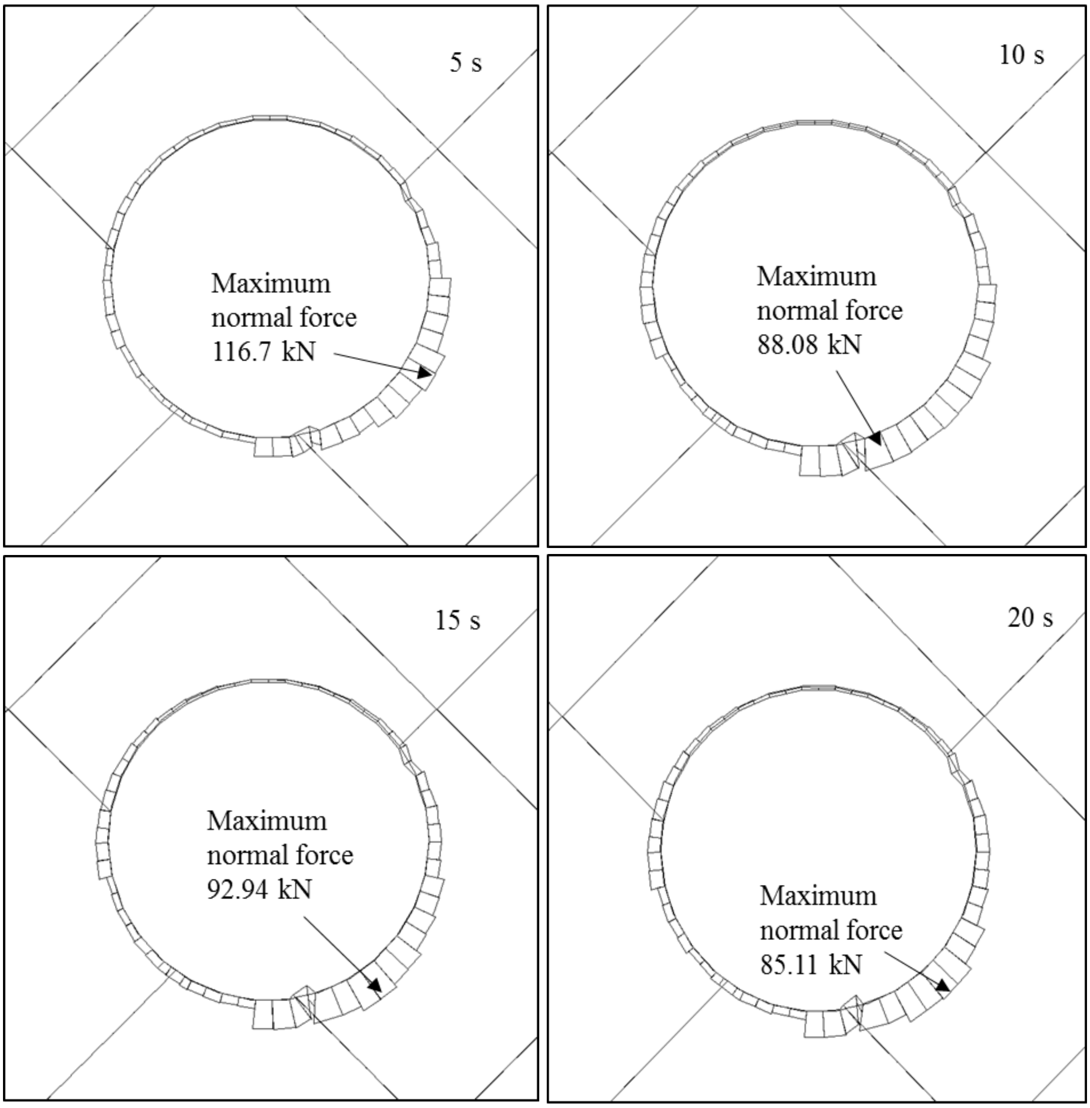

Figure 7.21: Normal force acting on the shotcrete for different incoming wave duration

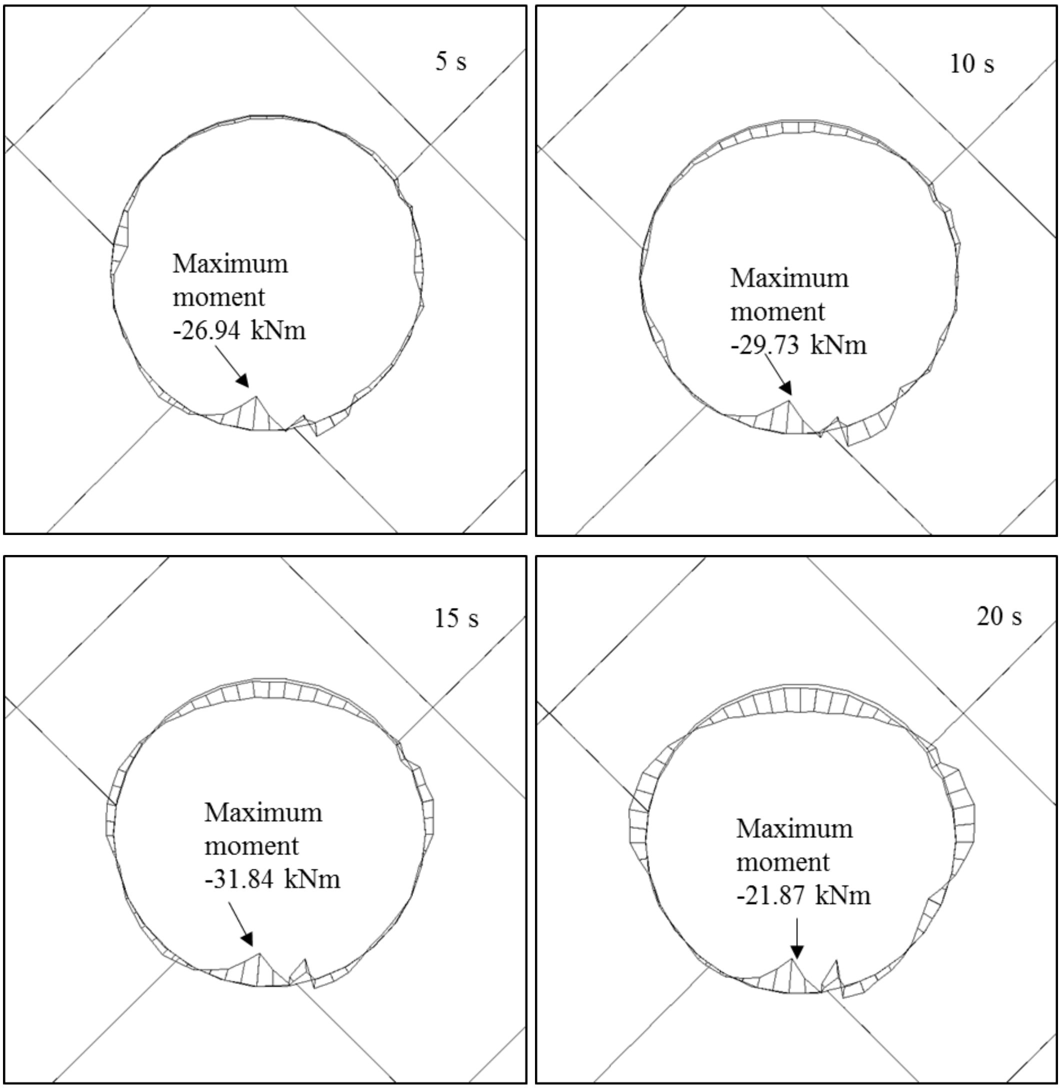

Figure 7.22: Bending moment acting on the shotcrete for different incoming wave duration

7.5.5 Amplitude of Dynamic Input Load

The tunnels were found to be affected by dynamic blast loads when the peak particle velocity is more than 800 mm/s (Dowding, 1984). To understand the effect of the amplitude of the incoming wave, the seismic load amplitude is varied from 400 mm/s to 1400 mm/s.

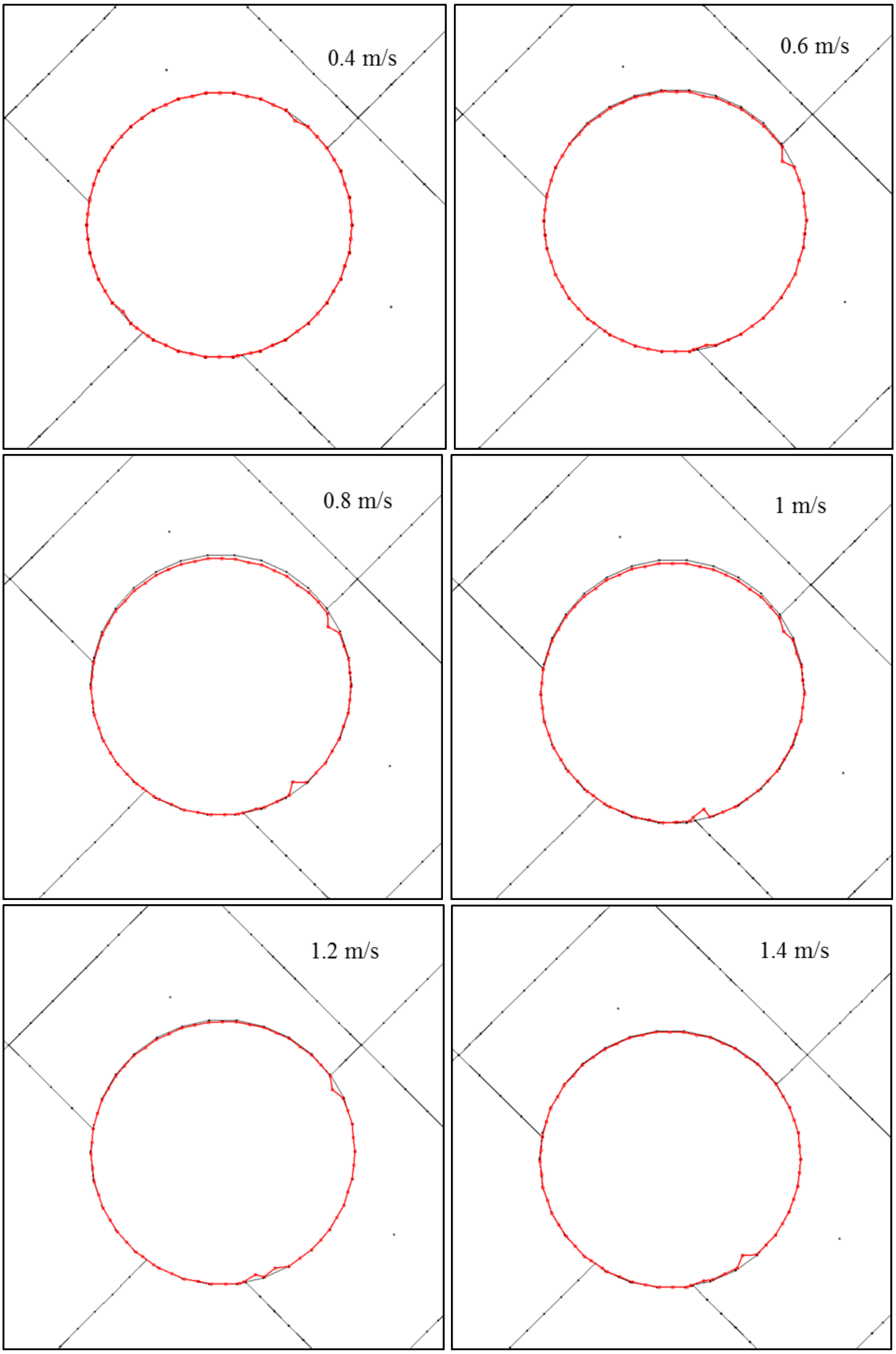

Figure 7.23: Performance of shotcrete under different incoming wave amplitude

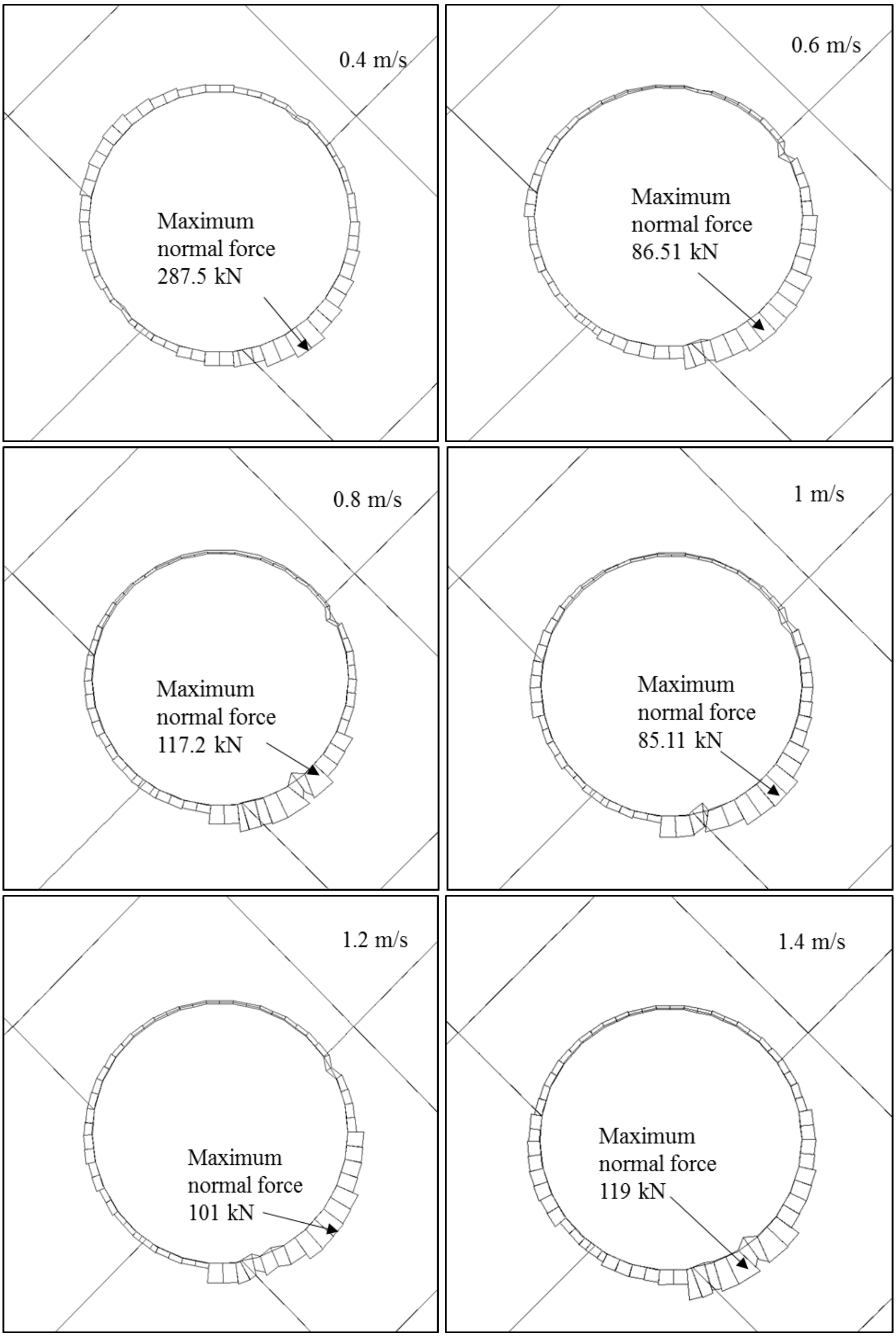

Figure 7.24: Normal force acting on the shotcrete for different incoming wave amplitude

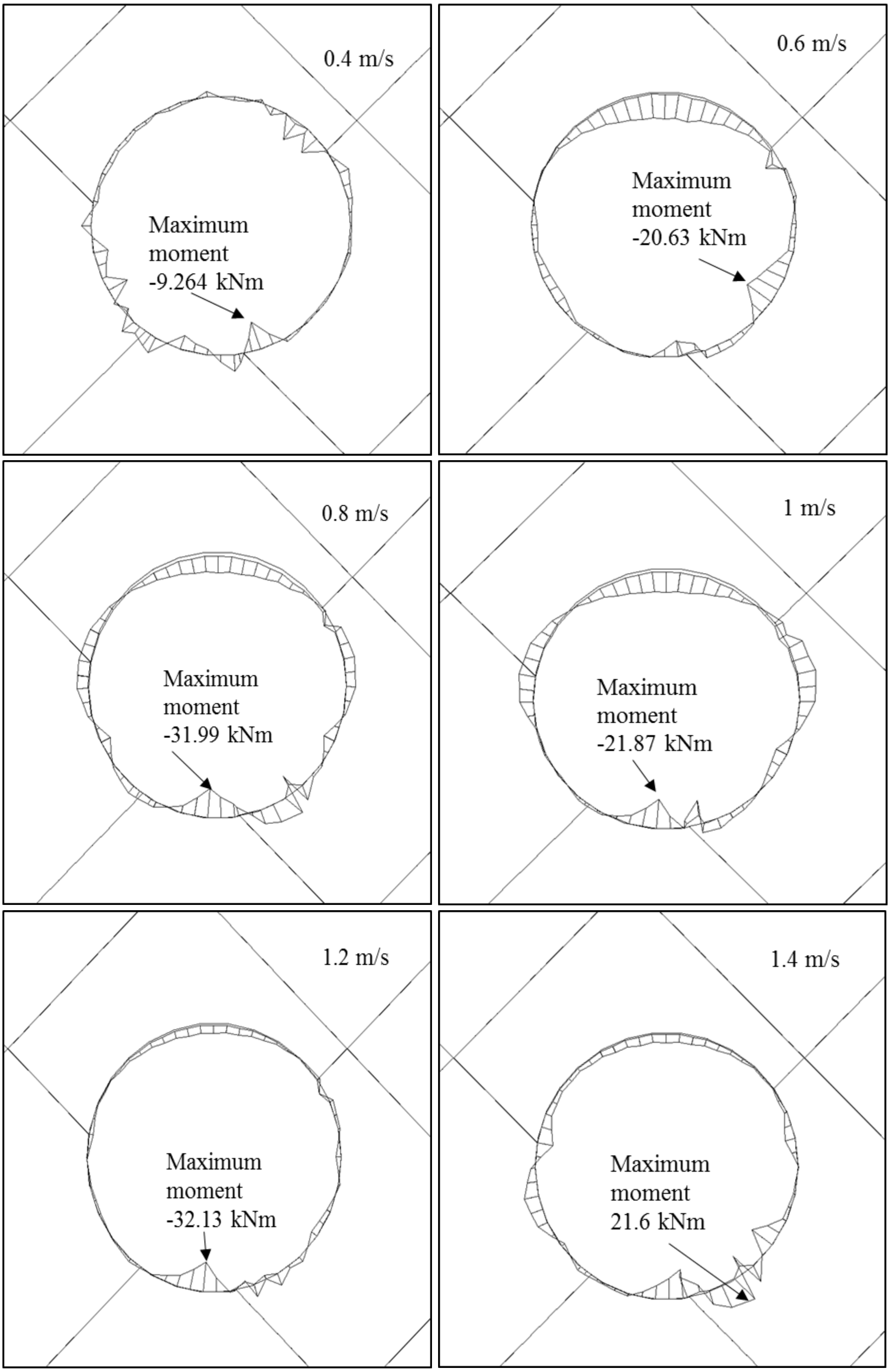

Figure 7.25: Bending moment acting on the shotcrete for different incoming wave amplitude

Figure 7.23 shows the variation in the shotcrete deformation for various wave amplitude. It can be seen from Figure 7.23 that as the amplitude of loading increases, the tunnel deformations increase. It is interesting to note that even the positions of shotcrete spalling changes under different loading amplitudes. For 400 mm/s amplitude, slight spalling is observed on the tunnel, one on the shoulder and the other diagonally opposite to it. The spalling on the shotcrete for amplitudes greater than 400 mm/s concentrated on the tunnel roof and shoulder. Slight spalling is also found between the invert and the sidewall. This spalling is found to increase with the increase in amplitude. The position of spalling between the invert and sidewall is also found to vary with different amplitude.

Figure 7.24 shows the variation in normal force acting along the shotcrete with an increase in amplitude. The normal force is found to decrease with the increase in wave amplitude. This is assumed due to the increased spalling on the shotcrete, which decreases the normal force. Figure 7.25 shows the variation of bending moment along the shotcrete. The bending moment acting on the shotcrete is found to increase with the increase in the amplitude of wave input. The decrease is spalling at the crown is due to the failure of the crown. This compares well with the previous research that peak particle velocity (PPV) beyond 800 mm/s causes failure in the tunnel. Spalling of the tunnel crown is found to be common failure pattern, especially with increasing incoming wave amplitude. The separation of tunnel liner or shotcrete from the crown is observed as seen in Wenchuan earthquake (2008, M_w=7.9) (Figure 7.26).

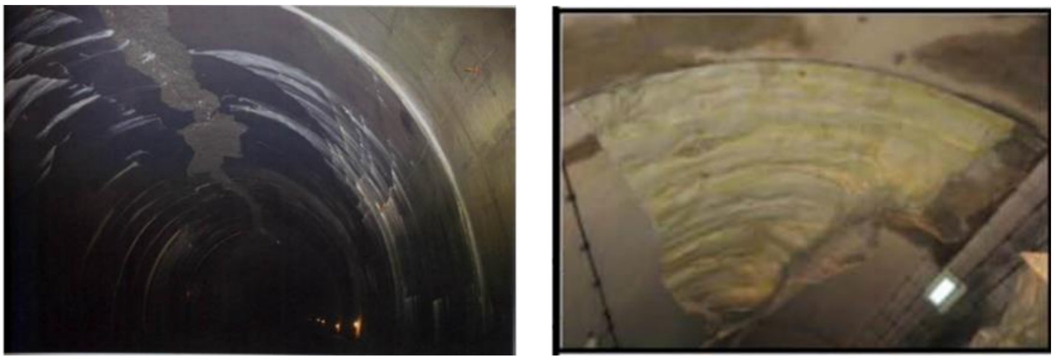

(a) (b)

Figure 7.26: Spalling of liner from roof of (a) Longxi tunnel in Wenchuan Earthquake (Yu et al., 2016) (b) Yingxiuwan Hydropower Station under the Wenchuan Earthquake (Wang et al. 2018)

7.6 SUMMARY

The current chapter focuses on the performance of shotcrete under the action of earthquake loads. The headrace tunnel of Tehri dam is considered assuming shotcrete as the only support system. The Uttarkashi earthquake (1991, M_w=6.8) and Nepal earthquake (2015, M_w=8.1) are used as the input data to study the performance of the tunnel under seismic conditions. The tunnel showed good stability under static condition when only shotcrete is used as support. No spalling or shotcrete deformations are observed under static conditions. Shotcrete is found to remain stable under the action of Uttarkashi earthquake (1991, M_w=6.8) as well. However, under the action of Nepal earthquake (2015, M_w=8.1), spalling took place at different places on the shotcrete. These positions are close to the shotcrete and rock joint intersection.

A parametric study is performed to understand the effect of different shotcrete parameters, wave parameters and joint parameters. Of all the parameters, the wave frequency and amplitude is found to have a significant effect on the tunnel support. It could be noticed that the position of force concentration and spalling varied with frequency and failure occurred when the amplitude is found to be greater than 800 mm/s. The pattern of shotcrete deformation is in line with the patterns found in the literature for different tunnels under the action of an earthquake. The findings from the current study compare well with the failure patterns from the literature.

CHAPTER 8

PERFORMANCE OF ROCKBOLT AND SHOTCRETE SUPPORT COMBINATION UNDER SEISMIC LOAD

8.1 INTRODUCTION

The tunnel support system consists of a combination of one or more supports. Different combinations of rockbolt, shotcrete and tunnel liners are used in tunnelling depending on the site conditions. Among these, the combination of rockbolt and shotcrete is most commonly used in tunnel construction, especially in NATM (ONORM B 2203, 1993; Bienwaski, 1989). For a ravelling tunnel in which joints cause a reduction in strength, combined shotcrete and rockbolt system in roof and at springline is recommended (Table 2.2). Combination of rockbolt with shotcrete is the most used support technique for jointed rock tunnels. The previous chapters analysed the effect of rockbolt and shotcrete independently under earthquake loads. This chapter tries to identify the forces acting on rockbolt and shotcrete as a combined system. Nepal Earthquake (2015, M_w=8.1) and Uttarkashi earthquake (1991, M_w=6.8), as discussed in chapter 6, are used in the analysis.in

8.2 NUMERICAL MODELLING OF THE TUNNEL

A UDEC model is developed to understand the effect of the earthquake on the combined support system of shotcrete and rockbolt (Figure 8.1). The headrace tunnel as discussed in chapter 6 (sections 6.4 and 6.6) is used in the current study. The rockbolts and shotcrete used in chapter 6 and 7 respectively is applied together to form a combined support system. The properties of the rock mass, rockbolt and shotcrete are as provided in Table 6.1, 6.2 and 7.1 respectively.

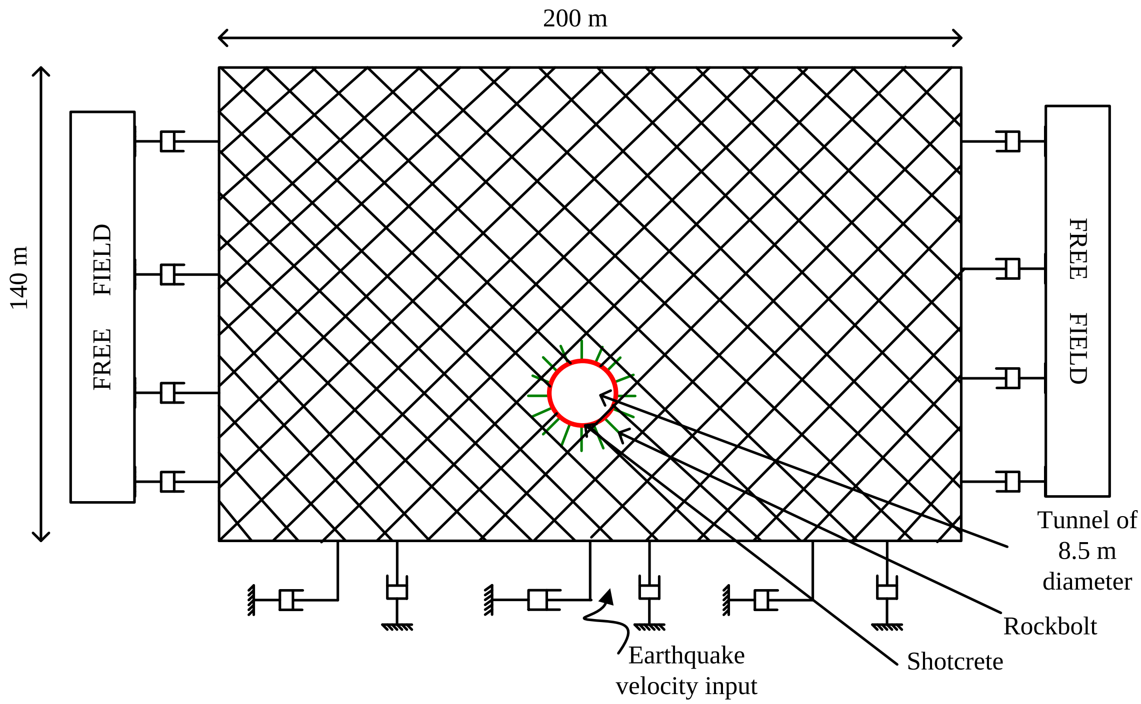

Figure 8.1: Numerical model for the Tehri dam tunnel

The tunnel is supported by a shotcrete liner of 10 cm thickness and rockbolts of 3 m length. The shotcrete is uniformly sprayed around the tunnel. The shotcrete liner is discretized into 60 nodes over which the mass of the liner is distributed. Rockbolts of 3 m length are placed around the tunnel at every 22.5° with a spacing of 3.3 m. Each rockbolt contains five nodes over which the mass of the rockbolt is concentrated. The reinforcing material follows the elastoplastic model, where the material yields. The rockbolt and the blocks are bonded by shear and normal springs as in Eq. 6.1 and 6.2. The properties of the rockbolt and shotcrete are as given in Table 6.2 and 7.1. The Nepal earthquake (2015, M_w=8.1) and Uttarkashi earthquake (1991, M_w=6.8) histories are converted to velocity histories using the Seismosignal software. The velocity histories (Figure 6.6 and 6.10) are applied as shear input at the base of the model. Figure 8.1 shows the numerical model. The rockbolt positions mentioned in the chapter are similar to the orientation shown in Figure 6.14

8.3 PERFORMANCE OF ROCKBOLT UNDER EARTHQUAKE

The performance of rockbolts under static and dynamic conditions is studied in chapter 7. The earlier results considered rockbolt as the only support system. However, in the field, a shotcrete layer accompanies the rockbolt. As part of the load is shared by the shotcrete there is a change in the forces acting on each rockbolt. The section tries to understand the variation in normal force, shear force and bending moment acting on the rockbolts in a combined system.

Figure 8.2 to 8.4 shows the normal force, shear force and bending moment acting on each rockbolt under static conditions and the action of Nepal earthquake (2015, M_w=8.1) and Uttarkashi earthquake (1991, M_w=6.8). In Figures 8.2 to 8.4, RB suffix stands for rockbolt being the only support system while RBS is for conditions with rockbolt and shotcrete combined to act as a support system. Legends Utksi EQ and Npl EQ stand for Uttarkashi (1991, M_w=6.8) and Nepal (2015, M_w=8.1) earthquakes, respectively in Figures 8.2 to 8.4.

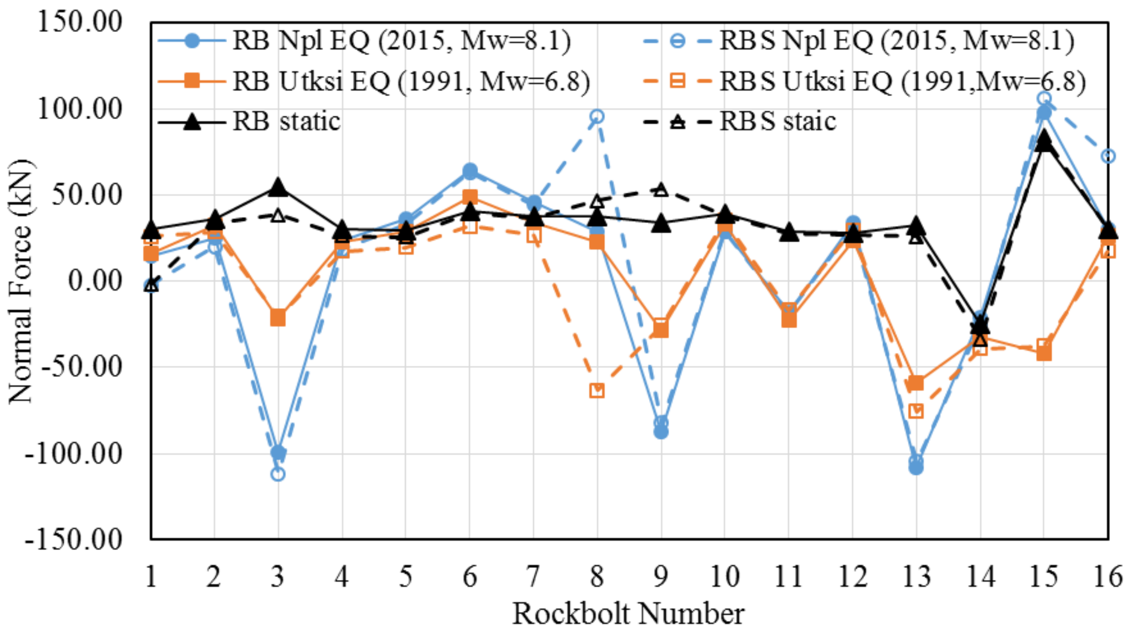

Figure 8.2: Normal force acting on rockbolt with and without shotcrete as support

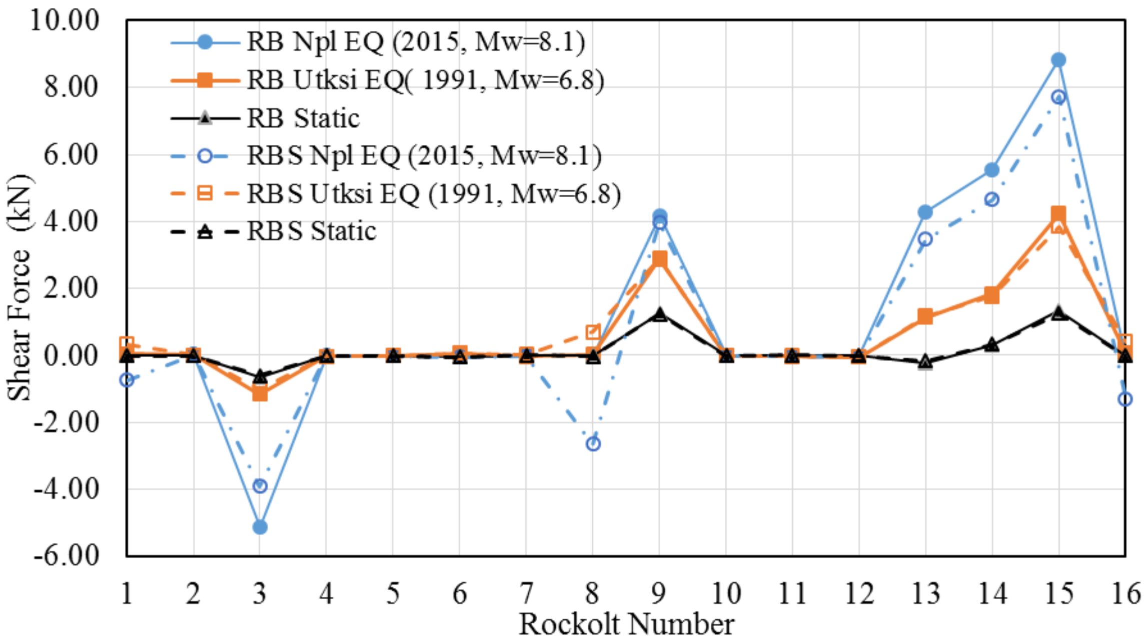

Figure 8.3: Shear force acting on rockbolt with and without shotcrete as support

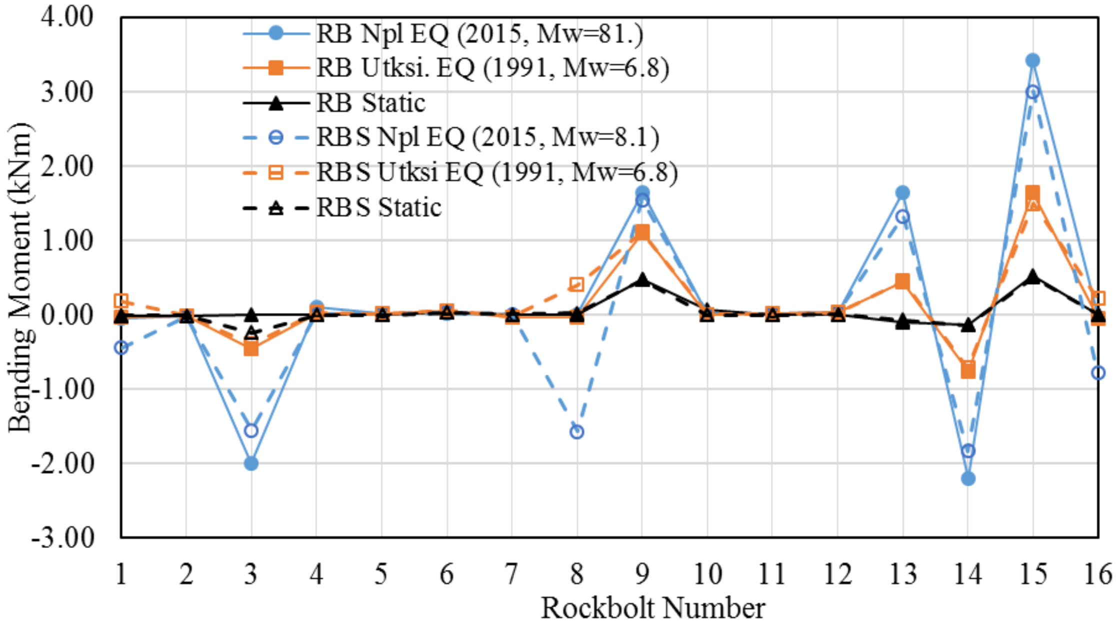

Figure 8.4: Bending moment acting on rockbolt with and without shotcrete as support

Figure 8.2 shows the normal forces acting on the rockbolts under static and earthquake loading. The normal force acting on the bolts passing through joints decreases under the static condition when the tunnel is given additional support by shotcreting. The decrease is predominant for the rockbolts in the bottom half of the tunnel, while the change in the normal forces at the crown and upper half are negligible.

An increase in normal force under static conditions occur for rockbolt 9 placed at 202.5˚, which is passing through a joint (Figure 8.2). Under earthquake conditions with rockbolt as the only support, the normal force acting on bolts passing through joints are lower at the bottom and sidewalls of the tunnel compared to the normal force on the upper half of the tunnel. However, the rockbolts at the sidewalls of the tunnel has an increase in the force exerted on the bolt with the addition of shotcrete layer. For the left sidewall, rockbolt 8 shows a higher increase in normal force on the addition of shotcrete support. This could be due to the additional force exerted on the tunnel walls by the shotcrete which gets transmitted to the rockbolt. The increase can also be found to depend highly on the earthquake magnitude and hence more severe for Nepal earthquake (2015, M_w=8.1). When shotcrete support is added together with Rockbolts, there is no change in the shear force acting on the rockbolts under static conditions (Figure 8.3). This is because shear forces act on the bolt when a relative displacement occurs along the blocks. However, during earthquake conditions, there is a decrease in the shear force acting on the rockbolts compared to rockbolt without shotcrete. This decrease could be due to the increased support to the rock blocks and relative lower displacements under the dynamic loading. However, an increased shear force acts on the sidewalls during an earthquake when a combination of shotcrete and rockbolt is placed. These bolts on the sidewalls are through intact blocks and are previously devoid from any shear force. This denotes that the reduction in shear force on bolts though joints are transferred to the shotcrete. Moreover, the redistribution of forces through shotcrete increased the force acting on the rockbolt in the sidewalls.

Figure 8.4 shows the bending moment acting on the rockbolts during static and earthquake loading. The bending moment variation is similar to that of the shear force. The bending moment acting on the bolts under static condition for a combination of rockbolt and shotcrete is mostly similar to the bending moment with rockbolts alone. However, under the action of earthquake load, a decrease in bending moment is found on bolts passing through joints, i.e. rockbolt number 3, 9, 13, 14 and 15 (Figure 8.4). This is possibly due to the bending moment shared by the additional supporting member, shotcrete. But an increase in bending moment is observed on rockbolts 1, 8 and 16 which are positioned on the tunnel sidewalls (Figure 8.4). This is due to the redistribution of bending moment on shotcrete transferred from rockbolts 3, 9, 13, 14 and 15.

8.4 PERFORMANCE OF SHOTCRETE UNDER EARTHQUAKE

Chapter 7 considered the performance of shotcrete as a single support system and analysed the forces acting along the shotcrete. However, when a combination of rockbolt and shotcrete system is placed, a change in the shotcrete behaviour is observed. Figure 8.5 shows the difference in shotcrete deformation behaviour when acting alone and along with rockbolt.

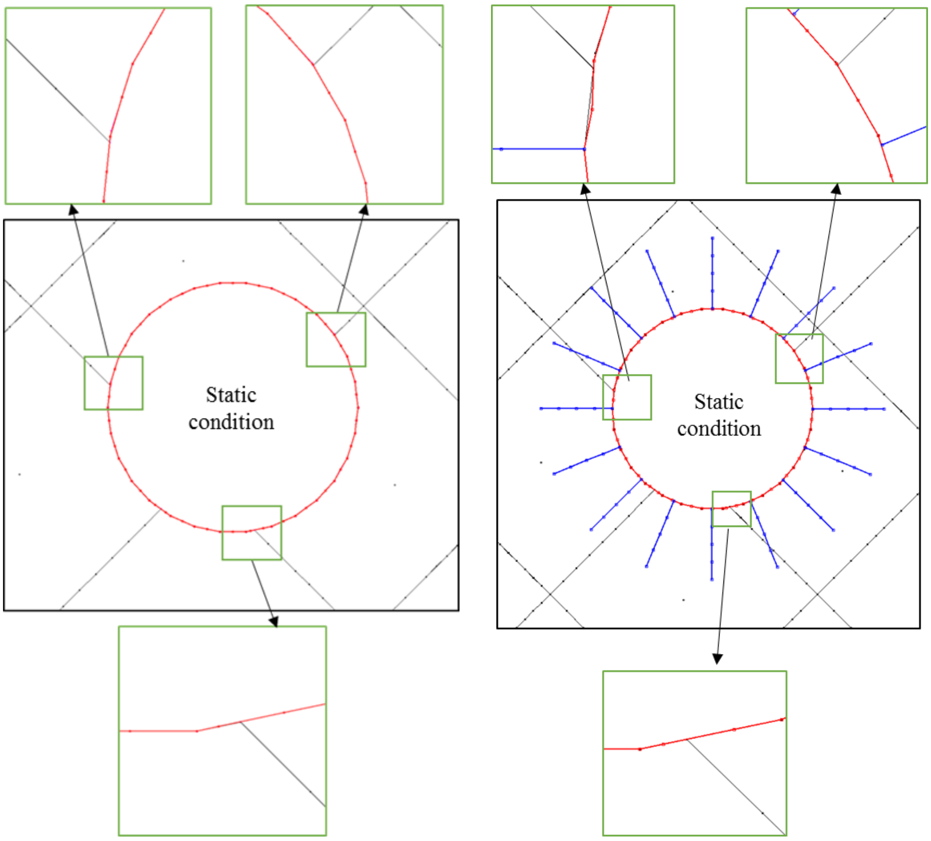

Figure 8.5: Tunnel deformation for static condition for shotcrete and a combination of shotcrete and rockbolt

Figure 8.5 shows that under static conditions, the shotcrete is stable with no deformation, while applied alone and as a combination with rockbolt support. The shotcrete, as well as rockbolt, show good compliance when applied as a support system. Figure 8.6 shows the performance of the support systems under the action of Uttarkashi earthquake (1991, M_w=6.8). This condition also points out that the support systems are safe against excessive deformation under Uttarkashi earthquake (1991, M_w=6.8).

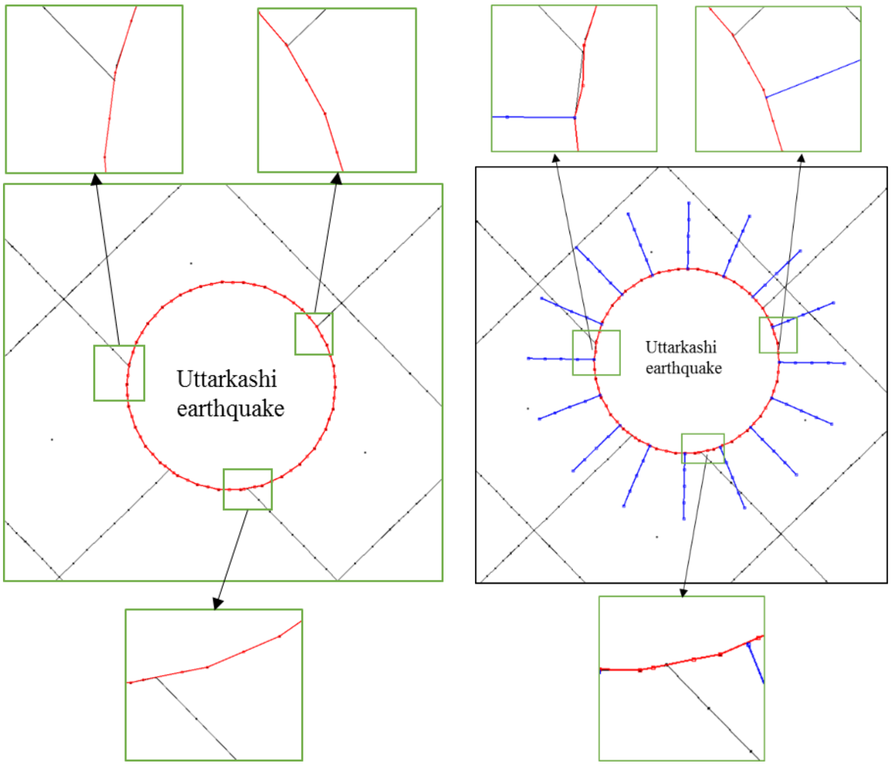

Figure 8.6: Tunnel deformation under Uttarkashi earthquake (1991, M_w=6.8) for shotcrete and a combination of shotcrete and rockbolt

Figure 8.7 shows the deformation of tunnel support under the action of Nepal earthquake (2015, M_w=8.1) for shotcrete as a single support system and shotcrete and rockbolt as a combined support system. Both the support systems under the action of Nepal earthquake (2015, M_w=8.1) show shotcrete spalling unlike Uttarkashi earthquake (1991, M_w=6.8). The positions in the shotcrete where spalling occurred in rockbolt shotcrete combination are similar to that of shotcrete alone and are in-line with the points of interaction with rock joint and shotcrete. This shows that even in well supported jointed rock tunnels with rockbolt-shotcrete combination, the relative movement along joints might cause spalling of shotcrete.

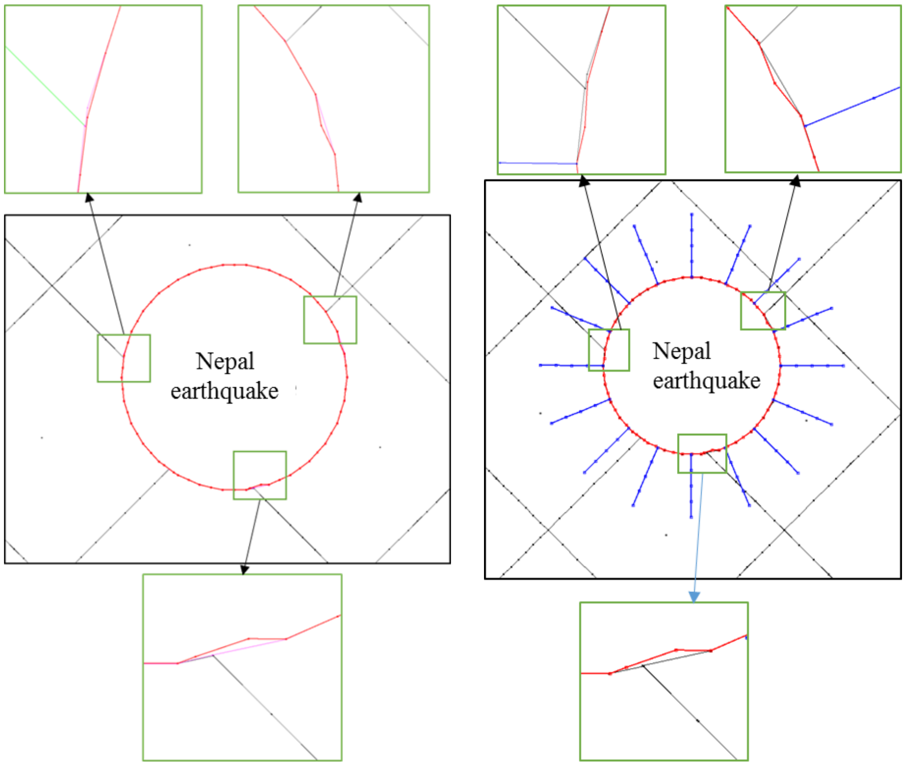

Figure 8.7: Tunnel deformation under Nepal earthquake (2015, M_w=8.1) for shotcrete and a combination of shotcrete and rockbolt

8.4.1 Normal Force acting on Shotcrete

Figure 8.8 shows the change in normal force acting on the shotcrete under static load when shotcrete is the only support and when used as a combination of shotcrete and rockbolt. The maximum normal force acting on the shotcrete decreases with rockbolt giving additional support and the position of the maximum normal force changes aswell. The normal force distribution pattern also shows a difference. The earlier point of maximum normal force is at the rockbolt position 9. From Figure 8.2, it can be seen that the force taken by rockbolt 9 has not changed under the combined effect of shotcrete and rockbolt. This leads to a decrease in the normal force coming on shotcrete at a position between 180˚ and 202˚. But the new maximum normal force acts at a position between rockbolt 13 and 14. Figure 8.2 shows a decrease in the normal force acting on rockbolts 13, 14 and 15 in the vicinity. This might be transferred as additional loads on shotcrete at tunnel position between 290˚ and 330˚.

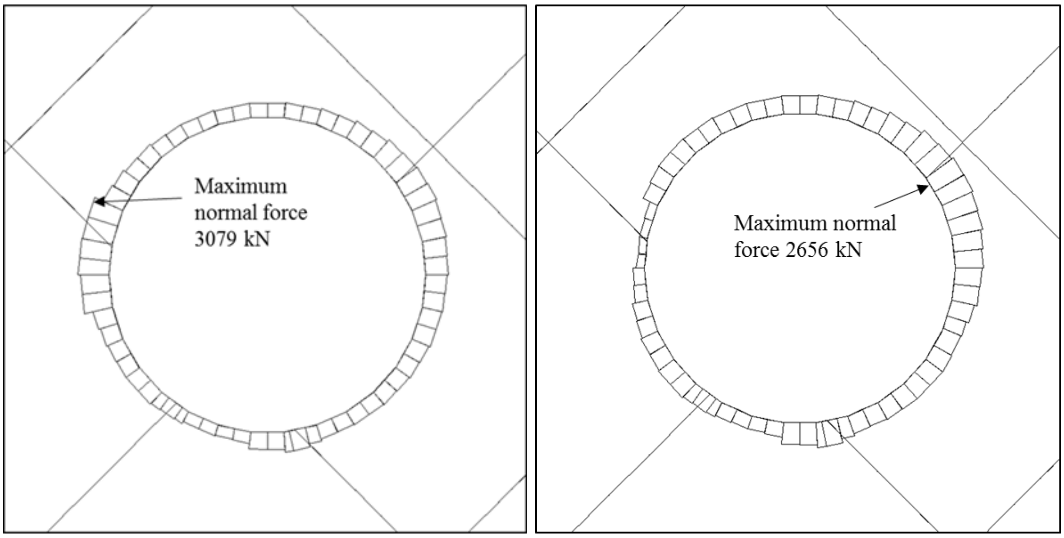

(a) (b)

Figure 8.8: Normal force acting on shotcrete lining under static condition (a) only shotcrete as support (b) shotcrete and rockbolt as support

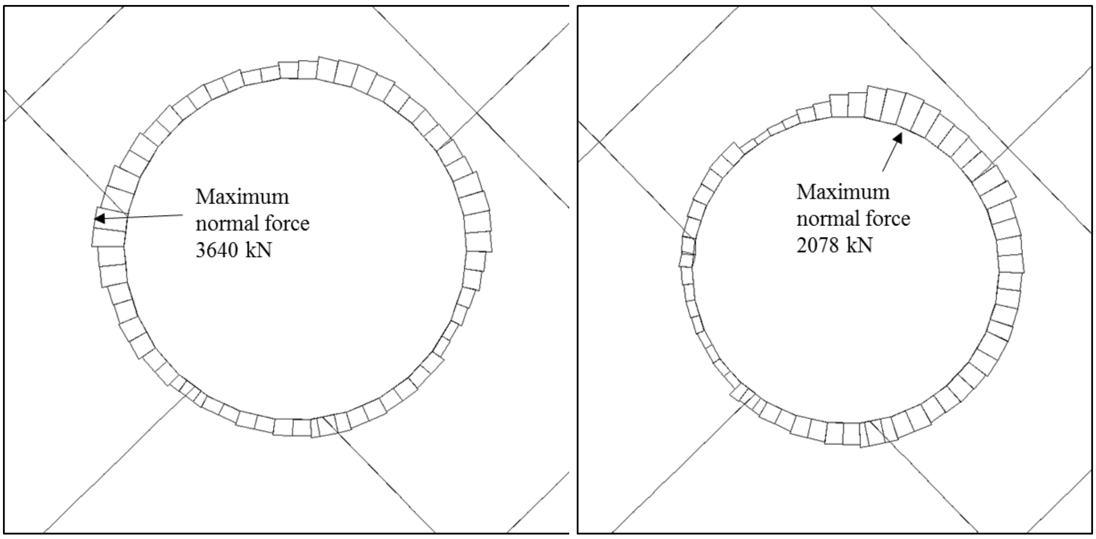

(a) (b)

Figure 8.9: Normal force acting on shotcrete lining during Uttarkashi earthquake (1991, M_w=6.8) (a) only shotcrete as support (b) shotcrete and rockbolt as support

The normal forces acting on the shotcrete under the action of Uttarkashi earthquake (1991, M_w=6.8) is shown in Figure 8.9. When shotcrete is the only supporting member, the sidewalls are found to experience maximum normal force. However, this changes to the tunnel shoulders when rockbolt is also used as a supporting member. In Figure 8.2, the forces acting on rockbolt shows an increase in the normal force acting on rockbolts on the tunnel sidewalls (rockbolt numbers 1, 8, 16). This shows that the sidewall forces are shared, which leads to a reduction of normal force on sidewalls. Thus, the maximum normal force value decreases from 3640 kN to 2078 kN when an additional rockbolt support system is provided.

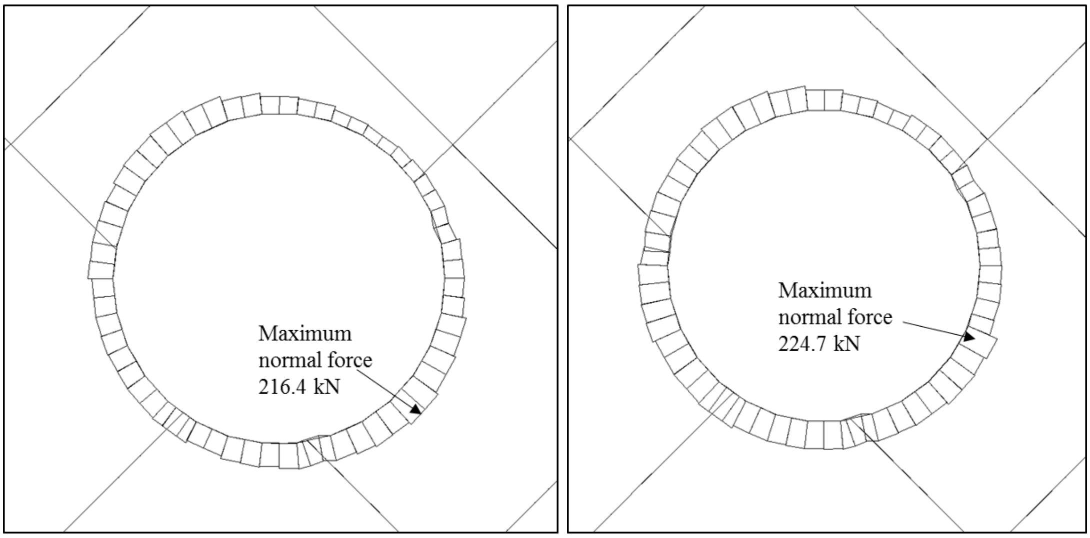

(a) (b)

Figure 8.10: Normal force acting on shotcrete lining during Nepal earthquake (2015, M_w=8.1), (a) only shotcrete as support (b) shotcrete and rockbolt as support

Figure 8.10 shows the shotcrete deformations for Nepal earthquake (2015, M_w=8.1) when it is the only support system and when a combination of rockbolt and shotcrete is used as support system. The liner deformations show that spalling of shotcrete happens on both support cases at points of maximum force on the action of Nepal earthquake (2015, M_w=8.1). Thus, the relocation of normal force happens primarily on the tunnel haunch. It can be seen that for Nepal earthquake (2015, M_w=8.1) a comparatively uniform redistribution of normal force occurs along the shotcrete.

8.4.2 Shear force acting on Shotcrete

Figure 8.11 shows the change in shear force on shotcrete under static conditions. A redistribution of shear force can be observed even under static conditions. The position of maximum shear force acting on the invert of the tunnel shifts to sidewalls of the tunnel. The positions 0˚ to 45˚ corresponding to rockbolt number 1, 8 and 9 are found to have increased shear force. However, according to Figure 8.4, there is no noticeable change in the shear force acting on rockbolt 1, 8 and 9 under static condition. But an increase in shear force occurs on these bolts under earthquake loading. The value of maximum shear force also changes and increases to 91.4 kN compared to 55.65 kN when only shotcrete is the supporting member.

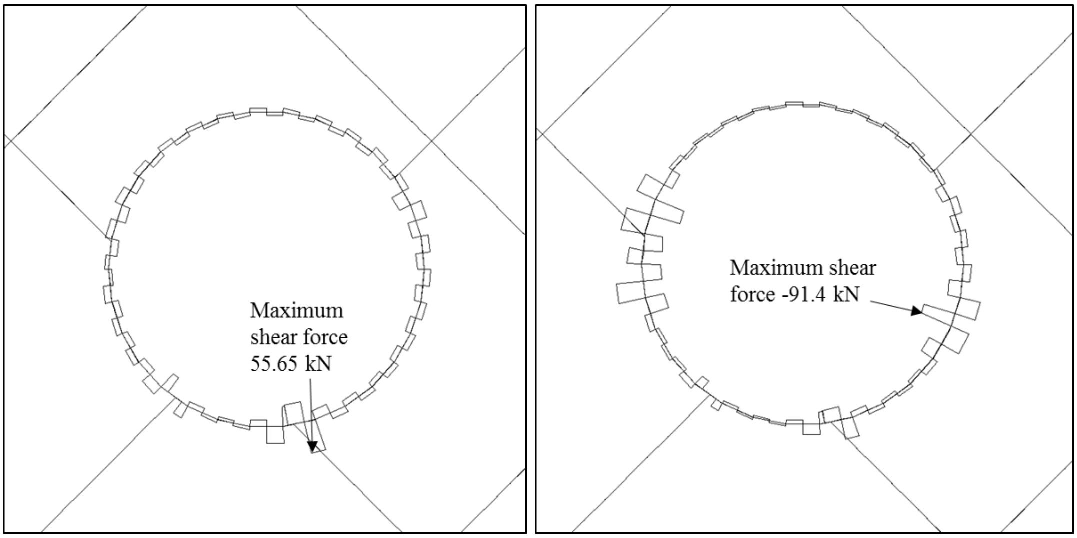

(a) (b)

Figure 8.11: Shear force acting on shotcrete lining under static condition (a) only shotcrete as support (b) shotcrete and rockbolt as support

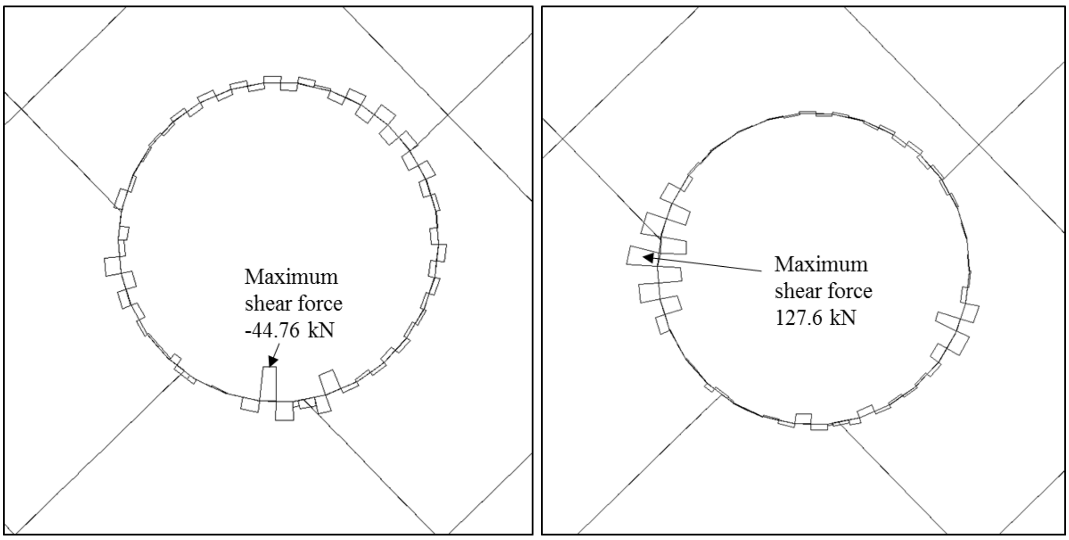

(a) (b)

Figure 8.12: Shear force acting on shotcrete lining during Uttarkashi earthquake (1991, M_w=6.8) (a) only shotcrete as support (b) shotcrete and rockbolt as support

Figure 8.12 shows the shear force variation on the shotcrete under the action of Uttarkashi earthquake (1991, M_w=6.8). Under the action of Uttarkashi earthquake (1991, M_w=6.8), a higher concentration of force acts on the points where shotcrete and rock joints intersect when shotcrete is the only support mechanism. However, when rockbolt and shotcrete is used as a support system, this increase of shear forces in zones of shotcrete and rock joint intersection is not visible for all joints. The increase in shear force is more concentrated on the sidewalls. The lowered effect of joints might be due to the presence of rockbolts, which reduces the interjoint slippage between the blocks.

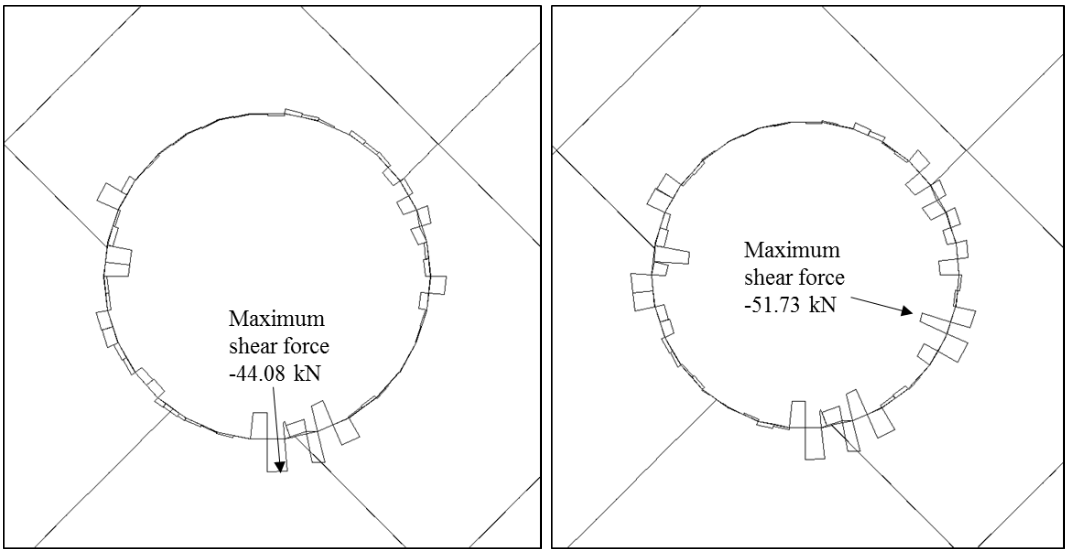

(a) (b)

Figure 8.13: Shear force acting on shotcrete lining during Nepal earthquake (2015, M_w=8.1) (a) only shotcrete as support (b) shotcrete and rockbolt as support

Figure 8.13 shows the shear force variation on the shotcrete lining under the action of Nepal earthquake. Compared to the static condition and Uttarkashi earthquake (1991, M_w=6.8) conditions, the Nepal earthquake (2015, M_w=8.1) has a pronounced effect on the shotcrete. This is true with and without rockbolt as additional support. Under the combination of rockbolt and shotcrete support, the action of shear force on the rock joint and shotcrete intersection has increased. The shear force acting on rockbolts passing through joints in Figure 8.14 shows a decrease under the action of Nepal earthquake (2015, M_w=8.1) when rockbolt and shotcrete is used. This might be due to the transfer of load to shotcrete, which is reflected as an increase in the forces along the rock joint and shotcrete interaction.

8.4.3 Bending Moment acting on Shotcrete

Figure 8.14 shows the variation of bending moment acting on the shotcrete under static load. The maximum bending moment occurs on the tunnel position positions 0˚ to 45˚ corresponding to rockbolt number 1, 8 and 9. The bending moment also increases from 11.78 kNm to 20 kNm.

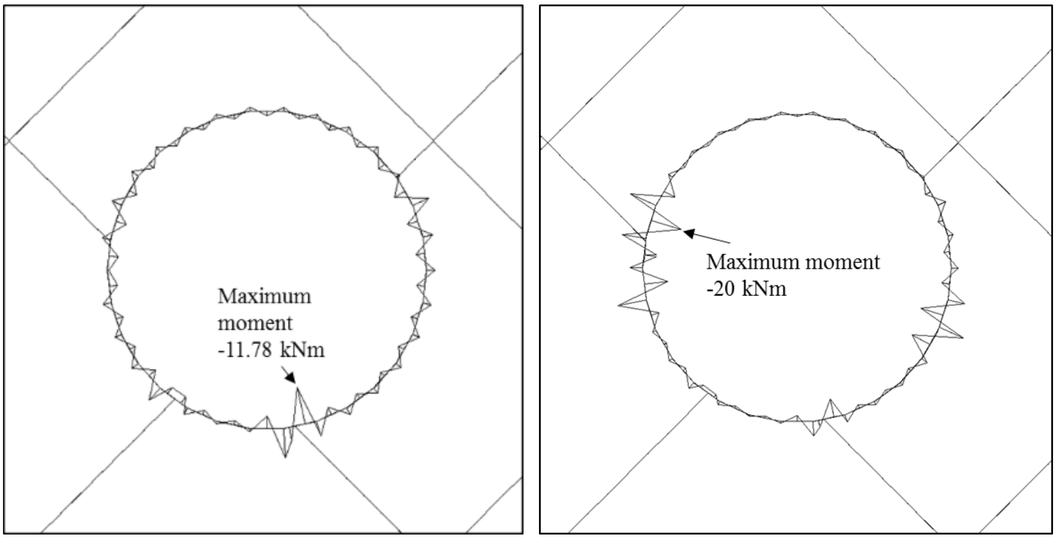

(a) (b)

Figure 8.14: Bending moment acting on shotcrete lining under static condition (a) only shotcrete as support (b) shotcrete and rockbolt as support

Figure 8.15 shows the bending moment acting on shotcrete at different points on the action of Uttarkashi earthquake (1991, M_w=6.8). When shotcrete is the only support system, the maximum bending moment and the bending moment concentration occurs on the tunnel invert as in the case of static condition. For the combined support of shotcrete and rockbolt, the bending moment variation pattern is similar to static condition, although the maximum bending moment increases from -13.84 kNm to 23.67 kNm.

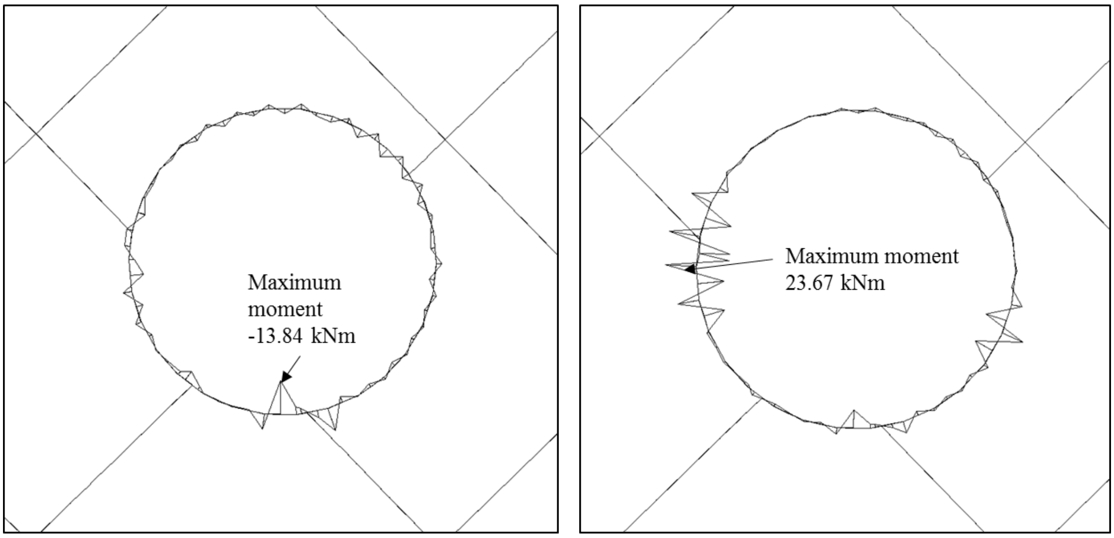

(a) (b)

Figure 8.15: Bending moment acting on shotcrete lining during Uttarkashi earthquake (1991, M_w=6.8) (a) only shotcrete as support (b) shotcrete and rockbolt as support

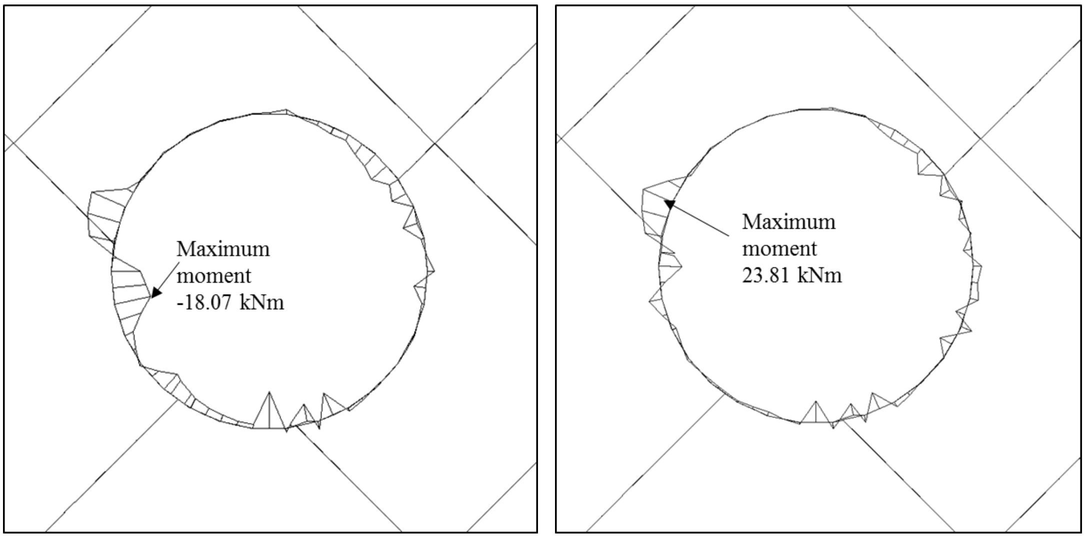

(a) (b)

Figure 8.16: Bending moment acting on shotcrete lining during Nepal earthquake (2015, M_w=8.1) (a) only shotcrete as support (b) shotcrete and rockbolt as support

Figure 8.16 shows the variation of bending moment under the action of Nepal earthquake (2015, M_w=8.1). The rock joint and shotcrete interaction induce a bending moment concentration in both cases when shotcrete alone as well shotcrete rockbolt combination. Though the magnitude of the variation is different, both have some concentration of bending moment on the sidewalls. This corresponds to an increased bending moment on the corresponding rockbolts as well. This could be due to the transfer of load from rockbolts passing through joints to the shotcrete, which creates an additional bending moment.

8.5 SUMMARY

The chapter was presented with studies to understand the performance of jointed rock tunnels supported by rockbolt and shotcrete. The Tehri dam head race tunnel, as discussed in chapter 6 is considered for analysis with rockbolt and shotcrete as a support system. The action of Uttarkashi earthquake (1991, M_w=6.8) and Nepal earthquake (2015, M_w=8.1) are used to understand its effect on rockbolt and shotcrete. The performance and load acting on rockbolt and shotcrete as a combination are compared when rockbolt and shotcrete when applied independently. The comparison of normal force acting on the rockbolt showed an increase in the sidewalls under the action of the earthquakes. The shear forces and bending moment for rockbolts passing through joints showed a decrease in force under the action of earthquake loads, though no effect is found under static conditions. The shotcrete support is found to be stable with no spalling under the static condition as well as Uttarkashi earthquake (1991, M_w=6.8). However, under the action of Nepal earthquake (2015, M_w=8.1), spalling of shotcrete occurred at points of intersection between shotcrete and rock joints. The areas of spalling are same for shotcrete with or without rockbolt support. The reduction of forces on rockbolts could be well reflected as an increase in force in shotcrete. The combined system facilitates a transfer of load from the shotcrete to the bolts passing through joints. Thus a recommendation of combined system for seismically active region will always be preferable.

CHAPTER 9

SUMMARY AND CONCLUSIONS

9.1 INTRODUCTION

The present study aims to understand the effect of stress waves originating from dynamic loads on rocks and rock joints. The effect of the stress waves on the rock also depends on the scale of the rock mass considered for analysis. For intact rocks, and rockmass with single or multiple joints, the wave propagation pattern is of primary importance. However, on a larger scale, when the study considers a structure constructed in the rockmass, the effect of the stress wave on the structure and its constituents become crucial. The present study considers the stress wave behaviour in rockmass while passing through single and multiple joints, on tunnels and tunnel supports. This chapter provides a summary of the study as presented in other chapters and the conclusions arrived from the study.

9.2 SUMMARY

The study intends to understand the effect of dynamic load on jointed rockmass and structures associated with it. The thesis is divided into nine chapters, and each chapter tries to give insights and contribute to different areas. The detailed literature review provides an in depth understanding of the existing knowledge and the research done in the area of rock dynamics.

The literature and findings on the wave propagation through rock joints are understood from the analytical, experimental and numerical perspectives. Most of the studies concentrated on the effect joint properties have on transmission and reflection coefficients. The studies showed that the dependence of wave amplitude and wave velocity on various factors like frequency of the wave, joint angle, joint infilling, joint roughness and number of joints. Many of the studies concentrated on blasting and rockburst conditions of a deep mine. The behaviour of tunnels under the action of earthquakes were also considered by many researchers with the help of suitable case studies. Though the tunnels are considered to be safe under the action of earthquakes, several literatures and case studies pointed out failures of tunnels under the action of different earthquakes. Some experimental studies and numerical modelling were done to understand the behaviour of tunnels under the action of dynamic load. The studies on the presence of joints showed an increased risk of failure in dynamic conditions due to joint slippage.

Reinforcements are used to support the tunnels in the field. Since rockbolt, shotcrete and concrete liners are the commonly used support systems, the same has been reviewed in the literature survey. The studies on rockbolt as a support system is mostly for dynamic loading and rockburst conditions. The failure and breakage of tunnels leads to deformation and breakage of these rockbolts. The effect of rockbolts under earthquake loading is given very little importance.. Many studies show the presence of cracks, spalling or breakage of these under dynamic loading. Even if the tunnels do not undergo complete failure, the tunnel support systems were found to undergo small and big damages.

An experimental study was conducted using ultrasonic pulse velocity test to understand the variation in longitudinal wave velocity with different joint conditions. The tests were conducted on laboratory prepared gypsum samples. Specimens of joint angle 0˚, 10˚, 30˚, 55˚ and 60˚ are tested. The joint angles are equal to the angle of incidence of the wave. The wave velocity was observed to decrease as the joint angle changes from 0˚ to 10˚. As the joint angle is changed from 10˚ to 55˚, negligible change in wave velocity was observed. However, the wave velocity suddenly increases as the joint angle is 60˚due to the change in phase. To understand the effect of joint roughness on wave velocity, stirrups of different roughness is introduced as per joint roughness coefficients (JRC). The wave velocity was found to decrease with the increase in joint roughness. The number of joints also found to have significant effects on the velocity of a wave transmitted through a joint. The joint numbers were increased to understand the variation with the increase in the number of joints. The wave velocity was found to decrease with increasing joints.

The experimental study posed many limitations with respect to sample sizes and the frequencies that could be studied. So a numerical approach which could successfully model the joints and consider the joint properties is adopted. The numerical tool UDEC working on distinct element method is used to analyse the wave propagation by adopting model tests similar to the experimental study. The material was modelled as elastic while the joints are assigned to follow the Coulomb slip condition. The end boundaries were modelled as quiet while the sides were roller supports with respect to wave propagation direction. The model is validated with the experimental results and also compared with the theoretical solution. The study extended the joint angle variation from 0˚ to 70˚ for a frequency range of 1 Hz to 500 kHz. The effect of block size was also analysed by varying it from 20 cm experimental size to 600 m long field size blocks. The effect of joint position is also analysed by changing the position of joint from 0.2 m to 0.8 m in a 2 m block and from 2 m to 9 m in a 10 m long block. The effect of number of joints and joint spacing is also studied. Relationships for prediction of longitudinal wave velocity in jointed rockmass with respect to intact rock are proposed.

The study is then extended to analyse the performance of unsupported jointed rock tunnels. Numerical studies are conducted on a laboratory scale with reference to the studies by CNWRA case study of Lucky Friday mine. The tunnel is subjected to scaled input motion of the 1985 Mexican earthquake and systematically validated. Further, the developed numerical model was extended to carry out parametric studies to understand the effect of various joint parameters on the deformation and stability of the tunnel under the earthquake input motion.

The jointed rock tunnels are rarely left unsupported. And the performance of the tunnel support system provides an insight into the working capability of tunnels under seismic conditions. The current study analyses the performance of rockbolt and shotcrete individually and also as a combined support system under the action of earthquake loading. The headrace tunnel of Tehri dam passing through a jointed rockmass was adopted for the study. The site was found suitable due to its critical positioning in seismic zone V. Uttarkashi earthquake (1991, Mw=6.8) and Nepal earthquake (2015, Mw=8.1) were provided as earthquake input. A parametric study is done to understand the performance of rockbolt, shotcrete and rockbolts with shotcrete.

9.3 CONCLUSIONS

The following conclusions were drawn from the current study:

9.3.1 Wave Propagation through Single and Multiple Joints

- A distinct variation in wave velocity is observed for different frequency ranges.
- Different joint parameters like joint angle, spacing or joint frequency, block length and corresponding roughness play significant roles and affect the wave characteristics in the rock mass.
- An increase in longitudinal wave velocity occurs at high angle of incidence. This is observed for input waves of very high and low frequency ranges but not for the intermediate frequency ranges.
- As the joint roughness coefficient increases, a non-linear decrease in longitudinal wave velocity occurs. This variation in longitudinal wave velocity with JRC is found to be relatively small when studied for the high frequency, which might be due to its higher energy content.
- Block length (length of the rockmass) affects the longitudinal wave velocity at low frequencies and very minor effect at higher frequencies. This influence is found to be dependent on the ratio of the wavelength to block length (λ/L_B). A sudden shift in the velocity can be observed when this ratio becomes 1. When $\lambda/2$ is more than the distance to the joint, a steep reduction of wave velocity can be observed.
- The change in longitudinal wave velocity is significant at ultrasonic range with an increase in the number of joints. A critical spacing to block length ratio exists for each frequency, at which the velocity is observed to be minimum. Also, a threshold value of spacing to block length occurs after which change in spacing to block length ratio causes no or little difference in the longitudinal wave velocity.
- Empirical equations to predict the value of longitudinal wave velocity with reference to functions of various joint parameters and intact rock velocity are proposed. The proposed equations are applicable to block with joints but it is not suitable for intact blocks or outside the ranges of joint or wave characteristics used.

9.3.2 Jointed Rock Tunnels under Seismic Load

- Displacements of joints are found to be cumulative under dynamic loads and the tunnel may fail after a series of repetitive loading. A threshold amplitude of dynamic load is observed specific to jointed rock tunnel, above which the tunnel deformations are more pronounced.
- Increase in tunnel deformations under seismic loading shows that tunnels in jointed rocks are highly susceptible to earthquake loads. A strain of at least 2-3% and as high as 15% is found to occur.
- Deformations around the tunnel increase with increasing lateral stress coefficients. For the same lateral stress coefficient, lower horizontal stress produces higher deformations. This implies that a tunnel at shallow depth is at higher risk of failure than the deep tunnels.
- The joints that are stable under static conditions are found to fail under seismic loading, specifically for some specific joint angle configurations. The rock blocks formed due to joint set are found to undergo loosening or separation if the wedge angle formed between the joints are found to be greater than the angle of joint friction.
- Under the dynamic loads, with an increase in joint normal stiffness, the tunnel deformations are found to decrease exponentially, unlike the static case where a linear decrease is seen. With the decrease in joint friction angle, the joint slip is found to increase linearly. This increase is more profound under seismic conditions compared to static conditions. The difference between static and dynamic case reduces for higher friction angle.
- Tunnel deformation values observed under seismic loads in the range of 1-5% strain with reference to the tunnel diameter can be considered significant for the field cases.
- The opening and closing of joints under dynamic loads may lead to possible slippage and strength losses degradation of the rock mass and eventual tunnel failure.

9.3.3 Performance of Rockbolts under Seismic Load

- The maximum force acting on each rockbolt is different. Normal force acts on all rockbolts under both static and seismic conditions with the maximum acts on bolts passing through joints.
- Shear force and bending moment act only on rockbolts passing through joints. The magnitude of shear force and bending moment increases under the action of earthquake load, and the effect is predominant in the bolts along the tunnel shoulders.
- The rockbolts undergo higher deformations under the action of dynamic load compared to a static load. The displacement patterns for Uttarkashi (1991, Mw=6.8) and Nepal (2015, Mw=8.1) earthquakes showed different trends. The peak values of forces, bending moment and displacement corresponds typically to the peak of the corresponding earthquake loads.
- Rockbolts were found to have an increase in the forces as the diameter increases. This increase is most predominant in the upper half of the tunnel compared to the lower half.
- An increase in embedment length led to a decrease in shear force and bending moment acting on the rockbolt. When a rockbolt initially in intact block coincides with a joint, an increase in shear force and bending moment occurs which later decrease with the increase in embedment length.
- The increase in joint friction leads to a decrease in relative displacement between the joints. This leads to a decrease in shear force and bending moment as the joint friction increases. Normal force acting on the rockbolts remain comparatively unaffected by the change in joint friction.
- Wave frequency affects different parts of the tunnel differently. Increase in the duration of loading leads to an increase in the forces acting on the rockbolt. However, these changes are comparatively small since the duration makes a negligible influence on the rockbolt when lower than the threshold value.
- The forces acting on each rockbolt was found to increase with an increase in amplitude. However, this increase was found to be different for the upper and lower half of the tunnels. The forces acting on the upper half of the tunnels were found to have a higher magnitude.

9.3.4 Performance of Shotcrete under Seismic Load

- The shotcrete is usually a relatively stable support system with no deformation under static conditions and earthquakes of lower magnitude. But under dynamic loads, substantial damage/spalling of shotcrete can occur especially with higher magnitude and duration.
- Spalling commonly occurs near points of intersection between shotcrete and joint. The concentration of shear force and bending moment occurs at locations of intersection between rock joint and shotcrete.
- The positions of normal force concentrations change from tunnel sidewall to tunnel haunch due to possible spalling**.** The positions of the stress concentration and spalling varied for each frequency. Wave frequency and amplitude are found to be vital factors affecting shotcrete support.
- The pattern and zones of spalling and cracking as observed in the numerical study compare well with the available literature for tunnel failure under actusl earthquake loading.

9.3.5 Performance of Rockbolt and Shotcrete combination under Seismic Load

- A reduction of forces occur on rockbolts passing through joints under combined support system along with a corresponding increase in the forces on shotcrete. This shows the transfer of load from rockbolt to shotcrete under seismic conditions.
- An increase in the concentration of stress was observed on the rockbolts at the sidewalls under the action of seismic load for a combined system. This is assumed to be due to the redistribution and transfer of load from the rockbolts on the shoulder to the sidewalls via shotcrete support system.
- Spalling of shotcrete occurs under high earthquake even in a combined support system. The points of shotcrete spalling are similar to independent shotcrete of shotcrete supports.

9.4 SCOPE OF FUTURE WORK

The current study area being comparatively new, many extensions for the future studies are also proposed. The following are some of the areas which will provide better insight into the subject,

- The experimental study on wave propagation needs to be extended for large strain problems.
- The study on wave propagation through joints were analysed only with longitudinal waves and a better understanding of the same with S wave needs to be done.
- Develop a design criteria and provide standards on allowable tunnel deformations under dynamic loads.

REFERENCES

1. Abokhalil, M. (2007). “Insights into the response of rock tunnels to seismicity”. Master's Thesis in Geosciences, Department of Geosciences, University of Oslo.
2. Adyan, Ö. (2016). “Large rock slope failures induced by recent earthquakes”. Rock Mechanics and Rock Engineering, 49, 2503–2524.
3. Adyan, Ö. (2017). “Rock dynamics”. ISRM Book Series, Taylor & Francis Group, London, ISSN: 2326-6872.
4. Adyan, Ö. and Kumsar. (2010). “An experimental and theoretical approach on the modeling of sliding response of rock wedges under dynamic loading”. Rock Mechanics and Rock Engineering, 43, 821–830.
5. Adyan, Ö., and Kawamoto, T. (2004). “The damage to lignite mines caused by the 2003 Miyagi-Hokubu earthquake and some considerations on its causes”. 3rd Asian Rock Mechanics Symposium, Kyoto, 1, 525-530.
6. Adyan, Ö., Ohata, Y., Genis, M., Tokashiki, N. and Ohkubo, K. (2010). “Response and stability of underground structures in rock mass during earthquakes”. Rock Mechanics and Rock Engineering, 43, 857–875.
7. Adyan, Ö., Shimizu, Y., and Karaca, M. (1994). “The dynamic and static stability of shallow underground openings in jointed rock masses”. The 3rd International Symposium on Mine Planning and Equipment Selection, Istanbul, 851-858.
8. Adyan, Ö., Ulusay, R., Hamada, M., and Beetham, D. (2012). “Geotechnical aspects of the 2010 Darfield and 2011 Christchurch earthquakes of New Zealand and geotechnical damage to structures and lifelines”. Bulletin of Engineering Geology and the Environment, 71(4), 637–662.
9. Ahola, M. P., Hsuing, S. M., and Kana, D. D. (1996). “Experimental study on dynamic behavior of rock joints. Coupled thermo-hydro-mechanical process of fractured media”. Developments in Geotechnical Engineering, 79, 467–506.
10. Arulnathan, R., Boulanger, R. W. and Riemer, M. F. (1998). “Analysis of bender element tests”. Geotechnical Testing Journal, ASTM, 21(2), 120-131.
11. Asakura, T., Kojima, Y., Matsunaga, T., Shigeta Y. and Tsukada, K. (2007) “Damage to mountain tunnels by earthquake and deformation mechanism”. 11th Congress of the International Society for Rock Mechanics – Ribeiro e Sousa,

Olalla & Grossmann (eds), Taylor & Francis Group, London, ISBN 978-0-415-45084-3.

12. Asakura, T., Shiba, Y., Matsuoka, S., Oya, T. and Yashiro, K. (2000). “Damage to mountain tunnels by earthquake and its mechanism”. Dobuku Gakkari Robunshu, Vol. 2000, Issue 659, 27-38.
13. ASTM C597-16. “Standard test method for pulse velocity through concrete".
14. ASTM D 2845-00 (2000). “Standard test method for laboratory determination of pulse velocities and ultrasonic elastic constants of rock”. Annual Book of ASTM Standards, 14(02).
15. Austrian Standards Institute: ONORM B 2203-1. 2001. “The Austrian practice of NATM tunnelling contracts”. Austrian Society for Geomechanics.
16. Aydan, Ö., Ohta, Y., Daido, M., Kumsar, H., Genis, M., Tokashiki, N., Ito, T. and Amini, M. (2011). “Earthquakes as a rock dynamic problem and their effects on rock engineering structures”. In: Advances in Rock Dynamics and Applications (Eds: Zhou, Y. & Zhao, J.). Boca Raton, FL, CRC Press, Taylor and Francis Group, 341–422.
17. Aydan, Ö., Tomiyama, J., Matsubara, H., Tokashiki, N. and Iwata, N. (2017). “The characteristics of damage to rock engineering structures induced by the 2016 Kumamoto earthquakes”. In: 14th Domestic Rock Mechanics Symposium, Kobe.
18. Babanouri, N. and Fattahi, H. (2018). “Evaluating orthotropic continuum analysis of stress wave propagation through a jointed rock mass”. Bulletin of Engineering Geology and the Environment, 77(20), 725-733.
19. Barbero, M. and Barla, G. (2010). “Stability analysis of a rock column in seismic conditions”. Rock Mechanics and Rock Engineering, (2010), 43:845–855.
20. Barla, G., Monacis, G., Perino, A. and Hatzor, Y. (2010). “Distinct element modeling in static and dynamic conditions with application to an underground archaeological site”. Rock Mechanics and Rock Engineering, 43, 877–890.
21. Barton, N. (1973). “Review of a new shear-strength criterion for rock joints”. Engineering Geology, 7 (4) , 287-332.
22. Barton, N. (1984). “Effect of rock mass deformation on tunnel performance in seismic regions”. Advances in Tunnelling Technology and Subsurface Use, 4(3), 89-99.

23. Barton, N. (2007) “Rock quality, seismic velocity, attenuation and anisotropy”. Taylor & Francis, London, UK.
24. Barton, N. R. (1974). “A review of the shear strength of filled discontinuities in rock”. Norwegian Geotechnical Institute Publication No. 105, Oslo: Norwegian Geotechnical Institute.
25. Barton, N. R. and Choubey, V. (1977). “The shear strength of rock in theory and practice”. Rock Mechanics, 10, 1-54.
26. Barton, N., Lien, R., and Lunde, J. (1974). “Engineering classification of rock masses for the design of tunnel support”. Rock Mechanics, 6(4), 189-236.
27. Bedford, A. and Drumheller, D. S. (1994). “Introduction to Elastic Wave propagation”. Wiley & Sons, Chichester.
28. Beer, A. J., Stead, D. and Coggan, J. S. (2002). “Estimation of joint roughness coefficient (JRC) by visual comparison”. Rock Mechanics and Rock Engineering, 35(1), 65-74.
29. Belem, T., Homand-Etienne, F. and Souley, M. (2000). “Quantitative parameters of rock joint surface roughness”. Rock Mechanics and Rock Engineering, 33(4),65-74.
30. Bhasin, R. and Pabst, T. (2014). “The behaviour of rock support in tunnels in seismic regions with a case study of a large underground cavern in the Himalayas”. Journal of Rock Mechanics and Tunnelling Technology, 20(1), 5-20.
31. Bhasin, R. K., Abokhalil, M., Kaynia, A. M., Hoeg, K., Paul, D. K. and Pal, S. (2010). "Numerical simulations of earthquake effect in underground structures." 14th Symposium on Earthquake Engineering, Roorkee, India, pp. 1384-1394.
32. Bhasin, R., Kaynia A. M., Paul, D. K., Singh, Y. and Pal, S. (2006). “Seismic behaviour of rock support in tunnels”. Proceedings 13th Symposium on Earthquake Engineering, Indian Institute of Technology, Roorkee, December 18-20.
33. Bhasin, R., Kaynia, A. M., Paul, D. K., Singh, Y. and Pal, S. (2006). “Seismic behaviour of rock support in tunnels”. Proceedings 13th Symposium on Earthquake Engineering, Indian Institute of Technology, Roorkee, December 18-20.
34. Bieniawski, Z. T. (1989). “Engineering rockmass classification”. Wiley, New York.

35. Boon, C.W. (2013). “Distinct element modelling of jointed rock masses: Algorithms and their verification”. PhD Thesis, University of Oxford.
36. Brady, B. H. G. and Brown, E. T. (1993). “Rock mechanics for underground mining”. George Allen & Unwin, London.
37. Bringnoli, E. G. M., Gotti, M. and Stokoe, K. H. (1996). “Measurement of shear waves in laboratory specimens by meas of piezoelectric transducers”. Geotchnical Testing Journal, ASTM, 19(4), 384-397.
38. Brummer, R. K., Vi, X., Tannant, D. D. and McDowell, M. (1994). “Rockbolt behaviour under dynamic loading: Field trials and numerical simulation”. Rock Mechanics, Nelson and Lauback (eds) © Balkema, Rotterdam, ISBN 905410 380 8.
39. Cai, J. G. and Zhao, J. (2000). “Effects of multiple parallel fractures on apparent attenuation of stress waves in rock masses”. International Journal of Rock Mechanics and Mining Sciences, 37, 661-682.
40. Cha, M. S., Sim, Y. J., Cho, G. C. and Lee, S. W. (2013). “The effect of joint conditions on longitudial and flexural wave velocities of a rock mass”. Key Engineeering Materials, Vols 321-323, pp. 306-309.
41. Cha, M. S., Sim, Y. J., Cho, G. C. and Santamaria, J. C. (2009). “Long wavelength P wave and S wave propagation in jointed rock masses”. Geophysics, 74, E205-E214.
42. Chai, S. B., Li, J. C., Zhang, Q. B., Li, H. B. and Li, N.N. (2016). “Stress wave propagation across a rockmass with two non-parallel joints”. Rock Mechanics and Rock Engineering, 49:4023-4032.
43. Chan, C. (2010). “Bender element test in soil specimens: Identifying the shear wave arrival time”. Electronic Journal of Geotechnical Engineering, 15, Bund. M, 1263-1276.
44. Chen, C., Wang, T., Jeng, F. and Huang, T. (2012). “Mechanisms causing seismic damage of tunnels at different depths”. Tunnelling and Underground Space Technology, 28, 31-40.
45. Chen, S. G. and Zhao, J. (1998). “A study of UDEC modelling for blast wave propagation in jointed rock masses”. International Journal of Rock Mechanics and Mining Science, 35(1), 93-99.
46. Chen, W. Y., Loveli, C. W., Haley, G. M. and Pyrak-Nolte, L. J. (1993). “Variation of shear-wave amplitude during frictional sliding”. International

Journal of Rock Mechanics and Mining Sciences and Geomechanics, 30(7), 779-784.

47. Chen, X., Li, J. C., Cai, M. F., Zou, Y. and Zhao, J. (2016). "A further study on wave propagation across a single joint with different roughness". Rock Mechanics and Rock Engineering, 49: 2701:2709.
48. Cook, N. G. W. (1992). "Natural joints in rocks: mechnical, hydraulic and seismic behaviour and properties under normal stress". International Journal of Rock Mechanics and Mining Sciences and Geomechanics, 29(3), 198-223.
49. COSMOS website. https://strongmotioncenter.org/vdc/scripts/default.plx
50. Cui, Z., Sheng, Q. and Leng, X. (2016). "Control effect of a large geological discontinuity on the seismic response and stability of underground rock caverns: A case study of the Baihetan surge chamber". Rock Mechanics and Rock Engineering, 49, 2099–2114.
51. Cundall, P. A. (1971). "A computer model for simulating progressive large scale movements in blocky rock systems". Proceedings of the Symposium of the International Society of Rock Mechanics, Society for Rock Mechanics (ISRM), France, Vol. 1, Paper No. 118.
52. Cundall, P. A. and Hart, R. D. (1992). "Numerical modelling of discontinua". Engineering Computations, 9, 101-113.
53. Daemen, J. J. K. (1977). "Problems in tunnel support mechanics". Underground Space, 1 (3):163-72.
54. D'Alembert (1747) "Recherches sur la courbe que forme une corde tenduë mise en vibration" (Researches on the curve that a tense cord [string] forms [when] set into vibration), Histoire de l'académie royale des sciences et belles lettres de Berlin,. 3, 214-219.
55. Deng, X. F., Zhu, J. B., Chen, S. G., Zhao, X. Y., Zhou, Y. X., Zhao, J. (2014). "Numerical study on tunnel damage subject to blast-induced shock wave in jointed rockmasses". Tunnelling and Underground Space Technology 43, 88–100.
56. Devali, K. and Babadagli, T. (1998). "Quantification of natural fracture surfaces using fractal geometry". Mathematical Geology, 30(8), 971-998.
57. Dhawan, R. K., Singh, D. N. and Gupta, I. D. (2004). "Dynamic analysis of underground openings". Rock Mechanics and Rock Engineering, 37(4), 299–315.

58. Do, N. A., Dias, D., Oreste, P. and Dheran-Maigre, I. (2015). "2D numerical investigation of segmental tunnel lining under seismic loading". Soil Dynamics and Earthquake Engineering, 72, 66-76.
59. Dowding, C. H. (1984). "Estimating earthquake damage from explosion testing of full- scale scale tunnels". Advances in Tunnelling Technology and Subsurface Use, 4 (3), 113–117.
60. Dowding, C. H. and Rozen, A. (1978). "Damage to rock tunnels from earthquake shaking". Journal Geotech Engineering Division, ASCE, GT2, 175–191.
61. Eitzenberger, A. (2012). "Wave propagation in rock and the influence of discontinuities". Doctoral Thesis, Luleå University of Technology, Sweden.
62. Elmo, D., Vyazmensky, A., Stead, D. and Rogers, S. (2012). "Applications of a finite discrete element approach to model cave mining". Innovative Numerical Modelling in Geomechanics (Eds. Sousa et al.) © Taylor and Francis Group, London, ISBN 978-0-415-6166.
63. Ewing, W. M., Jardetzky, W. S. and Press, F. (1957). "Elastic wave in layered media". McGraw-Hill, New York, NY.
64. Fan, L., Ma, G. and Li, J. (2012). "Nonlinear viscoelastic medium equivalence for stress wave propagation in a jointed rock mass". International Journal of Rock Mechanics & Mining Sciences, 50, 11–18.
65. Fratta, D. and Santamarina, J. C. (2002). "Shear wave propagation in jointed rock: State of stress". Geotechnique, 52(7), 495-505.
66. Genis, M. and Adyan, Ö. (2002). "Evaluation of dynamic response and stability of shallow underground openings in discontinous rock masses using model tests". Proceedings of 2002 ISRM Regional Symposium (3rd Korea-Japan Joint Symposium) on Rock Engineering Problems and Approaches in Underground Construction, Seoul, 2, 787-794.
67. Ghosh, A., Hsiung, S. M. and Chowdhury, A. H. (1996). "Seismic response of rock joints and jointed rockmass". Center for Nuclear Waste Regulatory Analysis, NUREG/CR-6388, CNWRA 95-013.
68. Goodman, R. E. (1989). "Introduction to Rock Mechanics". © John Wiley and Sons.
69. Goodman, R. E. and Dubious, J. D. (1971). "Static and dynamic analysis of rock bolt is support- Research on rock bolt reinforcement". Technical Report No. 6, AD 723 397, Omaha District, Corps of Engineers, Omaha, Nebraska.

70. Gu, B. L., Suarez, R., Nihei, K. T. and Myer, L. R. (1996). "Incidence of plane waves upon a fracture". Journal of Geophysical Research, 101(B11), 25, 337–25 346.
71. Gui, Y., Bui, H., Kodikara, J., Zhang, Q., Zhao, J. and Rabczuk, T. (2016). "Modelling the dynamic failure of brittle rocks using a hybrid continuum-discrete element method with a mixed-mode cohesive fracture model". International Journal of Impact Engineering, 87, 146-155.
72. Hart, R. D. (1993). "An introduction to distinct element modelling for rock engineering". Comprehensive rock engineering (Ed. in-chief: Hudson, J. A.), 2, 245-261. Pergamon Press, Oxford.
73. Hashash, Y. M. A., Hook, J. F., Schmidt, B. and Yao, J. I. (2001). "Seismic design and analysis of underground structures". Tunnelling and Underground Space Technology, 16, 247-293.
74. Hatzor, Y. H., Arzi, A. A., Zaslavsky, Y. and Shapira, A. (2004). "Dynamic stability analysis of jointed rock slopes using the DDA method: King Herod's Palace, Masada, Israel". International Journal of Rock Mechanics & Mining Sciences, 41, 813–832.
75. Heuze, F. E. and Morris, J. P. (2007). "Insights into ground shock in jointed rocks and the response of structures there-in". International Journal of Rock Mechanics & Mining Sciences, 44, 647–676.
76. Hoek, E. and Moy, D. (1993). "Design of large powerhouse caverns in weak rock". In Comprehensive rock engineering, (ed. J.A. Hudson) 5, 85-110. Oxford: Pergamon.
77. Hsuing, S. M. and Ghosh, A. (2006). "Seismic Responses of Underground Excavations in Jointed Rock Mass". ARMA/USRMS 06-974. Golden Rocks 2006, 41st U.S. Symposium on Rock Mechanics, Colardo, June, 17-21.
78. Huang, X., Qi, S., Guo, S. and Dong, W. (2014). "Experimental study of ultrasonic waves propagating through a rock mass with a single joint and multiple parallel joints". Rock Mechanics and Rock Engineering, 47, 549-559.
79. Huang, X., Qi, S., Williams, A., Zou, Y. and Zheng, B. (2014). "Numerical simulation of stress wave propagating through filled joints by particle model". International Journal of Solids and Structures, 69, 23-33.
80. Hwang, H., Juang, H., Ra, S., Kim, D. and Back, H. (2001). "Stability analysis of a tunnel supported by shotcrete-rockbolt system in hard bedrock". Rock

Mechanics in the National Interest, Elsworth, Tinucci and Heasley (eds.), © Swets and Zeltilinger Lisse, ISBN 90 2651 827 7.

81. Iai, S. (1989). “Similitude for shake table tests on soil-structure-fluid model in 1g gravitational field”. Soils and Foundations, 29,105-118.
82. Indraratna, B. and Haque, A. (2000). “Experimental and numerical modelling of shear behaviour of rock joints”. In: GeoEng 2000, An International Conference of Geotechnical and Geological Engineering, 1. Pennsylvania.
83. IS 13311-1(1992): “Method of Non-destructive testing of concrete, Part 1: Ultrasonic pulse velocity”. Bureau of Indian Standards.
84. IS 15026 (2002). “Tunnelling methods in rock masses- Guidelines”. Bureau of Indian Standards.
85. IS 5878 (1972). “Indian standard code of practice ofr construction of tunnels conveying water”. Bureau of Indian Standards, Reaffirmed in 2005.
86. ISRM(2010), website of the International Society for Rock Mechanics (ISRM), Commision on Rock Dynamics, http:// www.isrm.n et
87. Itasca Consulting group Inc. (2014) UDEC User Manuals.
88. Iyengar R. N. (1993). “How safe is the proposed Tehri dam to earthquakes”. Current Science, 65(5), 384-392.
89. Jaeger, J. C., Cook, N. G. W. and Zimmerman, R. W. (2007). “Fundementals of Rock Mechanics”. © Blackwell Publishing, Victoria, Australia.
90. Jain, S. K., EERI, M. and Das, S. (1993). “Analysis of strong motion records from Uttarkashi earhquake for assessment of code provisions for different seismic zones”. Earthquake Spectra, 9(4), 739-754.
91. Jalalifar, H., Aziz, N. and Hadi, M. (2005). “Rock and bolt properties and load transfer mechanism in ground reinforcement”. 20th World Mining Congress, Mining and Sustainable Development, 629-635.
92. Jalalifar, H., Aziz, N. and Hadi, M. (2006). “The effect of surface profile, rock strength and pretension load on bending behaviour of fully grouted bolts”. Geotechnical Geological Engineering, 24(5), 1203–1227.
93. Jia, P. and Tang, C. (2008). “Numerical study on failure mechanism of tunnel in jointed rock mass”. Tunnelling and Underground Space Technology, 23(5), 500-507.

94. Jiang, N. and Zhou, C. (2012). "Blasting vibration safety criterion for a tunnel liner structure". Tunnelling and Underground Space Technology, 32 (2012), 52–57.
95. Jiang, Y., Li, B. and Tanabashi, Y. (2006). "Estimating the relation between surface roughness and mechanical properties of rock joints". International Journal of Rock Mechanics and Mining Sciences, 43, 837-846.
96. Jing, L. (2003). "A review of techniques, advances and outstanding issues in numerical modelling for rock mechanics and rock engineering". International Journal of Rock Mechanics and Mining Sciences, 40, 283-353.
97. Jing, Y. and Stephansson, O. (2007). "Fundamentals of discrete element methods for rock engineering theory and application". Elsevier B.V., ISBN 978-0-444-82937-5.
98. Ju, Y., Sudak, L. and Xie, H. (2007). "Study on stress wave propagation in fractured rocks with fractal joint surfaces". Solids and Structures, 44, 4256-4271.
99. Kahraman, S. (2002). "The effects of fracture roughness on P wave velocity". Enginnering Geology, 63,347-350.
100. Kaiser, P. K. and Cai, M. (2012). "Design of rock support system under rockburst condition". Journal of Rock Mechanics and Geotechnical Engineeing, 4(3), 215-227.
101. Kaiser, P. K., Tannant, D. D. and McCreath, D. R. (1996). "Canadian rockburst support handbook".
102. Kana, D. D., Brady, B. H. G., Vanzant, B. W. and Nair, P. K. (1991). "Critical assessment of seismic and geomechanics literature related to a high-level nuclear waste underground repository". USA. doi: 10.2172/138128.
103. Kana, D. D., Fox, D. J., Hsuing, S. and Chowdhury, A. H. (1997). "An experimental scale model study of seismic responses of an underground opening in jointed rock mass". USA. doi:10.2172/464193.
104. Kaneshiro, J. Y., Power, M. and Rosidi, D. (2000). "Empirical correlations of tunnel performance during earthquakes and a seismic aspects of tunnel design". Proceedings of the Conference on lessons learned from recent earthquakes on Earthquakes in Turkey.
105. Kazerani, T. and Zhao, J. (2011). "Discontinuum-based numerical modelling of rock dynamic fracturing and failure". Advances in rock dynamics (Ed. Zhu, Y. and Zhao, J.), CRC Press,

106. Kimura, F., Okabayashi, N. and Kawamoto, T. (1987). “Tunnelling through squeezing rock in two large fault zones of Enasan Tunnel II”. Rock Mechanics and Rock Engineering, 20(3), 151-166.
107. Kirsch, E. G. (1898). “Die Theorie der Elastizität und die Bedürfnisse der Festigkeitslehre”. Zeitschrift des Vereines deutscher Ingenieure, 42, 797-807, 1898
108. Kolsky, H. (1953). “Stress Waves in Solids”. Clarendon Press, Oxford.
109. Kongai, K., Johansson, J., Zafeirakos, A., Numada, M. and Sadr, A. A. (2005). “Damage to tunnels in the October 23, 2004 Cuetsu earthquake”. JSCE Journal of Earthquake Engineering, 28, 75-81.
110. Kouretzis, G. P., Andrianopoulos, K. I., Sloan, S. W. and Crater, J. P. (2014). “Analysis of circular tunnels due to seismic P-wave propagation with emphasis on unreinforced concrete liners”. Computers and Geotechnics, 55, 187-194.
111. Kurtulus, C., Uckardes, M., Sari, U. and Guner, S. O. (2011). “Experimental studies in wave propagation cross a jointed rock mass”. Bulletin of Engineering Geology and the Environment, 71(2), 231-234.
112. Lang, T. A. and Bischoff, J. A. (1982). “Stabilization of rock excavations using rock reinforcement”. In: Proceedings of the Symposium on Rock Materials, American Rock Mechanics Association, 935-944.
113. Lee, J. S. and Santamarina, J. C. (2005). “Bender elements: Performance and signal interpretation” Journal of Geotechnical and Geoenvironmental Engineering, ASCE, 131(9), 1063-1070.
114. Li, C. (2017). “Principles of rockbolting design”. Journal of Rock Mechanics and Geotechnical Engineering, 9, 396-414.
115. Li, C., Stjern, G. and Myrvang, A. (2014). “A review on the performance of conventional and energy-absorbing rockbolts”. Journal of Rock Mechanics and Geotechnical Engineering, 6,315-327.
116. Li, J. C. and Ma, G. W. (2010). “Analysis of blast wave interaction with a rock joint”. Rock Mechanics and. Rock Engineering, 43(6), 777–787.
117. Li, J. C., Li, H. B., Ma, G. W. and Zhao, J. (2012). “A time-domain recursive method to analyse transient wave propagation across rock joints”. Geophysical Journal International, 188, 631-644.

118. Li, J. C., Li, X. B. and Zhao, J. (2015). “An improved equivalent viscoelastic medium method for wave propagation across layered rock masses”. International Journal of Rock Mechanics & Mining Sciences, Vol. 73, pp. 62–69.
119. Li, J., Ma, G. and Zhao, J. (2010). “An equivalent viscoelastic model for rock mass with parallel joints”. Journal of Geophysical Research, 115, B03305.
120. Li, W. and Pyrak-Nolte, L. J. (2010). “Seismic wave propagation in fractured carbonate rock”. Proceedings of Project Review, Geo-mathematical Imaging Group (Purdue Univeristy), Vol 1, 211-220.
121. Liu, K., Zhang, Q. B. and Zhao, J. (2018) “Dynamic increase factors of rock strength”. Rock Dynamics- Experiments, Theories and Applications ©2018 Taylor and Francis Group, London, ISBN 978-0-8153-9667-3.
122. Lukic, D., Maslak, E., Zlatanovic, E. and Manic, N. (2017). “Earthquake effects on the ground in the rock bolt area – A 3D computational model”. Contemporary achievements in civil engineering 21, April 2017, Subotica, Serbia.
123. Luo, X. and Z. Yang (2013). “Finite element modeling of a tunnel affected by dislocation of faults”. In Proceedings of 5th Asia Pacific Congress on Computational Mechanics & 4th International Symposium on Computational Mechanics (APCOM & ISCM), Singapore.
124. Ma, M. and Brady, B. H. (1999). “Analysis of the dynamic performance of an underground excavation in jointed rock under repeated seismic loading”. Geotechnical and Geological Engineering, Vol. 17, 1–20.
125. Manouchehrian, A. and Cai, M. (2017). “Analysis of rockburst in tunnels subjected to static and dynamic loads”. Journal of Rock Mechnics and Geotechnical Engineering, 9(6), 1031-1041.
126. Manouchehrian, A. and Cai, M. (2018). “Numerical modeling of rockburst near fault zones in deep tunnels”. Tunnelling and Underground Space Technology, 80, 164-180.
127. Miao, Y., Yao, E., Ruan, B. and Zhuang, H. (2018). “Seismic response of shield tunnel subjected to spatially varying earthquake ground motions”. Tunnelling and Underground Space Technology, 77, 216-226.
128. Miller, R. K. (1977). “An approximate method of analysis of the transmission of elastic waves through a frictional boundary”. Journal of Applied Mathematics, 44(4), 652–656.

129. Miller, R. K. (1978). “The effect of boundary friction on the propagation of elastic waves”. Bulletin of the Seismological Society of America, 68 (4), 987-998.
130. Mohd-Nordin, M. M., Song, K., Cho, G. and Mohamed, Z. (2014). “Long wavelength elastic wave propagation across naturally fractured rock masses". Rock Mech. Rock Engg., 47, 561-573.
131. Mollhoff, M., Bean, C. J. and Meredith, P. G. (2010). “Rock fracture compliance derieved from time delays of elastic waves”. Geophysical Prospecting, 58:111-1121.
132. Mortazavi, A. and Alavi, F. T. (2013). “A numerical study of the behavior of fully grouted rockbolts under dynamic loading”. Soil Dynamics and Earthquake Engineering 54, 66-72.
133. Mortazavi, A.and Alavi, F. T. (2013) “A numerical study of the behavior of fully grouted rockbolts under dynamic loading”. Soil Dynamics and Earthquuake Engineering, 54, 66-72.
134. Mow, C. C. and Pao, Y. H. (1971). “The diffraction of elastic waves and dynamic stress concentrations”. R-482-PR, Report for the U.S. Air Force Project Rand, April.
135. Myer, L. R. (2000). “Fractures as a collection of cracks”. International Journal of Rock Mechanics and Mining Sciences 37, pp 231-243.
136. Myer, L. R., Pyrak- Nolte, L. J., Hopkins, D., Cook, N. G. W. (1990). “Seismic characteristics of fracture properties”. US Department of Energy, Contract No. DE-AC03-76SF00098.
137. Noorzad, A., Aminpur, M. and Salari, H. (2008). “Seismic slope stability analysis of jointed rock masses on the northern abutment of Gotvand dam, Iran”. The 14th World Conference on Earthquake Engineering, October 12-17, 2008, Beijing, China.
138. ÖNORM B 2203 (1993). “The NATM Classfication”. © Austrian Standards Institute.
139. Ortelapp, W. D. and Stacy T. R. (1996). “The performance of containment rock support such as wire mesh under simulated rockburst loading”. Proceeding Geomechanics 96, Rotterdam: A.A. Balkema.
140. Ortlepp, W. D. (2001). “The behaviour of tunnels at great depth under large static and dynamic pressures”. Tunnelling and Underground Space Technology, 16, 41-48.

141. Ortlepp, W. D. and Stacey, T. R. (1998). “Performance of tunnel support under large deformation static and dynamic loading”. Tunnelling and Underground Space Technology 13(1), 15-21.
142. Otuonye, F. O. (1988). “Response of grouted roof bolts to blast loading”. International Journal Rock Mechanics and Mining Sciences & Geomechanics Abstracts, 25, 345-349.
143. Owada, Y. and Aydan, Ö. (2005) “Dynamic response of fully grouted rockbolts during shaking”. The School of Marine Science and Technology, Tokai University, 3(1), 9–18.
144. Owada, Y., Daido, M. and Aydan, Ö. (2004). “Mechanical response of rock anchors and rockbolts during earthquakes”. 34th Japan Rock Mechanics Symposium, 519–524.
145. Owen, G. N. and Scholl, R. E. (1981). “Earthquake engineering of large underground structures”. NASA STI/Recon Technical Report No. FHWA_RD-80_195. Federal Highway Administration and National Science Foundation.
146. Palmstrom, A. and Nilsen, B. (2000). “Engineering geology and rock engineering handbook”. Norwegian Rock and Soil Engineering Association, Trondheim.
147. Palmström, A. and Stille, H. (2010). “Rock Engineering”. © Thomas Telford Limited. ISBN : 978-0-7277-4083-0.
148. Panek, L. A. (1964). “Design for bolting stratified roof”. Transactions of the Society of Mining Engineers, 229,113-9.
149. Parija, M. P., Kumar, S., Tiwari, V. M., Rao, N. P., Kumar, N., Biswal, S. and Singh, I. (2018). “Microseismicity, tectonics and seismic potential in the Western Himalayan segment, NW Himalaya, India”. Journal of Asian Earth Sciences, 159, 1-16.
150. Park, D. and Yoo, J.K. (2014). “Seismic tunnel response in jointed rock mass”. Geotechnical Aspecta and Underground Construction in Soft Ground (Eds: Yoo, C., Park, S.W., Kim, B. and Ban, H.) ©Korean Geotechnical Society, Seoul, Korea, ISBN 978-1-138-02700-8.
151. Patel, A., Singh, D. N. and Singh, K. K. (2010). “Performance analysis of piezo ceramic elements in soils”. Geotechnical and Geological Engineering, 28(5), 681-694.
152. Perino, A. (2011). “Wave propagation through discontinuous media in rock engineering”. PhD. thesis. Polytechnic University of Turin, Italy.

153. Perino, A., Zhu, J. B., Li, J. C., Barla, G. and Zhao, J. (2010). “Theoretical methods for wave propagation across jointed rock masses”. Rock Mechanics and Rock Engineering, Vol. 43, pp. 799–809.
154. Power, M. S., Rosidi, D. and Kaneshiro, J. (1998). “Seismic vulnerability of tunnels and underground structures revisited”. In Proceedings of North American Tunneling, 98, Balkema, Rotterdam.
155. Pyrak Nolte, L. (2016). “Fracture specific stiffness as critical link among fracture properties”. Rock Dynamics: From Research to Engineering, (Eds: Li, H., Li, J., Zhang, Q. and Zhao, J.), Taylor and Francis Group, London, ISBN 978-1-138-02953.
156. Pyrak-Nolte, L. J. (1992). “Seismic response of fractures and interrelation among fracture properties”. International Journal Rock Mechanics and Mining Sciences and Geomechanics Abstracts, 73, 787-802.
157. Pyrak-Nolte, L. J. (1996). “The seismic response of fractures and the interrelation among fracture properties”. International Journal Rock Mechanics and Mining Sciences and Geomechanics Abstracts, 33(8), 787-802.
158. Pyrak-Nolte, L. J. (1996). “The seismic response of fractures and the interrelation among fracture properties”. International Journal Rock Mechanics and Mining Sciences & Geomechanics Abstracts, 33(8), 787-802.
159. Pyrak-Nolte, L. J. and Nolte, D.D. (1992). “Frequency dependence of fracture stiffness”. Geophysical Research Letters, 19(3), 325-332.
160. Pyrak-Nolte, L. J., Myer, L. R. and Cook, N. G. W. (1990a). “Transmission of seismic-waves across single natural fractures”. Journal of Geophysical Research, Solid Earth Planets, 95, 8617–8638.
161. Pyrak-Nolte, L. J., Myer, L. R. and Cook, N. G. W. (1990b). “Anisotropy in seismic velocities and amplitudes from multiple parallel fractures”. Journal of Geophysical Research, 95(11), 345–358.
162. Pytlik, A., Prusek, S. and Masny, W. (2016). “A methodology for laboratory testing of rockbolts used in underground mines under dynamic loading conditions”. Journal of South African Institute of Mining and Metallurgy, 116(11), 01-10.
163. Rabcewicz, L. (1969). “Stability of tunnels under rock load Part 2”. Water Power, July, 266-73.

164. Ramamurthy, T. (2014). "Engineering in rocks for slopes, foundations and tunnels". © PHI Learning Private Limited, Delhi.
165. Ramamurthy, T. and Arora, V.K. (1994). "Strength predictions for jointed rocks in confined and unconfined states". International Journal of Rock Mechanics and Mining Sciences and Geomechanics Abstracts, 31(1), 9-22.
166. Resende, R. (2010). "An investigation of stress wave propagation through rock joints and rock masses". Doctoral Thesis, Faculty of Engineering of the Porto University, Portugal.
167. Resende, R., Lamas, L., Lemos, J. and Calcada, R. (2004). "Stress wave propagation test and numerical modelling of an underground complex". International Journal of Rock Mechanics and Mining Sciences, 72, 26-36.
168. Romero, V. S. and Caulfield, R. J. (2012). "Improving the seismic resilience of lifeline tunnels". Proceedings of the 2012 New Zealand Society of Earthquake Engineering Conference, Paper Number 064.
169. Rosengren, L. (1993). "Preliminary analysis of the dynamic interaction between Norrra Lanken and a subway tunnel for Stockholm, Sweden". Tunnelling and Underground Space Technology, 8(4), 429-439.
170. Roy, N. and Sarkar, R. (2017). "A review of seismic damage of mountain tunnels and probable failure mechanisms". Geotechnical and Geological Engineering, 35 (1), 1–28.
171. Roy, N. and Sarkar, R. (2018). "Transverse dynamic response of circular tunnels in blocky rock mass using distinct-element method". International Journal of Geomechanics, 18 (10), 04018124.
172. Roy, N., Sarkar, R. and Bharati, S. D. (2018). "Transverse dynamic response of circular tunnels in blocky rock mass using distinct element method". Internatonal Journal of Geomechanics, 18(10), 04018124.
173. Sato, H., Fujikake, K. and Mindess, S. (2004). "Study on dynamic pullout strength of anchors: Based on failure modes". 13th World Conference on Earthquake Engineering,Vancouver, B.C., Canada, August 1-6, 2004.
174. Schoenberg, M. (1980). "Elastic wave behavior across linear slip interfaces". Journal of the Acoustical Society of America, 68(5), 1516–1521.
175. Schoenberg, M. and Sayers, C. M. (1985). "Seismic anisotropy of fractured rocks". Geophysics, 60 (1), 581-589.

176. Sebastian, R. (2015). “Elastic wave propagation and evaluation of low strain dynamic properties in jointed rocks”. Doctoral Thesis. IISc Bangalore.

177. Sebastian, R. and Sitharam, T. G. (2014). “Trasnsmission of Elastic waves through a frictional boundary”. International Journal of Rock Mechanics and Mining Sciences, 66, 84-90.

178. Sebastian, R. and Sitharam, T. G. (2015). “Long-wavelength propagation of waves in jointed rocks- Study using resonant column experiments and model material”. Geomechanics and Geoengineering, 33, 923-934.

179. Sharma, S. and Judd, W. R. (1991). “Underground opening damage to underground facilities”. Engineering Geology, 30, 263-276.

180. Shen, B. and Barton, N. (1997). “The disturbed zone around the tunnels in jointed rockmass”. International Journal of Rock Mechanics and Mining Sciences, 34 (1), 117-125.

181. Shigui, D., Yunjin, H. and Xiaofei, H. (2009). “Measurement of joint roughness coefficient by using profilograph and roughness ruler”. Journal of Earth Sciences, 20(5), 890-896.

182. St. John, C. M. and Zahrah, T. F. (1987). “Aseismic design of underground structures”. Tunneling Underground Space Technology, 2, 165-197.

183. Stacey, T. R. (2011). “Support of excavations subjected to dynamic (rockburst) loading”. In: Proceedings of the 12th ISRM Congress. [S.l.]: Taylor and Francis Group, 137–145.

184. Statens vegvesen, (2000). “Fjellbolting. Håndbok 215. Oslo: Trykkpartner AS”. (in Norwegian).

185. Stjern, G. and Myrvang, A. (1998). “The influence of blasting on grouted rock bolts”. Tunnelling and Underground Space Technology, 3(1), 65-70.

186. Sudbury, Ontario: Geomechanics Research Centre, Laurentian University.

187. Tahmasebinia, F., Canbulat, I., Onur, V. and Serkam, S. (2018). “A numerical study of the behaviour of fully grouted cable bolts under static and dynamic loading”. 10th Asian Rock Mechanics Symposium, 29 October -03 November, Singapore.

188. Tannant, D. D., Brummer, R. K. and Yi, X. (1995). “Rockbolt Behaviour under Dynamic Loading: Field Tests and Modelling”. International Journal of Rock Mechanics, Mining Sciences and Geomechanics Abstract, 32(6), 537-550.

189. Tao, S., Gao, B. and Xin, C. (2015). "Seismic damage analysis of tunnel front slope and shaking table tests on highway tunnel portal". EJGE Vol.20, Bund. 8.
190. Tehri Hydro Developent Corporation Limited. "Design Criteria for Rock Supporting System of Multiple Underground Caverns". Memorandum No. 17, Rishikesh, 1997.
191. Thomas, A. (2009). "Sprayed concrete lined tunnels". Applied Geotechnics. Volume 2, Taylor and Francis, 2 Park Square, Milton Park, Abingdon, Oxon OX14 4RN.
192. Tistel, J., Grimstad, G. and Eiksund, G. (2017). "Testing and modeling of cyclically loaded rock anchors". Journal of Rock Mechanics and Geotechnical Engineering, 9(6), 1010-1030.
193. Toomey, A., Bean, C. J. and Scotti, O. (2002). "Fracture properties from a seismic data- a numerical investigation". Geophysical Research Letters. 29(4), 1050, 1-4.
194. Tsesarsky, M. and Hatzor, Y. H. (2006). "Tunnel roof deflection in blocky rock masses as a function of joint spacing and friction–a parametric study using discontinuous deformation analysis (DDA)". Tunnelling and Underground Space Technology, 21(1), 29-45.
195. Viggiani, G. and Atkinson, J. H. (1995). "Interpretation of bender element tests". Geotechnique, 45(1), 149-154.
196. Walsh, J. B. (1966). "Seismic attenuation in rock due to friction". Journal of Geophysical Research, 71(N10), 2591-2600.
197. Wang, J. N. (1993). "Seismic design of tunnels: A state-of-the-art approach, monograph 7". Parsons, Brinckerhoff, Quade and Douglas Inc., New York.
198. Wang, T., Yang, C., Yan, X., Li, Y., Liu, W., Liang, C. and Li, J. (2014). "Dynamic response of underground gas storage salt cavern under seismic load". Tunnelling and Underground Space Technology, 43, 241-252.
199. Wang, W. L., Wang, T. T., Su, J. J., Lin, C. H., Seng, C. R. and Huang, T. H. (2001). "Assessment of damage in mountain tunnels due to the Taiwan Chi-Chi earthquake". Tunnelling and Underground Space Technology, 16(3), 133-150.
200. Wang, W. L., Wang, T. T., Su, J. J., Lin, C. H., Seng, C. R. and Huang, T. H. (2001). "Assessment of damage in mountain tunnels due to the Taiwan Chi Chi earthquake". 16, 133-150.

201. Wang, W., Song, Q., Xu, C. and Gong, H. (2018). " Mechnical behavior of fully grounted rock bolts under the joint action of pre-tension load and blast loading". Tunnelling and Underground Space Technology, 73, 82-91.
202. Wang, W., Song, Q., Xu, C. and Gong, H. (2018). "Mechanical behaviour of fully grouted GFRP rock bolts under the joint action of pre-tension load and blast dynamic load". Tunnelling and Underground Space Technology, 73, 82-91.
203. Wang, W., Song, Q., Xu, C. and Gong, H. (2018). "Mechanical behaviour of fully grouted GFRP rock bolts under the joint action of pre tension load and blast dynamic load". Tunnelling and Underground Space Technology, 73, 82-91.
204. Wang, X. and Cai, M. (2015). "Influence of wavelength-to-excavation span ratio on ground motion around deep underground excavations". Tunnelling and Underground Space Technology, 49, 438–453.
205. Wang, X., Chen, J. and Xiao, M. (2018). "Seismic damage assessment and mechanism analysis of underground powerhouse of the Yingxiuwan Hydropower Station under the Wenchuan earthquake". Soil Dynamics and Earthquake Engineering, 113, 112-123.
206. Wang, Z. L., Li, Y. C. and Shen, R. F. (2007). "Numerical simulation of tensile damage and blast crater in brittle rock due to underground explosion". International Journal of Rock Mechanics and Mining Sciences, 44(5), 730–738.
207. Wang, Z. Z., Jiang, Y. J. and Zhu, A. (2019). "Seismic energy response and damage evolution of tunnel lining structures". European Journal of Environmental and Civil Engineering, 29(6), 758-770.
208. Wang, Z. Z., Jiang, Y. J., Zhu, C. A. and Sun, T. C. (2015). "Shaking table tests of tunnel linings in progressive states of damage". Tunnelling and Underground Space Technology, 50, 109-117.
209. Wang, Z., Qiao, C., Song, C. and Xu, J.(2014). "Upper bound limit analysis of support pressures of shallow tunnels in layered jointed rock strata". Tunnelling and Underground Space Technology, 43, 171-183.
210. Wickham, G. E., Tiedemann, H. R. and Skinner, E. H. (1972). "Support determination based on geologic predictions". In Proceedings of North American rapid excavation tunneling conference, Chicago, (eds K.S. Lane and L.A. Garfield), 43-64. New York: Society of Mining Engineers, American Institute of Mining, Metallurgy and Petroleum Engineers.

211. Windsor, C. R. and Thompson, A. G. (1993). “Rock, reinforcement technology, testing, design and evolution”. Comprehensive Rock Engineering, (Ed. J.A. Hudson), Oxford: Pergamon Press.
212. Wu, W., Li, H. and Zhao, J. (2015). “Dynamic response of non-welded and welded rock fractures and implications for P wave attenuation in a rock mass”. International Journal of Rock Mechanics and Mining Sciences, 77, 174-181.
213. Wu, W., Li, H. and Zhao, J. (2015). “Rock of filling material in a P wave interaction with a rock fracture”. Engineering Geology 172, 77–84.
214. Wu, W., Li, J. C. and Zhao, J. (2014). “Role of filling materials in a P wave interaction with a rock fracture”. Engineering Geology, 172, 77-84.
215. Wu, X., Jiang, Y., Gong, B., Guan, Z. and Deng, T. (2019). “Shear performance of rock joint reinforced by fully encapsulated rock bolt under cyclic loading condition”. Rock Mechanics and Rock Engineering, https://doi.org/10.1007/s00603-018-1698-4
216. Yang, H., Huang, D., Yang, X. and Zhou, X. (2013). “Analysis model for the excavation damage zone in surrounding rock mass of circular tunnel”. Tunnelling and Underground Space Technology, 35, 78-88.
217. Yang, L., Mei, J., Li, S., Jiang, Y., Guo, K., Zhang, B. and Yang, W. (2018). “Experimental study of open fracture's multifarious effects on ultrasonic wave propagation in rock masses”. Journal of the Society of Materials Science, Japan. 67(8), 811-818.
218. Yang, Z., Lan, H., Zhang, Y., Gao, X. and Li, L. (2013). “Nonlinear dynamic failure process of tunnel-fault system in response to strong seismic event”. Journal of Asian Earth Sciences, 64, 125-135.
219. Yi, C. P., Lu, W., Zhang, P., Johansson, D. and Nyberg, U. (2016). “Effect of imperfect interface on the dynamic response of a circular lined tunnel impacted by plane P-waves”. Tunnelling and Underground Space Technology, 51, 68–74.
220. Yi, C., Zhang, P., Johansson, D. and Nyberg, U. (2014). “Dynamic response of a circular lined tunnel with an imperfect interface subjected to cylindrical P-waves". Computers and Geotechnics, 55, 165-171.
221. Yoo, J. K., Park, J. S., Park, D. and Lee, S. W. (2017). “Seismic response of circular tunnels in jointed rock”. KSCE Journal of Civil Engineering, 22(2), 1-9.

222. Yu, H., Chen, J., Bobet, A. and Yuan, Y. (2016). “Damage observation and assessment of the Longxi tunnel during the Wenchuan earthquake”. Tunnelling and Underground Space Technology, 54, 102-116.
223. Yu, H., Yuan, Y., Qiao, Z., Gu, Y., Yang, Z. and Li, X. (2013). “Seismic analysis of a long tunnel based on multi-scale method”. Engineering Structures, 49, 572-587.
224. Zhan, Z. and Qi, S. (2017). “Numerical Study on Dynamic Response of a Horizontal Layered-Structure Rock Slope under a Normally Incident Sv Wave”. Applied Science, 7, 716.
225. Zhang, L. (2017). “Engineering Properties of Rocks”. Elseviers Geo-Engineering Book Series, © Butterworth-Heinemann.
226. Zhang, Q. B. and Zhao, J. (2014). “A review of dynamic experimental techniques and mechanical behaviour of rock materials”. Rock Mechanics and Rock Engineering, 47(4), 1411-1478.
227. Zhang, X., Jiang, Y. and Sugimoto, S. (2018). “Seismic damage assessment of mountain tunnel: A case study on the Tawarayama tunnel due to the 2016 Kumamoto earthquake”. Tunnelling and Underground Space Technology, 71, 138-148.
228. Zhang, Z.X. (2016). “Rock Fracture and Blasting: Theory and Application”. © Elsevier Inc. ISBN: 9780128026885
229. Zhao, J. and Cai, J. G. (2001). “Transmission of Elastic P-waves across Single Fractures with a Nonlinear Normal Deformational Behavior”. Rock Mechanics and Rock Engineering, 34 (1), 3-22.
230. Zhao, J., Cai, J. G., Zhao, X. B. and Li, H. B. (2006). “Experimental study of ultrasonic wave attenuation across parallel fractures”. Geomechanics and Geoengineering, 1(2), 87-103.
231. Zhao, J., Zhou, Y. X., and Ma, G. W. (2008). “Rock failure, wave propagation and tunnel stability under dynamic loads”. Keynote Paper, 5th Asian Rock Mechanics Symposium (ARMS5), 24-26 November 2008 Tehran, Iran.
232. Zhao, J., Zhou, Y. X., Hefny, A. M., Cai, J. G., Chen, S. G., Li, H. B., Liu, J. F., Jain, M., Foo, S. T. and Seah, C. C. (1999). “Rock dynamics research related to cavern development for ammunition storage”. Tunelling and Underground Space Technology, 14(4), 513-526.

233. Zhao, X. B., Zhao, J., Cai, J. G. and Hefny, A. M. (2008). "UDEC modelling on wave propagation across fractured rockmasses". Computers and Geotechnics, 35, 97-104.
234. Zhou, Y. and Zhao, J. (2011). "Advances in rock dynamics and applications". Boca Raton, FL, CRC Press, Taylor and Francis Group. ISBN: 978-0-203-09320-7.
235. Zhu, J. B., Perino, A., Zhao, G. F., Barla, G., Li, J. C., Ma, G. W. and Zhao, J. (2011). "Seismic response of a single and a set of filled joints of viscoelastic deformational behaviour". Geophysical Journal International, 186, 1315–1330.
236. Zhu, J. B., Zhao, G. F., Zhao, X. B. and Zhao, J. (2011). "Validation study of the distinct lattice spring model (DLSM) on P-wave propagation across multiple parallel joints". Computers and Geotechnics, 38(2), 298-304.
237. Zou, Y., Jing, L., Sun, H. and Li, Y. (2012). "Analysis of Seismic Factors to Tunnels in the Earthquake". Applied Mechanics and Materials 166-169, 2182-2189.
238. Zou, Y., Li, J., He, L., Laloui, L. and Zhao, J. (2016). "Wave propagation in the vicinities of the rock fractures under obliquely incident wave". Rock Mechanics and Rock Engineering, 49, 1789-1802.
239. Zulficar, A. C., Alcik, H. and Cakti, E. (2012). "Analysis of earthquake records of Istanbul earthquake rapid response system stations related to the determination of site fundamental frequency". Proceedings of 15th World Conference on Earthquake Engineering, Lisbon, Portugal, 36, 28769-28776.

LIST OF PUBLICATIONS

Paper published /Under review in Journals

1. Varma, M., Maji, V. B. and Boominathan A. (2019). "Numerical modelling of a tunnel in jointed rocks subjected to seismic loading". Underground Space, Elsevier, 4(2), 113-146.
2. Varma, M., Maji, V.B. and Boominathan, A. (2019) A study on the effect of rock joints on wave response, International Journal of Rock Mechanics and Mining Sciences, Elsevier Pub. (Under Review)

Full Papers Published in Conference Proceedings,

3. Varma, M., Maji, V. B. and Boominathan, A. (2015). "Deformation Response of a Circular Tunnel in Jointed Rocks". Indorock proceedings 2016, IIT Bombay, Mumbai. Paper ID. INDOROCK201638.
4. Varma, M., Maji, V. B. and Boominathan, A. (2017). "A Study on Ultrasonic Wave Propagation Across Fractures in Jointed Rocks". ARMA 2017. 51st US Rock Mechanics / Geomechanics Symposium held at San Francisco, California, USA. Paper No. 483.
5. Varma, M., Maji, V. B. and Boominathan, A. (2018). "Effect of Joint Stiffness in Rock Tunnels under Dynamic Loading". 10th Asian Rock Mechanics Symposium, ARMS 10, Singapore. Paper ID. ARMS10-P-0558.